

**Redox regulation of protein phosphatase-1 and ER stress
regulation of connective tissue growth factor in
cardiomyocytes**

Doctoral Thesis

In partial fulfillment of the requirements for the degree

“Doctor of Philosophy (Ph.D.)”

in the Molecular Medicine Study Program

at the Georg-August University Göttingen



Submitted by

Simranjit Singh

Born in Barnala, Punjab

Göttingen, 2017

Dedicated to the Family

Members of the thesis committee

Prof. Dr. rer. nat. Susanne Lutz (Supervisor)

Email: susanne.lutz@med.uni-goettingen.de
Phone: +49 (0) 551 39 10665
Postal Address: Institute of Pharmacology and Toxicology
University Medical Center Göttingen
Georg-August University Göttingen
Robert-Koch-Str. 40, 37075 Göttingen
Germany

Prof. Dr. med. Ali El-Armouche (Supervisor)

Email: ali.el-armouche@tu-dresden.de
Phone: +49 (0) 351 458 6300
Postal Address: Institute of Pharmacology and Toxicology
Medizinisch-Theoretisches Zentrum
3rd Floor, Room C.20.050
Fiedlerstraße 42, 01307 Dresden
Germany

Prof. Dr. med. Dörthe Katschinski

Email: doerthe.katschinski@med.uni-goettingen.de
Phone: +49 (0) 551 39 5896
Postal Address: Institute of Cardiovascular Physiology
Humboldtallee 23, 37073 Göttingen
Germany

Prof. Dr. rer. nat. Viacheslav O. Nikolaev

Email: v.nikolaev@uke.de
Phone: +49 (0) 40 7410 51391
Postal Address: Institute of Experimental Cardiovascular Research
University Medical Center Hamburg-Eppendorf (UKE)
Martinistr. 52, 20246 Hamburg
Germany

Prof. Dr. rer. nat. Blanche Schwappach-Pignatro

Email: blanche.schwappach@med.uni-goettingen
Phone: +49 (0) 551 39 5962
Postal Address: Institute of Molecular Biology
Universitätsmedizin Göttingen
Humboldtallee 23
D-37073, Göttingen
Germany

Affidavit

Here I declare that my doctoral thesis entitled:

**“Redox regulation of protein phosphatase-1 and ER stress regulation in
connective tissue growth factor in cardiomyocytes”**

has been written independently with no other sources and aids than quoted.

Simranjit Singh

Göttingen, May 2017

Acknowledgement

I am very grateful to the director of the Institute of Pharmacology and Toxicology, Dresden, Prof. Ali El-Armouche, for accepting as Ph.D. student under his umbrella and being a constant source of inspiration during my early (and most difficult) days. Within Ali's group, I am particular thankful to several individual for taking me "under their wing" and sharing their wisdom. Alireza Saadatmand, a research associate in the lab, taught me everything from basic immunoblotting till making scientific presentation and posters. Christina Vettel, a senior research associate in the lab, has been inspiring in learning how to critically interpret and present experimental data. Last but not the least, my friends and colleagues, Simon Lämmle and Stefanie Meyer-Roxlau, for making everyday lab work easy and help in establishing many key experiments for the Ph.D. Also in then end time, thank you so much for support in proofreading the thesis. Just as well, my thesis committee has been very supportive and genuinely interested in helping me become a good scientist.

My sincere thanks to my supervisor, Head of the "GPCR-Signaling Research Unit", Göttingen, Prof. Susanne Lutz, for being a role model in the field of scientific carrier. Thank you very much for the continuous support and I can never think of completing it, without your immense scientific advice and patience during the Ph.D. time. I learned so many things from her – ranging from presentation of data, writing scientific reports and data analysis. Also, my deepest thanks to Dr. Naim Kittana for seeding the love for basic science in me and being an ideal mentor, his presence will always be missed. On top Anita Ongherth and Beate Ramba help and support, to which I am always in debt.

I would like to express my sincere gratitude to the director of the Institute of Pharmacology and Toxicology, Göttingen, Prof. Wolfram Zimmerman, for letting me part of the family during the Ph.D. and for his genuine support and valuable critics, comments and suggestion during the regular Monday meetings. I also thank the entire Institute of Pharmacology and Toxicology, Göttingen for welcoming me into their academic house and preceding me with every possible opportunity. I am also indebted to many other members of the laboratory for their constant support and advice. They include: Norman Liaw, Lavanya Iyer, Susanne Schlik, Svenja Hartmann, Sebastian Pasch, Matthias Dewenter, Sumon Sur, Satish Gala, Elif Levent, Eriona Heta, Felicitas Mügge, Claudia Noack, Iris Quentin, Andreas Schraut, and Tim Meyer.

I would like to say many thanks to my thesis committee members Prof. Dörthe Katschinski, Prof. Viacheslav O. Nikolaev and Prof. Blanche Schwappach-Pignatro for providing constructive comments and valuable suggestions during the regular progress report meeting

and also in writing the thesis. Many thanks also go to Prof. Steven Johnsen and Prof. Holger Reichardt for accepting to participate in the examination committee.

I am also very thankful to the 'International research training group 1816 (IRTG 1816) for offering me a Ph.D. position and for the great support they provided during the stay in Germany. My fellow members from IRTG 1816 program, Alex Johnston, Elisa Sanchez, Tohwid Islam, Theresa Riebleing and Angelika Beneke have also been very helpful in improvising the experiments and motivation.

It has been a true pleasure also with Head of "Functional Proteomics", Frankfurt, Dr. Ilka Witig and Head of "Mass Spectrometry" department, Frankfurt, Dr. Florian Richter for not just being expertise help in mass spectrometry but also provided valuable scientific inputs during the Ph.D.

To my beloved parents (Shamsher Singh and Sukhvinderjit Kaur) and my dearest sister (Damanjit Kaur), I am forever grateful for providing everything an individual could ever need (especially unconditional love and care). Education was never forced upon me as a youth, and I believe it is for this reason that I learned to truly embrace education. My Mother belief on faith, let me also grow from childhood with strong faith, which taught me how to be unshakable and love everyone unconditionally.

Index

Members of the thesis committee	i
Affidavit	ii
Acknowledgement	iii
Index	v
Abbreviations	viii
List of figures	xii
List of tables	xiv
Abstract	xv
1 Introduction	1
1.1 Oxidative stress	1
1.1.1 Sources of ROS and their role in the heart	2
1.2 Redox-nano switches – Cysteine residues	3
1.2.1 Reversible thiol modifications	5
1.2.1.1 Disulfide bridges	5
1.2.1.2 S-glutathionylation.....	5
1.2.1.3 S-sulfenylation	6
1.2.2 Irreversible thiol modifications.....	6
1.2.2.1 Sulfinic and sulfonic acid	6
1.3 Mass spectrometry	6
1.3.1 General strategies for peptide and disulfide bridge identification.....	8
1.4 The cardiac β-adrenergic signaling pathway	10
1.5 Serine/threonine phosphatases	12
1.5.1 Protein phosphatase 1 (PP-1)	12
1.5.2 Predicted oxidative modifications of PP-1.....	13
1.6 ER stress and the unfold protein response	15
1.6.1 ER-transmembrane proteins (IRE-1, PERK and ATF6).....	16
1.7 Connective tissue growth factor	17
1.7.1 Structural and functional properties of CTGF.....	18
1.7.2 Functional aspect of CTGF in heart diseases	19
2 Aim of the study	21
3 Materials & Methods	22
3.1 Materials	22
3.1.1 Antibodies.....	22
3.1.2 Buffers and solution	23
3.1.3 Chemicals and reagents.....	27
3.1.4 Kits	29
3.1.5 Cells	29
3.1.6 Primers and recombinant proteins.....	29
3.1.7 Laboratory instrument, general material and software	30
3.2 Methods	33
3.2.1 Cell culture methods.....	33
3.2.1.1 Preparation of cardiomyocytes from neonatal rats.....	33
3.2.1.2 Immunofluorescence of NRCM cells.....	35
3.2.1.3 Live cell imaging	35

3.2.1.4	Gene knockdown via siRNA transfection	36
3.2.2	Protein biochemical methods.....	36
3.2.2.1	Preparation of samples for western blotting.....	36
3.2.2.2	Protein quantification of samples via Bradford assay.....	37
3.2.2.3	Protein separation by SDS-polyacrylamide gel electrophoresis (SDS-PAGE) and detection by immunoblot	37
3.2.2.4	BIAM labeling assay	37
3.2.2.5	Phosphatase activity assay.....	38
3.2.3	Molecular biological methods	40
3.2.3.1	RNA isolation.....	40
3.2.3.2	cDNA synthesis.....	40
3.2.3.3	Quantitative real-time polymerase chain reaction (qRT-PCR)	40
3.2.4	Analytical methods	41
3.2.4.1	Differentiation of disulfide bridges assisted by protein structural analysis with Pymol.....	41
3.2.4.2	Performing the oxidative stress experiment and sample preparations for the identification of various PTMs in PP-1	42
3.2.4.3	Peptide purification via stage tips.....	42
3.2.4.4	LC-MS/MS analysis.....	43
3.2.4.5	Data analysis with Peaks 7.0 software	44
3.2.5	Statistical analysis.....	47
4	Results.....	48
4.1	Physiological effect of redox regulation in cardiac myocytes	48
4.2	Redox regulation of PP-1 in the heart.....	49
4.2.1	Importance of PP-1 in physiological functioning of NRCM.....	49
4.2.1.1	Investigation of phosphatase activity in human heart samples, NRCM, and whole heart mouse tissue	49
4.2.1.2	Impact of oxidative stress on phosphatase activity in NRCM and rPP-1	51
4.2.1.3	Impact of oxidative stress on cross talk between PKA and PP-1 signaling pathways	52
4.2.2	Identification of redox-sensitive Cys in PP-1	54
4.2.2.1	Investigating the disulfide bridges in phosphatases via immunoblotting.....	54
4.2.2.2	Analysis of disulfide bridges from bioinformatics tools in PP-1	57
4.2.3	Analysis via Mass Spectrometry	60
4.2.3.1	Investigating the PTMs in GST-tagged PP-1	60
4.2.3.2	Investigating PTMs in His-tagged PP-1.....	71
4.2.3.3	Oxidation of other amino acids in the vicinity of Mn ²⁺ ion in GST / His-tagged PP-1	74
4.3	Regulation of CTGF under stress conditions in cardiomyocytes	76
4.3.1	Expression of CTGF in physiological functioning of the heart	76
4.3.2	Influence of oxidative and ER stress on CTGF expression in NRCM	76
4.3.3	Impact of heat shock response and chaperone/heat shock protein on CTGF expression in NRCM.....	80
4.3.4	Impact of pH, MG132 and BFA on CTGF expression in NRCM.....	81
4.3.5	Impact of siRNA-CTGF knockdown on NRCM	82
5	Discussion.....	85
5.1	H₂O₂ influences the movement and morphology of cardiac cells	85
5.2	Oxidative stress influences cardiac β-adrenergic signaling pathway and PP-1 activity ...	87
5.3	Identification of redox-sensitive Cysteine residues in PP-1 via immunoblotting	89
5.4	Known oxidative state of Cysteine in PP-1.....	90
5.5	Impact of redox stress on PP-1 detected by mass spectroscopy.....	91
5.5.1	Redox-response of GST-tagged PP-1 involves glutathionylation of Cys: 140, 202 and 245 91	
5.5.2	Mn ²⁺ in external buffer plays a protective role for Cysteine oxidation	92
5.5.3	Network of disulfide bridges might play a protective role in maintenance of GST-tagged PP-1 activity under redox-stress	93

5.5.4	Redox response of His-tagged PP-1 involves sulfone formation	96
5.5.5	Do Histidine residues cage the dinuclear Mn ²⁺ ions to shield them from Cysteine residues?.....	97
5.5.6	Disulfide bridges determination in PP-1 using predictive computational methods and its correlation with mass spectrometry data	98
5.6	Proposed mechanism for protection of PP-1 from irreversible loss of activity	99
5.7	Clinical importance of redox-modified PP-1	100
5.8	Regulation of CTGF in response to ER stress	101
5.8.1	No evidence for the impact of pH, MG132 and BFA on CTGF expression in NRCM	103
5.8.2	Knockdown of CTGF affects ER stress markers in NRCM.....	103
5.9	Role of secretory cells with respect to ER stress	105
5.10	Higher expression of CTGF in the end stage heart failure.....	105
6	Appendix	107
6.1	Spectrum covered by MS	107
6.2	Summary of all disulfide bridges	113
7	References.....	128
8	Curriculum vitae	141

Abbreviations

α	alpha
Å	Ångström
Asp	aspartic acid
Asn	asparagine
Arg/R	arginine
ATF6	activating transcription factor 6
ATF4	activating transcription factor 4
APS	Ammonium persulfate
AMC	7-Amino-4-methylcoumarin
ABC	ammonium bicarbonate
β	beta
BiP	binding protein
BrdU	5'-bromo-2'-deoxyuridine
BFA	Brefeldin A
BPS	bottom precoll solution
CBFHH	Calcium- and bicarbonate- free Hanks with HEPES
cMyBP-C	cardiac myosin binding protein-C
CVD	cardiovascular disease
CTGF	connective tissue growth factor
°C	degree Celsius
cDNA	complementary DNA
CO ₂	carbon dioxide
CHOP	C/EBP homologous protein
cAMP	cyclic adenosine monophosphate
Ca ²⁺	calcium
Cys	cysteine
CT	cysteine knot
CR	cysteine-rich
CM	cardiomyocyte medium
DAPI	4',6-diamidino-2-phenylindole
DTT	Dithiothreitol
DMSO	dimethylsulfoxide
SS	disulfide
DNA	deoxyribonucleic acid
DiFMUP	6,8-difluoro-4-methylumbelliferyl phosphate
ER	endoplasmic reticulum
EBM-2	endothelial basal medium-2
e.g.	exempli gratia (for example)
EGM-2	endothelial growth medium-2
ECM	extracellular matrix
EDTA	ethylenediamine-tetraacetic acid

ECC	excitation-contraction coupling
ESI	electrospray ionization
eIF2 α	eukaryotic translation initiation factor 2 α
ESI	Electrospray ionization
et al.	et altera
FBS	fetal bovine serum
F-actin	filamentous actin
FITC	fluorescein thioisocyanate
g	gram
gDNA	genomic DNA
His	histidine
HCl	hydrochloric acid
hEGF	human epidermal growth factor
hFGF	human fibroblast growth factor
h	hour
H ₂ O ₂	hydrogen peroxide
•OH	hydroxyl radical
HUVEC	human umbilical vein endothelial cells
HRP	Horseradish peroxidase
HEPES	4-(2-hydroxyethyl)-1-piperazineethanesulfonic acid
HPLC	high-performance liquid chromatography
I-1	inhibitor-1
I/R	ischemia/reperfusion
IRE-1	inositol-requiring enzyme-1
IGFBP	insulin-like growth factor binding protein
IF	immunofluorescence
IAA	iodoacetamide
i.d	internal diameter
l	liter
LTCC	L-type Ca ²⁺ channels
LC	liquid chromatography
Lys/K	lysine
kDa	kilo dalton
MALDI	matrix-assisted laser desorption/ionization
MS	mass spectrometry
m/z	mass/charge
μ	micro
min	minute
M	molarmolar
mRNA	messenger RNA

mM	millimolar
μ	micro
μl	microliter
ms	milliseconds
n	nano
NOX	NADPH oxidases
NOS	nitric oxide synthases
NCM	non-cardiomyocyte medium
NRCM	neonatal rat cardiac cardiomyocytes
OM	opti-MEM
O ₂	oxygen
PLB	phospholamban
PKA	protein kinase A
pH	negative logarithm of the H ⁺ -ions
PP	Protein phosphatase
PP-1	protein phosphatase type-1
PP-2	protein phosphatase type-2
PTP	protein tyrosine phosphatase
PBS	phosphate buffered saline
PCR	polymerase chain reaction
PERK	protein kinase R-like ER kinase
PTM	post-translational modifications
PFA	paraformaldehyde
PDGF	platelet-derived growth factor
%	percent
P/S	penicillin/streptomycin
PBS	phosphate-buffered saline
ppm	parts per million
Q	quadrupole
ROS	reactive oxygen species
qRT-PCR	quantitative reverse transcription polymerase chain reaction
RNA	ribonucleic acid
RNase	ribonuclease
RT	room temperature
RyR2	ryanodine receptors
R110	bisamide rhodamine 110 peptide
rpm	rounds per minute
rPP-1	recombinant protein phosphatase type-1
SR	sarcoplasmic reticulum
SERCA2a	sarcoplasmic reticulum Ca-ATPase
Ser	serine
S.D.	standard deviation

sec	second
siRNA	small interfering RNA
O ₂ ^{•-}	superoxide
SOD	superoxide dismutases
SDS	sodium dodecyl sulfate
SAD-PAGE	sodium dodecyl sulfate-polyacrylamide gel electrophoresis
TEMED	tetramethylethylenediamine
TGN	thapsigargin
Thr	threonine
ToF	time of flight
TnI	troponin I
TSP1	thrombospondin motif
TGF-β	transforming growth factor-β
TPS	top precoll solution
UPR	unfolded protein response
vWF-C	von-Willebrand factor type C
v/v	volume by volume
W.B	western blot
H ₂ O	water
XO	xanthine oxidase
XBP-1	X-box binding protein 1 mRNA

List of figures

Figure 1 Chemical reactions involved in generating ROS	1
Figure 2 Sources of ROS in cardiomyocytes.....	3
Figure 3 Cys structure	4
Figure 4 Redox modification pathway of Cys by H ₂ O ₂	4
Figure 5 An overview of electrospray ionization	7
Figure 6 An overview of the generation of MS and MS/MS spectra used for the identification of peptides.....	8
Figure 7 A general strategy explaining the identification of peptide	9
Figure 8 Recent advances in redox regulation of β–adrenergic signaling pathway in cardiac myocytes	11
Figure 9 Sequence and detail structure analysis of PP-1 (PDB id: 4MOV).....	14
Figure 10 ER stress signaling pathways in eukaryotic cells.....	17
Figure 11 Schematic structure of CTGF protein.....	19
Figure 12 Percoll gradient showing three layers of fibroblast, cardiomyocytes and erythrocyte	34
Figure 13 Timeline for siRNA transfection.....	36
Figure 14 General assay format for BIAM labeling assay	38
Figure 15 Chromogenic reactions in the EnzChek Phosphatase Assay Kit	39
Figure 16 Scheme is showing generation of permuted Cys-peptide database	45
Figure 17 A robust strategy behind the identification of SS bridges.....	46
Figure 18 Analysis of NRCM relaxation-contraction ratio exposed to oxidative stress	49
Figure 19 Phosphatase activities in human NF, Hy and HF hearts	49
Figure 20 Phosphatase activities in NRCM and whole heart tissue of mouse	50
Figure 21 Phosphatase activity in rPP-1	51
Figure 22 Phosphatase activities in NRCM.....	52
Figure 23 Immunoblot and quantification of concentration dependency of H ₂ O ₂ mediated phospho I-1 expression in NRCM.....	52
Figure 24 Putative mechanism of PKA activation and PP-1 inactivation by H ₂ O ₂	53
Figure 25 Effect of increasing concentration of diamide and H ₂ O ₂ (15 min) on NRCMs under non-reducing and reducing conditions in PKA.....	54
Figure 26 Effect of increasing concentrations of diamide (15 min) on NRCMs under non- reducing condition in probed with anti-PP-1 (catalytic subunit)	55
Figure 27 Effect of increasing concentration of diamide (15 min) on NRCMs under non- reducing conditions probed with anti-PP-2A.....	56
Figure 28 Cell lysates from NRCM analyzed under non-reducing and reducing conditions probed with anti-SERCA2a, anti-PP-1 (catalytic subunit) and anti-PP-2A	56
Figure 29 Identification of oxidized proteins due to redox active Cys.....	57
Figure 30 Graphical representation of S-glutathionylation sites analyzed by dbGSH database in PP-1	60
Figure 31 In-vitro-assays for MS readout using the GST-tagged PP-1	64
Figure 32 Spectra and positions of the glutathione modified Cys ¹⁴⁰	64
Figure 33 Quantification of the amount of free, persulfide/disulfide and sulfonic acid - Cys residues by spectral counting	66
Figure 34 Disulfide-peptide conjugates (spectrum and fragment table).....	69
Figure 35 Spectrum and ion table for the inter-SS bridges with Cys ¹²⁷	70

Figure 36 In-vitro-assays for MS readout using the His-tagged PP-1	72
Figure 37 Cys ³⁹ and Cys ¹⁵⁵ Cys ¹⁵⁸ -SS-peptide conjugate (spectrum and fragment table) is the sole SS link induced in the His-tagged protein	73
Figure 38 Spectra and ion table of oxidized Histidine (His ²⁴⁸ /His ¹²⁵) caging around the dinuclear Mn ²⁺ ions	75
Figure 39 Spectra and ion table of oxidized Tyrosine (Tyr ²⁷²) close by Cys ²⁷³	75
Figure 40 Higher protein expression of CTGF in end-stage human heart failure.....	76
Figure 41 Protein expression of CTGF in cardiomyocytes exposed to H ₂ O ₂	77
Figure 42 Protein expression of CTGF in cardiomyocytes exposed to DTT and diamide....	78
Figure 43 Protein expression of CTGF in NRCM exposed to TGN	79
Figure 44 CTGF protein expression of NRCMs exposed to Tm.....	80
Figure 45 Effect of heat shock on the expression of CTGF.....	81
Figure 46 CTGF expression of NRCM exposed to pH, MG132 and BFA	81
Figure 47 Knockdown of CTGF in NRCM alters ATF6 localization	82
Figure 48 Partial knockdown of CTGF in NRCM alters the various ER stress markers at protein level.....	83
Figure 49 Knockdown of CTGF in NRCM shows XBP1 splicing	83
Figure 50 Knockdown of CTGF in NRCM does not alter the transcription of various ER stress markers	84
Figure 51 The X-ray structure of PP-1γ (PDB id: 4UT3) in its oxidized state	91
Figure 52 Proximities of several Cys residues forming a network.....	96
Figure 53 His caging Mn ²⁺ and Tyr ²⁷² arrangement correlated to Cys network	97
Figure 54 A proposed mechanism showing the vital role of glutathione, His, Cys and Mn ²⁺ ions in the activity of PP-1	99
Figure 55 Cys redox sensor in PP-1.....	100
Figure 56 Summary of all the effectors on CTGF.....	106
Append 1 Peak results indicating the Cys Peptides that were not detected with red boxes	107
Append 2 The new scrambled PP-1 sequence is displayed with the potential disulfide peptides boxed in red.....	111
Append 3 Spectra and positions of the glutathione modified Cys ²⁰² and Cys ²⁴⁵	112
Append 4 All disulfide-peptide conjugates are shown in their spectrum and fragment table	127

List of tables

Table 1 Primary antibodies.....	22
Table 2 Horseradish peroxidase (HRP)-conjugated secondary antibodies.....	23
Table 3 Fluorophore-conjugated secondary antibodies for immunofluorescence	23
Table 4 Composition of the used buffers, solutions, and media.....	23
Table 5 List of chemical and reagents.....	27
Table 6 List of kits.....	29
Table 7 List of bacterial and mammalian cells.....	29
Table 8 List of primers used for qPCR and RT-PCR.....	29
Table 9 List of recombinant protein	30
Table 10 List of instruments	30
Table 11 List of general material	31
Table 12 List of software	32
Table 13 Reagent preparation.....	33
Table 14 General assay format for 96 well plates used in Promega PP assay.....	39
Table 15 Master Mix for qRT-PCR	41
Table 16 qPCR Program	41
Table 17 Analysis of pKa of PP-1A (PDB id: 4MOV) by PROPKA 3.1.....	58
Table 18 Analysis of oxidation status of all Cys by COPA	58
Table 19 Analysis of disulfide oxidation state prediction of PP-1A by DiANNA 1.1 web	59
Table 20 Cross-reactivity scheme for disulfide linkages in GST-tagged PP-1A.....	68
Table 21 Distance measurements [Å] of the Cys residues with each other and Mn ²⁺	70
Table 22 Possible Cys residues that can undergo sulfonation in His-tagged PP-1.....	74

Abstract

Heart failure is one of the most common causes for morbidity and hospitalization in the western civilization. The prognosis is still poor and new therapies are needed. For decades, variations in phosphorylation and redox status of cardiac proteins have been characterized in different heart diseases to identify new drug targets. Both abnormal phosphorylation-levels of cardiac key proteins and elevated reactive oxygen species (ROS) production were found to contribute to contractile dysfunction and fibrosis in failing hearts.

In this context type-1 phosphatase (PP-1) was demonstrated to be a principal contributor to Ser/Thr PP activity (~45%) and has been implicated particularly in the regulation of basal cardiac contractility and in the responses to β -adrenergic stimulation (El-Armouche et al, 2009; Yin et al, 2009). Up until now redox sensitivity of cardiac PP-1 has not been addressed, despite well-known perturbations in PP-1 regulation in failing hearts. Therefore, one goal of this project was to identify the underlying mechanisms of PP-1 oxidation and to test whether oxidized PP-1 contributes to the pathophysiology of abnormal protein phosphorylation and myocardial dysfunction in failing myocardium. Immunoblotting revealed that the phosphorylation status of classical PP-1 downstream target proteins, such as phospholamban (PLB) and cardiac myosin binding protein-C (cMyBP-C) were differentially affected by H_2O_2 , indicating a complex layer of regulation of both redox sensitive kinases and phosphatases. Consistently, the phosphorylation status of protein phosphatase inhibitor-1 (I-1), a crosstalk protein between protein kinase A and PP-1 signaling, showed a bell-shaped phosphorylation response with a maximal peak at 100 μM . For the first time we demonstrated with mass spectrometry that PP-1 shows various post-translational modifications on the incubation with H_2O_2 as one of the majorly available intracellular reactive oxygen species. In summary, for PP-1 a mechanism is purposed which states that PP-1's cysteine residues in the presence of H_2O_2 , first form sulfenic acid with a fast response to protect higher oxidations by glutathione that enables a self-protective mechanism by forming transient inter-disulfide bridges. Intra-protein disulfide bridges with Cys¹²⁷ to form a dimer formation of PP-1 at 70 kDa might also play a role for the activity of the protein. In contrast, in the absence of glutathione, direct formation of sulfonic acid would make the protein irreversible inactive. The discovery of reversibility of PP-1 in the presence of the reducing agent (TCEP) after inactivation upon H_2O_2 treatment clearly shows that disulfide bridges are playing a crucial role in maintaining the activity of PP-1.

In addition, to the changed redox status of cytosolic proteins like PP-1 in diseased cardiomyocytes, an impairment of the redox balance in organelles was described. With this respect the occurring endoplasmic reticulum (ER) stress is of high interest as it could influence transmembrane and secreted proteins. Therefore, the redox- and ER stress-dependent regulation of the secreted connective tissue growth factor (CTGF) was investigated. CTGF is a cysteine-rich protein highly expressed during embryonic development and in fibrotic diseases, including cardiac fibrosis (Winter et al., 2008; Lok et al., 2015). Due to its high content in cysteines and intramolecular disulfide bonds, we hypothesize that ER stress modulates the oxidation status of CTGF, which in turn affects its activity and structure in cardiomyocytes. Moreover, it was unknown whether ER stress can be modulated by the expression of cysteine-rich proteins like CTGF. We first analyzed CTGF expression in human diseased heart samples and were able to show an up-regulation in

ischemic cardiomyopathy (ICM), which is associated with increased ER stress and changes in redox signaling. To further link the regulation of CTGF to these processes, isolated neonatal rat cardiomyocytes (NRCMs) were treated with pharmacological ER (DTT, thapsigargin) and oxidative (H_2O_2) stress inducers. DTT altered the molecular weight of CTGF in non-reducing immunoblots, suggesting conformational changes in the protein structure. In contrast, thapsigargin increased intracellular CTGF content, reaching the maximum after 6 hours of exposure to NRCMs. H_2O_2 had only a modest effect increasing intracellular CTGF within minutes. To further analyze the crosstalk of ER stress and CTGF regulation, CTGF expression was reduced with a specific siRNA in NRCMs, which led to a decrease in the expression of ER stress markers like PDI, BIP and IRE1- α . This data argues for an interconnection of CTGF and ER stress, as ER stress modulates CTGF and *vice versa*, CTGF expression modulates proteins of the ER stress cascade.

In summary, this thesis gives mechanistic insight in the redox-dependent regulation of PP1 and CTGF, which represent not only the cytosolic and secretory compartments of cardiomyocytes, respectively, but also the two major pathomechanisms contractile dysfunction and fibrosis in heart disease.

Key words: cysteine, disulfide bridges, heart failure, redox, cardiomyocytes, PP-1, CTGF

1 Introduction

1.1 Oxidative stress

During normal cellular aerobic function reactive oxygen species (ROS) such as hydrogen peroxide (H_2O_2), hydroxyl radical ($\cdot\text{OH}$) and superoxide ($\text{O}_2^{\cdot-}$) are produced in cells which react at both cellular and tissue levels (Griendling and FitzGerald, 2003). Intracellular ROS are formed from a single electron reduction of oxygen (O_2), which leads to the formation of radical $\text{O}_2^{\cdot-}$. In the presence of superoxide dismutase (SOD) enzymes, two molecules of $\text{O}_2^{\cdot-}$ can be converted to one molecule of H_2O_2 and one molecule of water (H_2O). In addition, by accepting an electron from free Fe^{2+} ions (Fenton reaction), H_2O_2 is converted to $\cdot\text{OH}$. With the potential presence of glutathione peroxidases, peroxiredoxins or catalase, H_2O_2 can be reduced to water. H_2O_2 can also potentiate the modification of redox-sensitive Cys residues to alter cellular signaling (Sullivan and Chandel, 2014; Figure 1). Further details about Cys redox modifications are discussed in Section 1.2.

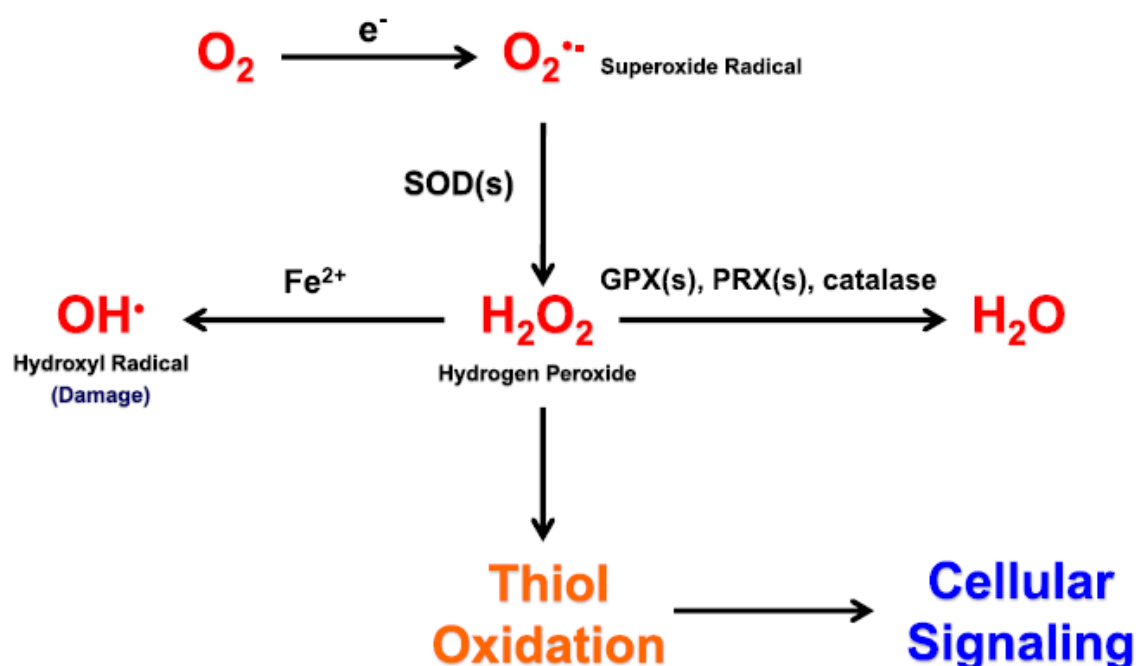


Figure 1 | Chemical reactions involved in generating ROS. Signaling pathway showing the formation of ROS species within the cell (Sullivan and Chandel, 2014).

Classically, oxidants have been considered as harmful elements mediating pathology. Oxidants are counterbalanced by antioxidants to maintain homeostatic levels of ROS. The most well-known antioxidant molecules are GSH, ubiquinol, thioredoxin, lipoic acid, beta carotene, retinol (vitamin A), ascorbic acid (vitamin C) and alpha-tocopherol (vitamin E)

(Charles and Eaton, 2008). Whenever oxidants and antioxidants are imbalanced, leads to an increase in ROS levels, a condition which is called oxidative stress (Sies, 1997).

On the other hand, redox signaling involves O_2 or O_2 -derived ROS to alter the cardiac function at the post-translational level. From a clinical perspective, oxidative stress has been associated with cardiac disease development (e.g., heart failure) with antioxidants in clinical trials showing little or no impact on rescuing the heart from diseases (Johnston et al., 2015).

1.1.1 Sources of ROS and their role in the heart

The primary sources of ROS in cardiac metabolism are known to be mitochondria, endoplasmic reticulum (ER), nicotinamide adenine dinucleotide phosphate (NADPH) oxidases (NOX), nitric oxide synthases (NOS), cytochrome P450 oxidases and xanthine oxidase (XO) (Sag et al., 2014; Figure 2). Electron leak from complexes I and III are the most well characterized sources of mitochondrial ROS production and have a significant impact on both disease pathogenesis and redox signaling transduction in the cardiovascular system (Chen and Zweier, 2014). However, recent studies suggest excessive mitochondrial ROS production in apoptosis, which leads to an abrupt remodeling of the heart (van Empel, Vanessa P M et al., 2005; Matsushima et al., 2006). Within the human end-stage of heart failure and in various heart failure models such as myocardial infarction and pressure overload-induced myocardial hypertrophy, XO has been found to be highly expressed (Berry and Hare, 2004; Maytin et al., 2004; Stull et al., 2004). In contrast, human clinical studies suggested that XO inhibitor treatment is not related to increased or decreased risk of cardiovascular diseases (Seoyoung C. Kim et al., 2015).

All seven isoforms of NADPH oxidase enzymes contain a core subunit NOX1-5 and DUOX1-2. NOX2 and NOX4 are expressed mainly in endothelial cells, cardiomyocytes, and fibroblasts. Studies of NOX2 knockout mice suggest that during pressure overload, ROS produced by NOX2 can affect the development of interstitial fibrosis and cardiac contractile dysfunction, but it is not shown to be important for the development of cardiac hypertrophy (Grieve et al., 2006). In eukaryotic cells, ER provides a typical oxidation environment for protein folding and disulfide bridge formation. Over time, as unfolded proteins are accumulated in the ER, leading to ER stress in the cell, an increase in ROS species can be observed due to a decrease in antioxidant levels (Rahal et al., 2014). More information related to ER-associated ROS will be discussed in Section 1.6.

For the physiological functioning and signaling of the cardiac cells, high amounts of endogenous H_2O_2 lead to various diseases, whereas lower levels are essential. Within

diseased tissues H_2O_2 concentrations of up to $100 \mu\text{M}$ have been measured (Burgoyne et al., 2007; Hartzell, 2007). However, $1\text{-}15 \mu\text{M}$ of H_2O_2 appears to be the peak level in normal physiological contexts. During scientific experimentation, intracellular concentrations of $1\text{-}15\%$ of externally applied H_2O_2 have been reported. External incubation with $10\text{-}10^3 \mu\text{M}$ H_2O_2 could largely mimic the discharge of H_2O_2 endogenously by growth factors and therefore such concentrations of exogenous H_2O_2 are physiologically relevant (Schroder and Eaton, 2008).

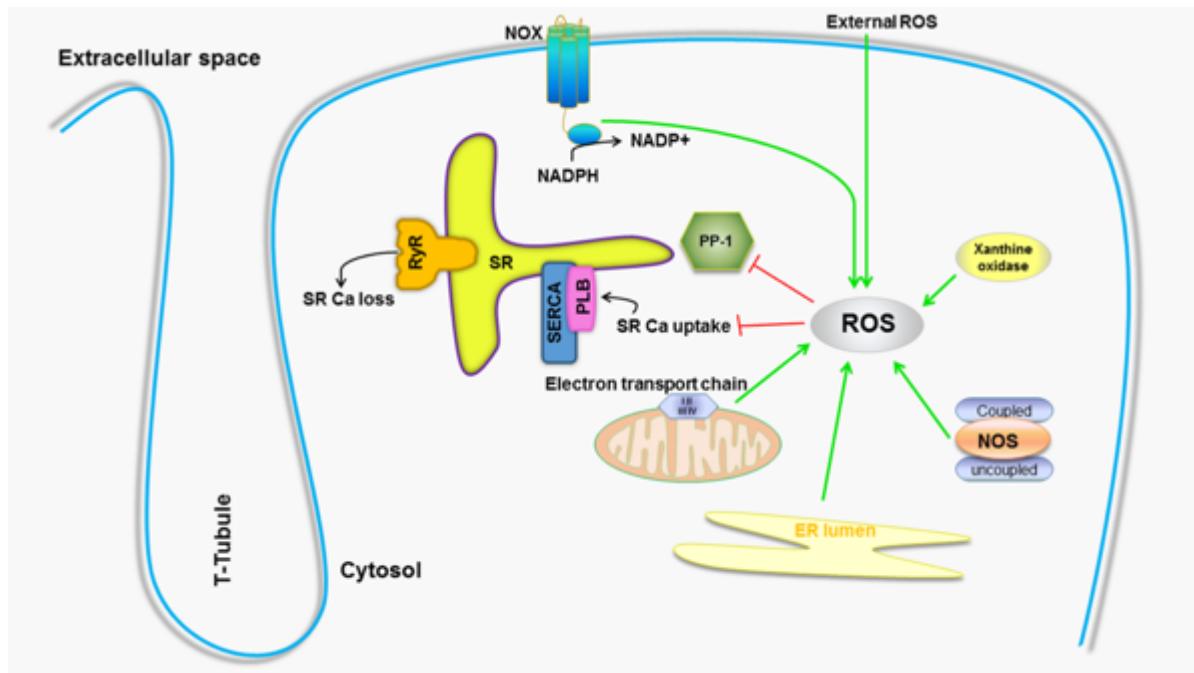


Figure 2 | Sources of ROS in cardiomyocytes. Under both baseline and pathophysiological conditions, ROS is produced by various sources in cardiac tissue. PP-1 is inhibited by ROS, playing an important role in calcium and ROS signaling within the cell (adapted from Erickson et al., 2011).

Previous clinical experiments using antioxidants have been largely disappointing as despite promising pre-clinical data in animal models, anti-oxidants failed to show any protective effects in large scale clinical trials (Steinhubl, 2008). These unanticipated results have been largely attributed to the unspecific nature of antioxidants. In such cases, exogenous application of anti-oxidants would also disrupt the physiological processes that oxidants contribute to. This therefore permits further research on the pathological and physiological roles of oxidants in order to develop specific treatments to target these mechanisms.

1.2 Redox-nano switches – Cysteine residues

Cysteine (Cys) is a molecule that consists of sulfur, carbon, nitrogen and hydrogen. In general, due to the presence of the thiol group, Cys side chains are known to be a highly potent nucleophile under physiological conditions (Figure 3). Within the thiol group, the

average pKa of Cys is 8.2 (Tajc et al., 2004). Thiol group reactivity is linked with its pKa value (Shaked et al., 1980).

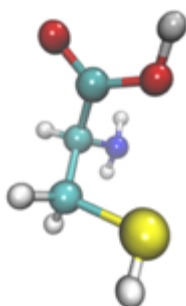


Figure 3 | Cys structure. Cartoon representation of the Cys molecule showing sulfur (yellow), carbon (cyan), oxygen (red), nitrogen (blue) and hydrogen (gray-white).

Thiol acidity could be increased by three to four-fold, if the thiol groups are in proximity to positively charged residues, i.e. lysine or arginine (Copley et al., 2004). Interactions with distinct residues and metal ions can also lead to stabilization of the thiolate form. Within the ER (a highly oxidizing compartment), Cys residues have a tendency to form disulfide bridges under physiological conditions. Whereas in the cytoplasm (a highly reducing environment), Cys residues are in the free thiol state.

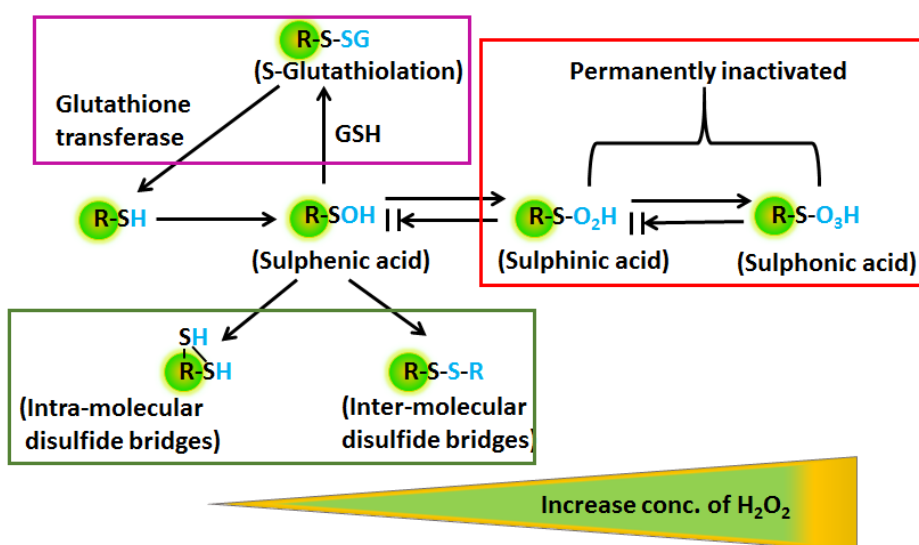


Figure 4 | Redox modification pathway of Cys by H_2O_2 . The catalytic thiol groups, representing oxidative modification by H_2O_2 : reversible modification (sulfenic acid, disulfide, and glutathionylation) and irreversible modification (sulfinic acid and sulfonic acid) (adapted from Meng C.T. et al., 2004).

When Cys is oxidized, kinases and phosphatases are activated and inactivated, respectively (Denu and Tanner, 1998; Brennan et al., 2006). Cys thiol groups are highly reactive and can trigger many biological pathways and act as a primary site for post translational modifications (PTM). Thiol modifications can be reversible, such as the formation of sulfenic acid (R-SOH), inter or intra-disulfide bonds and glutathionylation (R-S-SG) (Lim et al., 2001), or irreversible,

such as the formation of sulfinic acid (R-S-O₂H) and sulfonic acid (R-S-O₃H) (for review see Murray and van Eyk, 2012; Figure 4).

1.2.1 Reversible thiol modifications

1.2.1.1 Disulfide bridges

At the post-translational level, only Cys residues can undergo oxidation, which leads to the formation of disulfide bridges, which are particularly enhanced in secreted and membranous proteins. Disulfide bridges help to stabilize the protein's secondary structure through stronger covalent bonds (and not ionic or H-bridge formation) between two parts of the protein, or by linking various polypeptide chains. Normally proteins with only a single disulfide are available, but due to the presence of multiple Cys residues within one protein, formations of many disulfide bridges are also possible. Disulfide bridge formation within the cellular environment is also dependent on the oxidants present in the various cell compartments. Disulfide bridge formations are favorable within the lumen of ER due to a suitable pH (~7.2) for redox reactions of a thiol group (Kim et al., 1998). On the contrary, in the cytosol glutathione is the primary thiol-containing molecule, which prevents the formation of disulfide bridges. Within the cytosol of a resting cell, glutathione is present in either its reduced form (GSH) or oxidized state (GSSG) in the ratio 100:1; a ratio which has been demonstrated to reduce to 10:1 or even 1:1 in various models of oxidative stress (Chai et al., 1994).

Disulfide bridges can be of two types: intra, and inter - disulfide bridges. Some proteins such as thioredoxin, glutaredoxin, and protein disulfide isomerases contain CXXC motifs, which are a signature style of all proteins that form intra-disulfide bridges (Go et al., 2015). In addition, kinases are also well known to be redox regulated. It has been established that serine/threonine kinases PKG-1 α (Burgoyne, JR et al., 2007) and ATM (Guo et al., 2010) activation mechanism is dependent on the formation of intermolecular disulfide bridges between homodimers.

1.2.1.2 S-glutathionylation

One of the most common PTMs inside the cells is S-glutathionylation. When a protein undergoes the oxidation process, first the most unstable form of thiol-oxidation sulfenation happens, which is then resolved by a Cys GSH. This reaction stops further oxidation of the protein to form an irreversible form of thiol oxidation (sulfinic and sulfonic acid). The resulting product of the reaction is S-glutathionylation (R-S-SG), which can be reversed to the original state of the protein (R-SH), in the presence of glutathione transferase (GST). $GSSG \leftrightarrow$

GSH transfer to Cys residues is primarily dependent on the action of GST. This in return is mainly dependent on continued yield of GSH from the synthetic enzymes, such as glutathione synthetase and gamma-glutamylcysteine. This further helps in the removal of conjugates of GSH as a defined transporter. The principle role of GST is detoxification of xenobiotics by catalyzing the nucleophilic attack by GSH, which is possible with electrophilic carbon, nitrogen or sulfur atoms. This prevents any communication with crucial nucleic acids and cellular proteins (Ferre and Clote, 2005).

1.2.1.3 S-sulfenylation

When proteins are exposed to oxidants, sulfenic acid (R-SOH) is formed which can alter protein structure and hence protein activity. As this modification is highly unstable, the identification of this state remains challenging (Lo Conte and Carroll, 2013). It has been found that mainly protein tyrosine phosphatase (PTPs) are inactivated by H_2O_2 . Within the SH2 domain-containing PTPs (SHP-1 and SHP-2), two Cys residues form a stable disulfide bridge. This modification leads to an increase in catalytic pK_a value and hence a decrease in the activity of PTP protein (Chen et al., 2009).

1.2.2 Irreversible thiol modifications

1.2.2.1 Sulfinic and sulfonic acid

Two modifications of the thiol groups are considered to be permanently inactivated and irreversible: sulfinic (R-S-O₂H) and sulfonic (R-S-O₃H) acid. Recently, 181 R-S-O₂H/R-S-O₃H sites were recognized from rat myocardial tissue incubated with a physiological estimation of H_2O_2 (<100 μ M) or from ischemia/reperfusion (I/R) injury using the Langendorff perfusion. This study showed that I/R not only substantially increases both modified peptides from proteins involved in energy utilization and contractility, but also those engaged in oxidative damage and repair (Paulech et al., 2015).

1.3 Mass spectrometry

Mass spectrometry (MS) is an analytical technique mainly used to measure the molecular mass of a sample. It can also be used for more complex protein samples and structure analysis. The MS techniques is known to be very versatile due to the following attributes: (i) high sensitivity, (ii) detection of every molecule independent from its chemical nature, (iii) enabling of minor mass changes, e.g. alteration of one amino acid for another, and (iv) detection of PTMs with their exact modification site. The most common instruments in

biopharmaceutical MS are based on the matrix-assisted laser desorption/ionization (MALDI) and electrospray ionization (ESI) principle because they are available to large biomolecules. In principle, the liquid or gaseous sample first needs to be transferred from atmospheric pressure to the high vacuum regions and also from a non-charged molecule into the charged ion state. This is done by one of several ion sources available at front of the mass spectrometry unit. Then the particles pass through the mass analyzer, where they are separated according to their m/z ratio. At the end, they hit the detector plate that consumes the ions. Detection is enabled by the multiplication of a molecule in a secondary ion cascade, and this package of ions is recorded both the detector and by a PC framework. The PC shows the signals graphically as a mass spectrum: a two-dimensional plot of intensity versus m/z .

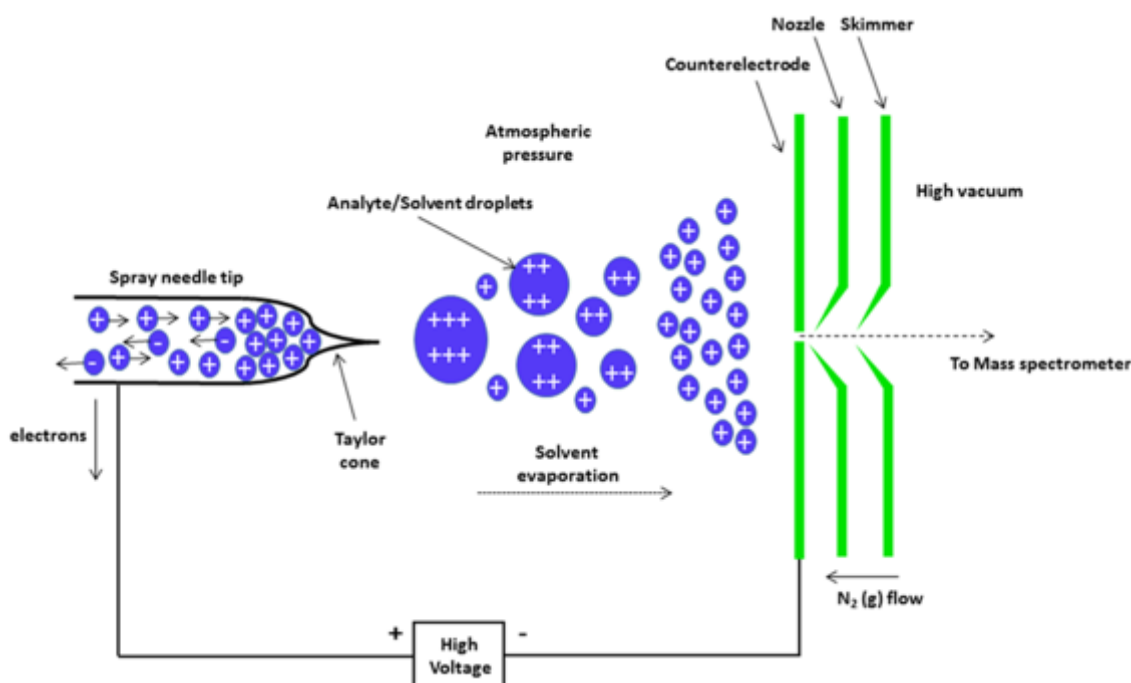


Figure 5 | An overview of electrospray ionization. ESI source produced a continuous stream of the sample solution, which is passed through quartz silica capillary, producing ions into multiple charge states that are trapped by MS.

Currently, most MS instrumentation is coupled with ESI, which has been established as one of the most important methods for small-scale chromatography coupling. A sample of interest is first brought into the tip of the conductive capillary, i.e. the ionization source of the MS. Then an electric field is established between the capillary and the mass spectrometer, which leads to the initial procurement of positive or negative charges. In ESI the molecules are present in solution and are then transformed into the gaseous state using high voltage. This process generates charged analyte/solvent droplets at the tip. Furthermore, atmospheric pressure reduces the size of the charged droplets and the solvent evaporates. Consequently,

droplets continue to contracting until the surface strain can no longer support the charge and the droplets are separated, and then analyzed by MS (for review see Yates et al., 2009; Figure 5).

1.3.1 General strategies for peptide and disulfide bridge identification

As discussed in Section 1.2, disulfide bridges formation is most common with secretory proteins, which could become one of the main targets in biopharmaceutical industry. Certainly, the PTMs in general, assume an essential role in the structural stabilization of the protein, and in the near future, it will be necessary to study the advancement of novel protein biopharmaceutical interventions (Sandra et al., 2014). Currently, detection of SS bridges or glutathionylation in proteins is difficult in MS analysis due to the high tendency for false-positive results. In MS-based disulfide mapping, the general rule is to produce and dissect fragments with a single disulfide bridge associating two peptides via proteolytic enzymatic digestion of the non-reduced protein. Further, it can then be recognized either by mass alone or by MS/MS sequencing. The predominantly used enzyme in proteomics is Trypsin, but in SS analysis it might be beneficial to digest at low pH, in such case Pepsin would be an ideal enzyme (Liu et al., 2014). Such cases result in the integration of an absence of enzymatic cleavage sites amongst Cys residues, and smaller disulfide bridges centers with firmly dispersed or even adjacent Cys residues (Goyder et al., 2013; Reinwarth et al., 2014).

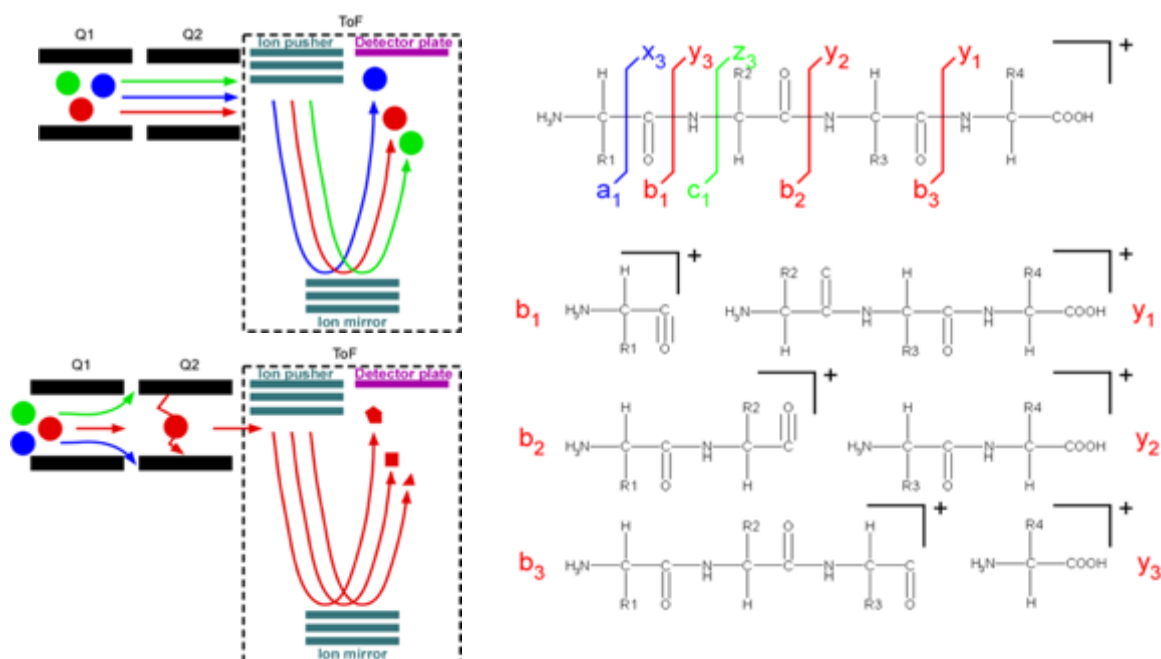


Figure 6 | An overview of the generation of MS and MS/MS spectra used for the identification of peptides. On the top left, the MS analysis of three different ions is shown. They bypass Q1 and Q2 and are separated in the ToF according to m/z . On the lower left, selection of one ion in Q1 and fragmentation in Q2 with subsequent detection in the ToF is shown. On the right hand, the

fragmentation pattern with the most typical ions of a short model peptide is represented (according to Biemann, 1988).

To understand the general strategy behind the unequivocal identification of a linear peptide, an example of a QToF instrument is explained (Figure 6). A QT of instruments consists of the following parts: (i) a selection Quadrupole (Q1), (ii) a fragmentation Quadrupole (Q2), and (iii) a Time of Flight (ToF) high-resolution mass analyzer. The latter can be interchanged with an Orbitrap which turns the instrument into the state of the art QExactive. When analyzing the intact mass of the peptides, the mixture transitions from Q1 to Q2, and is then separated according to its m/z in the ToF analyzer.

When the sequence or structural information of a peptide is required, the peptide is first selected in Q1, then fragmented in Q2 (by applying collision energy which is achieved by a lower vacuum value when inflating the cell with He or N₂ molecules), and the resulting fragments are separated according to their m/z in the ToF analyzer. Combined information on the intact mass and the sequence readout can be submitted to a database search for unequivocal identification of the peptide. Fragmentation of the peptide depends on the method and the gas used. Generally, the peptide breaks along the backbone exactly at the peptide bond, resulting in y-type (C-terminal) and b-type (N-terminal) ions. If using Trypsin as a proteolytic enzyme, the placement of a positive charge at the C-terminal Arginine (Arg/R) or Lysine (Lys/K) residue is visible, and another mobile proton is available for b-type ions.

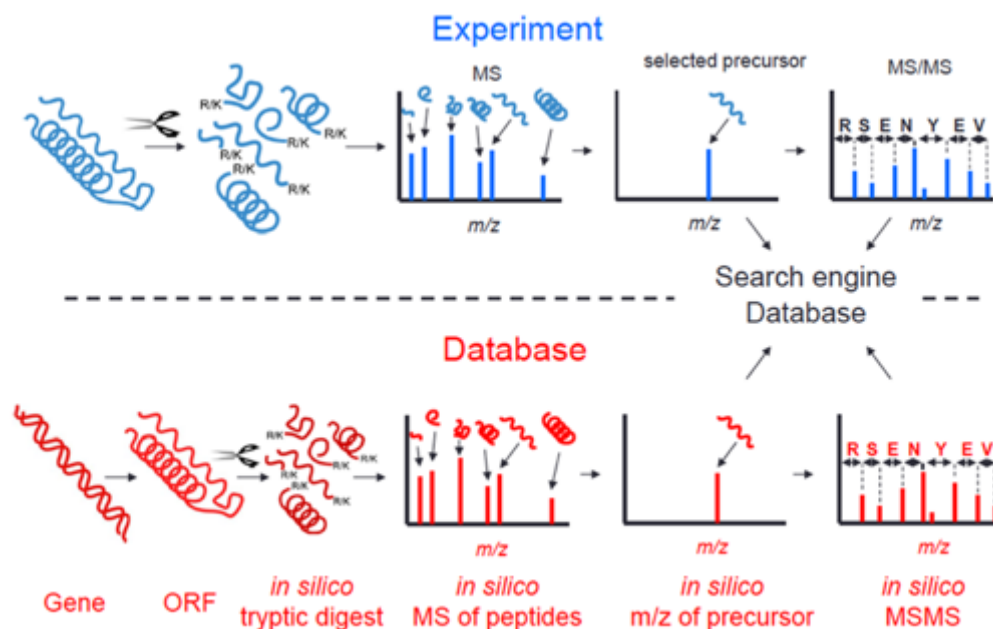


Figure 7 | A general strategy explaining the identification of peptide using MS/MS data. *In silico* generated MS/MS data from a complex database is compared with spectra obtained from the LC-MS/MS experiment. The blue side represents the real experiment, while the red side is an *in-silico* experiment performed by the search engine.

Identification of a peptide in a proteomics experiment is assisted with databases as shown in Figure 7. The intact protein is digested with a site-specific endoproteinase like Trypsin, leaving Arg/R or Lys/K residues at the C-terminus. These peptides are detected in the MS regime, one precursor ion (one peptide) is selected for fragmentation, and the sequence can be read out according to Figure 7.

Starting with a gene, the open reading frame (ORF) is in-silico transcribed, but modern proteome databases begin immediately with a curated database that contains only existing proteins. The proteins are in-silico digested and then an automated database search requires a spectrum comparison, which can be performed by two approaches: (1) One approach starts with comparing the intact mass of a peptide with all suitable intact masses from the *in-silico* digested database. Further spectrum searches are performed on a subset of corresponding peptide spectra. (2) The other approach starts with the determination of peptides sequences and searches them against a much smaller subset of possible precursor masses going along with it, which will greatly improve the confidence of peptide identification, particularly when PTMs are involved.

1.4 The cardiac β -adrenergic signaling pathway

Cardiovascular diseases (CVDs) are the primary cause of mortality worldwide, accounting for 17.3 million deaths per year, and mortalities are expected to increase to more than 23.6 million deaths per year by 2030. Even though the death rate from CVDs has fallen to 39% between 2001 and 2011, the concern and risk are high (Mozaffarian et al., 2015). Cardiac homeostasis is maintained by various post-translational modifications (PTMs), including phosphorylation, glycosylation, acetylation, hydroxylation, proteolytic cleavage as well as oxidative modifications. These altered PTMs can lead to heart failure, including contractile dysfunction and arrhythmias (Herren et al., 2013; Hoshino et al., 2014; Pryszyzhna and Eaton, 2015).

During physical activity or stress the sympathetic nervous system initiates a 'fight or flight' response. Within ventricular cardiomyocytes, norepinephrine and epinephrine act upon the β -adrenergic signaling system - activating adenylyl cyclase (AC) via stimulatory G proteins (Gs). This leads to an increase in cyclic adenosine monophosphate (cAMP), and hence activates protein kinase A (PKA) (Reuter H., 1983). Activated PKA further phosphorylates various pivotal proteins, such as ryanodine receptors (RyR2), phospholamban (PLB), troponin I (TnI), cardiac myosin binding protein-C (MyBP-C) and L-type calcium (Ca^{2+}) channels (LTCC). These aforementioned proteins regulate the excitation-contraction

coupling (ECC) cycle of the cardiomyocytes and hence the contraction of the heart (Bers, 2002; El-Armouche and Eschenhagen, 2009; Figure 8).

During ECC, Ca^{2+} plays an essential role in cardiac contraction by maintaining high cytosolic Ca^{2+} concentration to activate cross-bridge formation between myofilaments proteins, which in turn develops pressure in the heart chambers and hence provides energy for the ejection of blood (Luo and Anderson, 2013). Ca^{2+} enters the cardiomyocytes via tubular-dependent LTCC and later, with the phosphorylation of PLB at Ser¹⁶ by PKA, increases sarcoplasmic reticulum Ca-ATPase (SERCA2a) activity, thereby facilitating cytoplasmic Ca^{2+} reuptake into the sarcoplasmic reticulum (SR) lumen. The phosphorylation of PLB, cMyBP-C, and Tnl by PKA could be reversed by protein phosphatases (PP) (Figure 8). Phosphatases are discussed in more detail below.

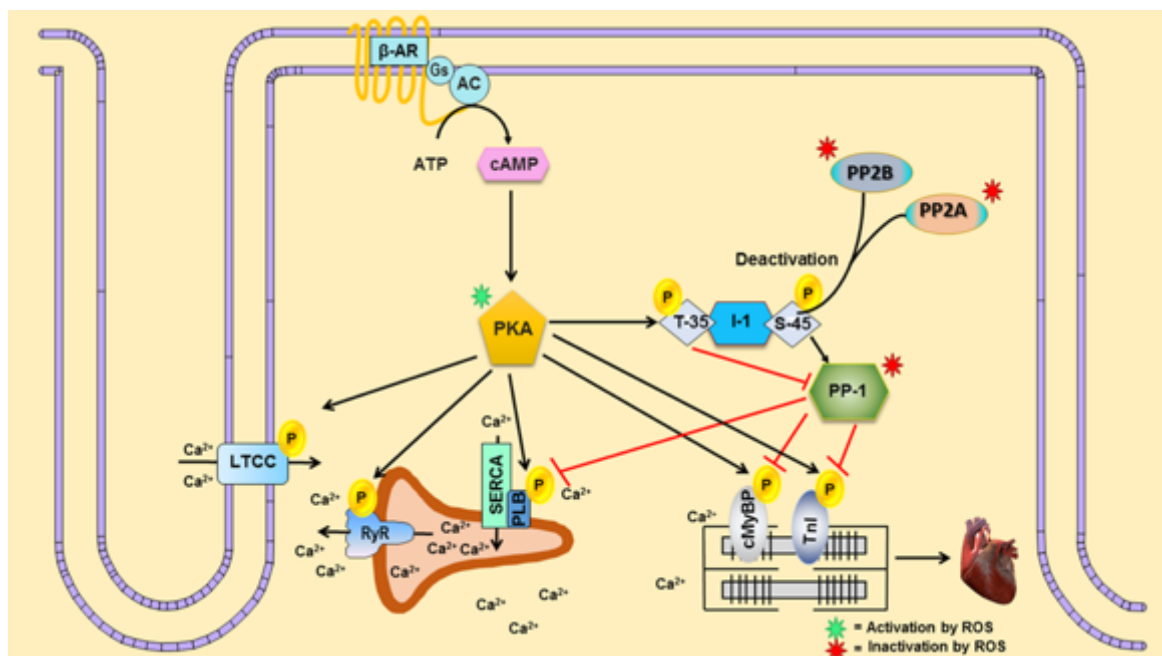


Figure 8 | Recent advances in redox regulation of β -adrenergic signaling pathway in cardiac myocytes. β -adrenergic (β -AR) receptors, localized in micro-domains of the sarcolemma formed by **t-tubules**, activate stimulatory G proteins (**Gs**) which stimulate adenylyl cyclase (**AC**) to make **cAMP**. **cAMP** then promotes an increase in protein kinase A (**PKA**)–dependent phospholamban (**PLN**) phosphorylation. This in turn promotes increased uptake of calcium ions (Ca^{2+}), via the sarcoplasmic reticulum Ca^{2+} ATPase (**SERCA**), into the sarcoplasmic reticulum (SR) increasing SR Ca^{2+} load, and SR Ca^{2+} release through ryanodine receptors (**RyR2**). In addition, activation of PKA also phosphorylates L-Type Ca^{2+} channel (**LTCC**), troponin I (**Tnl**) and cardiac myosin binding protein-C (**MyBP-C**). Moreover, activated **PKA**, also triggers phosphorylation of **I-1** at Threonine-35 to act as an inhibitor of phosphatase **PP-1**, resulting in dephosphorylation of **PLB**, **cMyBP** and **Tnl**. On the contrary, **PP-2A** and **PP-2B** deactivates **I-1** by dephosphorylation at Serine-45 and hence activation of **PP-1**. ROS alters the balance between kinase and phosphatase activity by activating and deactivating in a dose-dependent manner respectively and hence complex signaling paradigm with the downstream cardiac proteins (adapted from Bers, 2002).

1.5 Serine/threonine phosphatases

Many physiological functions are influenced by phosphorylation/de-phosphorylation events, such as cell differentiation, cell signaling, gene expression, neuronal activity, mitosis and metabolic functions (see reviews by McCluskey et al., 2002; Virshup and Shenolikar, 2009; Schulz and Wieczorek, 2013). Regulatory processes dictate the balance between two key enzymes; protein kinases, which transfer phosphate from ATP to the protein (phosphorylation), and protein phosphatases, which catalyze the opposite reaction (dephosphorylation). Protein phosphatases are considered to be relatively non-specific enzymes that exist only to reverse the action of protein kinases. In eukaryotic cells, phosphorylation's main targets are three hydroxyl-containing amino acids serine, threonine and tyrosine, and out of these, mainly serine is targeted. While understating the role of phosphatases and kinases, which are almost equal in number in the human genome i.e. 90 vs 107, whereas the number of catalytic subunits of serine/threonine phosphatases is much lower than that of Ser/Thr kinases (40 vs 428; Moorhead et al, 2007). Protein phosphatase families include: protein phosphatase type-1 (PP-1, ~38.5 kDa; Figure 9), type-2 (PP-2), consisting of PP-2A, PP-2B (calcineurin) and PP-2C. Recently, this set has been extended to PP-4, PP-5, PP-6 and PP-7 (Herzig and Neumann, 2000; Shi, 2009). PP-1 and PP-2 are the major constituents of phosphatase activity (~90%). Specifically, PP-1 is ubiquitously expressed in most cardiac cell types, including cardiomyocytes (El-Armouche and Eschenhagen, 2009).

1.5.1 Protein phosphatase 1 (PP-1)

PP-1 is a monomeric 37-kDa protein (Bollen et al., 2010) containing 330 residues. PP-1 plays a leading role in Ser/Thr PP activity (~45%). All isoforms of PP-1 contain thirteen Cys residues that hold two manganese (Mn^{2+}) ions at the center of the structure. Mn^{2+} is an essential element in biological systems and occurs in various oxidation states (+2. +3. +4. +6 and +7). It is also a cofactor for important enzymes and metalloproteins that are necessary for proper functioning (Martinez-Finley et al., 2013). Mammalian cells have three genes which encode four isoforms of PP-1's catalytic subunits PP-1 α , PP-1 β (or δ), PP-1 γ 1 & PP-1 γ 2 (Cohen 1988). Moreover, different isoforms of PP-1 shares similar sequence of percentages - 93% (γ 1/ γ 2), 91% (α / γ 1), 89% (α / β), 88% (α / γ 2), 87% (γ 1/ β) and 85% (γ 2/ β). All aforementioned isoforms of PP-1 have a distinctive tissue distribution and subcellular localization, which assembled to a favored binding to regulatory subunits and perform distinct functions (MacMillan et al., 1999).

PP-1 is highly conserved throughout evolution and is involved in a diverse array of cellular processes including muscle contraction, gene transcription, synaptic plasticity, glycogen metabolism and cell cycle progression (Cyert and Thorner, 1989). In the heart PP-1 has been shown to specifically regulate basal cardiac contractility and feedback to β -adrenergic stimulation. There are two types of PP-1 inhibitors: natural small molecular toxins and protein inhibitors. Various toxins exist inhibiting PP-1 activity, including tautomycin, calyculin A, microcystin and okadaic acid (OA). However, many endogenous proteins, such as the acid- and heat-stable inhibitor proteins – inhibitor-1 (I-1), inhibitor-2 (I-2), dopamine- and cyclic-AMP-regulated phosphoprotein (DARPP-32) have been shown to inhibit PP-1, leading to changes in localization and activity.

1.5.2 Predicted oxidative modifications of PP-1

ROS are capable of modulating the response of numerous cell-signaling pathways and serve as secondary messengers that control signal transduction by oxidizing cysteines of various kinases and phosphatases (Chiarugi, 2005). Oxidative modifications of PKA have been shown to enhance cardiac contractility via increased phosphorylation of key proteins (Brennan et al., 2006). In general, PKA inhibits PP-1 activity by phosphorylating PP inhibitor-1 (I-1) at Thr³⁵ and PP-2B dephosphorylating I-1 at Ser⁴⁵, acting as a counterbalance (MacLennan and Kranias, 2003; El-Armouche and Eschenhagen, 2009). In contrast, ROS can inhibit the activity of phosphatases and improve the ability of PKA to phosphorylate various downstream cardiac proteins (Figure 8). So far it has been shown that inactivation of PP-2B occurs in a thiol-oxidation-dependent manner (Li et al., 2004).

PP-1 contains highly conserved motifs with putative reactive Cys residues (Cys¹⁵⁵ and Cys¹⁵⁸) in proximity to the active site similar to thioredoxin (CXXC) (Figure 9.A). In the presence of oxidants, the Cys residues are expected to form a disulfide bridges, which results in loss of PP-1 activity (Fetrow. et al., 1999). This putative mechanism will be examined in this thesis.

Interestingly, besides targeting Cys for redox regulation, the PP-1 structure also has binuclear metal ions which reside about 3.3 Å apart at the center of the catalytic subunit. The two metal ions, manganese (Mn²⁺), are surrounded by four histidines (His), two aspartic acids (Asp), and one asparagine (Asn). On top, exclusively Cys residues (Cys⁶², Cys¹²⁷, Cys¹⁴⁰, Cys¹⁵⁵, Cys¹⁷¹, Cys²⁰², Cys²⁴⁵ and Cys²⁷³) also lie near the Mn²⁺ ions (Figure 9.B).

α -helices are represented as cylinders, β -strands are indicated with arrows, and metal coordinated residues are highlighted in yellow (Peti et al., 2013). (B) Binuclear metal center surrounded by Cys residues in the PP-1 structure, showing the networking Cys residues as red in color, the distance between them as red dotted lines and the rest of the backbone peptide is shown as a blue cartoon (B.1). The two Mn^{2+} ions are shown as pink balls surrounded by close Cys residues (B.2), with four Histidines surrounding the Mn^{2+} ions (B3).

1.6 ER stress and the unfold protein response

Cardiovascular studies have intensively focused on the function of the sarcoplasmic/endoplasmic reticulum (SR/ER) in cardiomyocytes, mainly due to SR's role as a primary source of intracellular Ca^{2+} , which regulates the contraction and relaxation of myofilaments. Currently, it is well accepted that a relationship exists between disturbances in Ca^{2+} handling and heart disease, and thus the regulation of Ca^{2+} is an important pharmaceutical target for treatment of cardiovascular diseases. In addition, there is increasing evidence showing that the ability of protein handling in the SR/ER is also affected by heart disease. This leads to ER stress which has been first described in 1988 in simian cells (Kozutsumi et al., 1988).

A network of membranes, known as cisternae, builds the ER in eukaryotic cells. Membrane and secretory proteins are produced in the ER, then processed, folded, and exported via the Golgi apparatus to the cell membrane or released into the interstitial space. In the ER lumen, balanced protein folding is primarily maintained by levels of calcium, molecular chaperones, protein glycosylation and the redox-status. Perturbations in the balance of accumulation and removal of misfolded/unfolded proteins can lead to physiological/pathological consequences, a condition which is called ER stress (Glembotski, 2007). To overcome this and to restore function back to the cell, a series of events takes place, including the degradation of misfolded proteins, the increase in production of chaperones, and the downregulation of protein translation. This process is known as unfolded protein response (UPR). If UPR is not successful, the cell will undergo apoptosis (Fribley et al., 2009). In the heart, it has also been shown that UPR is activated during I/R; furthermore long-term stresses that lead to cardiac hypertrophy and heart failure (Glembotski, 2008).

ER stress is prominently led by three ER-transmembrane proteins, i.e. inositol-requiring enzyme-1 (IRE-1) (Cox et al., 1993), protein kinase R-like ER kinase (PERK) (Shi et al., 1998) and activating transcription factor 6 (ATF6) (Zhu et al., 1997). These proteins act as the primary proximal effectors of the UPR signaling pathway. When the ER protein folding machinery functions efficiently, the ER luminal domains of IRE-1, PERK and ATF6 resides at the ER-resident chaperone called binding protein (BiP). Upon perturbation of ER protein

folding machinery, aggregation of misfolded proteins begins: BiP dissociates from IRE-1, PERK and ATF6, and attaches to the hydrophobic regions of misfolded proteins in order to support their folding. This translocation of BiP activates the three proximal effectors, which in turn activates the UPR signaling pathway (Bertolotti et al., 2000; Minamino and Kitakaze, 2010; Kimata and Kohno, 2011).

1.6.1 ER-transmembrane proteins (IRE-1, PERK and ATF6)

The IRE-1 gene was first discovered in mammals which encodes a type 1 ER transmembrane protein (Mori et al., 1993). IRE-1 functions as a kinase and as an endoribonuclease. In the UPR, IRE-1 gets detached from BiP due to the accumulation of misfolded proteins in the ER. Autophosphorylation by its kinase activity occurs and dimerization activates IRE-1 leading to the subsequent activation of endoribonuclease activity. IRE-1 α is the most important isoform for UPR, it efficiently splices the X-box binding protein 1 mRNA (XBP-1). After the spliced mRNA is translated, the splice variant, i.e. XBP-1s moves to the nucleus and triggers the activation of ER-stress responsive genes, which regulate the protein folding machinery, transportation and protein degradation (Calfon et al., 2002; Figure 10).

PERK is a type 1 ER transmembrane protein kinase and found as a monomer under unstressed conditions (Shi et al., 1998). Without ER stress, the luminal part of the monomeric PERK associates with the ER chaperone BiP. As soon as ER stress is initiated, BiP relocates from PERK to misfolded ER proteins. BiP relocalization permits PERK to dimerize, which facilitates trans-autophosphorylation in a mechanism similar to growth factor receptor activation (Ma et al., 2002). After dimerization and autophosphorylation, PERK is activated, which further phosphorylates and activates eukaryotic translation initiation factor 2 α (eIF2 α) at Ser⁵¹, which in turn prevents the initiation of global translation (Bertolotti et al., 2000). Global translational inhibition decreases the protein-folding load on the ER, aiding in the recovery of ER homeostasis and the amelioration of efficient protein folding machinery (Harding et al., 1999). With respect to translational arrest, eIF2 α phosphorylation also translates specific mRNAs such as the activating transcription factor 4 (ATF4). This results in increased expression of ATF4, which assists in regulating transcription factors such as C/EBP homologous protein (CHOP). This protein contributes to programmed cell death (Figure 10).

Similar to IRE-1 and PERK regulation, ATF6 is an ER transmembrane protein that, during the unstressed state, exists as a dimer linked by intermolecular SS bridges in the luminal domain and is associated with BiP. During ER stress, protein misfolding increases which

leads to the sequestration of BiP away from the ER-luminal domain of ATF6. In contrast to the other two effectors, which remain in the ER lumen upon dissociation of BiP and disulfide bridge cleavage, a 90 kDa form of ATF6 translocates to the Golgi-complex, where it is cleaved by site-1 and site-2 proteases (S1P and S2P) (Figure 10). The resulting cleaved 50 kDa ATF6 is a cytosolic fragment, which translocates to the nucleus where it can form homodimers or heterodimers with a small group of basic leucine zipper transcription factors which trigger UPR genes expression in the nucleus. Therefore, activated ATF6 is an essential element of the UPR (Glembotski, 2014).

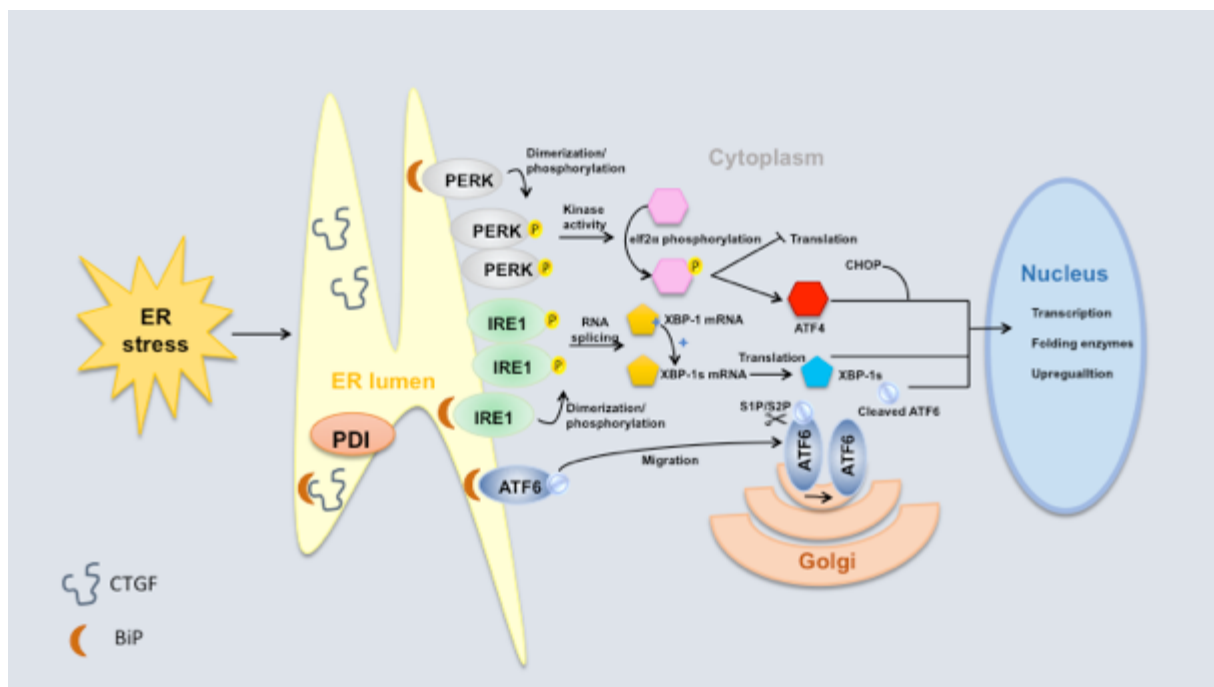


Figure 10 | ER stress signaling pathways in eukaryotic cells. ER stress is triggered by disturbance in nutrient or energy balance of a cell, results in misfolded protein accumulation in the ER and hence activation of the UPR as a surviving process. Three ER transmembrane proteins play an essential role in maintaining the balance between ER stress and UPR: Inositol-requiring enzyme-1 (**IRE-1**), protein kinase R-like ER kinase (**PERK**) and activating transcription factor 6 (**ATF6**)—in combination with the ER chaperone **BiP** (adapted from Groenendyk et al., 2013).

1.7 Connective tissue growth factor

CCN proteins are known to have abundant amounts of Cys (>10%) and a complete conservation of the 38 Cys residues position in the sequence (Bork, 1993). In total, there are six exclusive proteins within the CCN family, which share the same sequence homologies and secondary structure. The CCN family of secreted Cys-rich proteins with similar structure are grouped together and abbreviated according to these proteins: Cys-rich protein 61 (cyr61=CCN1), connective tissue growth factor (CTGF=CCN2) and nephroblastoma overexpressed protein (NOV=CCN3) (Leask and Abraham, 2006). The other three members

of the CCN family are Wnt-1-induced proteins (WISP): WISP-1 (CCN4), WISP-2 (CCN5) and WISP-3 (CCN6) (Rachfal and Brigstock, 2005). CTGF was discovered in 1991. Gary et al. described a platelet-derived growth factor (PDGF)-related mitogen in the medium of human umbilical vein endothelial cells (HUVECs) and termed it CTGF (Bradham DM et al., 1991).

1.7.1 Structural and functional properties of CTGF

CTGF is a 36 kDa matricellular protein of the CCN family containing four distinct structure modules: (1) an insulin-like growth factor binding protein (IGFBP), (2) a von-Willebrand factor type C (vWF-C), (3) a thrombospondin motif (TSP1), and (4) a Cys knot (CT) at the carboxyterminal end (Figure 11.A). Between modules (2) and (3), CTGF has a hinge region which can be cleaved by proteases into two fragments of similar molecular weights.

All four modules are involved in different physiological functions such as cell proliferation, migration, adhesion, differentiation, matrix production and apoptosis. From the pathobiology perspective CTGF is overexpressed in fibrotic lesions, fibrogenesis, cancer, atherosclerosis (Au et al., 2010; Leeuwis et al., 2010; Jacobson and Cunningham, 2012) and is also involved in wound healing, angiogenesis and epithelial-mesenchymal transition (Alfaro et al., 2013; Sonnylal et al., 2013; Liu et al., 2014b).

CTGF contains 39 conserved Cys residues, spread over four modules and can form intra- and inter-disulfide bridges. The IGFBP N-terminal domain contains twelve Cys residues (Hwa et al., 1999). vWF-C, also known as chordin-like Cys-rich (CR) repeats, contains ten Cys residues. The first motif 'Cys²XXCys³XCys⁴' lies in the middle and the second motif 'Cys⁸Cys⁹XXCys¹⁰' lies at the end of the repeat (Bork, 1993). In total, TSP-1 contains six Cys residues and the motif 'CSXTCG' (Tan et al., 2002). The last domain, located at the carboxy-terminal end, is known as the CT module or Cys knot. It has been suggested that the CT module may be involved in dimerization as it serves this function in transforming growth factor- β (TGF- β), nerve growth factor and PDGF (Bork, 1993).

The CT is stable in structure with two SS bridges forming a ring structure and the fifth Cys projecting through the ring to allow the formation of a third SS bridge (Perbal et al., 1998) (Figure 11.B). Within the aqueous environment, this structure enhances the availability of hydrophobic residues in monomers and supports the formation of homo- or heterodimers. To initiate signal transduction through their respective receptors, dimers serve as an active state of the CT bearing growth factors. Individual domains of CTGF show a distinct functions, where the C-terminal arbitrate fibroblast proliferation and the N-terminal domain arbitrates myofibroblast differentiation and collagen synthesis (Grotendorst and Duncan, 2005).

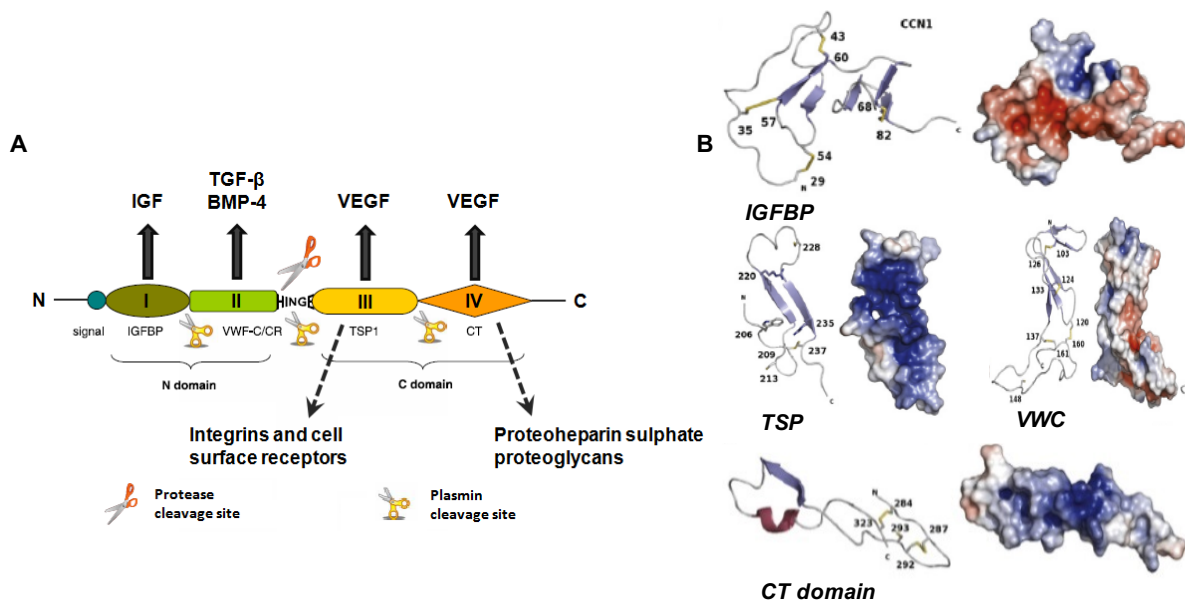


Figure 11 | Schematic structure of CTGF protein. (A) Structural CTGF is composed of four modules: IGFBP, vWF-C, TSP1 and the CT (adapted from Winter et al., 2008). (B) 3D chemical structure with various domains of CTGF showing intra and inter-SS bridges (Holbourn et al., 2008).

1.7.2 Functional aspect of CTGF in heart diseases

Previous studies on CTGF have focused on cardiac fibrosis (Jatho et al., 2015; Ongherth et al., 2015); yet it is still uncertain whether CTGF plays any role in cardiomyocytes. Contrary to studies on the negative impacts of CTGF during fibrogenesis, several reports suggest that CTGF plays a cardio-protective role. This cardio-protective role was shown by Ahmed et al., as CTGF restored phosphokinase signaling by promoting the inhibition of GSK-3 β and activating phospho-SMAD2 (Ahmed et al., 2011).

CTGF can also attenuate hypertrophic signaling in cardiac myocytes in response to chronic pressure (Gravning et al., 2013a). The same research group suggested that paracrine regulation of GRK5 activity in cardiomyocytes may contribute to cardio-protective actions of CTGF in heart failure (Gravning et al., 2013b). In adult cardiac myocytes CTGF has also been shown to directly trigger the Akt/GSK-3 β signaling pathway, which leads to increasing tolerance to hypoxia and oxidative stress (Moe et al., 2013). One of the studies furthermore describes an antagonizing function of CTGF by using a CTGF monoclonal antibody. The results showed that the antibody may decrease the danger of hypertensive coronary illness in patients (Szabo et al., 2014).

In the context of cellular proliferation, CCN1 and CTGF are known to be positive regulators of growth, whereas CCN3 and CCN5 are negative growth regulators (Brigstock, 1999; Lau and Lam, 1999). In different tissues and organs, CCN1 and CTGF (structurally related, but

functionally distinct multimodular proteins) are expressed during pathological or developmental events. In one of the studies, it was shown that, using *in vitro* computation of biological activities, CCN1 expression triggered a genetic reprogramming of structural, adhesive and angiogenic proteins, whereas CTGF induced aggregation of the extracellular matrix, a primary stage of fibrotic diseases (Chaqour and Goppelt-Struebe, 2006).

Further comparisons by the Park group showed differential expression of CTGF and CCN5 during the process of cardiac remodeling and opposite regulation during the fibrosis and cardiac hypertrophy. In other words, CTGF and CCN5 were shown to be pro-and anti-hypertrophic, respectively. The CT domain is absent in CCN5, which is known to have hypertrophic activity in CTGF. The deletion of the CT domain in CTGF restores hypertrophic function similar to a CCN5-like dominant negative molecule (Yoon et al., 2010). The same group demonstrated that CCN5 expression was significantly decreased in end-stage heart failure samples compared to non-failing heart samples. In addition, both *in vivo* and *in vitro* experimentation showed that CCN5 triggers apoptosis only in myofibroblasts, but surprisingly not in cardiomyocytes or fibroblasts. The authors suggest that CCN5 could reverse cardiac fibrosis (Jeong et al., 2016).

In 2001 it was reported that, in dermal fibroblasts and activated hepatic stellate cells, CTGF protein is quantitatively emitted through the Golgi apparatus and is rapidly degraded in the endosome (Chen et al., 2001). In chondrocytes it was found that the loss of CTGF triggers deformed extracellular matrix (ECM) organization and chondrocyte death, accompanied by increased cellular stress (Hall-Glenn et al., 2013). CTGF and its role in ER stress in the heart has not been fully understood. Therefore, the involvement of CTGF in the ER stress response and UPR signaling pathway was analyzed.

2 Aim of the study

Abnormal phosphorylation levels of cardiac key proteins and elevated reactive oxygen species (ROS) production were shown to contribute to contractile dysfunction and fibrosis in failing hearts. Within this context this thesis aimed to investigate the redox sensitivity of the cytosolic PP1 and the secreted CTGF in cardiomyocytes. Both proteins were demonstrated before to be dysregulated in the diseased heart, however, the influence of a changed redox status on their regulation in cardiomyocytes had been not assessed.

Given that redox sensitivities of cardiac PP-1 and CTGF are involved in contractile dysfunction and fibrosis, which are the main pathomechanisms of cardiac diseases, the thesis addresses the following objectives:

- **Identify the mechanisms of PP-1 oxidation and test whether oxidized PP-1 contributes to the pathophysiology of abnormal protein phosphorylation and myocardial dysfunction in failing myocardium**

More specifically, the following questions were addressed:

1. Does PP-1 activity change, due to cysteine oxidation status or dinuclear metal (Mn^{2+}) ions in response to oxidative stress?
2. Does glutathionylation play any role in the activity of PP-1?

The main experimental procedure consisted of activity assays to identify the PP-1 activity. Mass spectrometry was used, as a method to analyze different Cys-based post-translational modification in PP-1.

- **Test the hypothesis whether redox and ER stress affects CTGF and *vice versa***

In detail, the following questions were addressed:

1. Is CTGF affected by redox and ER stress in cardiomyocytes?
2. Is ER stress and the UPR pathway affected by the expression of CTGF?

We attempted to answer the above questions using a combination of non-reducing gels and incubation of the cells with redox and ER stress eliciting agents. Furthermore, we also used si-RNA techniques to knockdown CTGF expression in cardiomyocytes and assessed the impact on various ER stress markers.

3 Materials & Methods

3.1 Materials

3.1.1 Antibodies

Table 1 | Primary antibodies

Primary antibody	Dilution		Source	Type/ Clone	Catalogue No.	Company
	W.B	IF				
α -actinin	1:2000	1:500	Mouse	Monoclonal/6-11B-1	T6793	Sigma-Aldrich
ATF6	1:500	1:50	Rabbit	Polyclonal	H-280	Santa Cruz
BiP	1:500	-	Rabbit	Monoclonal	C50B12	Cell Signaling
CHOP	1:500	1:3200	Mouse	Monoclonal	L63F7	Cell Signaling
CTGF	1:200	1:50	Goat	Polyclonal/L-20	sc-14939	Santa Cruz
CSQ	1:1000	-	Rabbit	Polyclonal	9102S	Dianova
Phospho cMyBP-C-Ser ²⁸²	1:5000	-	Rabbit	Polyclonal	ALX-215-057-R050	Enzo Life Science
Phospho-Inhibitor-1-Thr ³⁵	1:1000	-	Rabbit	Polyclonal	#2302	Cell Signaling
IRE1- α	1:1000	-	Rabbit	Monoclonal	14C10	Cell Signaling
PDI	1:1000	1:100	Rabbit	Monoclonal	C81H6	Cell Signaling
Phospho PLB-Ser ¹⁶	1:1000	-	Rabbit	Polyclonal	9102S	Badrilla
PKA RI	1:200	-	Mouse	Monoclonal	610166	BD Transduction Laboratories
PP-1	1:200	-	Mouse	Monoclonal	E-9	Santa Cruz
PP-1 alpha (α)	1:1000	-	Mouse	Polyclonal	C-19	Santa Cruz
SERCA2	1:200	-	Goat	Polyclonal	Sc-8094	Santa Cruz
α -tubulin (~Tubulin)	1:2000	-	Mouse	Monoclonal	T 5168	Sigma-Aldrich

Table 2 | Horseradish peroxidase (HRP)-conjugated secondary antibodies

Secondary antibody	Dilution	Source	Catalogue No.	Company
Goat	1:10000	Donkey	Sc-2020	Santa Cruz
Mouse	1:10000	Rabbit	A9044	Sigma-Aldrich
Rabbit	1:40000	Goat	A9169	Sigma-Aldrich

Table 3 | Fluorophore-conjugated secondary antibodies for immunofluorescence

Secondary antibody	Dilution	Fluorophore	Source	Catalogue No.	Company
Goat	1:300	Cy3	Rabbit	305-165-003	Jackson Immuno Research
Goat	1:100	FITC	Rabbit	305-095-003	Jackson Immuno Research
Goat	1:150	FITC 488	Rabbit	305-095-003	Jackson Immuno Research
Rabbit	1:500	Alexa-fluor 594	Goat	111-475-144	Jackson Immuno Research

3.1.2 Buffers and solution

Table 4 | Composition of the used buffers, solutions, and media

Immunoblotting	
GST-fish buffer (500 ml)	25 ml 1 M Tris (pH 7.4 with HCl) 75 ml 1 M NaCl 2 ml 1 M MgCl ₂ 50 ml glycerol 5 ml Igepal CA-630 up to 500 ml distilled water
4x SDS-PAGE sample loading buffer (50 ml)	25 ml glycerol 5 ml β-Mercaptoethanol 3.25 g SDS 15 ml 300 mM Tris (pH 6.8 with HCl) 0.125 g bromophenol blue up to 50 ml distilled water
Blocking buffer	10 ml 1 M Tris-HCl pH 7.4 20 ml 0.5 M maleimide 20 ml 10% SDS up to 50 ml H ₂ O
2x Non-reducing loading buffer	4 ml 1 M Tris-HCl pH 6.8 1.6 gm SDS 8 ml Glycerol, 87% 4 mg bromophenol blue

	8 ml 0.5 M maleimide
2x Reducing loading buffer	4 ml 1 M Tris-HCl pH 6.8 1.6 gm SDS 8 ml Glycerol, 87% 4 mg bromophenol blue 8 ml 0.5 M maleimide 0.617 gm DTT
10x TBS buffer (1000 ml)	12.12 g Tris 87.65 g NaCl up to 1000 ml distilled water pH 7.4 with HCl
TBS-T buffer (1000 ml)	1000 ml 10x TBS 1 ml tween 20
5x SDS-PAGE electrophoresis buffer (1000 ml)	15.1 g Tris 94 g glycine 5 g SDS up to 1000 ml distilled water pH 8.3 with KOH
Blotting buffer (1000 ml)	3.02 g Tris 14.4 g glycine 200 ml methanol up to 1000 ml distilled water
12% SDS-polyacrylamide gel (50 ml)	16.5 ml distilled water 20 ml acrylamide rotiphorese gel 30 solution 12.5 ml 1.5 M Tris (pH 8.8 with HCl) 0.5 ml 10% SDS 0.5 ml 10% APS
15% SDS-polyacrylamide gel (50 ml)	11.5 ml distilled water 25 ml acrylamide rotiphorese gel 30 solution 12.5 ml 1.5 M Tris (pH 8.8 with HCl) 0.5 ml 10% SDS 0.5 ml 10% APS 0.02 ml TEMED
5% SDS-polyacrylamide gel (20 ml)	13.6 ml distilled water 3.4 ml acrylamide rotiphorese gel 30 solution 2.5 ml 1 M Tris (pH 6.8 with HCl) 0.2 ml 10% SDS 0.2 ml 10% APS 0.02 ml TEMED
10% SDS (100 ml)	10 g SDS up to 100 ml distilled water
10% APS (10 ml)	1 g APS up to 10 ml distilled water
Ponceau S stain (100 ml)	5 ml glacial acetic acid 0.2 g Ponceau S powder up to 100 ml distilled water

Immunofluorescence (IF)	
4% paraformaldehyde (PFA) (250 ml)	10 g paraformaldehyde 50 µl 10 N NaOH 25 ml 10x PBS up to 250 ml distilled water pH adjusted to 7.0 with HCl
0.05% Triton (50 ml)	250 µl 10x Triton up to 50 ml PBS
1x Roti-Immunoblock (50 ml)	5 ml 10x Roti-Immunoblock up to 50 ml distilled water
Agarose gel electrophoresis	
1% Agarose gel (50 ml)	0.5 g agarose powder 50 ml 1x TAE buffer 2 µl ethidium bromide (10 mg/ml)
50x TAE buffer (1000 ml)	242.28 g Tris 57.1 ml glacial acetic acid 200 ml 0.25 M EDTA (pH 8.0 with NaOH) up to 1000 ml distilled water
Bacterial culture media and plates	
LB medium (1000 ml)	10 g tryptone 5 g yeast extract 10 g NaCl up to 1000 ml distilled water pH 7.0 autoclave
LB agar plates with carbenicillin (1000 ml)	10 g tryptone 5 g yeast extract 10 g NaCl 15 g agar up to 1000 ml distilled water pH 7.0 with NaOH autoclave let cool to about 50°C, then add 1 ml carbenicillin stock (50 mg/ml), then cast as 20 ml/10 cm petri dish
SOB medium (1000 ml)	20 g tryptone 5 g yeast extract 0.5 g NaCl 10 ml 25 mM KCl up to 1000 ml distilled water pH 7.4 autoclave 5 ml autoclaved 2 M MgCl ₂
SOC medium (100 ml)	1 ml filter-sterilized 2 M glucose up to 100 ml SOB medium

Cell Isolation	
Calcium- and bicarbonate- free Hanks with HEPES (CBFHH) (1000 ml)	40 ml NaCl stock (200 g/l) 10 ml MgSO ₄ *H ₂ O stock (20 g/l) 10 ml KH ₂ PO ₄ stock (6 g/l) 10 ml Na ₂ HPO ₄ *2H ₂ O stock (5.97 g/l) 10 ml glucose dihydrate stock (100 g/l) 100 ml HEPES stock (47.66 g/l) up to 1000 ml distilled water, sterile by filtration pH 7.4 with NaOH
Heat inactivated FCS (50 ml)	50 ml FCS was incubated in a water bath adjusted to 56°C for 30 minute (min), during which it was shaken gently every 5 min.
Non-cardiomyocyte medium (NCM)	500 ml DMEM GlutaMAX 1 g/l glucose 50 ml heat-inactivated FCS 5 ml P/S (100x)
0.4% Trypan blue (100 ml)	0.4 mg trypan blue 100 ml distilled water
Neo-natal rat cardiomyocyte (NRCM) culture media	
Cardiomyocyte medium (CM)	Minimal Essential Medium (MEM-Earle, 2.2 g / l NaHCO ₃ , without L-glutamine) FCS (inactivated) 10% (v/v) L-glutamine, 1% (v/v) Penicillin / streptomycin, 1% (v/v) BrdU (10 mM) 1% (v/v) freshly added
BrdU (5-bromo-2'-deoxyuridine)	BrdU 10 mM In aqueous solution, sterile filtered. Stable for one week at 4°C.
Other buffers and solution	
BIAM labeling buffer	1 ml 10 mM Tris (pH 6.8 with HCl) 1ml 1% Triton X-100 6.6 ml 100mM Nacl 10 ml 1% SDS up to 100 ml distilled water (Prior to use, add 100 µM BIAM to solution)
Stage A buffer	0.5% (v/v) acetic acid in water
Stage B buffer	80% (v/v) acetonitrile 0.5% (v/v) acetic acid in water
Loading buffer for MS	1% (v/v) acetonitrile 0.1% (v/v) formic acid in water

3.1.3 Chemicals and reagents

Table 5 | List of chemical and reagents

Chemical and Reagents	Manufacturer
Acetic acid (100%)	Carl Roth
Acetonitrile	AppliChem
Agar	Peqlab
Agarose	AppliChem
Ammonium bicarbonate	Sigma-Aldrich
Ammonium persulfate (APS)	AppliChem
Ascorbic acid	AppliChem
Aqua B. Braun	Braun
N-(Biotinoyl)-N'-(Iodoacetyl)Ethylenediamine (BIAM)	Thermo-Scientific
Brefeldin a (BFA)	Sigma-Aldrich
Bromophenol blue	AppliChem
Carbenicillin	Applichem
Control siRNA-A	Santa Cruz
CTGF siRNA	Santa Cruz
Cycloheximide	Santa Cruz
4',6-diamidino-2-phenylindole (DAPI)	Sigma-Aldrich
Diamide	Sigma-Aldrich
Dimethylsulfoxide (DMSO)	Sigma-Aldrich
DMEM Glutamax, 1 g/l glucose, pyruvate	Life Technologies
DMEM Glutamax, 4.5 g/l glucose	Life Technologies
DNA loading buffer (6x)	Thermo-Scientific
DNA molecular weight standard (1 kb DNA ladder)	Thermo Scientific
Dithiothreitol (DTT)	Applichem
Ethanol, absolute	J.T. Baker
Ethidium bromide	Sigma-Aldrich
EvaGreen dye for qPCR	Solis Biodyne
Fetal calf serum (FCS)	Life Technologies
Formaldehyde (37%)	Merck
Formic acid	AppliChem
GeneRuler 1 Kb plus DNA ladder	Thermo-Scientific
Glucose	AppliChem
Glycerol	AppliChem
Glycine	AppliChem
Hydrogen peroxide (H ₂ O ₂) solution	Sigma-Aldrich

4-(2-hydroxyethyl)-1-piperazineethanesulfonic acid (HEPES)	Carl Roth
Igepal CA-630	Sigma-Aldrich
Iodoacetamide (IAA)	Sigma-Aldrich
Isopropanol	Carl Roth
Lipofectamine RNAiMAX transfection reagent	Life Technologies
6x Loading Dye (Agarose gel electrophoresis)	Thermo Scientific
Lumi-Light PLUS Western Blotting Substrate	Roche
Magnesium chloride (MgCl ₂)	AppliChem
Manganese chloride (MnCl ₂)	AppliChem
Maleimide	Sigma-Aldrich
β-Mercaptoethanol	AppliChem
Methanol	Carl Roth
MG132	Sigma-Aldrich
Okadaic acid	Enzo life sciences
Paraformaldehyde (PFA)	Sigma-Aldrich
Penicillin/streptomycin (P/S)	Life Technologies
Phosphate-buffered saline (PBS) without Ca ²⁺	Life Technologies
PolyFect transfection reagent	Qiagen
Ponceau S	Sigma-Aldrich
Protein Marker „Roti-Mark Standard.“	Carl Roth
Roti-Block (Blocking Reagent) 10X	Carl Roth
Roti-Nanoquant (Bradford reagent)	Carl Roth
Sodium chloride (NaCl)	Sigma-Aldrich
Sodium dodecyl sulfate (SDS)	AppliChem
Streptavidin agarose	Thermo-Scientific
Streptavidin, horseradish peroxidase conjugate	Thermo-Scientific
SuperSignal West Femto	Thermo Fisher Scientific
Bond-Breaker TCEP Solution, Neutral pH	Thermo-Scientific
Tetramethylethylenediamine (TEMED)	Merck
Thapsigargin (TGN)	Calbiochem
Tris ultrapure (Tris base)	AppliChem
Triton X-100	Carl Roth
Trypan blue	Fluka
Trypsin-EDTA 0.05%	Life Technologies
Tunicamycin	Santa Cruz
Tween-20	Carl Roth
Urea	AppliChem

3.1.4 Kits

Table 6 | List of kits

Kit	Application	Manufacturer
EnzChek Phosphatase Assay Kit	Phosphatase activity assay	Molecular probes
Exprep plasmid SV mini	Miniprep plasmid purification from bacteria	GeneAll
GoTaq green master mix	PCR	Promega
High pure PCR product purification kit	PCR product purification	Roche
5x HOT FIREPOL EvaGreen qPCR Mix Plus	qPCR	Solis Biodyne
Lumi-light western blotting substrate	Chemiluminescence protein blot visualization	Roche
Neonatal Heart Dissociation Kit	Isolation of beating cardiomyocytes	Miltenyi Biotec
ProFluor Ser/Thr PPase Assay Kit	Phosphatase activity assay	Promega
Revert Aid First Strand cDNA Synthesis Kit	RNA reverse transcription into cDNA	Thermo-Scientific
RNeasy	Total RNA isolation	Qiagen

3.1.5 Cells

Table 7 | List of bacterial and mammalian cells

Cells	Description
HSP47 knock out (KO)	Isolated from MEFs
Primary neo-natal rat cardiomyocytes (NRCM)	Isolated weekly from neonatal Wistar rats (1-3 days old)

3.1.6 Primers and recombinant proteins

Table 8 | List of primers used for qPCR and RT-PCR

Gene	Primer	Sequence (5' → 3')	Annealing temperature
CTGF	Forward	CCG GGT TAC CAA TGA CAA TA	58°C
	Reverse	CAC ACC CCA CAG AAC TTA GC	
PBGD	Forward	CCT GAA ACT CTG CTT CGC TG	58°C

	Reverse	CTG GAC CAT CTT CTT GCT GAA	
PDI	Forward	CTT CTT CAA GGA CGC AGG GT	58°C
	Reverse	GCG GCC TTC ATC AAA CTT CTT	
XBP-1	Forward	TTA CGA GAG AAA ACT CAT GGG C	58°C
	Reverse	GGG TCC AAC TTG TCC AGA ATG	

Table 9 | List of recombinant protein

Enzyme	Source	Company
PP-1A, active, GST-tagged, human recombinant	Sf9 insect cells	Sigma-SRP5338
PP-1A, His-tagged	E.coli	Sigma-P7937

3.1.7 Laboratory instrument, general material and software

Table 10 | List of instruments

Instrument	Model No.	Manufacturer
Autoclave	VX-150	Systec
Cell counting chamber	Fuchs-Rosenthal bright-line	Marienfeld-Superior
Cell culture incubator	Steri-cult 200 Incubator	Forma Scientific
Cell culture incubator	Labotect Incubator C 200	Labotect
Cell sieve	Cell dissociation sieve - tissue grinder kit (250 µm pore size)	Sigma-Aldrich
Centrifuge bench top	Centrifuge 5804 R	Eppendorf
Centrifuge bench top	Sigma 3K30	Sigma
Centrifuge table top	Tabletop centrifuge 5415 D	Eppendorf
Centrifuge table top	Combi-spin FVL-2400N	Biosan
Centrifuge table top	Centrifuge 5417 R	Eppendorf
Chemiluminescence imaging system	Versa doc MP	Bio-Rad
Double distilled water system	Milli-Q	Millipore
Electric power supply and control	Powerpac	Bio-Rad
Heating block	Thermomixer compact	Eppendorf
Incubator	CFC-free	Sanyo
Inverted fluorescence microscope	Axiovert 200	Zeiss
Inverted fluorescence microscope with climate chamber	Olympus IX 81	Olympus

Inverted microscope	Axiovert S100 TV	Zeiss
Microplate reader	Flex Station 3	MDS Analytical Technologies
Microscope camera	CAM-XM10-T-Camera	Olympus
Nanospray Flex ion-Source	ES071	Thermo-Scientific
pH meter	WTW	Inolab
Pipettes	Pipetman	Gilson
Plate reader	FlexStation3	Molecular Devices
Pump	ME2	Vacuubrand
Q Exactive Plus System	LTQ Orbitrap XL	Thermo-Scientific
Real-Time-PCR-System	TaqMan 7900HT Fast Real-Time-PCR System	Applied Biosystems
Rocker	Diomax 1030	Heidolph
Rotation shaker	Reax 3	Heidolph
Scale	Portable	Sartorius
Shaker	GFL 3016	GLF
Shaker	Vibramax 100	Heidolph
Shaking incubator	Innova 4300	New Brunswick Scientific
Spectrophotometer	Nanodrop 1000	Peqlab
Sonicator	Sonifier B-12	Branson Sonic Power
Temperature control chamber	Certomat	B. Braun
Thermocycler	Mastercycler gradient	Eppendorf
Ultracentrifuge	L8-70M	Beckman
Ultracentrifuge rotor	SW-27	Beckman
Ultra-high performance liquid chromatography unit (UPLC)	Dionix Ultimate 3000	Thermo-Scientific
UV agarose gel imaging system	Gel doc XR	Bio-Rad
Vortexer	VF 2 Vortexer	Janke u. Kunkel IKA Labortechnik
Water bath	2764	Eppendorf
Western blotting setup	Mini-protean tetra cell 4-gel system	Bio-Rad

Table 11 | List of general material

General material	Manufacturer
Acclaim PepMap100 C18 column	Thermo-Scientific
Cell culture dishes	Greiner Bio One
Cell scrapers	Sarstedt
Centrifuge tubes	Beckman
Empore SPE Disks	Sigma-Aldrich (66883-U SUPELCO)
Filter syringes	Sarstedt
Liquid junction emitters	New Objective
Multi-well cell culture plates	Greiner Bio One

Nitrocellulose membrane, Whatman, Protran	GE Healthcare
PCR reaction tubes	Sarstedt
Pipette tips	Sarstedt
Pipette tips with filters	4titude
Protein desalting spin columns	Thermo-Scientific
Reaction tubes (15, 50 ml)	Greiner Bio One
Reaction tubes (0.5, 1.5, 2 ml)	Sarstedt
Reprosil Saphir	Dr. Maisch GmbH
Serological pipettes	Sarstedt
Silica beads	Amerbruch
96 well microtiter plates	Thermo-Scientific
96 well solid black microplates	Corning
Wide opening, serological pipettes	Falcon

Table 12 | List of software

Program	Application	Manufacturer
Citavi	Managing references	Swiss academic software
GraphPad Prism 6.0c	Statistical calculations and graphs drawing	GraphPad
ImageJ 1.51a	Evaluation of fluorescence intensity	National Institutes of Health, USA
Image Lab 5.1	Operating the Versa Doc MP system and for semi-quantification of western blots	Bio-Rad
Peaks 7.0 Search engine	Analysing Mass-Spectrometry's data	Bioinformatics solutions Inc.
PyMOL 0.99rc6-bin-win32	Structural analysis of proteins	Schrödinger, Inc.
SDS 2.4	Operating the TaqMan 7900HT Fast Real-Time-PCR System, and its data analysis	Applied Biosystems
Xcellence pro	Operating the Olympus microscopy system for cell imaging	Olympus

3.2 Methods

3.2.1 Cell culture methods

3.2.1.1 Preparation of cardiomyocytes from neonatal rats

Neonatal rats were sacrificed on postnatal day 0-3 (P0-P3) in accordance with ethical standards. Hearts were extracted using forceps and ventricular tissues were collected in cell culture dishes with ice-cooled Calcium- and bicarbonate- free Hanks with HEPES (CBFHH). Ventricular tissues were cut in half and transferred to a new culture dish with 20 ml of CBFHH and washed one additional time to remove excess blood. The tissues were minced into small pieces (1-2 mm³) and then transferred via a 10ml pipette tip to a gentle MACS C-tube (up to ~20 neonatal rat hearts).

The following enzymes were prepared from the neonatal heart dissociation kit (for 20 neonatal rat hearts) according to the manufacturer's instructions. Reagent preparation summarized in Table 13:

Table 13 | Reagent preparation

Enzyme mix 1		Enzyme mix 2		
Enzyme P	Buffer X	Buffer Y	Enzyme A	Enzyme D
62.5 µl	2300 µl	25 µl	12.5 µl	100 µl

The enzyme mix 1 was preheated for 5 minutes (min) at 37°C and mixed with enzyme mix 2. 2.5 ml of the enzyme mix was transferred to the C-tube containing the tissues and incubated in an inward position with the cap down for 15 min at 37°C. The C-tube was then attached to the sleeve of a gentle MACS Dissociator and followed by the program named 'h_Tumour_01.' Incubation steps were repeated twice to complete the digestion of tissue. After the completions of the program, C-tubes were removed from the gentleMACS Dissociator and samples were carefully resuspended in 7.5 ml of a non-cardiomyocyte medium (NCM).

To separate the tissue from the suspension, a sieve was moistened (pore size 250 µm) with 3-4 ml of NCM. The cell suspension was transferred through the sieve, collected in a fresh cell culture dish and added to a falcon tube. Cell suspensions were centrifuged at 300 g for 5 min (20°C), and the supernatant was carefully discarded and re-suspended in 4 ml of 1x Phosphate-buffered saline (PBS), homogenized and then filtered.

The percoll gradient method was used to extract and purify only the cardiomyocytes fraction from the heterogeneous cell suspensions (consisting of a mixture of fibroblasts, cardiomyocytes, and erythrocytes). The percoll stock solution was prepared by mixing 40.5 ml of percoll (4°C) with 4.5 ml of 10x PBS. Then, a top and bottom percoll solution (TPS, BPS) was prepared, by mixing 9 ml of percoll stock with 11 ml of 1x PBS and 13 ml percoll stock with 7 ml of 1x PBS respectively. To differentiate between both solutions, 200 µl of phenol red stock solution was added to TPS. Subsequently, 4 ml of TPS was added to two 15 ml reaction tubes, and 3 ml of BPS was slowly added to the bottom while transferring the pipette upward. Next, 2 ml of cell suspension mixed with 1x PBS was slowly added and centrifuged at 750 g for 30 min at 20°C. The percoll gradient (Figure 12) was divided into three different gradients (as per density of tissue), i.e. fibroblasts, cardiomyocytes, and erythrocytes.

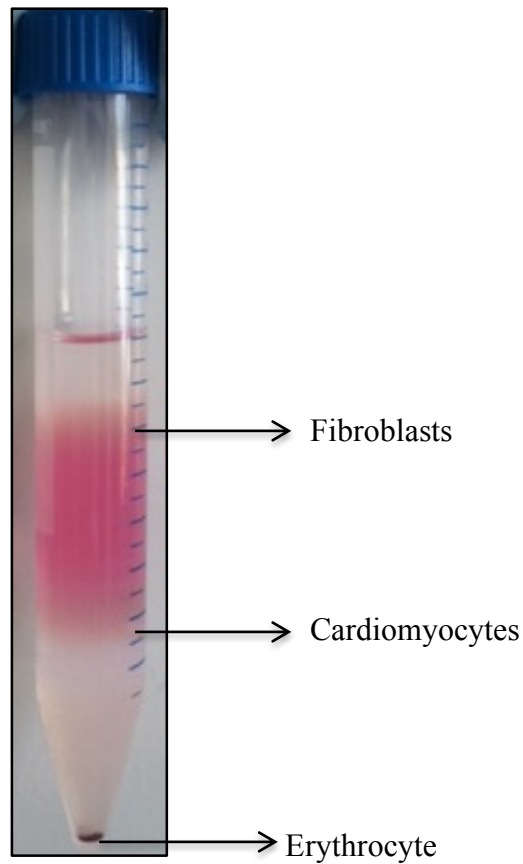


Figure 12 | Percoll gradient with three distinct layers consisting of fibroblasts, cardiomyocytes, and erythrocytes.

The upper 5 ml of the solution composed of fibroblasts was removed, and 2 ml of cardiomyocyte layer was carefully transferred into a new 50 ml tube and washed twice with pure DMEM cardiomyocyte medium (CM) at 300 g for 5 min at 20°C. The supernatant was discarded, and the pellet was resuspended in 10 ml of pre-warmed DMEM CM. The overgrowth of fibroblasts within cardiomyocytes was prevented by the adding 10 mM of

antimetabolite 5'-bromo-2'-deoxyuridine (BrdU) in the cardiomyocytes medium, which selectively inhibited the DNA synthesis and consequently cell proliferation of fibroblasts.

Cells were counted as follows: 10 μ l of cell suspension was mixed with 10 μ l tryphan blue and transferred to a Neubauer counting chamber. The cell number was counted in all four corner chamber, and the average value was used to quantify the cell number as shown below:

$$\text{Cell quantity} \times 2 (\text{dilution}) \times 10^4 = \text{cell amount/mL}$$

Cells were seeded into 1% collagen (diluted in PBS) coated plates. For six or twelve well plates, 1×10^6 or 0.5×10^6 cells/well were added, respectively. The neo-natal rat cardiomyocytes (NRCM) culture was maintained at 37°C in 5% CO₂ in a humidified incubator. The medium was exchanged after 48 hours (h).

3.2.1.2 Immunofluorescence of NRCM cells

After the specific treatment of cells, the medium was aspirated, and the cells were fixed with 4% paraformaldehyde (PFA) for 15 min at room temperature (RT). The cells were then washed twice with PBS and incubated for 5 min with 0.05% Triton solution to permeabilize the cell membranes. Cells were washed twice with 1X PBS, before being incubated with 1x Roti-Immunoblock for 1 h at RT. Next, the cells were incubated overnight in the dark at 4°C with PBS containing the primary antibody against the protein of interest. Cells were then washed twice with 1x PBS and incubated overnight at 4°C in the dark with the specific fluorophore-conjugated secondary antibodies and DAPI to stain the nuclei (see Table 4 for respective dilutions). Finally, the cells were washed twice with PBS and images were taken using inverted fluorescence microscopy (Olympus).

3.2.1.3 Live cell imaging

The experiments were performed in a 6 well plate with cells incubated with 2 ml of medium. The cells were incubated with 10^2 μ M, 10^3 μ M and 10^4 μ M of H₂O₂ for 90 min in the climate chamber of the inverse fluorescence microscope (Olympus), keeping the ideal environment at 37°C, 5% CO₂, 57.37% lamp intensity and the exposure time of 20 ms. A 40x objective and a bright-field filter were used to capture the video. The time-lapse recording was setup at one frame every 20 min for a total duration of 24 h, with the first frame taken at 0 sec. The change in the morphology of cells was further analyzed with Image J.

3.2.1.4 Gene knockdown via siRNA transfection

After seeding NRCMs (day 1), the first transfection was performed after 19-20 h (day 2). For the transfection, 2 different siRNA constructs were used: a siRNA, which does not bind to mammalian mRNA to serve as a control (siRNA ctrl) and a second siRNA construct that binds to the mRNA of CTGF (siRNA ctgf) and blocks its translation. For each well (6 well plate) transfection, RNAi duplex-Lipofectamine RNAiMAX complexes were first produced as follows:

- (1) 9.9 μ l siRNA (22nM) was gently mixed with 900 μ l Opti-MEM (OM).
- (2) In parallel, 9.9 μ l Lipofectamine RNAiMAX was mixed with 900 μ l OM.
- (3) Both solutions were mixed and incubated for 20 min at RT.

For the transfection, the cells were washed twice with warm PBS. Then 600 μ l of 37°C warm OM was added together with 400 μ l of transfection solution in each well for 6 h at 37°C. Later the cells were washed twice with warm PBS and then incubated with fresh CM (day 2). The second transfection was performed 24 h after the first transfection as described above (day 3). The next medium change was conducted after 24 h (day 4). The next day (24 h later) the cells were used for particular experiments (Figure 13).

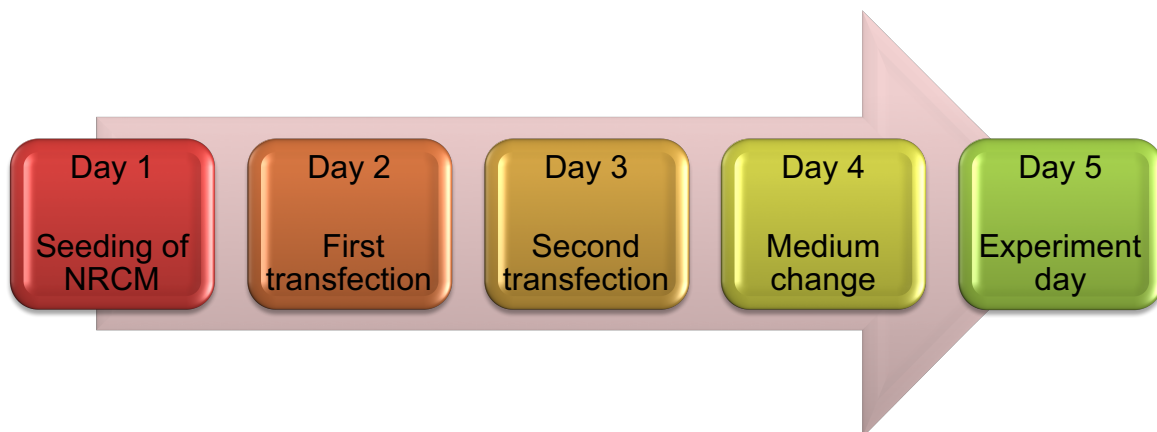


Figure 13 | Timeline for siRNA transfection.

3.2.2 Protein biochemical methods

3.2.2.1 Preparation of samples for western blotting

NRCMs were kept at 37°C and 5% CO₂ in a humidified incubator for 3-4 days with one medium exchange. On the day of the experiments, the cells were incubated with respective reagents for the definite period under controlled conditions. For protein analysis, the cells were lysed with ice-cold GST-fish lysis buffer and afterwards centrifuged at 13000 g for 10

min at 4°C to remove the cell debris. The supernatant was mixed with 4x sample loading buffer. Subsequently, the samples were incubated at 95°C for 5 min on a heating block and then gently centrifuged.

For reducing and non-reducing gel, the cells were lysed with a blocking buffer containing maleimide, which blocks the free thiol groups. The cells were later mixed with a 2x loading buffer (including maleimide) with and without, DTT respectively. To keep the disulfide bridges intact, non-reduced samples were not heated, whereas reduced samples were heated at 95°C for 5 min.

3.2.2.2 Protein quantification of samples via Bradford assay

To measure protein concentration, a colorimetric protein assay was used, which was based on a shift in the absorbance maximum when dye associates with proteins. A standard curve was established with BSA dilutions of known concentrations. 200 µl of 1x Roti-Nanoquant solution was mixed with 1 µl of the protein sample (diluted 1:150) and incubated for 5 min at RT. Together with the standard curve, the absorbance of each sample was detected at 595 nm with the microplate reader Flexstation3, and the protein concentrations were calculated by linear regression analysis.

3.2.2.3 Protein separation by SDS-polyacrylamide gel electrophoresis (SDS-PAGE) and detection by immunoblot

The electrophoresis for the immunoblotting was carried out in 12-15% SDS-PAGE. Protein samples from Section 3.2.2.1 were separated at 200 V on polyacrylamide gels. They were then blotted onto a nitrocellulose membrane for 1 h at 100 V. The membranes were blocked for 1 h with 1x Roti-Block, washed with the TBST and incubated overnight with a primary antibody at 4°C. The following day, the membrane was washed three times for 10 min with TBST and incubated with the secondary antibody for 1 h at RT. At the end, the membrane was washed again three times for 10 min with TBST. For protein-antibody complex detection, west-dura extended duration substrate was used, and for imaging a chemiluminescence imager equipped with the software Quantity one.

3.2.2.4 BIAM labeling assay

The N-(Biotinoyl)-N-(Iodoacetyl) Ethylenediamine (BIAM) labeling assay was performed to confirm Cys oxidation status change in response to ROS. Briefly, NRCMs were incubated at 37°C for 15 min in a NRCM medium containing 10^2 µM H₂O₂. Then the cells were washed with PBS and lysed with a BIAM labeling buffer. The control samples were treated without a

BIAM labeling buffer. Debris was removed by centrifugation at 13000 g for 10 min, and supernatants were further incubated at 37°C for 30 min. Excess BIAM was withdrawn from the lysates using protein desalting columns. The lysates were aliquoted into input and output samples. Output lysates were mixed with 50 µl streptavidin beads and incubated overnight on a shaker at 4°C. The next day the beads were washed thrice with a labeling buffer and the sample was cooked with loading buffer at 95°C for 5 min. Both input and output samples were then loaded for immunoblotting (Figure 14) (see Section 3.2.2.3).

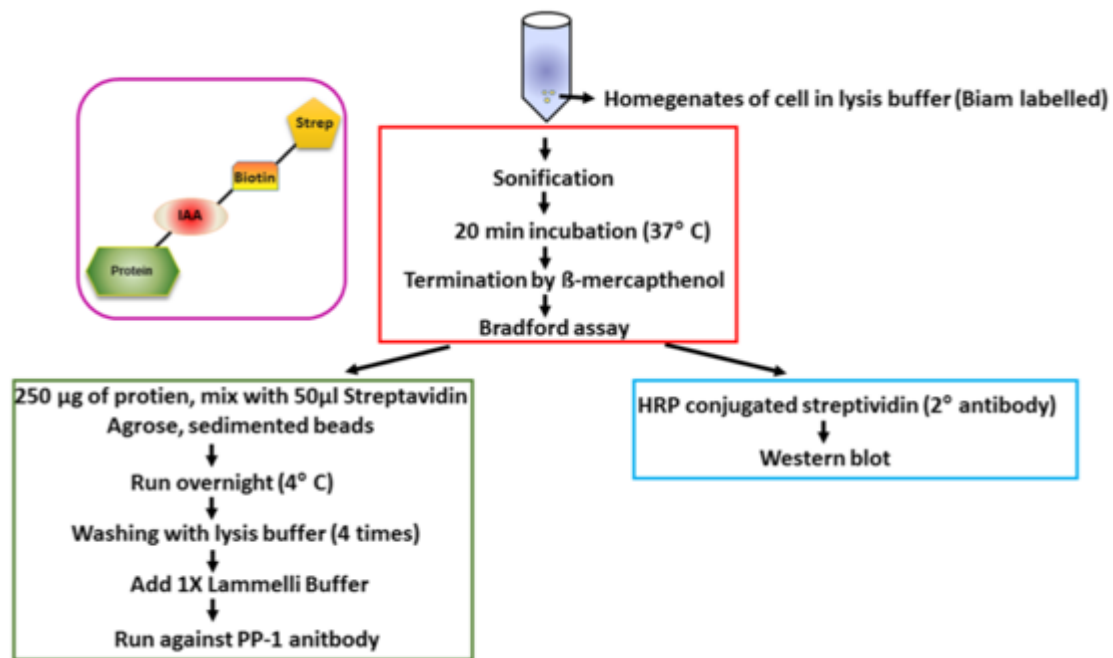


Figure 14 | General assay format for the BIAM labeling assay

3.2.2.5 Phosphatase activity assay

Total PP activity was measured using the EnzChek Phosphatase Assay Kit. Human heart tissue homogenates, NRCM and whole heart mouse tissue were generated in a passive lysis buffer (20 mM Tris-HCl pH 7.5, 1 mM Na₂EDTA, 150 mM NaCl, 1 mM EGTA, 1% Triton and protease inhibitor). Afterwards the protein content (20 µg total protein) was measured using a Pierce BCA Protein Assay Kit. The 100 µM 6,8-difluoro-4-methylumbelliferyl phosphate (DiFMUP) substrate was mixed with a 100 mM reaction buffer (sodium acetate pH 5.5), which was then added to the protein and incubated at RT for 15 min. Fluorescence was measured using an excitation wavelength of 360 nm and an emission wavelength detection at 460 nm on a Flexstation 3 (Molecular Devices; Figure 15). The fluorescence values were used as read out to calculate the PP activity.

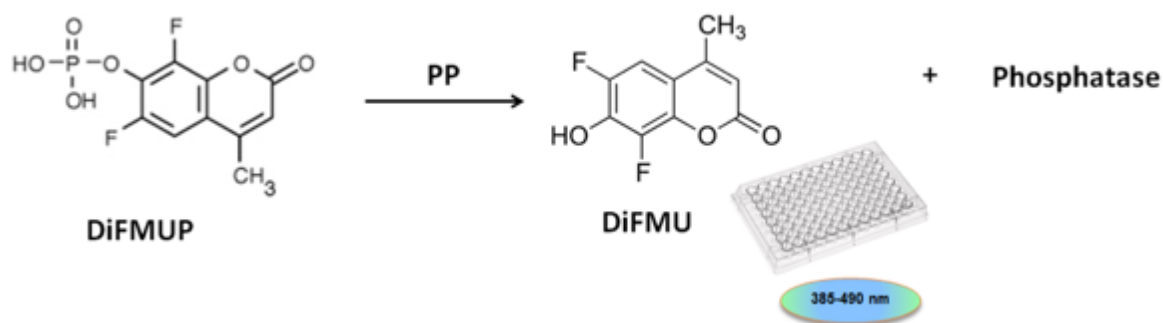


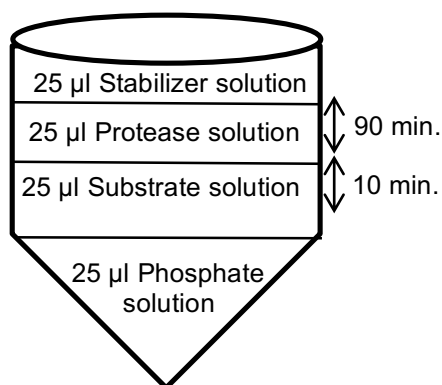
Figure 15 | Chromogenic reactions in the EnzChek Phosphatase Assay Kit. In the presence of reaction buffer, PP cleave the DiFMUP substrate, converting into phosphatase and hydrolyzed DiFMU (6, 8-Difluoro-7-Hydroxy-4-Methylumbelliferone) as a fluorogenic product (excitation/emission =385/490 nm).

For calculating the PP-1 activity, a recombinant protein (rPP-1) was used as a source of phosphatases and a commercial Promega PP activity assay. The phosphate activity was measured in 96 well formats and involved 'add, mix and read' steps (Table 14). The assay started with a reaction of rPP-1 with a reaction buffer including phosphorylated bisamide rhodamine 110 peptide (R110 substrate) and control 7-Amino-4-methylcoumarin (AMC substrate). The latter serves as a control for compounds that inhibit the protease. In this context, both R110 and AMC substrate were non-fluorescent. However, after the phosphatase reaction, the addition of a protease solution stopped the reaction. Then both substrates were digested, producing highly fluorescent R110 and AMC. A phosphate solution was prepared including MgCl_2 and MnCl_2 , and the assay was initiated by adding a 25 μl substrate solution. The reaction was continued for 10 min, and then a protease solution was added for 90 min. To stabilize the reaction, 25 μl of stabilizer solution was added. The R110 signal was measured using an excitation wavelength of 485 nm and an emission wavelength at 530 nm. The AMC signal was measured using excitation wavelength of 360 nm and emission wavelength at 460 nm. The ratio between R110 and AMC signal was used to calculate the PP-1 activity.

Table 14 | General assay format for 96 well plates used in Promega PP assay

Phosphatase solution		Reaction buffer (μl)	Control (μl)
Reaction buffer		5	5
PP-1		0	10
MgCl_2		1	1
MnCl_2		3.125	3.125
H_2O		15.9	5.9
Total		25	25

Substrate solution	
5x Reaction buffer (μl)	200
R11 substrate (μl)	1
AMC substrate (μl)	1
H_2O (μl)	798
Total (ml)	1
Protease solution	
5x Termination buffer (μl)	200



Protease Reagent (μl)	20
Okadaic acid (300 μM)	10
H ₂ O (μl)	770
Total (ml)	1
Stabilizer solution	
5x Termination buffer (μl)	200
Stabilizer reagent (μl)	1
H ₂ O (μl)	799
Total (ml)	1

3.2.3 Molecular biological methods

3.2.3.1 RNA isolation

NRCM were grown to 80% confluence, washed once with PBS and total RNA was extracted using the RNeasy mini kit, according to the supplier's procedure with an additional homogenization step using a QIA shredder. Afterwards the RNA concentration was determined using a Nanodrop 1000 device. Samples were stored at -80°C .

3.2.3.2 cDNA synthesis

cDNA synthesis was performed using Revert Aid First cDNA Synthesis Kit from 1 μg RNA (extracted from NRCM at step 3.2.3.1) according to manufacturer's protocol. Samples were stored at -20°C .

3.2.3.3 Quantitative real-time polymerase chain reaction (qRT-PCR)

qRT-PCR was performed to detect the expression level of various genes in NRCM. As the housekeeping gene, PBGD was used for normalization. In general, qPCR was performed using 5x HOT FIREPOL EvaGreen qPCR Mix Plus Kit as per manufacturer's protocol. Primers for each gene were diluted to 10 μM , and cDNA samples were diluted to 1:20 with RNase free water. For each sample four replicates were performed with a master mix for each gene, which was prepared as shown in Table 15:

Table 15 | Master Mix for qRT-PCR

Reagent	Volume
Primer for (10 pmol/ μ L)	1 μ L
Primer rev (10 pmol/ μ L)	1 μ L
Template DNA /Standard DNA (1:20)	1 μ L
RNase-free water	13 μ L
5x EvaGreen qPCR mix	4 μ L

Initially, 1 μ l of the diluted cDNA was added per well (Micro-Amp optical reaction 384-well plate), and mixed with 19 μ l of the master mix. Analyzes were carried out with TaqMan 7900HT Fast Real-Time-PCR System and as per the following program (Table 16):

Table 16 | qPCR Program

Cycle	Temperature	Time	Number of Cycles
Initial Denaturation	95°C	15 min	
Denaturation	95°C	15 s	30
Annealing	60°C	20 s	
Elongation	72°C	40 s	
Dissociation curve	95°C	15 s	
	60°C	15 s	
	95°C	15 s	

In the end, threshold cycle values (C_T) were calculated for each gene. Finally, to calculate gene expression, $\Delta\Delta c_t$ value was used by the following formula:

$$2^{-\Delta\Delta c_t} = 2^{(c_{tSample} - c_{tHousekeeping\ gene\ in\ sample}) - (c_{tControl} - c_{tHousekeeping\ gene\ in\ control})}$$

3.2.4 Analytical methods

3.2.4.1 Differentiation of disulfide bridges assisted by protein structural analysis with Pymol

Pymol 0.99rc6-bin-win32 was used to generate structural plots. A Pymol script file was prepared that enabled a prior selection of several residues and their labeling either as colored sticks or balls. Another feature of the Pymol program was the measurement of molecular distances that are summarized in the cross-correlation Table 21. The red dotted lines indicate the distances that could be measured (Figure 9) and that are also shown in

Table 21 for every reasonable combination of two Cys residues. Generally, the molecular distance for forming a bridge lies within 3 Å. However, small structural changes could also induce other proximities since most of the Cys residues are in about 6 Å distance (Figure 9).

3.2.4.2 Performing the oxidative stress experiment and sample preparations for the identification of various PTMs in PP-1

The experimental design was simplified by incubating GST-tagged PP-1A (supplied in 50 mM Tris-HCl, pH 7.5, 150 mM NaCl, 10 mM glutathione, 0.1 mM EDTA, 0.25 mM DTT, 0.1 mM PMSF, and 25% glycerol) in 50mM TRIS pH 7.5 buffer with the following four treatments: (1) without Mn^{2+} , without H_2O_2 , (2) without Mn^{2+} , 500 μM H_2O_2 (15 min), (3) 0.1 mM Mn^{2+} , without H_2O_2 , and (4) 0.1 mM Mn^{2+} , 500 μM H_2O_2 (15 min).

After the oxidation, 10 mM (final concentration) of iodoacetamide (IAA) were immediately added to the samples to block free Cys residues within 20 min. Then 4% SDS solution was added to obtain a final SDS concentration of 1% and immediately afterwards the samples were subjected to a filter-aided sample preparation (FASP) (Wisniewski et al., 2009). The buffer exchange was performed twice for 8 M Urea and twice for 50 mM ammonium bicarbonate (ABC). This was followed by an overnight protein digestion at 37°C using a digestion buffer (1 μg trypsin/100 ng with 50 mM ABC in 100 μl total volume). The membrane was not allowed to dry during the digestion.

The above experiment was repeated with the 100 ng of the His-tagged recombinant PP-1 alpha protein for each of the above conditions. The advantage of using this protein was that the reducing reagents were omitted from the buffers. Hence, the reactions can be performed under “real” oxidative conditions, and the FASP digestions were performed as described in above FASP protocol.

3.2.4.3 Peptide purification via stage tips

After 18 h the digest was spun through the filter and then subsequently washed with 50 μl 50 mM ABC buffer, 50 μl 0.5 M NaCl and 100 μl Stage A buffer. All fractions were collected in the microspin tube. Samples were then desalted according to the stage tip protocol (Rappsilber et al., 2007). Three discs of the desalting material (Empore SPE Disks; C18-Octadecyl, diameter 47 mm) were prepared in yellow pipette tips and activated with 50 μl methanol, washed with 50 μl Stage B buffer and then equilibrated with 100 μl Stage A buffer. After loading the sample, the stage tips were washed with another 100 μl Stage A buffer and

either stored until measurement or directly eluted with two times 40 μ l Stage B buffer into 96 well microtiter plates.

3.2.4.4 LC-MS/MS analysis

For the experimental design with GST-tagged PP-1A, measurements were performed on a Q Exactive Plus interfaced with an ultra-high performance liquid chromatography (UPLC) unit and a Nanospray Flex Ion-Source Ion Source. Peptides were loaded onto a C18 PepMap100 column (300 μ m internal diameter (i.d) x 5mm length) with 5 μ M particle size and 100 \AA pore width using the capillary pump of the UPLC. The loading pump was operated at a flow rate of 25 μ l/min with the loading buffer (1% acetonitrile (v/v), 0.1% formic acid (v/v) in water). For shorter separation, the nano-LC pump unit was operated at 0.5 μ l/min and delivered a linear binary gradient from 5% to 44% buffer B (80% acetonitrile (v/v) in 0.1% formic acid in water) in 28.53 min or 31.02 min, respectively. It was followed by a wash-out at 99% buffer B for 4 min and re-equilibration to 1% buffer for 10 min or 5 min, respectively. Data acquisition started at 2 min when the concentration of buffer B had increased by 5% from the starting conditions. The total acquisition time was 48.53 min or 47.52 min, respectively. The gradient times were adjusted to the dead volume of the pre-column 1 or pre-column 2 connections. The in-house columns were packed directly into liquid junction emitters (100 μ m i.d, tip 10+/- 1 μ m) with 2.4 μ m Reprosil Saphir fused silica beads. The length of the columns varied between 12 cm and 15 cm.

Ionization power of the source was 2.6 keV, and the MS spectra was recorded in 45 min with the following parameters: the full MS scan was 200 m/z with a resolution of 70,000; an automatic gain control (AGC) target value of 3×10^6 total ion counts with maximal ion injection time of 250 ms; the mass spectra were recorded in the profile mode within a mass range of 300-2500 m/z. All precursor ions with a charge state between two and six were chosen for fragmentation, applying an isolation window of 2 m/z if they met the intensity threshold of $6,7 \times 10^3$. This threshold is calculated from the AGC target value of 10^5 and the underfill ratio of 1%. To achieve this target value, a maximal injection time of 150 ms for any precursor was allowed. The MS/MS spectra were recorded with the following parameters: the resolution was 17,500 at 200 m/z. All selected Precursor ions underwent higher-energy collisional dissociation (HCD) fragmentation with a normalized energy of 30. MSMS spectra were recorded in the centroid mode within the mass range of 200-2000 m/z. All precursors being fragmented were dynamically excluded for 30sec within 10 ppm mass accuracy for a second fragmentation event in order to increase the sensitivity for low abundance precursors.

For the repeated experiment with the His-tagged PP-1, the experimental design for the measurement was altered again: the measurement time was now 60 min and the system was operated in the one-pre-column setup. Measurements were performed on a Q Exactive Plus System, interfaced with FlexSource Electrospray Ion Source. The spray voltage was 3.3 keV using a direct junction emitter (stainless steel emitter) with a capillary temperature of 250°C. No extra gas supply was used for sheath gas, auxiliary gas or spare gas. Data acquisition was performed in the positive ion mode. MS Spectra were recorded with the following parameters: resolution at 200 m/z was 70,000, AGC target value 3×10^6 , max injection time 160 ms, and all MS spectra were recorded in profile mode within a mass range of 200-2000 m/z. All precursor ions with a charge state between 2 and 6 were chosen for fragmentation, applying an isolation window of 2 m/z if they met the intensity threshold of 6.7×10^3 . The threshold was calculated from the AGC target value of 1×10^5 and the underfill ratio of 1% and underwent HCD fragmentation with a stepped energy fragmentation scheme. This scheme included three fragmentations at the normalized fragmentation energies 30, 35 and 40 and the subsequent overlay of the obtained spectra to a single spectrum. The MSMS spectra were recorded with the following parameters: resolution at 200 m/z 17,500 and max injection time 150 ms. All MSMS spectra were recorded in the centroid mode within the mass range of 200-2000 m/z. Finally, all precursors within 10 ppm mass accuracy eluting within a time frame of 30sec were excluded from fragmentation for a second time to increase the sensitivity for low abundance precursors.

3.2.4.5 Data analysis with Peaks 7.0 software

Spectra were searched with the Peaks 7.0 search engine. Briefly, regular redox-modifications were examined, and a search strategy for the identification of disulfide-linked spectra from a known/identified protein was established. For the former, the following parameters were used: the database was UniProt human (July, 7th, 2015) comprising 68605 proteins. Variable modifications in the case of GST-tagged PP-1 used were Carbamidomethylation (c, +57.02), Cysteine oxidation to cysteic acid (c, +47.98), Cysteinyl C (c, +119.00), Deamidation (NQ) (d, +0.98), Disulfide Bridge unpaired fragmentation (d, -2.02), Dehydroalanine C (d, -33.99), Deoxidation (M) (d, +31.99), Glutathione disulfide (g, +305.07), Hydroxylation (h, +15.99), Oxidation (M) (o, +15.99), Oxidation (HW) (o, +15.99), Oxidation or Hydroxylation (C) (o, +15.99), Persulfide C (p, +31.97) and Phosphorylation (STY) (p, +79.97). The parent mass tolerance allowed was set to 10 ppm and fragment mass tolerance was set to 0.02 Da. The enzyme specificity used was Trypsin, missing cleavages were limited to four, but cutting before Proline was authorized in contrast to the standard

Trypsin settings. Variable modifications permitted for the search were five. Extraction of data points was set to the top 100 peaks for each spectrum.

Variable modifications in the case of His-tagged PP-1 used were: Acetylation (N-term) (a, +42.01), Arginine oxidation to glutamic semialdehyde (a, -43.05), Carbamidomethylation (c, +57.02), Deamidation (NQ) (d, +0.98), Disulfide CID breakage (d, +33.99), Dehydroalanine (d, -33.99), Dehydration (d, -18.01), Dihydroxy (d, +31.99), Hydroxylation (h, +15.99), internal disulfide bond (i, -1.01), internal disulfide bond unpaired fragmentation (i, -2.02), Methyl ester (m, +14.02), Oxidation (M) (o, +15.99), Oxidation (HW) (o, +15.99), Oxidation or Hydroxylation (C) (o, +15.99), Proline oxidation to pyroglutamic acid (p, +13.98), Sulfone C (s, +47.98) and S-Persulfide C (s, +31.97). Otherwise the same conditions were used as with the GST-tagged protein.

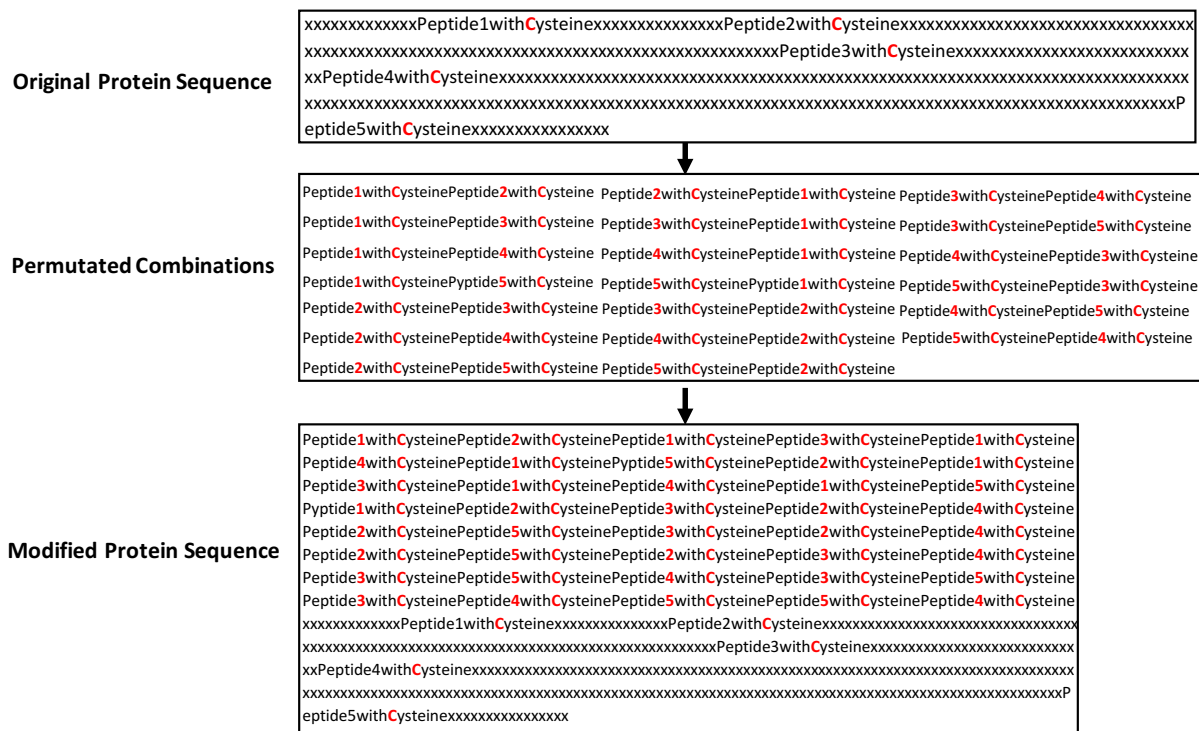
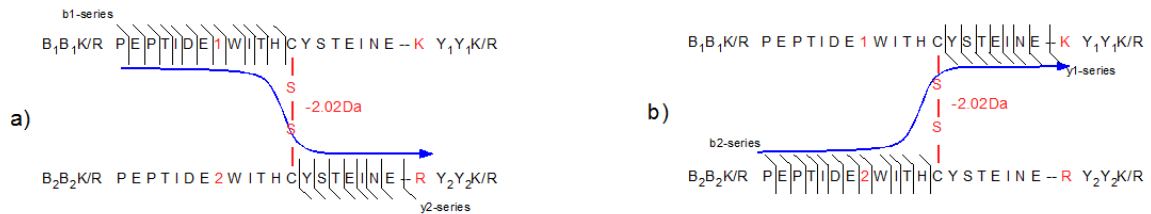


Figure 16 | Scheme is showing the generation of permuted Cys-peptide database. The top box shows the original protein sequence with the Cys-containing peptides indicated within any other sequence x. The Cys residues are highlighted in bold red. In the middle box, the Cys-containing peptides were excised and permuted with each other. In the bottom box, all combinations were reassembled with the original protein sequence to form the new database entry.

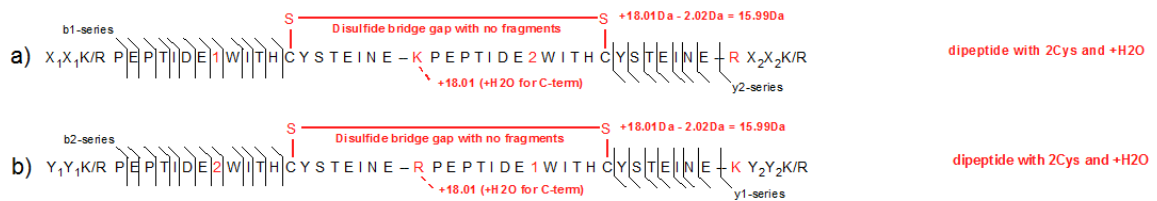
Since a database search from a linear protein database does not allow the simultaneous detection of two structurally close but sequence-wise distant peptides, an automatic search strategy for this data was created. For the identification of disulfide-linked peptides, a new linearized database entry was created that contained two peptides combinations in a permutation. An artificial disulfide-protein was incorporated to the normal human database in order to perform the search with the normal search engine. This protein allowed the detection

of the intact disulfide-linked peptides from a non-reduced sample, considering them as longer peptides with a missed cleavage in the middle either as AB or BA combination. The method used to detect these peptides is described in detail in Figure 16 (above).

1) Starting Point: Two Cysteine Peptides somewhere in the protein cause a data search problem



2) Solution 1: Permuted Cysteine Database to solve the data Search Problem...but only small fragments!



3) Solution 2: Identification of Disulfides Spectra with b - or y- type series that jumps the gap!

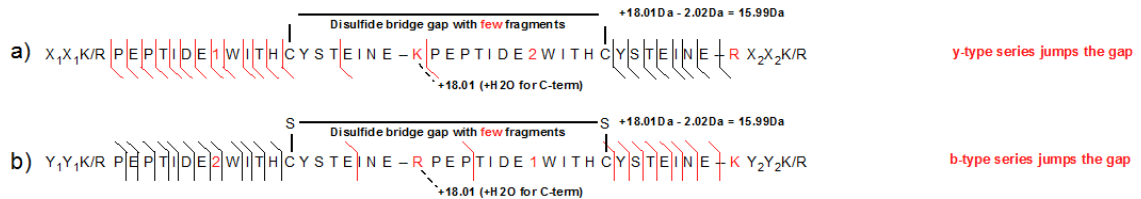


Figure 17 | A robust strategy behind the identification of disulfide bridges. Point 1) brings out the drawbacks searching disulfide-link spectra in a normal linear database when the peptides are distant in the protein sequence. Fragmentation of one peptide might be favored and then it jumps over the disulfide-link. Point 2) and 3), illustrated how a novel solution is applying permuted combination of the Cys peptides in the database and how further identification works. Hereby case a) represents the order of Peptide1Peptide2 and case b) the reverse order Peptide2Peptide1 for the spectrum annotation.

From previous studies on cross-linked peptides, often the b-type or the y-type ion series breaks at the site of crosslinking so that a dipeptide is identified by a partial series from the one and a partial series from the other peptide. There are also studies about branched peptides, which observed that the ion series might jump from one peptide to the other over the site of interaction (e.g. Hsiao et al., 2009a). Measurements on the QE favors the generation of y-type ion series. In order to unequivocally identify two disulfide linked peptides, they need to show fragmented ions in the spectrum that argue for this “jumping the gap”-mechanism. When searching the data on behalf of the permuted database, the spectra have to match both the intact molecular weight and the fragmentation pattern. For these peptides, two main characteristics were taken into account: the loss of two hydrogen (-2.02 a.m.u.) Da because of the disulfide bridge, and the hydroxylation of the free C-terminus of the second peptide (+18.01 a.m.u.), that is now buried in the sequence of the permuted

database. This provides a C-terminal modification (e.g. positioned at the K or R for a trypsin digestion) of +15.99 a.m.u. (equal to oxidation). In order to evaluate whether spectra were correctly annotated, the search was conducted both for the position of the +15.99 a.m.u modification as well as for the occurrence of large molecular weight fractions that complemented either the y-type or the b-type ion series (Figure 17).

3.2.5 Statistical analysis

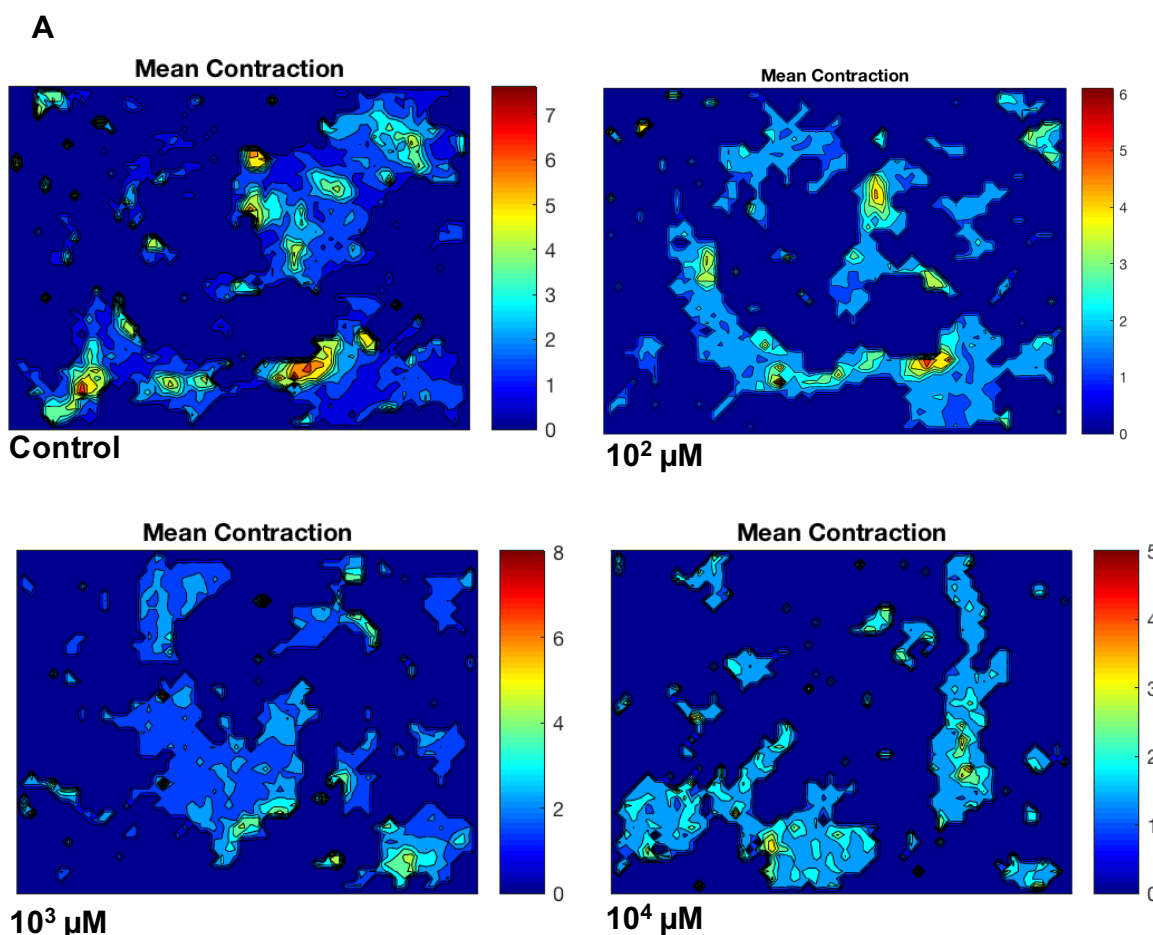
Data are reported as the mean of $n=2$ or mean \pm SEM of $n>3$. Experiments with $n=2$ are showing the solid data as second independent experiments were performed to confirm the finding. Statistical analyses were performed with GraphPad Prism 6. Multiple group comparisons were calculated by one or two-way ANOVA, followed by Bonferroni's multiple comparison tests. Comparison of two group experiments was performed using a t-Test. The significance definitions are $*p<0.05$, $**p<0.01$, $***p<0.001$ and $****p<0.0001$ vs. control.

In the case of mass spectroscopy experiments, samples were injected twice in the instruments. Only one out of two experiments give us consistent results along with the theory. Spectral count is different for every Cys site and every modification.

4 Results

4.1 Physiological effect of redox regulation in cardiac myocytes

To initially investigate the effect of oxidative stress on cardiac myocytes, a very simple experiment was established by making live cell imaging of NRCM with increasing concentrations of H_2O_2 to force oxidative stress. NRCM was incubated at 37°C until it was fully mature and beating. A movie was recorded with one frame taken every 20 min for 24 h (with the first frame taken at 0 sec), with control ($0\ \mu\text{M}$), $10^2\ \mu\text{M}$, $10^3\ \mu\text{M}$ and $10^4\ \mu\text{M}$ of H_2O_2 (movie available on CD; Figure 18). Without H_2O_2 , the NRCM cell contraction was, as expected, normal and its hold same with exposure to the physiological dose of $10^2\ \mu\text{M}$ H_2O_2 . With higher concentration doses of $10^3\ \mu\text{M}$, reduced contraction of cells was observed and at $10^4\ \mu\text{M}$ cell death was observed. After video recording of the cultured NRCM, a matlab based script according to Huebsch et al. was used to generate a heat map of the mean contraction of the contractile regions for each given H_2O_2 concentrations (Huebsch et al., 2015; Figure 18.A). The same script was afterwards used to quantify the contraction velocity and the relaxation velocity of the myocytes at each H_2O_2 concentration. From this values the relaxation-contraction ratios were calculated to give a measure of myocyte vitality.



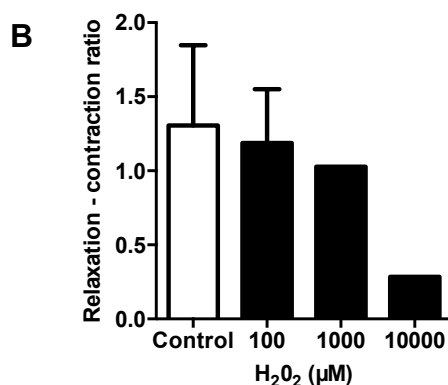


Figure 18 | Analysis of NRCM relaxation-contraction ratio exposed to oxidative stress. (A) Heat map depicting the mean of the time-averaged magnitude of every motion (myocyte contraction). A center of mean contraction is defined as a region from which contractions (inward motion) and relaxation (outward motion) are maximized over the time-averaged course of the movie. (B) Quantitative analysis representing ratio of relaxation to contraction. Values are given as mean \pm SEM, n=2-4.

Quantitative analysis of the ratio between contraction to relaxation, suggested that ratios remains similar with 10^2 μ M H₂O₂, and gradually decreased at higher concentrations of H₂O₂ (Figure 18.B).

4.2 Redox regulation of PP-1 in the heart

4.2.1 Importance of PP-1 in physiological functioning of NRCM

4.2.1.1 Investigation of phosphatase activity in human heart samples, NRCM, and whole heart mouse tissue

To calculate Phosphatase activity, two different kits were used. For human heart samples, NRCM and whole heart tissue Enzchek kit, and for recombinant protein the Promega phosphatase activity assay were used (Section 3.2.2.5).

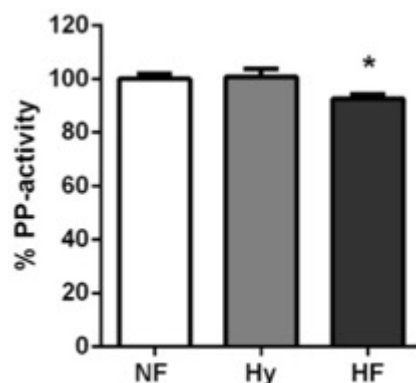


Figure 19 | Phosphatase activities in human NF, Hy and HF hearts. Total phosphatase activities of human heart homogenates (20 μ g total protein); non-failing (NF), hypertrophy (Hy) and heart failure(HF) patients were measured using EnzChek Phosphatase Assay Kit. Values are given as

mean \pm SEM, NF=5, Hy=15 and HF=23. Statistical comparison was performed by t-test, * $p < 0.05$ vs. NF.

To differentiate between different types of phosphatases, i.e. PP-1 and PP-2A, OA as phosphatase inhibitor, was used in the Enzchek kit assay. Total phosphatase activity in heart failure (HF) patients was 7.38% lower as compared to non-failing (NF) and hypertrophy (Hy) samples (Figure 19). The inhibitory activity of 10 and 100 nM of OA was expected to inhibit mainly PP-2A and PP-1 activity respectively. In NRCM and total heart tissue from mice, PP-1 contributes to approximately 10% of total PP-activity (Figure 20). Heart samples were kind gift from Dr. Thomas H. Fischer, Clinic for Cardiology and Pneumology, Goettingen.

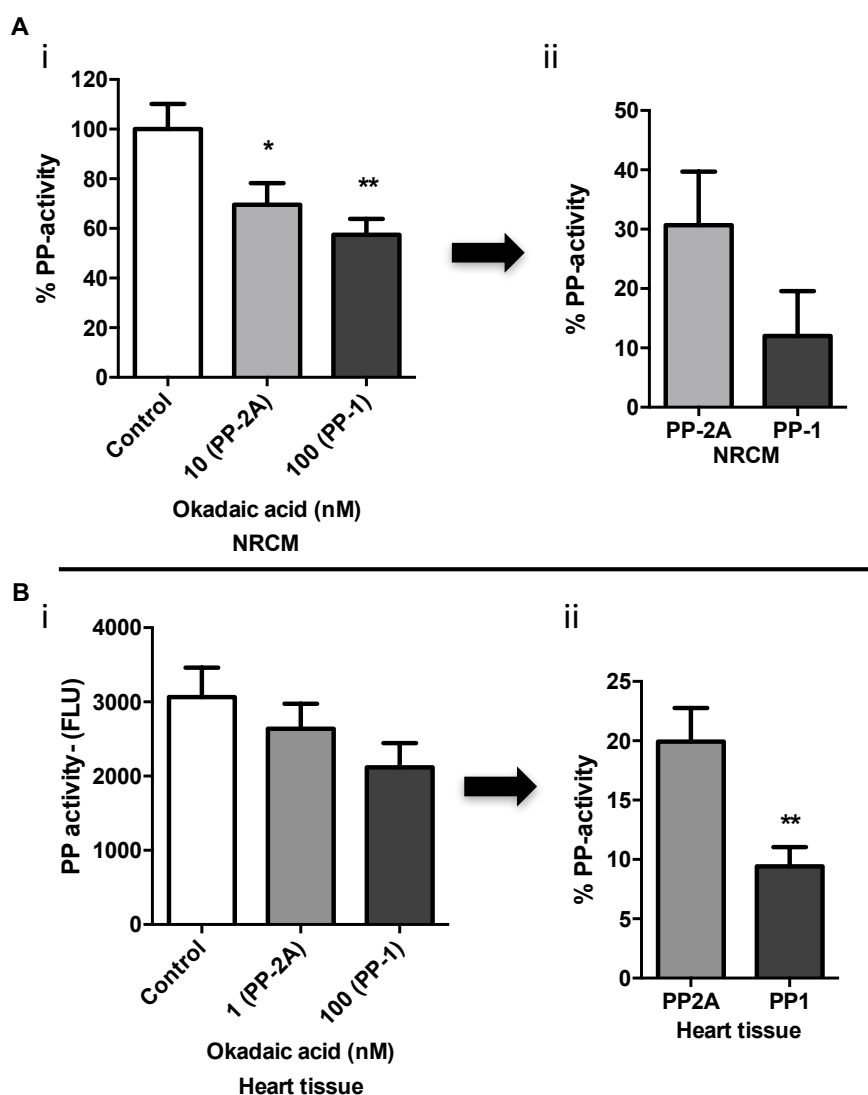


Figure 20 | Phosphatase activity in NRCM and whole heart tissue of mouse. Total phosphatase activities depicting percentage of PP-2A and PP-1 activity in (A) NRCM and (B) whole heart tissue of mouse. Activity was measured using ProFluor Ser/Thr PPase Assay in the presence of 10 nM (PP-2A) and 100 nM (PP-1) OA. Panel A, B – Figure ii represents the %PP-activity after calculations as per following formula $\{PP-2A = [Control - 10(PP-2A)]/Control$; $PP-1 = [10(PP-2A) - 100(PP-1)]/Control$. Values are given as mean \pm SEM, n=3-6. Statistical comparison was performed

by t-tests, * $p < 0.05$, ** $p < 0.01$ vs. control (Panel A, B – Figure i), ** $p < 0.01$ vs PP-2A (Panel A, B – Figure ii).

4.2.1.2 Impact of oxidative stress on phosphatase activity in NRCM and rPP-1

To test the effect of oxidative stress on PP-1 activity, in the presence of Mn^{2+} buffer, the experiments were conducted using either recombinant PP-1 alpha (rPP-1-GST tagged) *in vitro* or in living neonatal rat cardiomyocyte (NRCM) treated with the oxidizing agent H_2O_2 . Results show that increasing concentrations of H_2O_2 induced a significant reduction in recombinant PP-1 activity (Figure 21.A); with a maximum effect of H_2O_2 after 10-30 min incubation time (Figure 21.B). Consistently, the reducing agent Tris-(2-carboxyethyl) phosphine (TCEP), when added to recombinant PP-1, reversed H_2O_2 -induced PP-1 inactivation (Figure 21.C). However, when NRCM was treated with H_2O_2 , the net decrease in PP-activity reached around 25%, indicating that not only PP-1 activity was affected by oxidation (Figure 22).

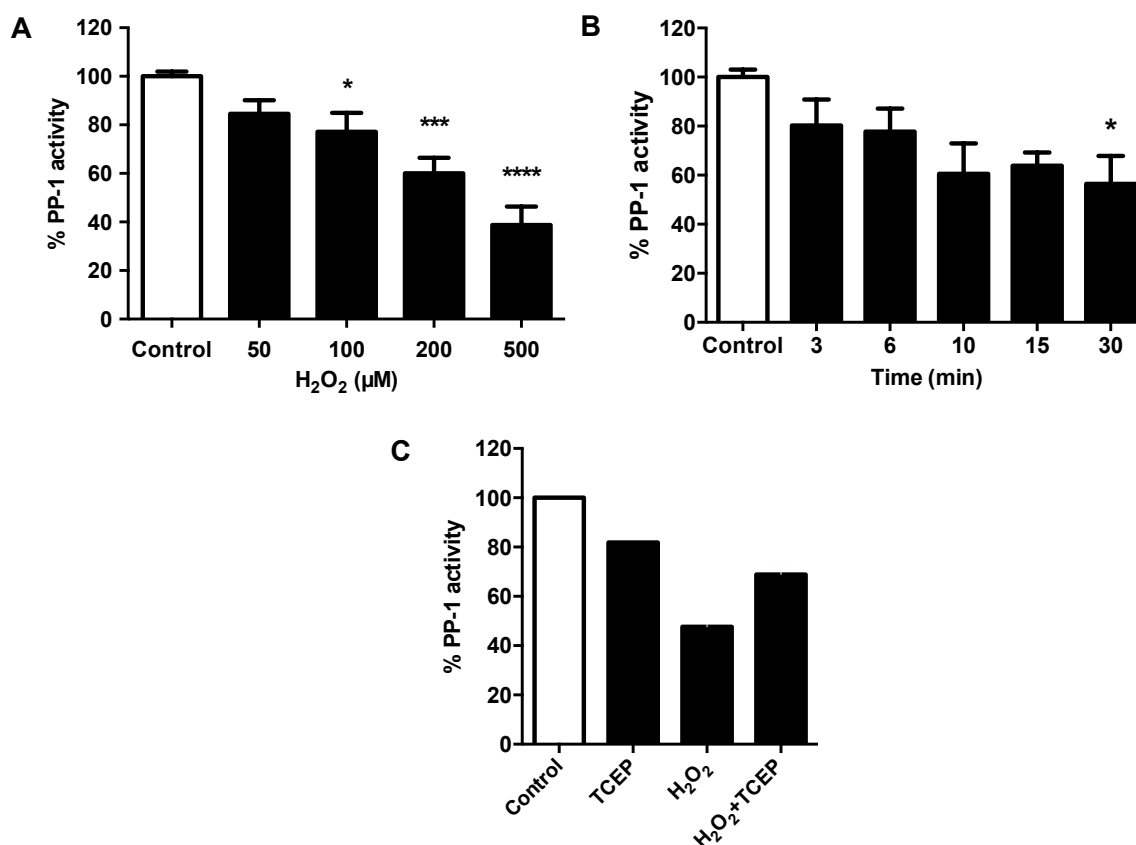


Figure 21 | Phosphatase activity in rPP-1. (A) Activity of recombinant-PP-1 (rPP-1) incubated with H_2O_2 (0, 50, 100, 200, 500 μM) for 10 min. Values are given as mean \pm SEM, $n=3-4$. (B) The activity of rPP-1 incubated with H_2O_2 (200 μM) for the indicated time period. Values are given as mean \pm SEM, $n=2-4$. (C) Reversibility of rPP-1 activity, when incubated with H_2O_2 (200 μM , 15 min) followed by TCEP (100 mM) for 5 min. Values are given as mean, $n=2$. Statistical comparison was performed by one-way ANOVA, and post hoc correction with Bonferroni's multiple comparison tests, * $p < 0.05$, *** $p < 0.001$, **** $p < 0.0001$ vs. control.

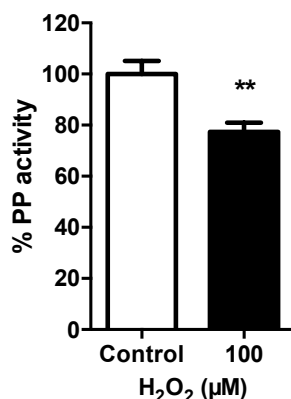


Figure 22 | Phosphatase activities in NRCM. Total phosphatase activity in NRCM incubated with H₂O₂ (100 μM) for 3 min was measured using EnzChek Phosphatase Assay Kit. Values are given as mean ± SEM, n=5. Statistical comparison was performed by t-test, **p<0.01 vs. control.

4.2.1.3 Impact of oxidative stress on cross talk between PKA and PP-1 signaling pathways

Regarding the impact on downstream targets, immunoblotting revealed that the phosphorylation status of classical PP-1 downstream target proteins such as phospholamban (PLB) and cardiac myosin binding protein-C (cMyBP-C) were differentially affected by H₂O₂, indicating a complex layer of regulation of both redox-sensitive kinases and phosphatases (Figure 24.A). Whereas the phosphorylation status at Thr³⁵ of protein phosphatase inhibitor-1 (I-1), a crosstalk protein between protein kinase A and PP-1 signaling showed a bell-shaped phosphorylation response with a maximal peak at 100 μM (Figure 23).

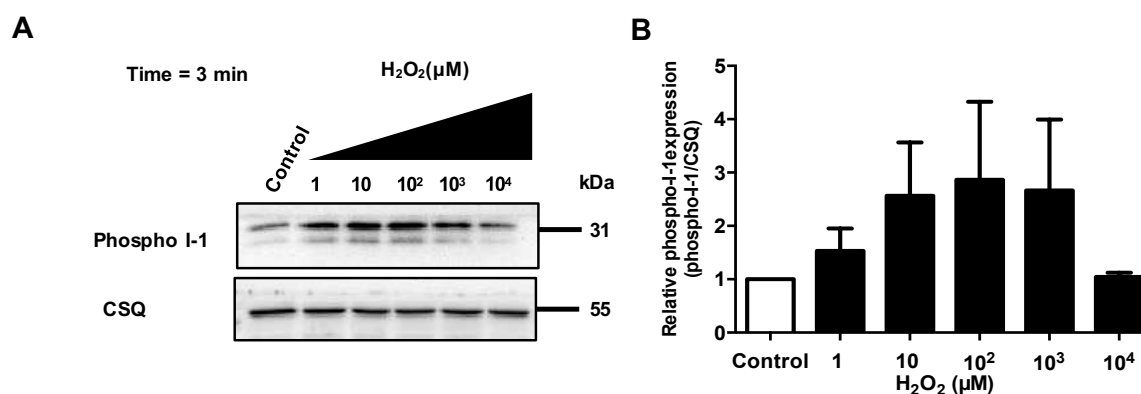


Figure 23 | Phospho I-1 phosphorylation after H₂O₂ treatment. (A) Immunoblot and (B) quantification of concentration dependency of H₂O₂ mediated phospho I-1 expression in NRCM. The analysis was normalized to CSQ, and the change in phospho I-1 expression was estimated relative to the control. Values are given as mean ± SEM, n=3. Statistical comparisons were performed by one-way ANOVA, and post hoc correction with Bonferroni's multiple comparison tests, *p< 0.05 vs. control.

There was no effect of H₂O₂ at physiological concentration on PLB phosphorylation at Ser¹⁶ (p-PLB-Ser¹⁶) or cMyBPC phosphorylation at Ser²⁸² (p-cMBPC-Ser²⁸²) after 3 min (Figure 24.C). Time-dependent experiments, however, showed a remarkable decrease in PLB-Ser¹⁶

phosphorylation after 10 min. In contrast, cMyBPC-Ser²⁸² phosphorylation was bell-shaped, peaking after 10 min of H₂O₂ incubation (Figure 24.B).

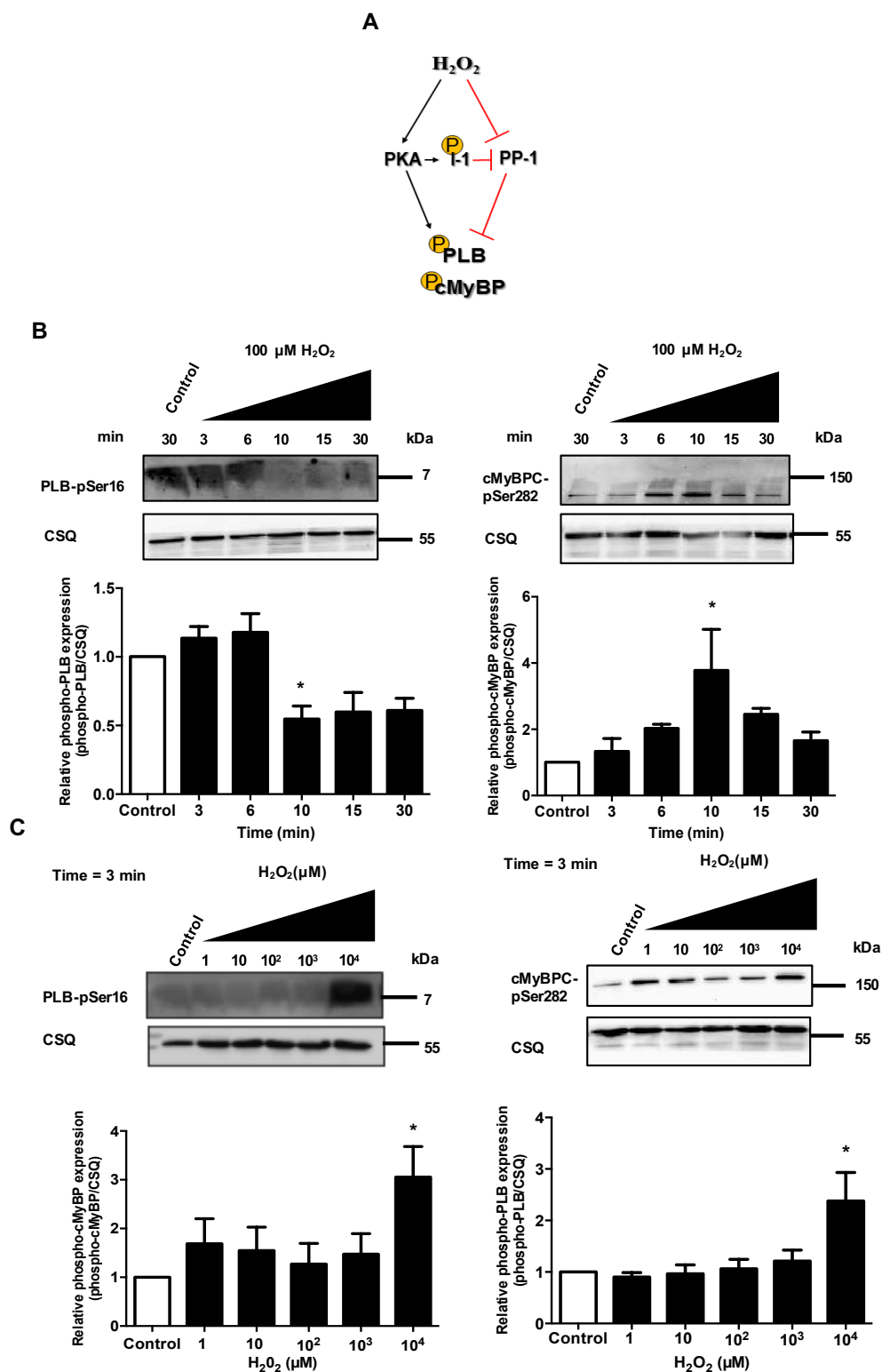


Figure 24 | Putative mechanism of PKA activation and PP-1 inactivation by H₂O₂. (A) The mechanism is showing the summary of activating and inhibitory effect of H₂O₂ on PKA and PP-1 respectively, and hence changes in phosphorylation of downstream cardiac protein, PLB and cMyBPC. Immunoblot and quantification of (B) time course and (C) concentration dependency of H₂O₂ mediated PLB-pSer¹⁶ and cMyBPC-pSer²⁸² expression in NRCM. The analysis was normalized to

CSQ, and the change in PLB-pSer¹⁶ and cMyBPC-pSer²⁸² expression was estimated relative to the control. Values are given as mean \pm SEM, n= 3. Statistical comparisons were performed by one-way ANOVA, and post hoc correction with Bonferroni's multiple comparison tests, *p < 0.05 vs. control.

4.2.2 Identification of redox-sensitive Cys in PP-1

4.2.2.1 Investigating the disulfide bridges in phosphatases via immunoblotting

A PKA regulatory subunit-1 (PKA RI) dimer formation in NRCM was established to identify any disulfide bridges within the PP-1 protein. In the presence of maleimide NRCM were then treated with increasing concentrations of oxidizing agents, i.e. diamide and H₂O₂. Afterwards the sample was processed on a gel under non-reducing conditions which formed a RI subunit of PKA and resulted in an SDS-resistant dimer.

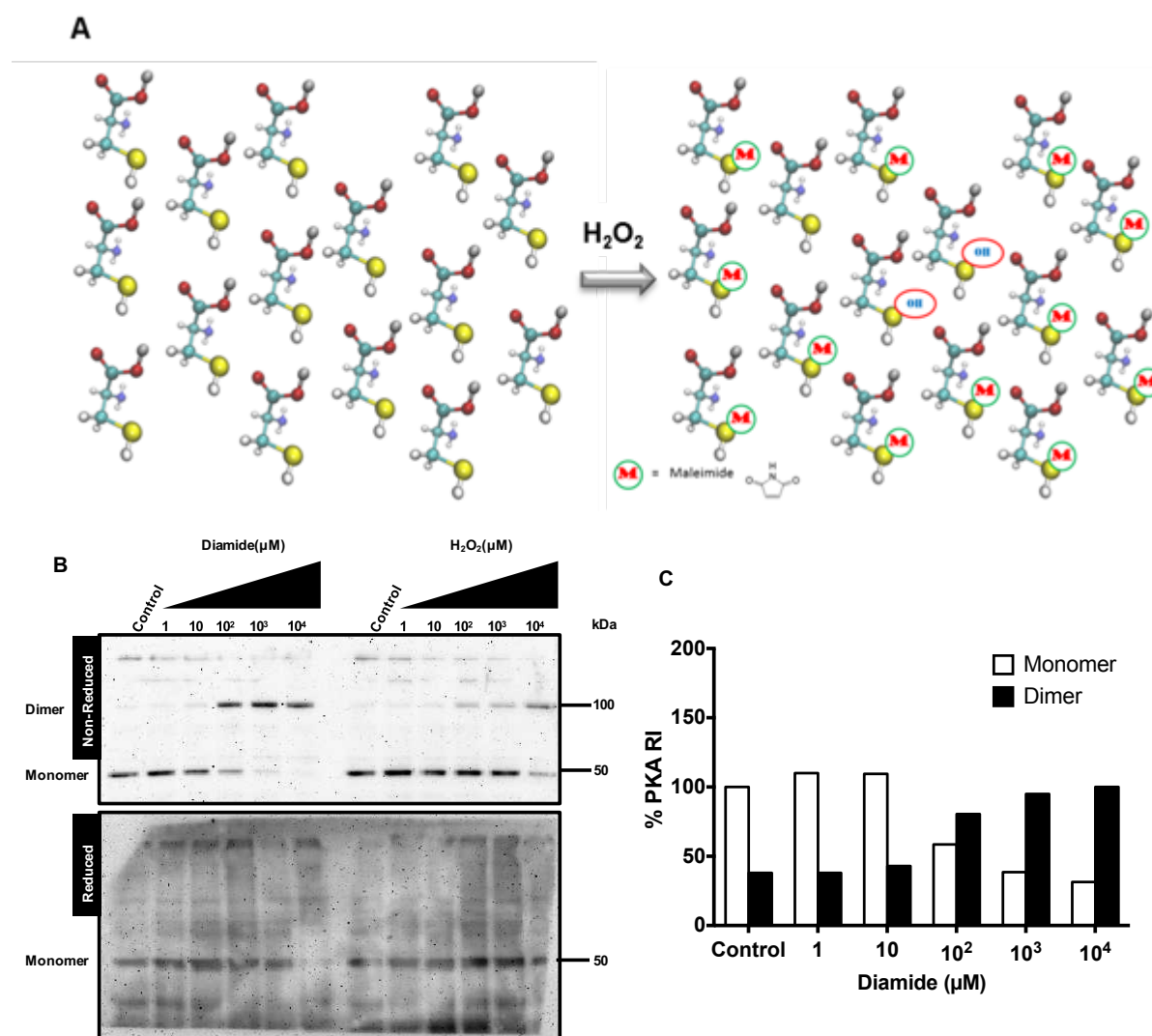


Figure 25 | Effect of increasing concentration of diamide and H₂O₂ (15 min) on NRCMs under non-reducing and reducing conditions in PKA. (A) Mechanism depicting the blocking of free thiols with maleimide during the oxidation process in the protein (B) Immunoblots probed with anti-PKA RI and (C) densitometric analysis showing the percentage of PKA-RI that exists as monomer or dimer. Values are given as mean, n=2.

This dimer formation was no longer present when samples were run on reduced gel (inclusive of DTT). This data shows a shift of bands from 50 kDa to 100 kDa, was due to intermolecular disulfide bridges formations. disulfide bridge formation was dose dependent, since more than 50% of PKA RI in NRCM becoming dimeric after 15 min with 100 μ M, in contrast to the treatment of H₂O₂, same observation was observed at 10⁴ μ M (Figure 25.B). The bar chart shows the quantitative data of two experiments, when treated with diamide, indicating the percentage of PKA-RI having monomer and dimer formation (Figure 25.C).

The same samples were run which were used to establish PKA-RI dimer formation. This step allowed us to identify any inter-molecular disulfide bridge formations in PP-1. Figure 26 shows that with dose dependence of diamide, PP-1 expression decreased, and no shift in the gel was observed as per PKA immunoblots. The bar chart shows the quantitative data of two experiments, when treated with diamide, indicating the decreasing expression of PP-1 (Figure 26.B). However, interestingly a dimer formation was observed at 70 kDa both in control and increased concentrations of diamide, which were less expressed at 10³ μ M diamide and eventually disappeared at 10⁴ μ M diamide.

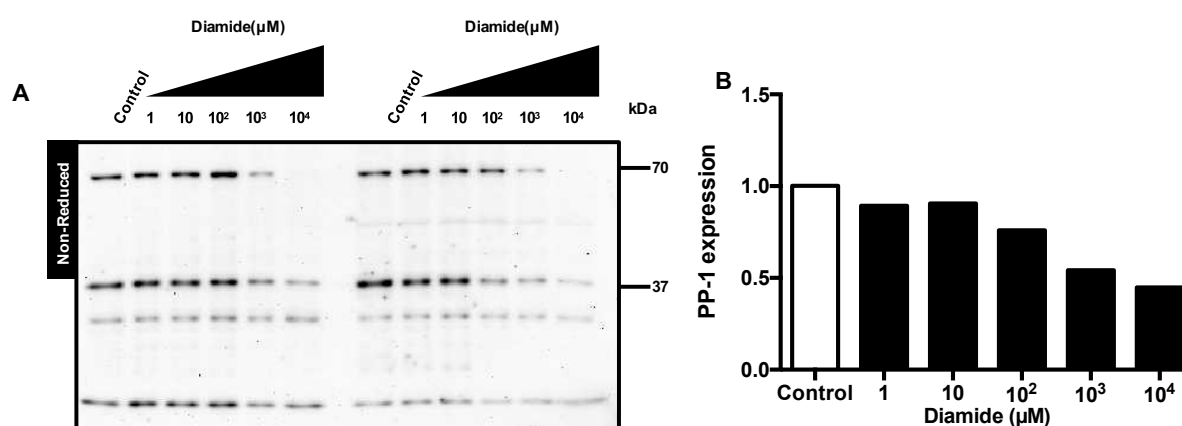


Figure 26 | Effect of increasing concentrations of diamide (15 min) on NRCMs under non-reducing condition probed with PP-1 (catalytic subunit). (A) Immunoblot representing the decreasing expression of PP-1 (37 kDa) and a dimer formation at 70 kDa, which eventually disappears at 10⁴ μ M diamide. (B) Densitometric analysis showing the decreasing expression of PP-1. Values are given as mean, n=2.

PP-2A was examined more closely to check for disulfide bridge formation within the family of phosphatases. Some literature has suggested that PP-2A might also have redox-sensitive Cys. Therefore, the same samples were run on non-reduced gel with PP-2A antibody. In the end, it was discovered that no shift in gel occurred. However, at 10⁴ μ M diamide, less expression of PP-2A was observed which concurs with the findings of PP-1 (Figure 27).

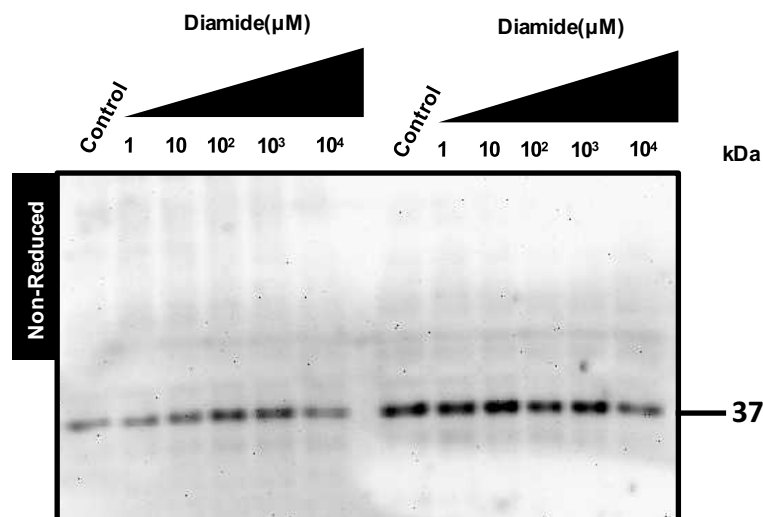


Figure 27 | Effect of increasing concentration of diamide (15 min) on NRCMs under non-reducing conditions probed with anti-PP-2A. Immunoblot representing the reduction of expression of PP-2A (37 kDa) at 10^4 μM diamide. Similar results were obtained in a second independent experiment.

While running blots for PP-1, PP-2A and PKA under non-reducing and reducing conditions, an interesting finding was discovered regarding SERCA2a. Without DTT as the reducing agent, a band shift was observed in the non-reducing state with respect to SERCA2a, which was not visible in PP-1 and PP-2A blots. Hence, in conclusion, SERCA2a, which has redox-sensitive Cys, appears to lead to a band shift, whereas phosphatases do not (Figure 28).

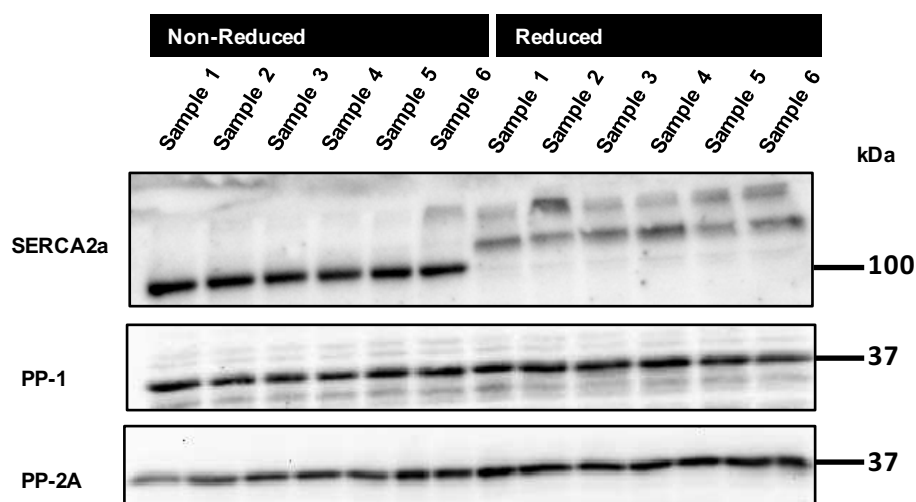


Figure 28 | Cell lysates from NRCM analyzed under non-reducing and reducing conditions probed with anti-SERCA2a, anti-PP-1 (catalytic subunit) and anti-PP-2A. Immunoblots representing a shift in band with respect to SERCA2a, which is not visible for PP-1 and PP-2A. Similar results were obtained in a second independent experiment.

To further confirm that PP-1 Cys-oxidation status changes in response to ROS, a cell permeable, biotinylated iodoacetamide (BIAM) was applied to label free Cys thiol groups

following exposure of NRCM cells to oxidizing agent H_2O_2 . For HRP conjugated streptavidin immunoblots, results showed that by the addition of H_2O_2 , unexpectedly there was little difference between control and treated cells. However, in comparison to pH 6.5, a visible change occurred with the sample treated with pH 8.5, after BIAM and H_2O_2 were added. No change was observed in the pull-down of PP-1 expression all above-mentioned conditions (Figure 29).

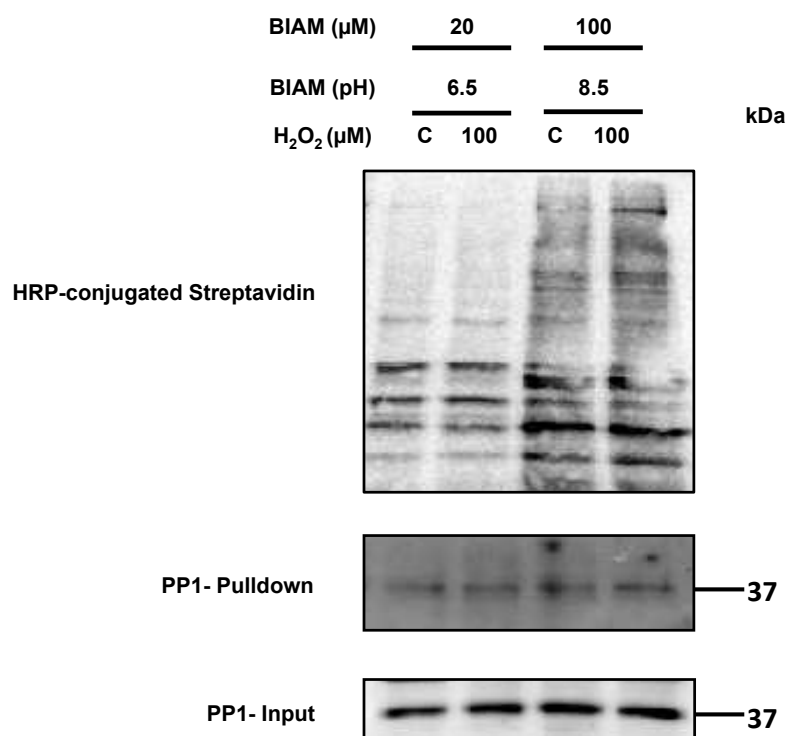


Figure 29 | Identification of oxidized proteins due to redox active Cys. NRCM were treated with 0 μ M (Control) and 100 μ M H_2O_2 for 15 min, followed by an incubation with BIAM (20 μ M - 6.5 pH and 100 μ M - 8.5 pH) for 30 min and protein-BIAM adducts were purified using streptavidin pull-down and then subjected to Western blot analysis using PP-1 antibodies in BIAM labeling buffer. Similar results were obtained in a second independent experiment.

4.2.2.2 Analysis of disulfide bridges from bioinformatics tools in PP-1

To calculate pK_a values, PROPKA 3.1 (Søndergaard et al., 2011) was used, to semi-quantitatively estimate pK_a values of all the Cys residues of PP-1A. It is empirical pK_a predictors, based on the better physical description of the desolvation and dielectric response for the protein. Table 18 shows that out of thirteen Cys residues, only two (Cys¹⁵⁵ and Cys¹⁷¹) had the lowest pK_a i.e. 8.01 and 8.97 respectively.

Table 18 | Analysis of pKa of PP-1A (PDB id: 4MOV) by PROPKA 3.1. The representative table represents the pKa of all Cys in the PP-1 α . Cys¹⁵⁵ and Cys¹⁷¹ are susceptible to oxidation because of pK_a near to 8.

Pos.	pKa
CYS 39 A	18.69
CYS 62 A	12.64
CYS 105 A	12.94
CYS 127 A	10.12
CYS 140 A	13.30
CYS 155 A	8.01
CYS 158 A	10.65
CYS 171 A	8.97
CYS 172 A	12.59
CYS 202 A	11.56
CYS 245 A	18.55
CYS 273 A	9.76
CYS 291 A	11.94

The Cysteine Oxidation Prediction Algorithm (COPA) is an algorithm used to predict oxidation-susceptible sites, which can further help a protein's Cys residues susceptible to redox-mediated regulation and identify possible enzyme catalytic sites with reactive cysteine thiols (Sanchez et al. 2008). Table 17 demonstrates that Cys 39, 155, 171 and 245 were susceptible to oxidation by sulfur distance, and that the oxidation status was reduced. Also, Cys¹²⁷ and Cys²⁷³ are vulnerable to oxidation due to a low pK_a and a reduced oxidation state.

Table 17 | Analysis of oxidation status of all Cys by COPA. Representative table represents the oxidation status, pK_a and various other predictions, whose full form are as follow: Oxidation Status Codes: RED – Reduced, DSB - Disulfide Bond, OXI – Oxidized; Prediction Codes: SOD - Susceptible to Oxidation by Sulfur Distance, SEP - Susceptible to Oxidation by Exposure and pKa, NOS - Not Oxidation Susceptible, N/P - No Prediction.

SEQUENCE POSITION	SEQUENCE	OXIDATION STATUS	PREDICTION	-	ASA	pKa
39	QLTENEIRGLCLKSREIFLSQ	RED	SOD		0	13.15
62	LLELEAPLKICGDIHGQYYDL	RED	NOS		0.07	12.33
105	DRGKQSLETICLLAYKIKYP	RED	NOS		1.65	12
127	NFFLLRGNHECASINRIYGFY	RED	SEP		4.87	5.96
140	INRIYGFYDECKRRYNIKLWK	RED	NOS		0	10.6
155	NIKLWKTFDFCNCLPIAAIV	RED	SOD		0.26	9.78
158	LWKTFDFCNCLPIAAIVDEK	RED	NOS		0	8.52
171	IAAIVDEKIFCCHGGLSPDLQ	RED	SOD		0	11.98
172	AAIVDEKIFCCHGGLSPDLQS	RED	NOS		0	12.72
202	PTDVPDQGLLCDLLWSDPKD	RED	NOS		0.21	10.73
245	FLHKHDLDLICRAHQVVEDGY	RED	SOD		0	14.28
273	LVTLSAPNYCGEFDNAGAMM	RED	SEP		17	8.1
291	AMMSVDETLMCSFQILKPA--	RED	NOS		4.45	9.67

The third prediction software for Cys oxidation that was used was DiANNA (version 1.1), a software program composed of an artificial neural network located on a web server. The software provides information on various Cys oxidation states and disulfide connectivity of proteins. The amino acid sequence of PP-1 α was analyzed in DiANNA with the help of the support vector machine (SVM) with spectrum kernel. SVM predicts whether a Cys is reduced or involved in a disulfide bridge or bound to the metallic ligand. The results in Table 19 show that only Cys²⁷³ obtained a score of 1, an indication that the compound is highly likely to both oxidize and form disulfide bridges. (Ferre and Clote, 2005).

Table 19 | Analysis of disulfide oxidation state prediction of PP-1A by DiANNA 1.1 web. It is a neural network, which takes the input of evolutionary information of symmetric window centered on each Cys. It tells us a score of a Cys oxidation state prediction with the score of 1. The program provides a score for a Cys oxidation state prediction, with a score of 1 indicating high susceptibility to oxidation and a strong likelihood to form disulfide bridge.

Sequence Position	Cysteine neighborhood window	Score
39	EIRGLCLKSRE	0.0
62	APLKICGDIHG	0.0
105	SLETICLLLAY	0.0
127	RGNHECASINR	0.0
140	GFYDECKRRYN	3e-05
155	KTFTDCFNCLP	0.0
158	TDCFNCLPIAA	0.0
171	DEKIFCCHGGL	0.0
172	EKIFCCHGGLS	0.0
202	DQGLLCDLLWS	0.0
245	DLDLICRAHQV	0.0
273	SAPNYCGEFDN	1.0
291	DETLMCSFQIL	0.0

Furthermore, Cys S-glutathionylation (GSH) sites from PP-1 A (PDB id: 3N5U) were also verified in human species with the dbGSH database. The database integrates all experimentally verified S-glutathionylated peptides from research articles using a text mining approach. The Figure 30 refers to the identified Cys, i.e. 140, 158 and 245 which were S-glutathionylated (Chiang et al., 2012). The top part of the figure shows the proposed S-glutathionylation sites in the context of solvent accessibility and protein secondary structure. Both Cys¹⁴⁰ and Cys²⁴⁵ were located at the end or beginning of a helical structure, respectively, and at a solvent accessible area. The predicted Cys¹⁵⁸ was found in the middle of a helical structure and hence was not solvent accessible. The lower part of the picture shows two consensus motifs for probable glutathionylation sites. It is easily visible that the acidic amino acid residues Asp (D) and Glu (E) are in close proximity.

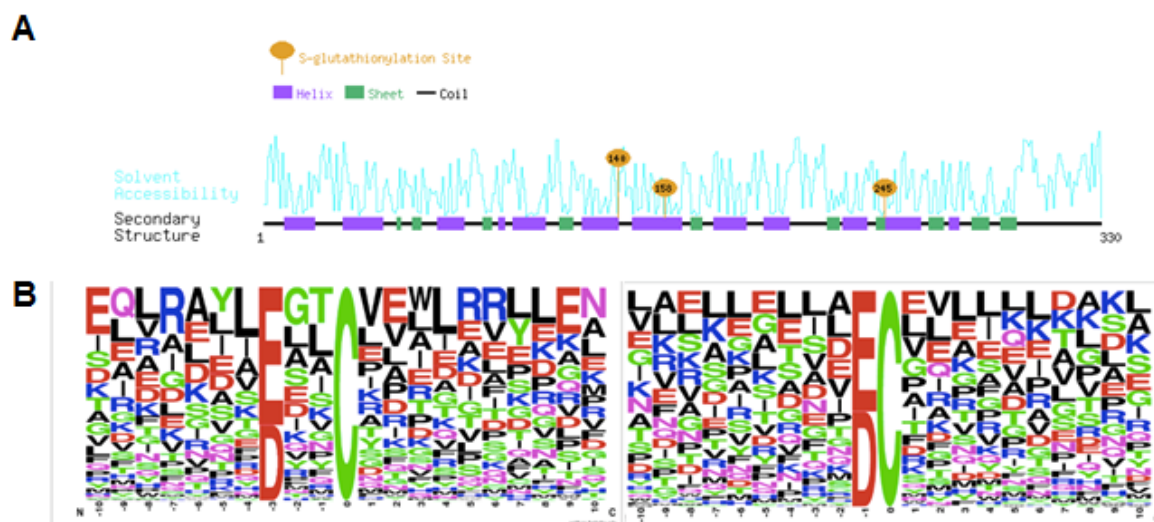


Figure 30 | Graphical representation of S-glutathionylation sites analyzed by the dbGSH database in PP-1. (A) An overview of protein S-glutathionylation sites with functional and structural information of human PP-1 (PDB id: 3N5U) showing Cys¹⁴⁰, Cys¹⁵⁸ and Cys²⁴⁵ to be S-glutathionylated. (B) Substrate motifs are showing a conserved region for Cys¹⁴⁰ and Cys²⁴⁵.

4.2.3 Analysis via Mass Spectrometry

The reason for beginning the analyses with mass spectrometry (MS) was to prove the existence of the predicted disulfide bridges. The Pymol software for measuring the molecular distances from the non-oxidized protein structure did not predict any intra-molecular disulfide bridges. The immunoblots, on the other hand, were able to show band shifts which represented inter-disulfide bridges (Section 4.2.2.1), however, it is unclear whether these disulfide bridges are artifacts. MS is the only method that maps all PTMs and sites in a single experiment without *a priori* knowledge.

4.2.3.1 Investigating the PTMs in GST-tagged PP-1

According to the computational prediction (Section 4.2.2.2), possible Cys residues were identified, which could be oxidized and may be susceptible to disulfide bridge formation. The experiment was performed with four different conditions (1: $-\text{Mn}^{2+} -\text{H}_2\text{O}_2$; 2: $-\text{Mn}^{2+} +\text{H}_2\text{O}_2$; 3: $+\text{Mn}^{2+} -\text{H}_2\text{O}_2$; 4: $+\text{Mn}^{2+} +\text{H}_2\text{O}_2$) so that one can draw some conclusions about the protective effect of Mn^{2+} and the oxidative effect of high H_2O_2 conditions. In addition to the common PTMs, a new database search strategy was created to unequivocally identify disulfide linked peptides from non-reduced and proteolytic digested samples. Although in principle many different PTMs could be formed under oxidative stress, the main emphasis was given on the identification of (i) free cysteines (which were protected by alkylation with IAA), (ii) glutathionylated Cys, (iii) potential disulfides being indicated by an unheterolytic cleavage of the disulfide link forming one persulfide and one dehydroalanine peptide, and (iv) sulfone

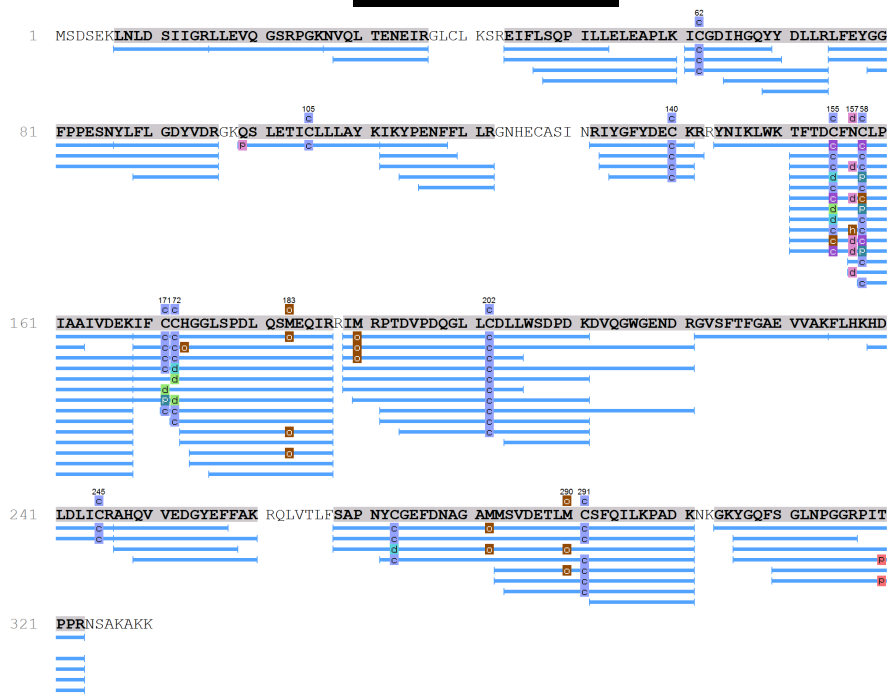
oxidized cysteines (which is the highest oxidative form of cysteines). The experiment was performed as described in Section 3.2.4. The H₂O₂ (500 μM) concentration used in the experiment would more than out-compete the protective effect of Mn²⁺ ions in the buffer.

The data was generated with LC-MS/MS using an Ultimate 3000 chromatography system coupled to a Q-Exactive Plus system. The sample was loaded onto the precolumn and eluted in reverse to the separation column. Data acquisition was performed with a top ten-centroid mode method. It was then searched with Peaks 7.0 with semi-Trypsin specificity because some long nonspecific fragments could have been undetectable. With this method, a longer fragment was identified that had a non-specific cleavage site comprising Cys²⁷³ and Cys²⁹¹ but starting at Ser²⁶⁸. However, the two short peptides that included Cys³⁹ and Cys¹²⁷ were not detectable (Appendix 1) under all condition, so in conclusion, they might be involved in some intra-molecular interaction or unexpected modification.

The search included all relevant Cys modifications, namely dehydroalanine, persulfide, sulfenic acid, sulfonic acid, glutathionylation, internal disulfide bridges on one peptide (but which could also be represented by a combination of the first two modifications), and carbamidomethylation. Furthermore, all other types of amino acid oxidations were included: phosphorylations of Ser, Thr and Tyr, N-terminal protein acetylation and side reactions such as pyrolysis of Gln and Pyro Asn and deamidations of Glu and Asp.

Glutathionylation in the non-protective buffer was observed under harsh oxidative stress (Figure 31.B) for the three Cys residues Cys¹⁴⁰, Cys²⁴⁵ with good spectra and Cys²⁰² with a lower quality spectrum. Many Cys residues were observed with dehydroalanine and persulfide modifications only under these experimental conditions, which suggest that these Cys residues form disulfide bridges. The over-oxidation of the Cys residues was also displayed. Figure 31 provides a sequence summary of the four distinct buffer conditions. The above-mentioned modified Cys residues are highlighted with green or gray boxes, respectively.

A) - Mn²⁺, - H₂O₂

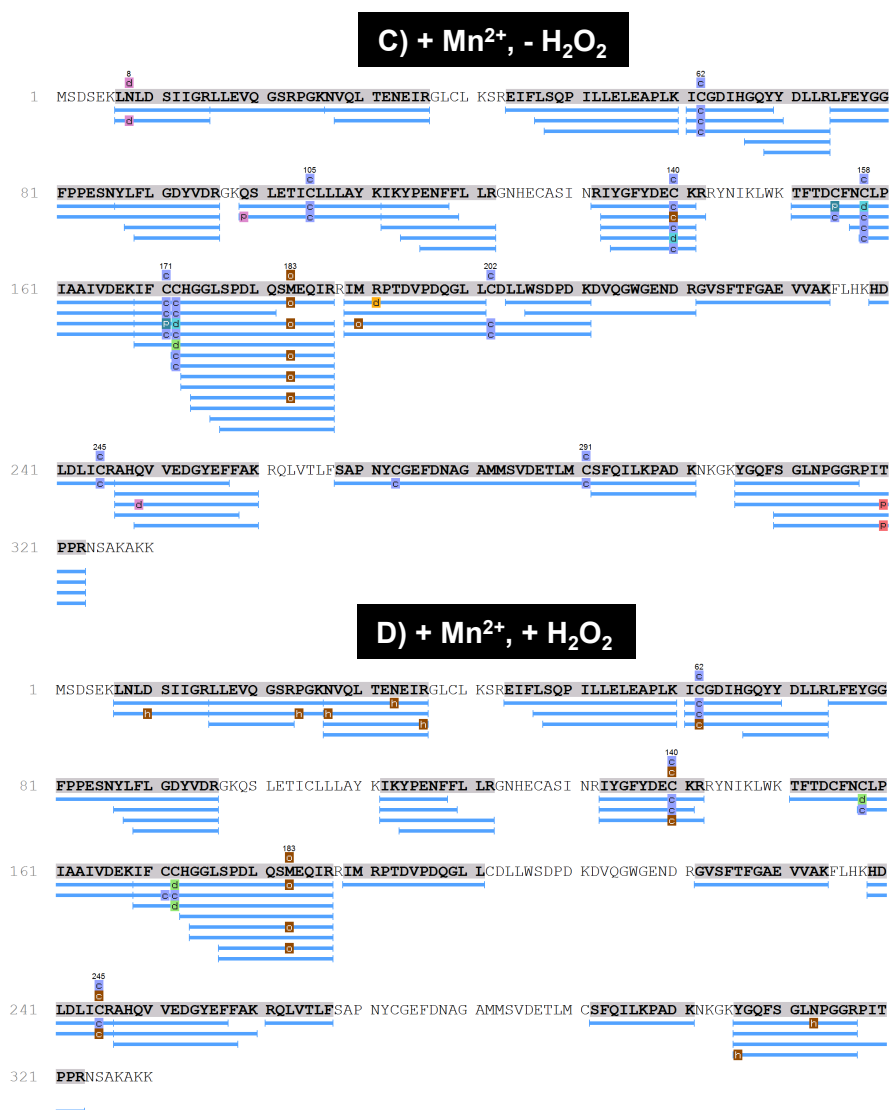


B) - Mn²⁺, + H₂O₂



**Persulfide/ Dehydroalanine
Generated by MS/MS
fragmentation of Disulfides**

Glutathion peptides



- Carbamidomethylation (+57.02)
- Cysteine oxidation to cysteic acid (+47.98)
- Cysteinylation (+119.00)
- Deamidation (NQ) (+0.98)
- Disulfide Bridge unpaired fragmentation (-2.02)
- Dehydroalanine C (-33.99)
- Dioxidation (M) (+31.99)
- Glutathione disulfide (+305.07)
- Hydroxylation (+15.99)
- Oxidation (M) (+15.99)
- Oxidation (HW) (+15.99)
- Oxidation or Hydroxylation (C) (+15.99)
- Persulfide C (+31.97)
- Phosphorylation (STY) (+79.97)

Figure 31 | *In vitro*-assays for MS readout using the GST-tagged PP-1 protein. All sequences which were successfully identified by Peaks 7.0 software are depicted by a blue bar below the sequence. All PTMs, their abbreviations and their color code are shown on the left. With respect to four different conditions, output PTM was generated with specifically (B) showing glutathionylated Cys¹⁴⁰, Cys²⁰² and Cys²⁴⁵ in the gray and persulfide/dehydroalanine generated by MSMS fragmentation of disulfide in a green box with respective spectra.

The spectrum shown for Cys¹⁴⁰ (Figure 32) shows that Cys underwent glutathionylation. Furthermore, the ion tables and the error bar plots are shown as they were extracted from Peaks 7.0 software. The remaining spectra for Cys²⁰² and Cys²⁴⁵ is shown in Appendix 3. The table in Figure 32 summarizes the following ions: on the left side of the peptide sequence are Immonium ions, b-type ions, b-H₂O ions, b-NH₃ ions, a-type ions and B (2+) ions. On the right side of the peptide sequence are y t-type ions, y-H₂O ions, y-NH₃ ions and y (2+) ions. The error plot below shows all fragment ions within 0.02 Da mass deviations that were allowed for the search. Since almost the entire ion series was covered, the correct identification could be made with confidence.

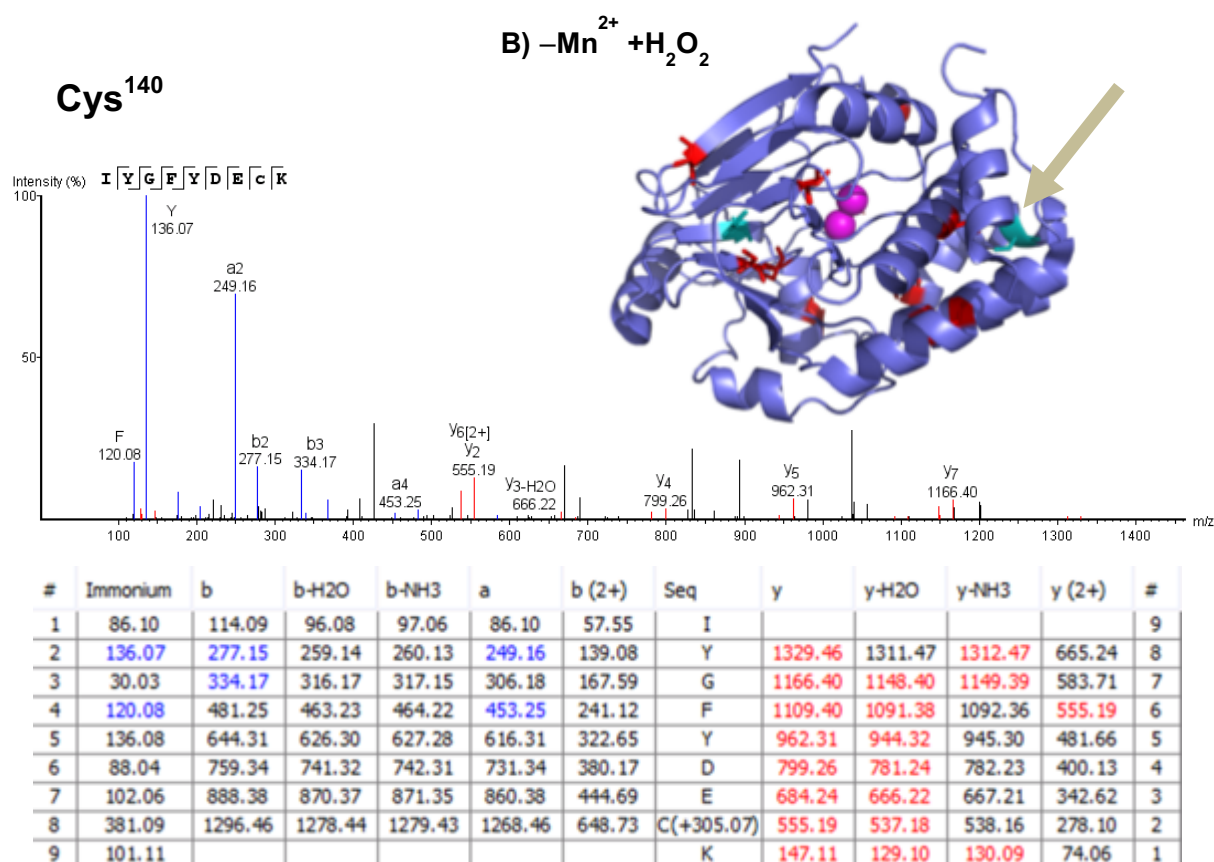


Figure 32 | Spectra and positions of the glutathione-modified Cys¹⁴⁰. The top shows the spectrum with y-type ions in red and b-type ions in blue. The ion table below displays the exact masses of each of the ions and indicates the site of the PTM. In the structure, Cys residues are highlighted in red, glutathione-modified in cyan, and indicated by an arrow.

In order to describe the different solvent accessibilities and the reactivity of the diverse Cys residues, the above-mentioned modifications were quantified using the spectral count approach. The data from the GST-tagged PP-1 for the four experimental conditions demonstrated that the Cys residues are subtyped in 2-3 groups (Figure 33). Overall, free Cys spectral counts were higher in number in both conditions $-Mn^{2+} -H_2O_2$ and $+Mn^{2+} -H_2O_2$. persulfide/disulfide bridge and sulfone formation was higher when $-Mn^{2+} +H_2O_2$ was

incubated. In contrast, the presence of additional Mn^{2+} ions protected the Cys residues from further oxidation. Three Cys residues also formed glutathionylation.

The PTMs of the 13 Cys residues were quite different from one another. Data for Cys¹⁵⁵ and Cys¹⁵⁸ as well as Cys¹⁷¹ and Cys¹⁷² has to be interpreted pairwise because they most likely form an internal disulfide bridge upon sample preparation. Mn^{2+} ions in the buffer protect them completely from sulfone formation. Disulfide bridges are observed under all conditions, but to a lesser extent when no H_2O_2 is applied. Apparently, the presence of the Mn^{2+} does not alter this effect. For instance, Cys¹⁵⁵ and Cys¹⁵⁸, disulfide formation dominated in the condition with $-Mn^{2+} + H_2O_2$ and no free Cys in the 4th condition with $+Mn^{2+} + H_2O_2$: 50% of persulfide/disulfide bridge and 50% free Cys or 50% of persulfide/disulfide bridge and 40% free Cys, respectively. However, spectral counting results demonstrated, that Cys¹⁵⁸ formed 10% of sulfone Cys in the condition with $-Mn^{2+} + H_2O_2$ which hints at the fact, that it might be free under some circumstances while Cys¹⁵⁵ is more protected. Cys¹⁷¹/Cys¹⁷² showed a similar trend but about 20-25% of persulfide/disulfide bridge formation under condition 2. When no H_2O_2 treatment was performed, spectral count for Cys¹⁷¹ and Cys¹⁷² showed 62-70% of free Cys and only the rest to be persulfide/ disulfide bridges, which can be explained by the disfavored orientation of the sulfhydryl groups in the peptide. Around 58-62% of persulfide/ disulfide bridge spectral count was discovered in the condition with $-Mn^{2+} + H_2O_2$ and was reduced to 12-20% in the condition with $+Mn^{2+} - H_2O_2$ and rest free Cys.

Cys²⁷³ and Cys²⁹¹ lie at the outermost region of the structure show a complete 100% persulfide/disulfide bridge spectral count in the condition with $-Mn^{2+} + H_2O_2$. This result is reversed with 100% free Cys in the condition with $+Mn^{2+} - H_2O_2$. No spectra were found for the last condition with $+Mn^{2+} + H_2O_2$.

For Cys¹⁴⁰, Cys²⁰² and Cys²⁴⁵ glutathionylation (in gray) was detected, that apparently competes with the disulfide formation; and further also showed 62%, 47% and 50% of sulfone spectra counts, respectively, with the condition $-Mn^{2+} + H_2O_2$. Cys¹⁴⁰ also forms sulfone with Mn^{2+} in the buffer. However, in Cys²⁰² and Cys²⁴⁵, no sulfone formation was observed with the condition $+Mn^{2+} - H_2O_2$. In Cys¹⁴⁰ and Cys²⁴⁵, 35% and 50% of Cys residues formed sulfone, respectively, with the condition $+Mn^{2+} + H_2O_2$ and no spectral count was identified for Cys²⁰² for the latter condition. Mn^{2+} completely protected Cys⁶² and Cys¹⁰⁵. In the condition with $-Mn^{2+} + H_2O_2$, around 33% and 68% of sulfone formations were identified in the two aforementioned Cys, respectively. In the last condition, almost 35% sulfone formations were identified in Cys⁶² and however no spectra were identified for the Cys¹⁰⁵.



Figure 33 | Quantification of the amount of free, persulfide/disulfide and sulfonic acid -Cys residues by spectral counting. Columns show the percentage distribution of all the four modifications. Yellow represent sulfone formation, grey represent glutathione formation, green represent persulfide/disulfide formation and blue represent free Cys residues.

In order to verify the results from persulfide/dehydroalanine detection and unequivocally identify the disulfide-linked peptides within the data set, a new data search strategy was

introduced. Though the fact that other software packages are available such as StavroX (Gotze et al., 2012), SearchXlinks (Wefing et al., 2006), XlinkX (Liu et al., 2015) or several commercial software from the mass spectrometry vendors e.g. the PepFinder Software from ThermoFischer Scientific. The results were compared with the StavroX software, but the quality of the identified spectra was not satisfying, since the program annotated the peptide fragments just from the free N-and C-termini of the two peptides (data not shown). An interesting question would be, if a more robust strategy might be able to detect the higher order b-type or y-type fragments. Similar to the observation with simulated peptides (Hsiao et al., 2009b), that the ion series jumped from one to the other peptides for branched species. Based on this idea a search database was generated, as was described in detail in the Section 3.2.4.5. In the at end, tall linear peptides were identified. The actually disulfide-linked region would not be identified by fragmented ions, but high molecular fragments were observed in the second peptide after jumping the linkage. Hence, this behavior for some of the following spectra was observed and incorporated into the database to optimize the search strategy. The strategy worked well for a single or few known proteins but a general strategy for the understanding of the disulfide network of an entire proteome is still needs to be developed. Two example spectrums are shown in Figure 34. The modification in the middle of the peptide is calculated as follows:

$$\text{Water (free C-terminus) – Hydrogen} = \text{Jump over Disulfide bridge}$$

$$18.01 \text{ Da} - 2.02 \text{ Da} = 15.99 \text{ Da}$$

Table 20 summarizes the observed disulfide spectra from the four experimental conditions in a reactivity scheme. The previously described Cys¹⁵⁵ and Cys¹⁵⁸ are located in a distance that is suitable for inter-disulfide bridge formation. The olive-green squares being identified under all conditions are Cys¹⁵⁵Cys¹⁵⁸ and Cys¹⁷¹Cys¹⁷² that are placed on the same Trypsin derived peptide and hence could be generated from sample preparation. Interestingly, the – Mn²⁺ +H₂O₂ condition resulted in a significant increase in the occurrence of disulfide peptides, which is concurrent with our prior observation of the persulfides/dehydroalanines. The light green squares were generated by a weaker spectrum. However, only Cys residues in the upper left part of the figure involved with a strong emphasis of the Cys³⁹ and Cys¹²⁷, as they were not identified as non-modified peptides in these samples. For Cys¹²⁷-Cys¹⁴⁰ a disulfide link was found under all conditions except for the last one. The same holds true for the Cys³⁹-Cys¹²⁷ link. Without the addition of Mn²⁺, a Cys¹²⁷-Cys²⁴⁵ disulfide link was also observed. Disulfide exchange might be in concurrence with the protection of the Mn²⁺. Many disulfide peptides were positively identified and were in proximity within the 3D structure (Cys¹⁴⁰ XL Cys³⁹, Cys¹⁰⁵ XL Cys³⁹, Cys¹⁴⁰ XL Cys¹²⁷, Cys¹⁴⁰ XL Cys¹⁵⁴Cys¹⁵⁸ and Cys¹²⁷ XL

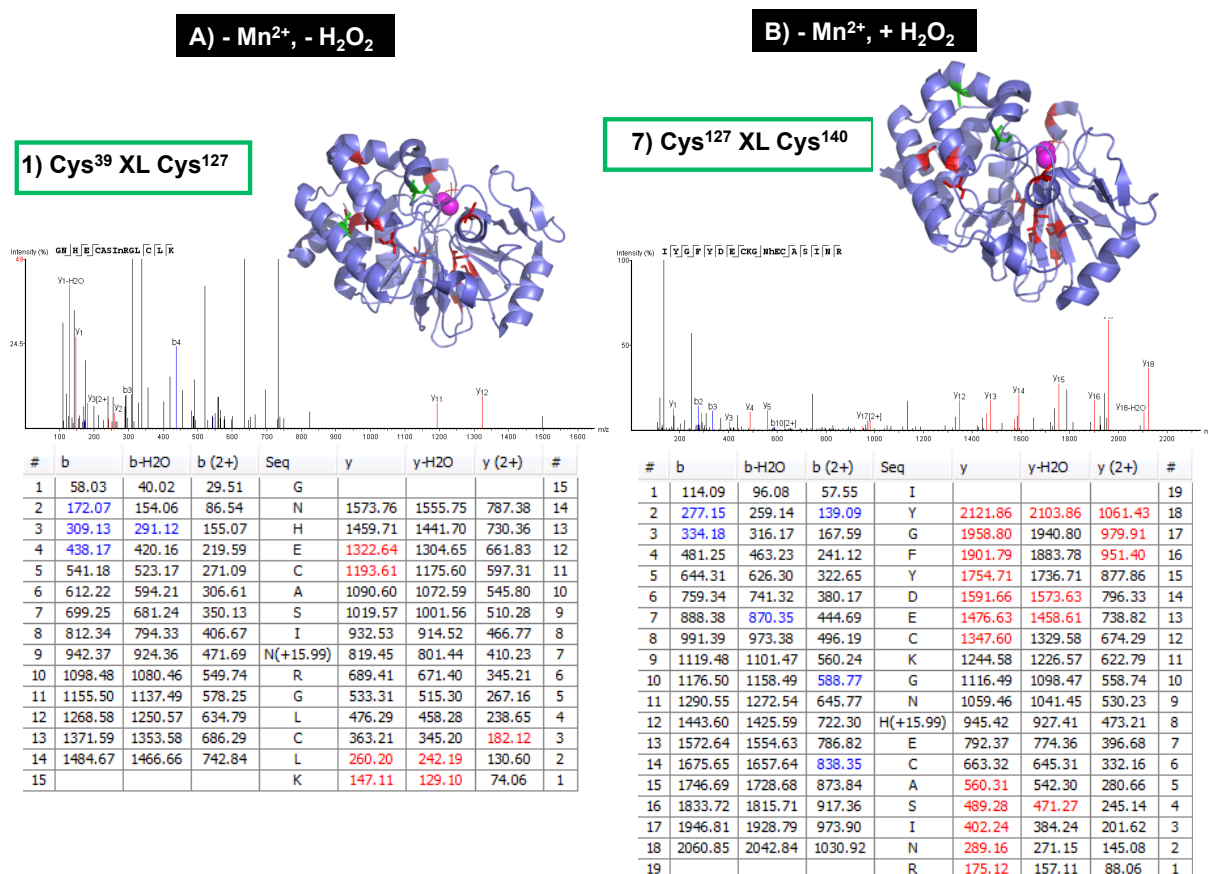


Figure 34 | Disulfide-peptide conjugates (spectrum and fragment table) of (A) Cys³⁹ and Cys¹⁴⁰ (B) Cys¹²⁷ and Cys¹⁴⁰. In the structure plot, the two involved Cys are indicated with green color.

Results from Figure 26 proposed the native inter-disulfide bridges forming a dimer at 70 kDa, which were then analyzed by the mass spectrometry approach. Only one inter-disulfide bridge with Cys¹²⁷ was discovered. However, it was only discovered in the condition $-Mn^{2+} + H_2O_2$, which contradicted the results from the immunoblot. It even showed inter-disulfide bridge under control conditions. Figure 35 represents the protein surface of PP-1 (PDB id: 4MOV), with Cys residues in red (Cys¹²⁷, Cys²⁷³ and Cys³⁹) at the surface. These residues are prone to oxidation and might form inter-disulfide bridges with other proteins. Also, the structure nicely shows the entry point for manganese ions in green and pink (Histidines and Mn²⁺).

Pymol and the PDB structure 4MOV were used to map all the possible distances of Cys residues with each other and the Mn²⁺ ions to understand the data obtained from the MS/MS fragmentation experiments (Table 21). The color-coding ranges from the heavy blue (shortest distance) to white (longest distance). The approximate color-coding distribution is shown on the right side of the table. The solid black boxes indicate the two possible Cys networks over closer interaction, showing, that the protein could be seen as divided into two halves. The Cys residues at the rim carry another color code: green boxes indicate Cys with

persulfide/dehydroalanine modification as a strong indicator for a cleaved disulfide bridge (only in the $-Mn^{2+} + H_2O_2$ condition, compare supplemental information) and in grey for glutathione-modified sites. Cys²⁰² was found within both above mentioned modifications. Mn²⁺ ions are indicated in pink in the structure. The values are given in Å.

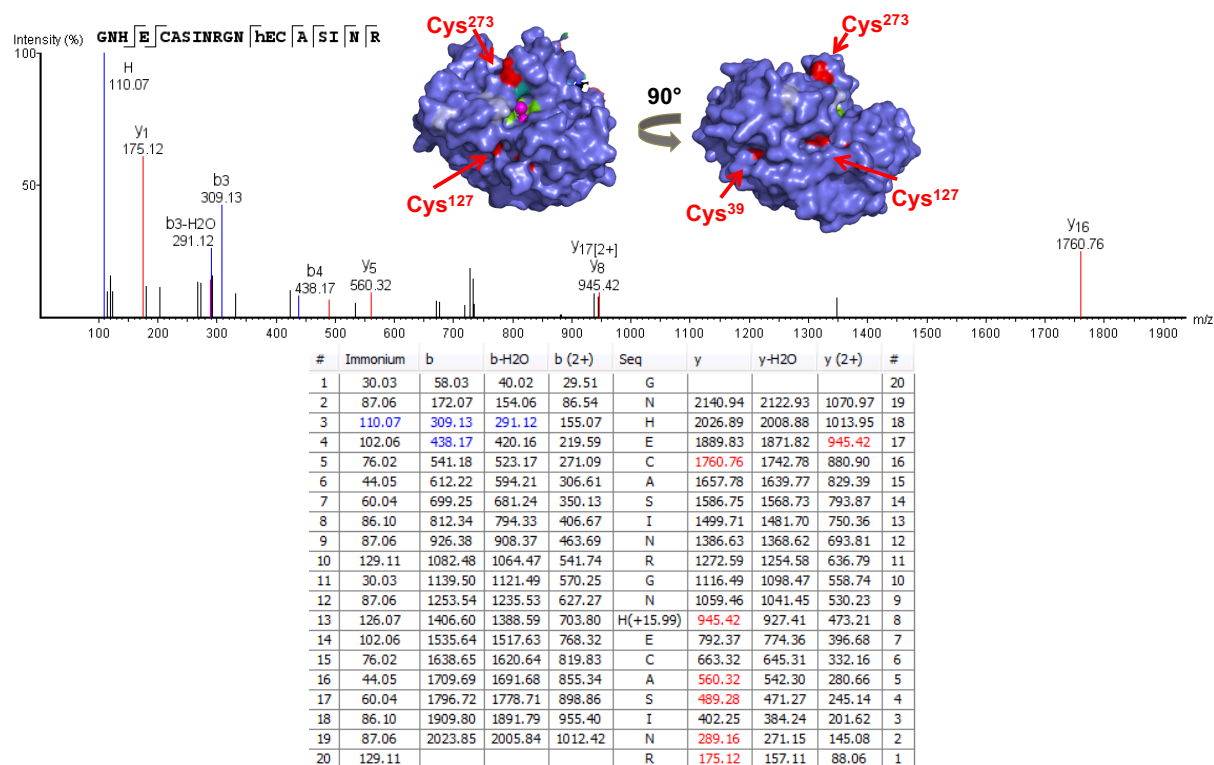
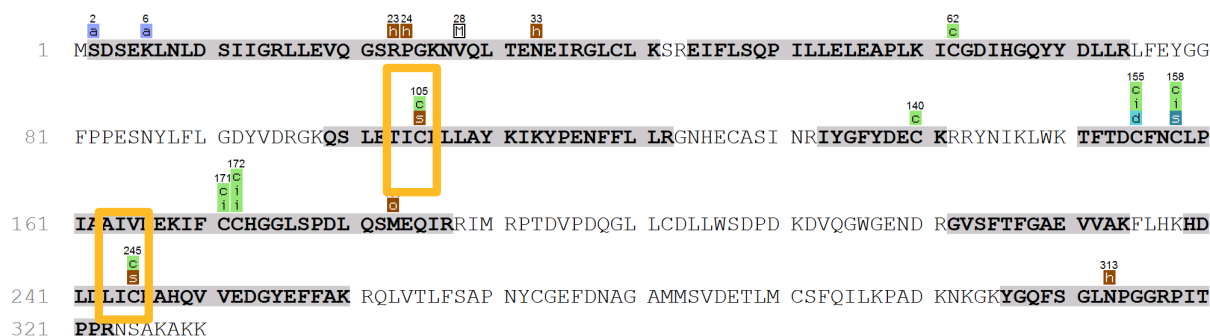
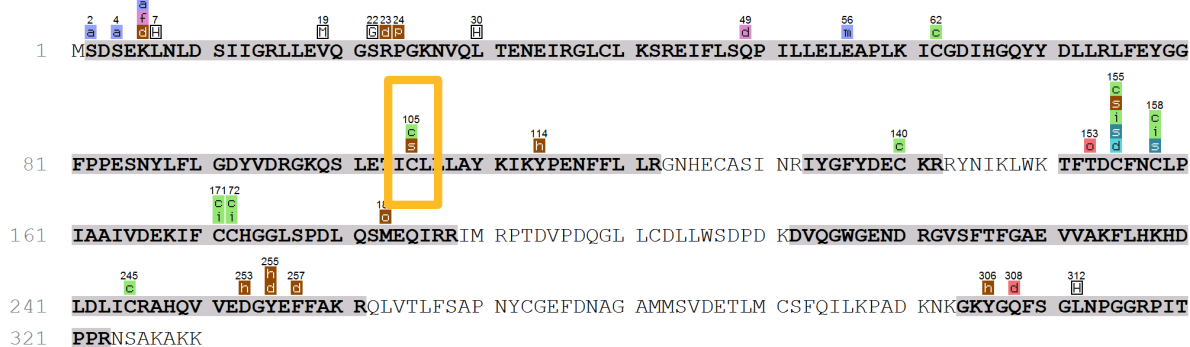


Figure 35 | Spectrum and ion table for the inter-disulfide bridges with Cys¹²⁷. Surface structure is showing the outer bound Cys residues- 127, 273 and 39, which could be prone to oxidation.

Table 21 | Distance measurements [Å] of the Cys residues with each other and Mn²⁺. The PDB file 4MOV contains structural information of the PP-1A under non-oxidative conditions and was used in Pymol to measure all cysteine distances with each other and the Mn²⁺.

	Cys 39	Cys 62	Cys 105	Cys 127	Cys 140	Cys 155	Cys 158	Cys 171	Cys 172	Cys 202	Cys 245	Cys 273	Cys 291	Mn ²⁺	colorcode
Cys 39		19,68	6,97	15,72	8,68	4,54	16,54	24,20	22,15	23,69	25,46	23,86	33,78	19,92	30,00
Cys 62	19,68		6,82	18,44	22,31	17,76	10,41	8,60	7,78	19,53	6,91	18,04	13,11	11,82	27,00
Cys 105	6,97	6,82		18,96	8,66	9,65	16,64	24,81	23,01	7,04	25,08	21,18	30,20	20,19	24,00
Cys 127	15,72	18,44	18,96		10,72	14,07	13,94	21,41	15,82	12,56	23,80	16,44	28,94	11,00	21,00
Cys 140	8,68	22,31	8,66	10,72		11,64	16,65	27,56	23,75	23,16	27,53	18,62	33,79	17,45	18,00
Cys 155	4,54	17,76	9,65	14,07	11,64		6,98	20,33	18,59	20,82	22,60	23,76	27,07	17,75	15,00
Cys 158	16,54	10,41	16,64	13,94	16,65	6,98		20,98	19,30	12,02	23,67	27,99	29,58	19,72	12,00
Cys 171	24,20	8,60	24,81	21,41	27,56	20,33	20,98		5,96	19,42	4,57	24,22	9,08	15,24	10,00
Cys 172	22,15	7,78	23,01	15,82	23,75	18,59	19,30	5,96		13,56	6,43	19,11	15,03	19,24	9,00
Cys 202	23,69	19,53	7,04	12,56	23,16	20,82	12,02	19,42	13,56		19,87	21,33	26,59	12,41	8,00
Cys 245	25,46	6,91	25,08	23,80	27,53	22,60	23,67	4,57	6,43	19,87		21,25	7,15	14,37	7,00
Cys 273	23,86	18,04	21,18	16,44	18,62	23,76	27,99	24,22	19,11	21,33	21,25		26,60	9,08	6,00
Cys 291	33,78	13,11	30,20	28,94	33,79	27,07	29,58	9,08	15,03	26,59	7,15	26,60		20,86	5,00
Mn ²⁺	19,92	11,82	20,19	11,00	17,45	17,75	19,72	15,24	19,24	12,41	14,37	9,08	20,86		4,00

C) +Mn²⁺ -H₂O₂D) +Mn²⁺ +H₂O₂

Sulfone formation

- Acetylation (N-term) (+42.01)
- Arginine oxidation to glutamic semialdehyde (-43.05)
- Carbamidomethylation (+57.02)
- Deamidation (NQ) (+0.98)
- Disulfide CID breakage (+33.99)
- Dehydroalanine (-33.99)
- Dehydration (-18.01)
- Dihydroxy (+31.99)
- Hydroxylation (+15.99)
- Internal disulfide bond (-1.01)
- Internal disulfide bond unpaired fragmentation (-2.02)
- Methyl ester (+14.02)
- Oxidation (M) (+15.99)
- Oxidation or Hydroxylation (C) (+15.99)
- Oxidation (HW) (+15.99)
- Proline oxidation to pyroglutamic acid (+13.98)
- Sulphone C (+47.98)
- S-Persulfide (+31.97)
- Mutation

Figure 36 | *In vitro*-assays for MS readout using the His-tagged PP-1 (data based on analysis from Peaks7.0 software). All PTMs, their abbreviations and their color code are shown on the left. With respect to four different conditions, output PTM was generated with specifically (B) showing sulfone formation at various Cys residues in the yellow box with respective bar chart and spectra.

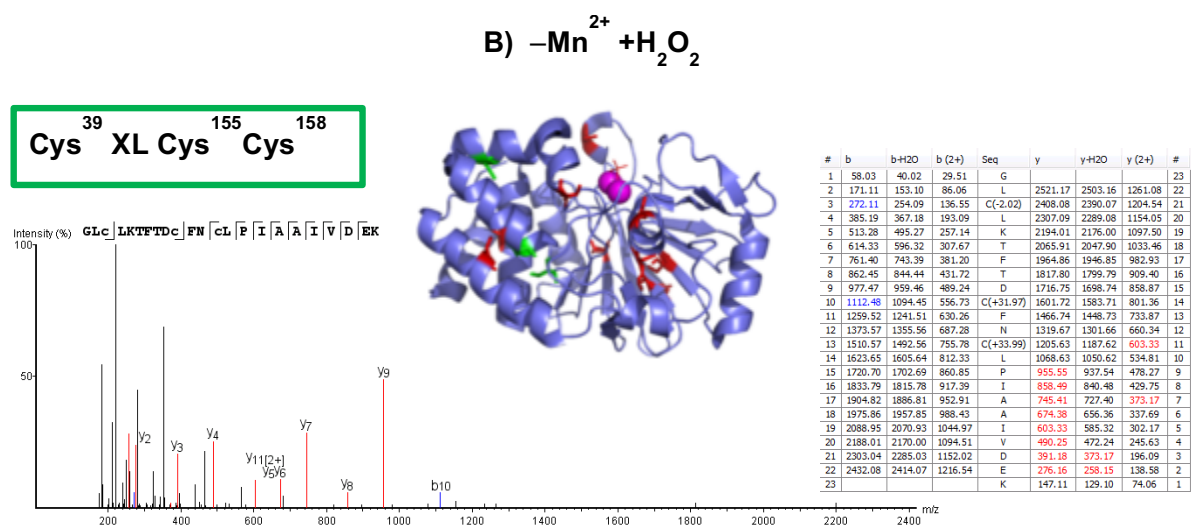


Figure 37 | Cys³⁹ XL Cys¹⁵⁵ Cys¹⁵⁸ disulfide-peptide conjugates (spectrum and fragment table) is the disulfide link induced in the His-tagged PP-1. In the structure plot, the two involved Cys are indicated in green. They are located in a local proximity that makes the formation of a disulfide bridge.

Finally, the amount of free and hyper-oxidized Cys residues (sulfonic acid) was quantified by extracting the label free quantification (LFQ) of each peptide using PEAKS 7.0 software. The color code of Table 22 ranges from green (lowest value) to red (highest value). The amount of free Cys residues is highest with $+Mn^{2+} - H_2O_2$ in the buffer and slightly lower with $-Mn^{2+} - H_2O_2$ in the buffer, which suggests that oxidation could also occur in Cys residues exposed to the air. Cys¹⁰⁵ and Cys²⁴⁵ have interesting values: the lowest values were observed as expected by treatment with H_2O_2 and no protective Mn^{2+} present. However, for one Cys the opposite was observed, however it was not displayed in the sequence. In accordance with these observations, Table 22 shows the highest values for the formation of sulfonic acid, when no protective Mn^{2+} ions counteracted the H_2O_2 treatment. From a structural perspective, Cys¹⁰⁵ is the furthest distance from the Mn^{2+} binding centrum and also completely shielded by the His residues that cage the two Mn^{2+} ions. Cys¹⁴⁰ is almost equally prone to form sulfonic acid as it is close to the Mn^{2+} binding centrum.

Table 22 | Possible Cys residues that can undergo sulfonation in His-tagged PP-1. The color code is from green for lowest value to red for the highest value. Dark green labeled boxes=free cysteine; Orange labeled boxes=Sulfonic acid (SO₃).

Peptide	Cys	Free Cys				Color Code
		no Mn + no H ₂ O ₂	no Mn + with H ₂ O ₂	with Mn + no H ₂ O ₂	with Mn + with H ₂ O ₂	
ICGDIHGQYYDLLR	Cys62	1,36E+06	2,73E+05	2,89E+06	8,04E+05	1,60E+07
QSLETICLLLAYK	Cys105	6,01E+06	4,85E+05	1,60E+07	2,09E+06	8,50E+06
GKQSLETICLLLAYK	Cys105	3,13E+06	1,00E+03	2,07E+06	1,00E+03	5,00E+06
GNHECASINR	Cys127	6,10E+04	2,68E+05	1,00E+03	1,00E+03	1,00E+06
IYGFYDECKRR	Cys140					5,00E+05
TFTDCFNCLPIAAIVDEK.I	Cys155Cys158	3,02E+06	1,00E+03	3,61E+06	2,64E+05	1,00E+05
IFCCHGGLSPDLQSM(+15.99)EQIR	Cys171Cys172	1,32E+06	1,00E+03	4,60E+06	9,20E+05	5,00E+04
IFCCHGGLSPDLQSMQEQIRR	Cys171Cys172	9,19E+05	1,00E+03	5,96E+06	2,27E+05	1,00E+04
IM(+15.99)RPTDVPDQGLLCDLLWSDPK	Cys202					5,00E+03
FLHKHDLDLICR	Cys245	3,98E+06	1,44E+05	3,49E+06	1,00E+03	2,00E+03
HDLDLICR	Cys245	1,93E+06	1,00E+03	1,16E+07	8,37E+05	1,00E+03
Peptide	Cys	Sulfone Cys				
		no Mn + no H ₂ O ₂	no Mn + with H ₂ O ₂	with Mn + no H ₂ O ₂	with Mn + with H ₂ O ₂	
ICGDIHGQYYDLLR	Cys62	1,00E+03	1,09E+06	1,00E+03	1,00E+03	
QSLETICLLLAYK	Cys105	7,10E+04	8,40E+06	1,00E+03	1,46E+05	
GKQSLETICLLLAYK	Cys105	1,00E+03	3,73E+06	1,00E+03	3,67E+04	
GNHECASINR	Cys127					
IYGFYDECKRR	Cys140	1,00E+03	7,30E+06	1,82E+05	2,13E+05	
TFTDCFNCLPIAAIVDEK.I	Cys155Cys158	1,00E+03	2,41E+05	6,40E+04	1,00E+03	
IFCCHGGLSPDLQSM(+15.99)EQIR	Cys171Cys172	1,00E+03	8,27E+05	1,00E+03	1,00E+03	
IFCCHGGLSPDLQSMQEQIRR	Cys171Cys172					
IM(+15.99)RPTDVPDQGLLCDLLWSDPK	Cys202	1,00E+03	2,96E+05	1,00E+03	1,00E+03	
FLHKHDLDLICR	Cys245	1,00E+03	1,01E+06	1,00E+03	1,00E+03	
HDLDLICR	Cys245	1,00E+03	1,98E+06	4,17E+05	5,51E+05	

4.2.3.3 Oxidation of other amino acids in the vicinity of Mn²⁺ ion in GST / His-tagged PP-1

The X-ray structure of PP-1 has revealed four Histidines (His) close to dinuclear metal ions. While finding the PTM in both, GST and His-tagged PP-1, surprisingly His²⁴⁸ was solely identified to be oxidized in the GST-tagged protein experiment. This might suggest that it is more solvent exposed as the other His residues and probably not involved in the binding of the Mn²⁺ ions. An unexpected result was found in the His-tagged protein experiment, where His²⁴⁸ was unaffected while His¹²⁵ was oxidized with buffer B (–Mn²⁺ –H₂O₂). The spectra are shown in Figure 38.

Tyr²⁷² can be oxidized, however it is only 4.4 Å from the Mn²⁺ ion and 3.68 Å from His⁶⁶, hence do not have a protective effect. The oxidizable His²⁴⁸ is only 8.55 Å from the Mn²⁺ ion (Figure 39). The sample containing GSH and GST resulted in surprising oxidations in the presence of additional Mn²⁺. Fairly consistent mono-oxidation occurred under all conditions except in buffer condition B (–Mn²⁺ +H₂O₂).

B) $-Mn^{2+} + H_2O_2$

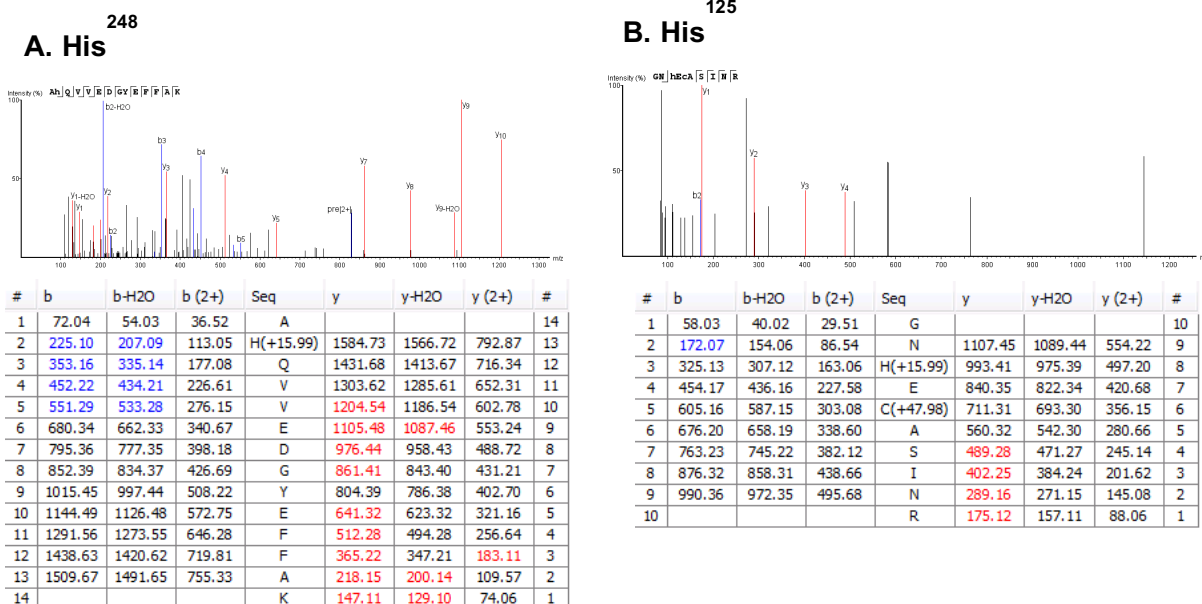


Figure 38 | Spectra and ion table of oxidized Histidine (His²⁴⁸/His¹²⁵) caging around the dinuclear Mn²⁺ ions. In the structure of PP-1, the two Mn²⁺ ions are caged by the four His residues (His⁶⁶, His¹²⁵, His¹⁷³ and His²⁴⁸). Spectra under H₂O₂ treatment represent show mono-oxidized His²⁴⁸ and His¹²⁵ in the (A) GST and (B) His-tagged- PP-1, respectively.

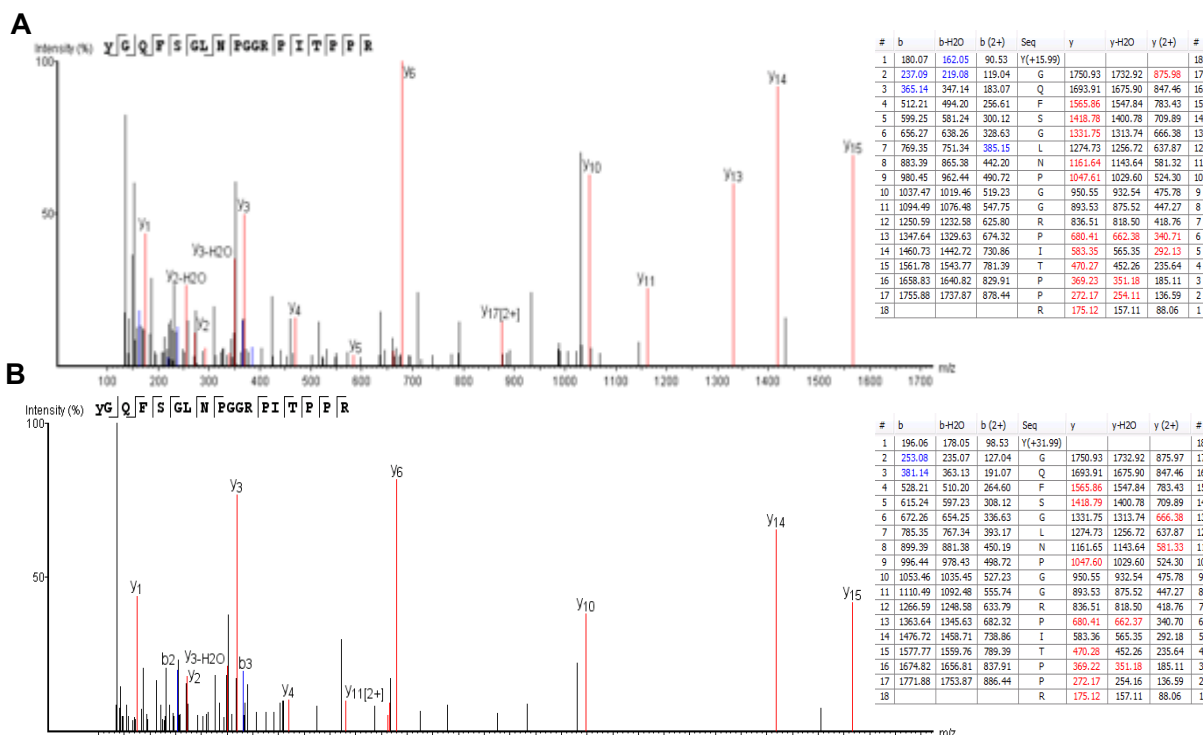


Figure 39 | Spectra and ion table of oxidized Tyrosine (Tyr²⁷²) close to Cys²⁷³ in the (A) GST and (B) His-tagged PP-1 respectively.

4.3 Regulation of CTGF under stress conditions in cardiomyocytes

4.3.1 Expression of CTGF in physiological functioning of the heart

Human non-failing (NF), ischemic (ICM), and dilated cardiomyopathy (DCM) heart samples were used to examine the expression of CTGF in heart disease. Immunoblotting analysis demonstrated that CTGF expression was significantly higher in DCM samples as compared to NF samples (Figure 40.A). In ICM samples, CTGF expression was slightly but not significantly increased compared to NF samples (Figure 40.B).

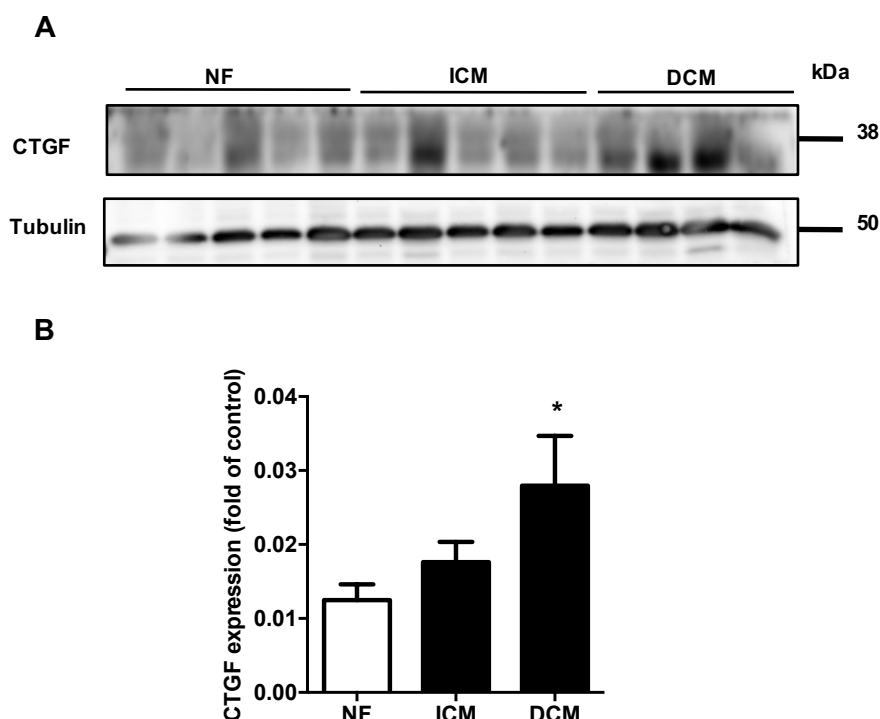


Figure 40 | Higher protein expression of CTGF in end-stage human heart failure. (A) Immunoblot and (B) relative analysis of CTGF expression in non-failing (NF) hearts, end-stage heart failure ischemic cardiomyopathy (ICM) and dilated cardiomyopathy (DCM). Analysis was normalized to Tubulin, and the change in CTGF expression was estimated relative to the control. Values are given as mean \pm SEM, NF=5, ICM=5 and DCM=4. Statistical comparison was performed by one-way ANOVA, and post hoc correction with Bonferroni's multiple comparison tests, * $p < 0.05$ vs. NF. The heart samples were kindly provided by Dr. Thomas H. Fischer, Clinic for Cardiology and Pneumology, Goettingen.

4.3.2 Influence of oxidative and ER stress on CTGF expression in NRCM

The influence of the oxidative environment on CTGF expression was subsequently analyzed in NRCM with 100 μ M H_2O_2 for short incubation times of up to 30 min (time intervals of 3, 6, 10, 15 and 30 min) and longer incubation times of up to 6 h (time interval of 2, 4 and 6 h). In both settings, the last time point was kept as control time point. The relative analysis of

immunoblots (Figure 41) revealed that no significant change in CTGF levels occurred after H₂O₂ treatment.

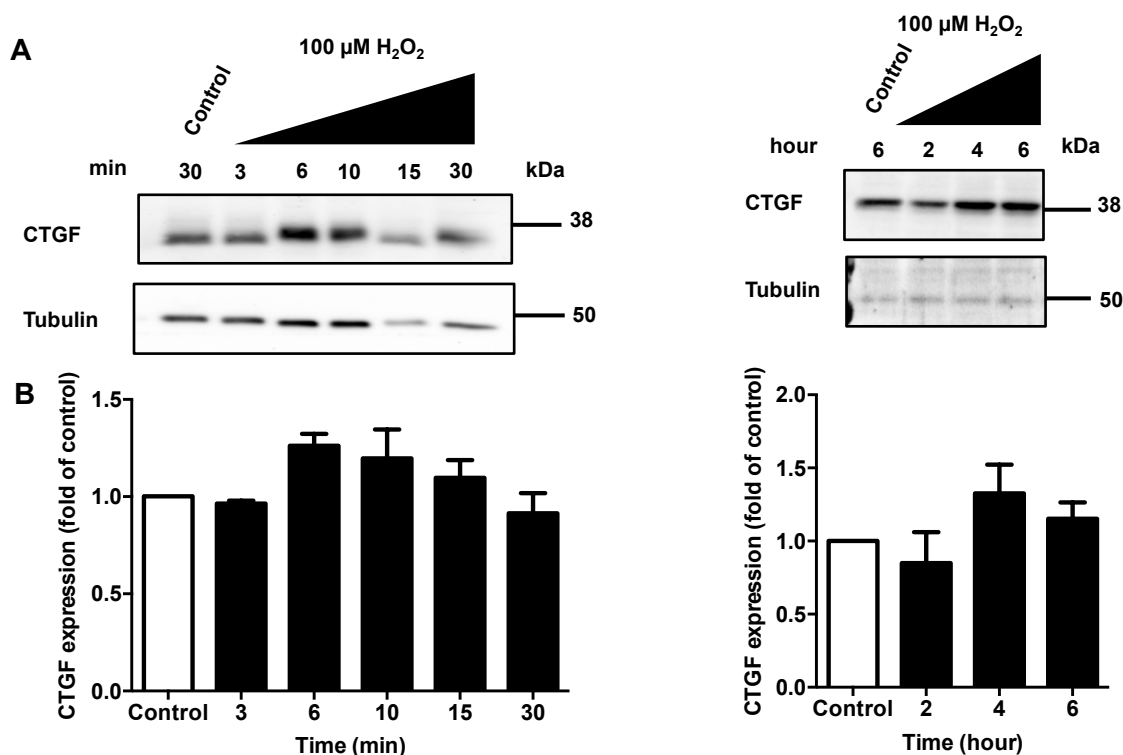


Figure 41 | Protein expression of CTGF in cardiomyocytes exposed to H₂O₂. (A) Immunoblot and (B) relative analysis of CTGF in neonatal rat cardiomyocytes (NRCM) exposed to 100 μM H₂O₂ at different time points. Analysis was normalized to Tubulin, and the change in CTGF expression was estimated relative to the control. Values are given as mean ± SEM, n=3-5. Statistical comparisons were performed by one-way ANOVA, and post hoc correction with Bonferroni's multiple comparison tests, *p<0.05 vs. control.

To determine the effect of reducing conditions on CTGF, the NRCMs were treated with 50 mM DTT for up to 30 min (time interval with 3, 6, 10, 15 and 30 min). In the respective immunoblot analysis, CTGF showed a time-dependent staircase pattern. This likely reflects different structural forms of CTGF in the cells, with the lower band having a molecular weight of 36 kDa and the top band with a molecular weight of 38 kDa in non-reducing SDS-PAGE. Furthermore, by the addition of the reducing agent in SDS-PAGE sample buffer (reducing condition), the staircase pattern was no longer present supporting the hypothesis of in cell reduction of CTGF by DTT (Figure 42.A). In addition, the concentration-dependent effect of DTT and diamide on CTGF in a non-reducing condition was analyzed. The results demonstrated that the staircase pattern of CTGF was dependent on the DTT concentration. The oxidizing agent diamide was without effect (Figure 42.B)

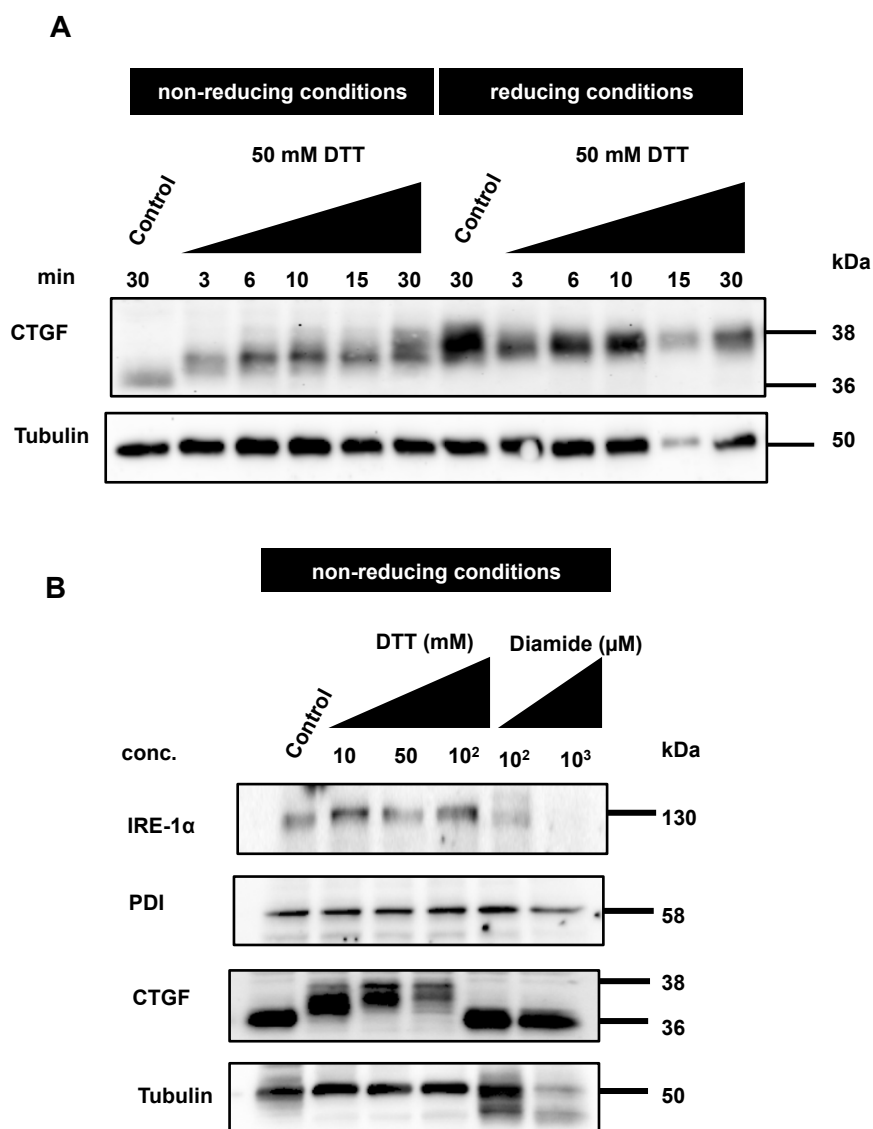


Figure 42 | Protein expression of CTGF in cardiomyocytes exposed to DTT and diamide. (A) Immunoblot of CTGF in NRCM exposed to 50 mM DTT for different time periods analyzed under non-reducing and reducing conditions. Tubulin is shown as loading control. (B) Immunoblot analysis of the ER stress markers IRE-1 α and PDI and CTGF in NRCM exposed to increasing concentrations of DTT and diamide under non-reducing conditions. Tubulin is shown as loading control, n=3.

Further, the intracellular Ca²⁺-depleting agent thapsigargin (TGN) was studied as it has been described to induce ER stress similar to DTT (Zhang et al., 2010). As shown in Figure 43, CTGF expression was significantly increased after 6 h when NRCM were treated with 3 μ M TGN. Under the used conditions the ER stress markers PDI and IRE1- α were only up-regulated by trend.

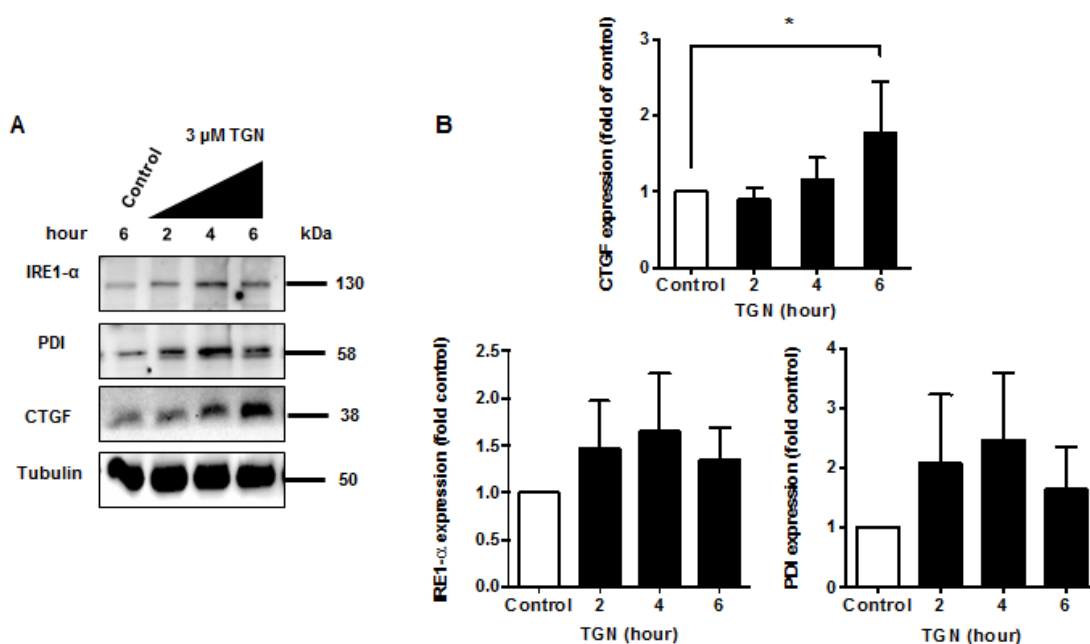
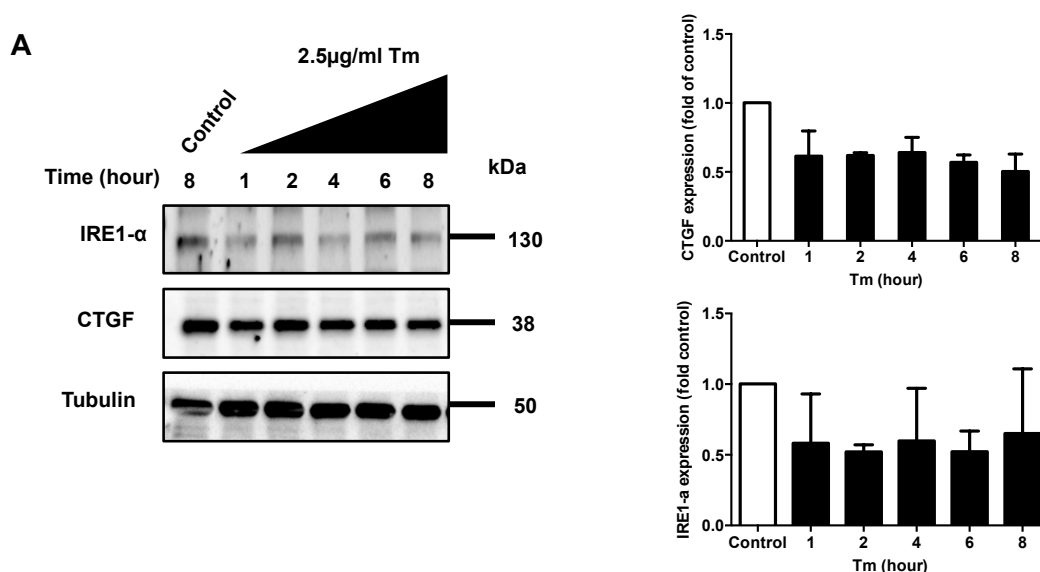


Figure 43 | Protein expression of CTGF in NRCM exposed to TGN. (A) Immunoblot and (B) relative analysis of CTGF, IRE1- α , and PDI in NRCM exposed to 3 μ M thapsigargin (TGN) for the indicated time periods. Analysis was normalized to Tubulin, and the change in CTGF expression was estimated relative to the control. Values are given as mean \pm SEM, $n=3-5$. Statistical comparisons were performed by one-way ANOVA, and post hoc correction with Bonferroni's multiple comparison tests, * $p < 0.05$ vs. control.

Aside from DTT and TGN, tunicamycin (Tm) has been demonstrated to induce ER stress (Kaufman, 1999). Therefore, the NRCMs were treated with Tm for different time periods and with various concentrations and CTGF was again analyzed by immunoblot. However, under neither conditions a change in CTGF expression as well as in the ER stress marker IRE1- α could be observed (Figure 44).



B

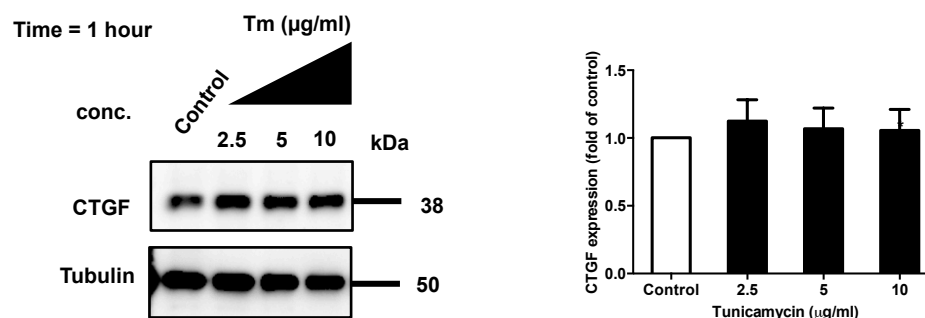


Figure 44 | CTGF protein expression in NRCM exposed to Tm. (A) Immunoblot and relative analysis of CTGF and IRE1- α in NRCM exposed to (A) 2.5 μ g/ml Tm for different time periods. Values are given as mean \pm SEM, n=4. (B) treated with different concentrations (2.5, 5 and 10 μ g/ml) for 1 hr. Values are given as mean \pm SEM, n=3. Analysis was normalized to Tubulin, and the change in CTGF expression was estimated relative to the control. Statistical comparisons were performed by one-way ANOVA, and post hoc correction with Bonferroni's multiple comparison tests, *p<0.05 vs. control.

4.3.3 Impact of heat shock response and chaperone/heat shock protein on CTGF expression in NRCM

As ER stress induced by DTT and TGN influenced CTGF in its oxidative state and expression, respectively, the effect of other stressors was investigated next. To analyze the influence of the heat shock protein hsp47, CTGF expression was analyzed in control mouse embryonic fibroblasts (MEF) and hsp47 knockout mouse embryonic fibroblasts. In this experiment, CTGF was found to be less expressed in hsp47 MEF compared to control cells. Next, the NRCM were incubated at 42°C for 1h with a subsequent recovery phase for different time periods. CTGF was found to be up-regulated 2 h after the heat shock (Figure 45).

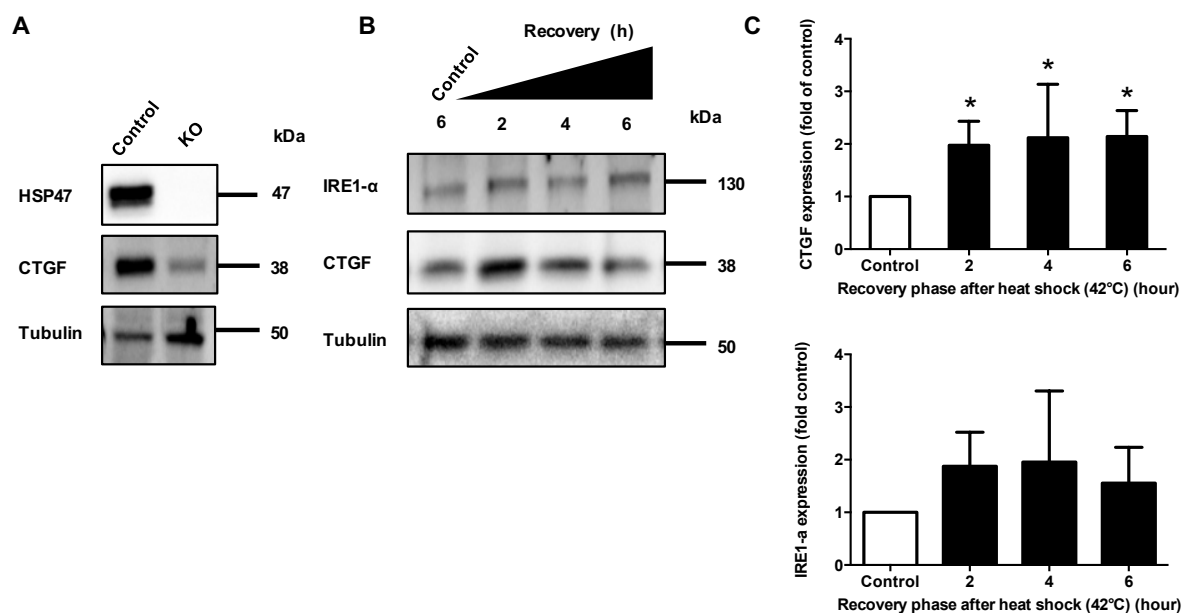


Figure 45 | Effect of heat shock on the expression of CTGF. (A) Protein expression of CTGF, HSP47 and Tubulin in control and HSP47 knockout mouse embryonic fibroblasts, $n=1$. (B) Immunoblot and (C) relative analysis of CTGF, IRE1- α and Tubulin as a loading control in cell extracts from NRCM after heat shock at 42°C for 1 h and recovery phases of 2-6 h. Values are given as mean \pm SEM, $n=5-6$. Statistical comparisons were performed by one-way ANOVA, and post hoc correction with Bonferroni's multiple comparison tests, $*p<0.05$ vs. control.

4.3.4 Impact of pH, MG132 and BFA on CTGF expression in NRCM

To further examine the effects of the pH of the culture medium on CTGF expression, the NRCMs were cultivated under different pH conditions (pH 8, 7, 7.5 and 6) for 1 h. However, no effect was detectable (Figure 46.A). Moreover, inhibition of the proteasome with different concentrations of MG132 was also without effect (Figure 46.B). And finally blockade of the transport from the ER to the Golgi apparatus by brefeldin A (BFA) showed no effect (Figure 46.C).

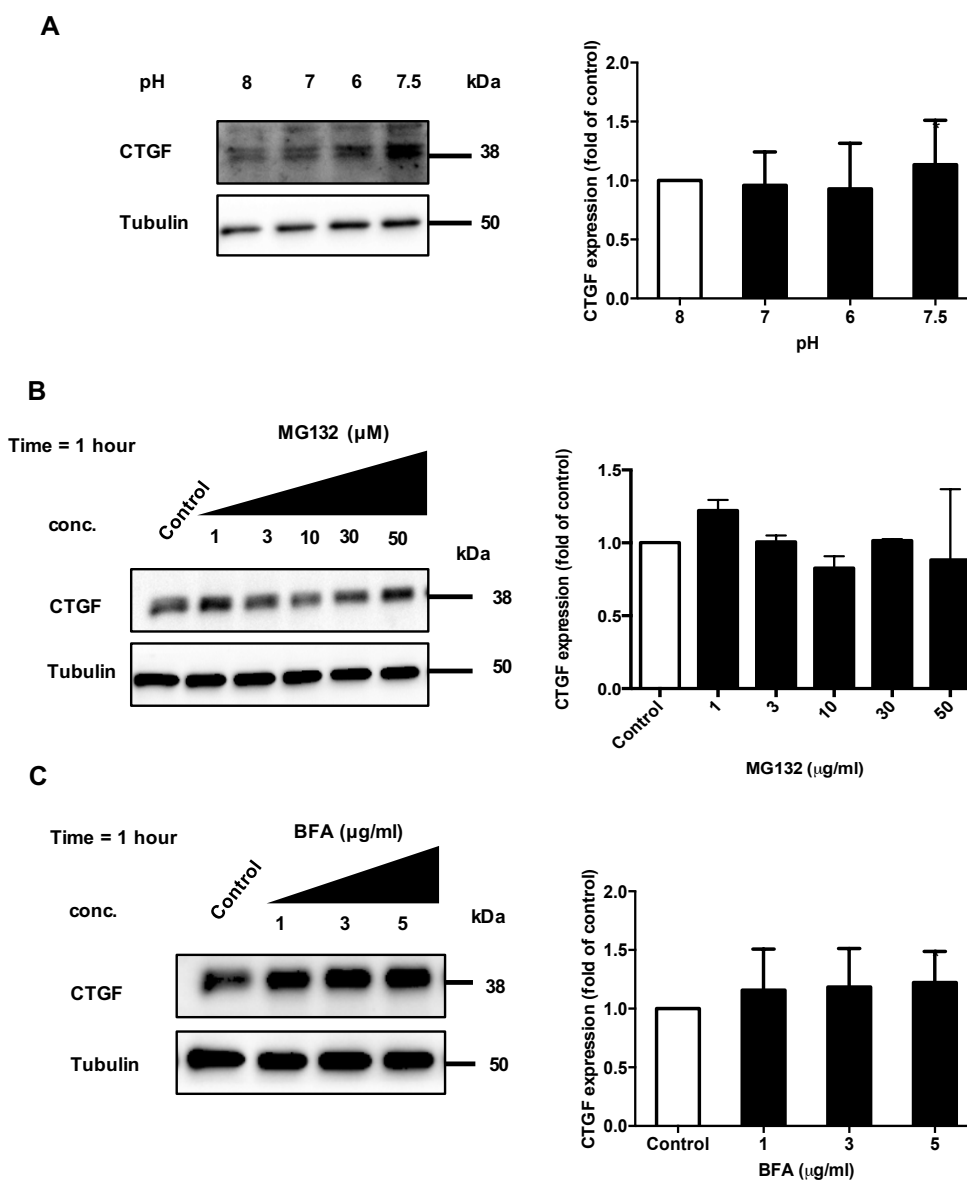


Figure 46 | The effect of pH, MG132 and BFA treatment on CTGF expression in NRCM. Immunoblot and relative analysis of CTGF in NRCM exposed to (A) Different pH over 1 h. Value are given as mean \pm SEM, n=6. (B) Concentration-dependent of MG132 over 1 h. Value are given as mean \pm SEM, n=3 (C) Concentration-dependent of BFA over 1 h. Value are given as mean \pm SEM, n=3. Tubulin is shown as loading control. Statistical comparisons were performed by one-way ANOVA, and post hoc correction with Bonferroni's multiple comparison tests, *p<0.05 vs. control.

4.3.5 Impact of siRNA-CTGF knockdown on NRCM

As CTGF was demonstrated to be regulated by cellular stressors like DTT and TGN, in the next step the effect of CTGF expression on the ER stress response was analyzed. Therefore, CTGF expression was reduced by a siRNA approach. Immunofluorescence analysis demonstrated that the knockdown of CTGF appeared to lead to a translocation of ATF6 to the nucleus (Figure 47).

Moreover, the knockdown of CTGF led to a significant downregulation of the ER stress markers IRE-1 α , PDI, and BiP (Figure 48). Only CHOP was not changed in its expression.

Next, the splicing of the XBP1 mRNA was analyzed by PCR which had been demonstrated to occur during the unfolded protein response (Wang et al., 2014). In these experiments, the knockdown of CTGF resulted in the amplification of two PCR products representing the unspliced (US) and spliced (S) XBP1 mRNA (Figure 49).

To validate, the immunoblot data, the expression of ER markers at mRNA level was examined. As shown in Figure 50, with successful knockdown of CTGF at mRNA level, other ER stress markers were not changed.

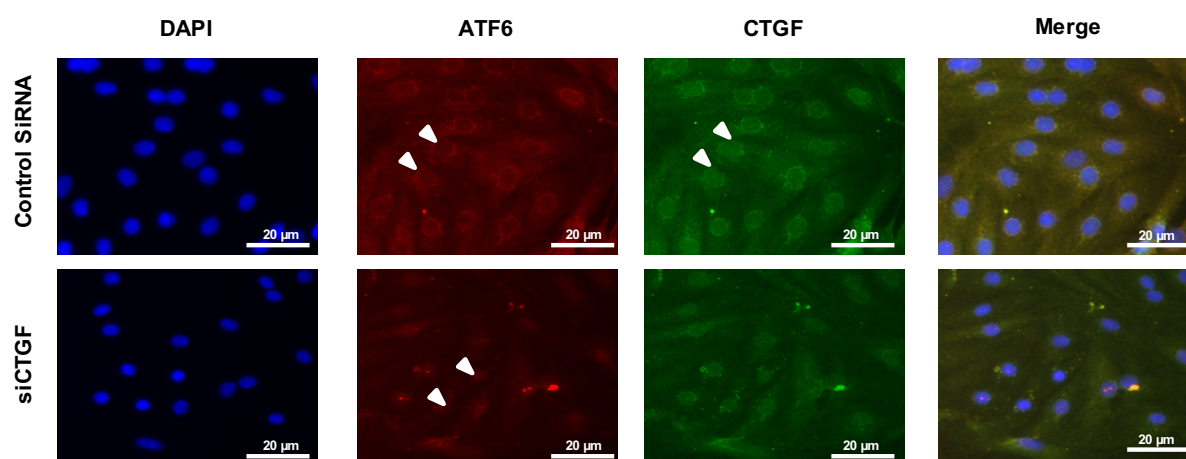


Figure 47 | Knockdown of CTGF in NRCM and ATF6 localization. siRNA was used to partially knockdown CTGF in NRCM. In the control siRNA, ATF6 was localized at endomembranes (arrow heads), whereas in the cells treated with the siRNA, ATF6 was moved to the nucleus (arrow heads). Immunofluorescence staining was performed to detect CTGF (green), ATF6 (red) and the nuclei were stained with DAPI (blue), n=2, Scale bar: 20 μ m.

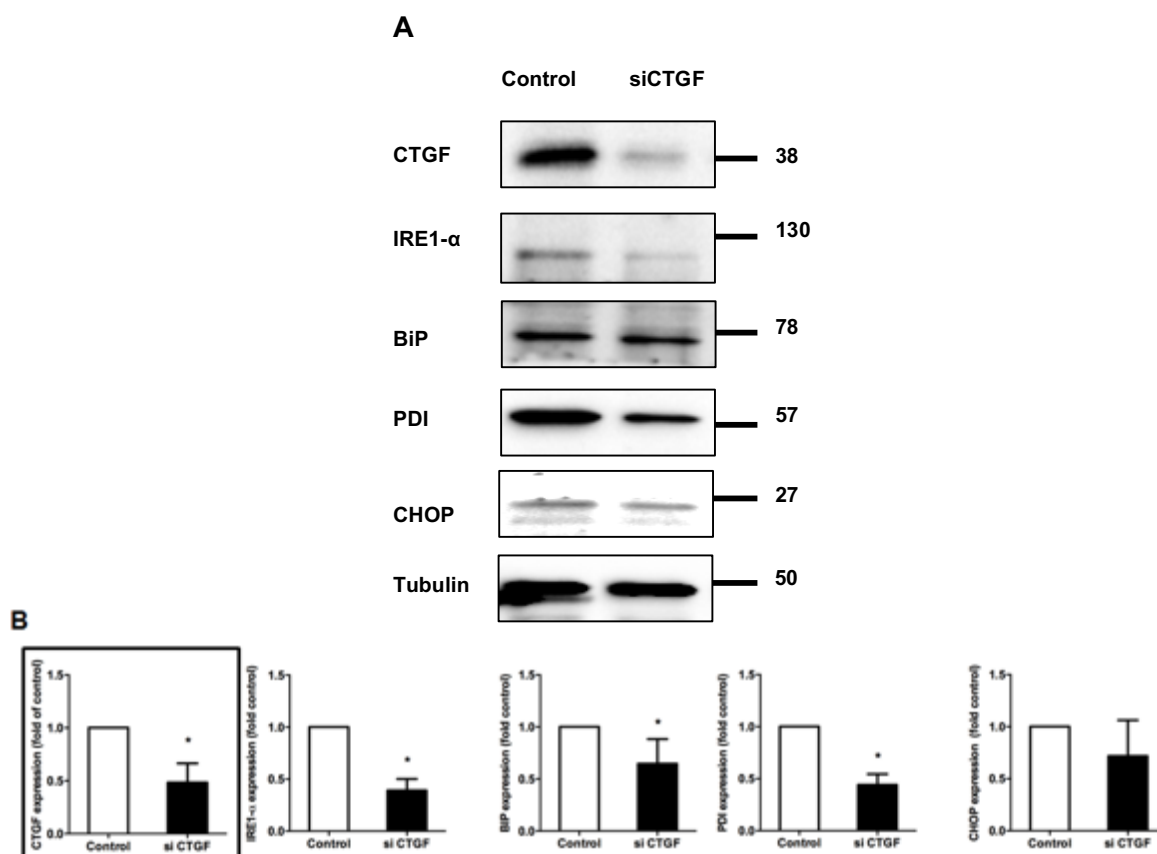


Figure 48 | Partial knockdown of CTGF in NRCM and various ER stress markers at the protein level. (A) Immunoblot and (B) relative analysis of CTGF, IRE1- α , BiP, PDI and CHOP (markers of ER stress) on siCTGF-partial knockdown NRCM. Values are given as mean \pm SEM, $n=4-7$. Statistical comparisons were performed by an unpaired t-test, * $p < 0.05$ vs. control.

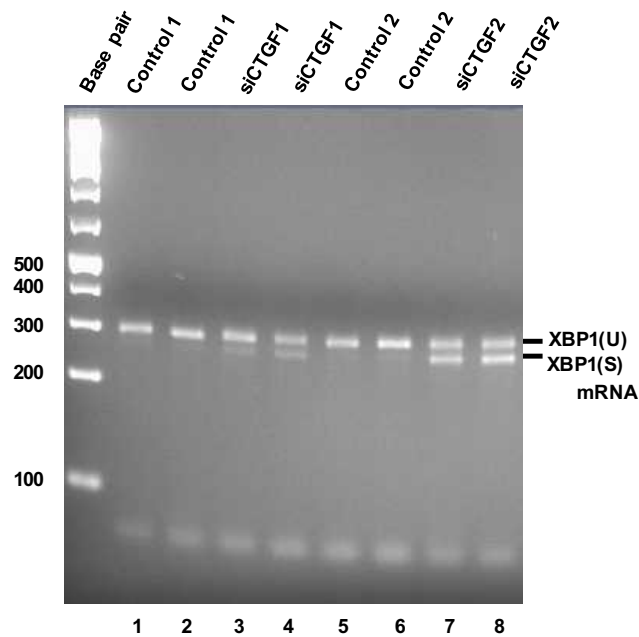


Figure 49 | Knockdown of CTGF in NRCM with XBP1 splicing. XBP1 mRNA was detected by RT-PCR. XBP1US was observed as a 289 bp band, and XBP1S was observed as a 263 bp band on siCTGF-partial knockdown NRCM, $n=2$.

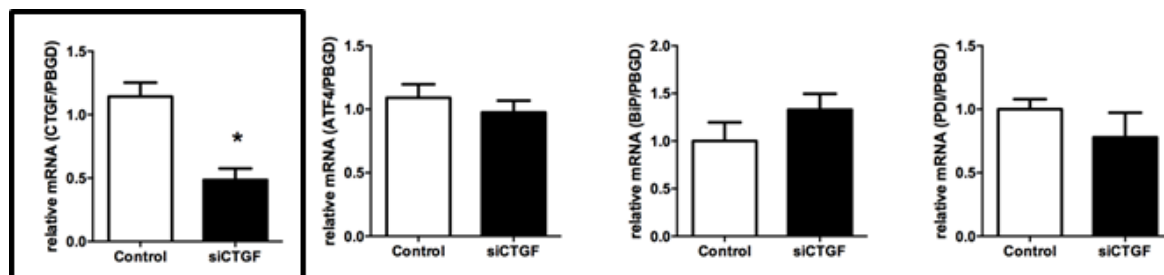


Figure 50 | Partial knockdown of CTGF in NRCM and various ER stress markers at the transcription level. mRNA level of CTGF, ATF4, PDI, and BiP was assessed by qPCR in control and CTGF knockdown NRCM. The values are given as mean \pm SEM, n=4. Statistical comparisons were performed by a paired t-test, *p<0.05 vs. control.

5 Discussion

In spite of significant improvements in the treatment of cardiovascular diseases, heart failure remains a prevalent problem. Heart failure describes a critical state in which the heart is not able to maintain normal cardiac output, and thus blood supply to the organs is diminished. The leading causes of heart failure include arrhythmia, cardiomyopathy, hypertension, myocardial infarction and ischemic heart disease (Drazner, 2011; Minicucci et al., 2011; Yancy et al., 2013; Diez, 2014; Lip et al., 2016; Marti-Carvajal and Kwong, 2016). For decades variations in the phosphorylation and redox status of various proteins have been characterized in different areas of heart diseases, however this has unfortunately not resulted in many new therapeutic treatments. Both abnormal phosphorylation states of essential cardiac proteins and elevated ROS production contribute to contractile dysfunction and fibrosis in failing hearts. Cys residues are subjected to oxidation, however the interplay between oxidation and downstream phosphorylation events remains unclear. Despite its important role in the cardiovascular system whether redox changes to PP-1 affect the regulation of its targets is not fully understood. In this study, mass spectrometry was used to explore the oxidation state and various PTMs of PP-1. In addition to irreversible modifications, such as sulfonic acid formation of Cys residues, mass spectrometry may work as a robust strategy to identify transient modifications such as disulfide bridge formation and glutathionylation of PP-1.

The effect of oxidative stress is, however, not restricted to the cytoplasm of a cell. Also other compartments are affected by increased oxidative stress. With that respect, the endoplasmic reticulum (ER) is of special interest as oxidative stress can induce ER stress leading to an accumulation of unfolded transmembrane and secreted proteins. This results in the unfolded protein response which itself is a reactive oxygen species producing mechanism (Santos CX et al., 2009). Therefore, the secreted protein CTGF, which is strongly induced in heart failure, was studied as a target of oxidative changes in the ER and as a potential regulator of ER stress.

5.1 H₂O₂ influences the movement and morphology of cardiac cells

Exogenous H₂O₂ application is a valuable tool for altering oxidant-dependent signaling in cardiac tissue and cells. For maintenance and efficient physiological functioning of the cardiovascular system, it has been well established that levels of endogenous H₂O₂ need to be lower and that higher levels are associated with various diseases (Halliwell et al., 2000; Gough and Cotter, 2011). Recently it has become clear that H₂O₂ is not exclusively

associated with deleterious functions but also mediates normal physiological processes (Schroder and Eaton, 2008). The mechanisms by which oxidation alters the heart's contractile properties resulting in myocardial remodeling is not entirely understood.

To investigate the possibility that H_2O_2 exogenously regulates cardiac function, NRCMs were treated with different concentrations of H_2O_2 for 24 h and a time-lapse movie was recorded. Heat maps were generated from the movies showing the spots of myocyte contraction as mean of the time-averaged magnitude of every motion. For that a matlab based script was used, according to Huebsch et al, which also quantified the contraction velocity and the relaxation velocity of the myocytes at each H_2O_2 concentration (Huebsch et al., 2015). From this values the relaxation-contraction ratios were calculated to give a measure of myocyte vitality. A resolution of $0.6442 \mu\text{m}/\text{pixel}$ ($20\times$ objective) was used and dead floating cells were tried to filter with the script build-in cleaning mechanism. The script first determines spatiotemporal information about motion vector direction and intensity of every beating cardiac myocyte which will then be translated into the results seen in Figure 18. Results demonstrated that a concentration of $10^4 \mu\text{M}$ H_2O_2 significantly damaged NRCM vitality. However, NRCMs were resistant to lower concentrations 100 or $10^3 \mu\text{M}$ of H_2O_2 (Figure 18). During disease states when ROS is elevated cardiac function is compromised altering calcium homeostasis and negatively affecting myofilament proteins responsible for mediating contractile functioning. The reciprocal synergy between ROS and calcium signaling has been shown to modify various calcium channels, pumps, and exchangers (Görlach et al., 2015). Lower levels of endogenous H_2O_2 are essential for normal physiological functioning and signaling, whereas higher levels are associated with altered cell morphology in cardiac myocytes (Schroder and Eaton, 2008). Another study showed that acute treatment of $100 \mu\text{M}$ H_2O_2 for 45 min in NRCM, triggers MAP kinase activation which could further be stopped by catalase (Sabri et al., 1998). In addition, treating the cardiomyocytes or fibroblast with $0-200 \mu\text{M}$ H_2O_2 for 30 min induces MAPK, and while the cells are remaining healthy, some downstream phosphorylation targets were downregulated by EGF receptor inhibitors (Purdom and Chen, 2005). Interestingly, another group revealed that different concentrations of H_2O_2 showed a different effect in rat cardiomyocytes over the period of 24 h, such that $10-30 \mu\text{M}$ triggered protein synthesis, $200 \mu\text{M}$ induced apoptosis and $300-1000 \mu\text{M}$ triggered both apoptosis and necrosis (Kwon et al., 2003). In summary, exogenous application of H_2O_2 to tissues or cells in the range of $0.1-1.0 \text{ mM}$ over several hours will not lead to the death of cells but rather triggers downstream signaling pathways.

5.2 Oxidative stress influences cardiac β -adrenergic signaling pathway and PP-1 activity

According to the enzymatic activities, there are two enzyme subclasses within the family, PP-1, and PP-2, which further consists of PP-2A and PP-2B (calcineurin) and PP-2C (Ingebritsen and Cohen, 1983). In the cardiovascular system PP-1, PP-2A and PP-2B are responsible for 90% of protein phosphatase activity (El-Armouche and Eschenhagen, 2009). Neumann et al first identified increased PP-1 activity as a hallmark of cardiovascular disease (Neumann et al., 1997). Almost one decade ago it was established that both *in vitro* and *in vivo* PP-1 activity is inhibited by H₂O₂ (3 mM) treatment and further that it could be reversed *in vitro* by thiol-oxidant *N*-acetyl-cysteine (NAC) and reduced glutathione (GSH). Moreover, it was found that NAC pretreatment protected from H₂O₂ triggered PP-1 inactivation, eradicating H₂O₂ triggered eIF2 α phosphorylation and protein synthesis inhibition (O’Loughlen et al., 2003). In the following year, it was also shown in rat hippocampal and SHSY5Y human neuroblastoma cells, that there was a decrease in the phosphorylation of I-2 and PP-1 activity due to H₂O₂ incubation; the authors proposed that oxidative stress-induced activation of Cdk5 led to I-2 phosphorylation, preventing its inhibitory effect on PP-1 (Zambrano et al., 2004). How oxidative stress and β -adrenergic signaling pathways converge via PP-1 in cardiac cells was analyzed. To assess PP activity two assays were utilized: EnzChek kit assay (DiFMUP as substrate; Figure 15) and ProFluor Ser/Thr PPase Assay (R110 as substrate; Table 14).

Using the ProFluor Ser/Thr PPase assay, PP-1 and PP-2A activity was calculated by using a selective inhibitor, i.e. OA in NRCM and whole heart tissue of mice (Figure 20). Using this assay, findings are in line with previous work, demonstrating a 10% contribution of PP-1 in both species. Structure-function analysis suggests that PP-1 activity may be regulated by two redox-sensitive Cys residing in proximity to its active site (Fetrow. et al., 1999). To further validate whether PP-1 activity is oxidant-dependent, a recombinant PP-1-GST tagged peptide was used with the abovementioned kit. PP-1 activity was inhibited by the exogenous addition of H₂O₂ in both a concentration and time-dependent manner (Figure 21.A-B). Furthermore, the reversibility of the inhibition of PP-1 activity was elucidated via the reducing agent (TCEP) (Figure 21.C). The EnzChek kit assay was used to calculate total phosphatase activity in human non-failing (NF), ischemic cardiomyopathy (ICM) and dilated cardiomyopathy (DCM) donor hearts. Interestingly, the total phosphate activity was lower (~7%) in DCM as compared to ICM and NF (Figure 19). Consequently, using the same kit, in NRCM the inhibition of total PP activity was identified by 25%, in the presence of 100 μ M H₂O₂ as exogenous oxidant (Figure 22). In parallel recently, Santos et al, demonstrated that,

recombinant PP-1 was also concentration-dependently inactivated by H₂O₂. However, thiol reductant such as DTT, glutathione and Cys did not restore PP-1 activity as removal of excess of H₂O₂ by catalase treatment. But with a one-electron reductant, ascorbate, efficiently reversed PP-1 inactivation (Santos et al., 2016).

The PP-1-inhibitory subunit I-1 is strongly expressed in the cytosol of cardiomyocytes, and thus plays a primary role in phosphorylation feedback loops and expedites crosstalk between phosphatases and kinases. During β -adrenergic stimulation, I-1 was activated via PKA, consequently inhibition of PP-1, which leads to the formation of a positive feedback loop augmenting the phosphorylation of several cardiac substrates such as PLB, RyR2, cMyBPC and Tnl (El-Armouche et al., 2003; Heijman et al., 2013). Also, many cardiac proteins are dephosphorylated by PP-1 and PP-2A, for example PP-1 triggers the dephosphorylation of Tnl at Ser^{23/24} (Solaro and Kobayashi, 2011). The results in NRCM demonstrated a novel impact of oxidative stress on various cardiac proteins playing a vital role in the functioning of the β -adrenergic signaling pathway (Figure 24). The phosphorylation status of protein phosphatase inhibitor-1 (I-1), a crosstalk protein between PKA and PP-1 signaling, showed a bell-shaped phosphorylation response with a maximal peak at 100 μ M H₂O₂ (Figure 23). This data is in line with results from the Eaton group, i.e. the oxidant-induced bell-shaped PKA phosphorylation was highest at 100 μ M H₂O₂ (5 min) in adult rat ventricular myocytes; after which there was a loss of phosphorylation (Brennan et al., 2006). However, no effect on phosphorylation of both PLB-Ser¹⁶ and cMyBP-C-Ser²⁸² was observed in concentration dependent manner (Figure 24.C). For PLB-Ser¹⁶, phosphorylation was decreased after 10 min incubation with 100 μ M H₂O₂, whereas phosphorylation of cMyBP-C-Ser²⁸² showed a bell-shaped curve with the highest peak at 10 min (Figure 24.B). One possible explanation could be that PP-1 activity was decreased after 10 min (Figure 21.A) and that might suggest for the cMyBP-Ser²⁸² phosphorylation to be high after 10 min. Nevertheless, it is surprising that PLB-Ser¹⁶ phosphorylation is decreased after 10 min. If H₂O₂ is incubated longer, it is possible that it has more time to phosphorylate and activate I-1 via PKA oxidant dependent activation (Brennan et al., 2006), which will inhibit PP-1 more strongly and therefore increase phosphorylation at PLB-Ser¹⁶. However, on the other hand, a study done in cardiomyocytes directed NOX2 transgenic mouse model, Ang II-stimulated NOX2-ROS production increased cardiac contractile performance by augmenting SERCA activity driven by enhanced PLB phosphorylation and led to faster contraction and relaxation. Further, it was established that PP-1 activity was strongly inhibited in Ang II-treated transgenic mice, which is in line with the mechanism where NOX2 inactivates PP-1, permitting for an increase in PLB phosphorylation. Still, the spatial interrelationship between NOX2, PP-1 and PLB or how PP-1 is inhibited by NOX2, remains elusive at this stage. One possible suggestion could be that,

NOX2 inhibits PP-1 locally at the junctional SR and this then transduces the signal to PLB at the network SR (Zhang et al., 2015).

In summary, these results suggest that the activity of PP-1 is inhibited in the presence of oxidation and that it can be reversed in the presence of the reducing agents. Our findings also demonstrated that the expression of PLB-Ser¹⁶ and cMyBP-C-Ser²⁸² were differentially affected by H₂O₂, indicating a complex layer of regulation of both redox-sensitive kinases and phosphatases. Results from failing human samples show that PP activity is diminished in failing myocardium. The pathway described in this study could therefore be novel possibility with which to treat cardiovascular disease.

5.3 Identification of redox-sensitive Cysteine residues in PP-1 via immunoblotting

In 2006, it was demonstrated that the regulatory subunit of type I PKA contain redox-sensitive Cys residues. With respect to the availability of cellular H₂O₂, this leads to the two RI subunits of the tetrameric holoenzyme to form inter-protein disulfide bridges (Brennan et al., 2006). The same experiment with H₂O₂ and diamide was successfully replicated in NRCM. In addition, samples were also treated with maleimide, which reacts with free thiol groups and further stops oxidative reactions or disulfide bridge formation. Interestingly, using similar protocols in NRCM samples, PP-1 immunoblots show the formation of a dimer at 70 kDa (Figure 26) suggesting that inter-molecular disulfide bridges may be formed in PP-1 in its native state. These results are similar to those obtained from the Brautigan group which showed that purified PP-1 from rabbit skeletal muscle formed a 70 kDa polypeptide as a potential dimer of the 38 kDa monomer (Brautigan and Shriner, 1989). Surprisingly, Cys¹²⁷ was also identified to form inter-disulfide bridges as one of the PTMs using mass spectrometry (Figure 35). One of the limitation of these findings is that although the dimer formation was identified from control samples up to 10⁴ μM diamide, including 37 kDa. However, mass spectrometry results indicated that only Cys¹²⁷ was identified to form inter-disulfide bridges and only with condition -Mn²⁺ and +H₂O₂, in contrast to the immunoblot data. In addition to this reduced expression of PP-1 was identified with increasing concentration of diamide at 37 kDa. An explanation for the above-mentioned result may be that the epitope of the antibody is less available after a dose of 10³ and 10⁴ μM diamide.

In 2007, it was discovered in rat cerebral cortex, that inhibition of PP-2A activity was associated with the formation of intramolecular disulfide bridges (Foley et al., 2007). With the same above-mentioned samples, band shifts were also checked and immunoblots showed

that the same results as PP-1 but no intramolecular disulfide bridge formation in PP-2A (Figure 27).

As SERCA in previous experiments with HPLC-ESI (electrospray ionization)-MS/MS (tandem MS) showed two Cys residues (Cys³⁴⁴ and Cys³⁴⁹) forming internal disulfide bridges (Sharov et al., 2006). To some extent the formation of an internal disulfide bridge in SERCA2a could be demonstrated by immunoblotting of shifted bands (Figure 28). One conclusion from the observation of a shift to lower size when running the NRCM samples under non-reducing conditions is that SERCA2a is forming an internal disulfide bridge. However, under the above-mentioned conditions for PP-1, no such shift was observed therefore contradicting the idea of internal disulfide bridges formation in PP-1. Similar results were observed for PP-2A.

A biotin-conjugated iodoacetamide (BIAM) labeling assay was used to investigate whether PP-1 Cys-oxidation changes in response to ROS. From the results, one conclusion is that, free Cys residues are mostly protected from oxidations at very acidic pH and performing the assay at slightly acidic or slightly basic conditions does not protect the Cys residues from being oxidized. These results suggest that, under the chosen conditions, the Cys residues of PP-1 are not susceptible to oxidation by H₂O₂ (Figure 29). However, the 'Biotin-switch assay' should be used as an indirect method to check for oxidized Cys in proteins as an alternative to the BIAM labeling assay (Forrester et al., 2009).

In summary, immunoblots demonstrated the PKA's dimerization and SERCA's band shift, thus representing Cys oxidations in the respective protein. With respect to PP-1, results suggest the dimerization formation at 70 kDa, however a band shift was not observed. Section 5.5.6, illustrates the prediction software results, which concur with above mentioned findings.

5.4 Known oxidative state of Cysteine in PP-1

The recent X-ray structure of oxidized PP-1 γ (PDB id: 4UT3; Figure 51) reveals that only two Cys residues Cys¹²⁷ and Cys²⁷³ are oxidized. Cys²⁷³ resides on the outskirts of the structure, might be one of the reasons, for not identifying any connection towards disulfide bridges. In contrast, since Cys¹²⁷ lies in the vicinity of various other Cys, it is expected that it interchanges disulfide bridges with the network around it in the, those disulfide links were identified with mass spectrometry (see Figure 31). The same results were identified in the recent crystallographic studies, stating that Cys¹²⁷ and Cys²⁷³, were often oxidized to a sulfenic derivative in electron density maps (Santos et al., 2016).

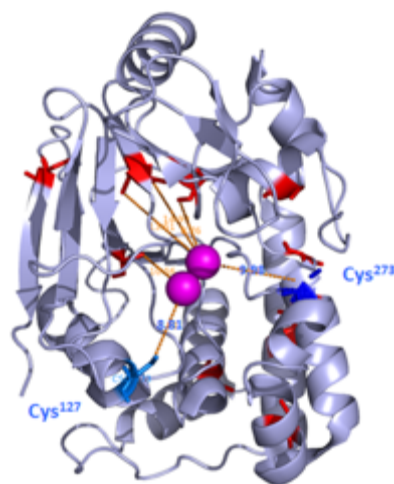


Figure 51 | The X-ray structure of PP-1y (PDB id: 4UT3) in its oxidized state. The two blue Cys residues (Cys¹²⁷ and Cys²⁷³) are oxidized in the presence of H₂O₂. The distances between oxidized Cys and Mn²⁺ are measured as follows: Cys¹²⁷-Mn²⁺ = 8.81 Å; Cys²⁷³-Mn²⁺ = 9.98 Å.

5.5 Impact of redox stress on PP-1 detected by mass spectroscopy

The varied chemistry of Cys residues is due to the electronic structure of its thiol group, resulting in multiple oxidation states (-2 to +6) and redox modifications (sulfenylation, -SOH; sulfinylation, -SO₂H; sulfonylation, -SO₃H; glutathionylation, -SSG; SS formation, etc.). All of which contribute to various signaling pathways. For example, it has been well established that tyrosine phosphatases are sensitive to oxidation by ROS, especially H₂O₂, acts as an intracellular second messenger in the cells (den Hertog et al., 2005; Tonks, 2005). In the following sub-sections, the key focus will be to discuss the structure of PP-1 with respect to its various PTMs, Mn²⁺ role, networking of disulfide bridges and predictive computational methods.

5.5.1 Redox-response of GST-tagged PP-1 involves glutathionylation of Cys: 140, 202 and 245

PTP-1B is the most studied redox-sensitive signaling protein which consists of reversible oxidized Cys involving Cys²¹⁵ to be glutathionylated (Barrett et al., 1999). Though H₂O₂ is known to be a secondary messenger, excessive concentrations may also damage various amino acids (Berlett and Stadtman, 1997). Cys residues are first oxidized to sulfenic acid, which is reducible, however they may be further oxidized to irreversible sulfinic and sulfonic acid. Another possible pathway could involve the protective pathway by reacting with glutathione to form a reversible disulfide link, which prevents excessive oxidation. S-glutathionylation is reversible and so protects and modifies structures/functions of proteins.

Thus it can consequently regulate signaling pathways to maintain cellular homeostasis (Grek et al., 2013).

In the course of the experiments, it should be considered that, PP-1 is tagged with glutathione S-transferase (GST), and supplied with 10mM of excess glutathione (GSH) in the buffer for the stability of the protein. In this thesis, results (Figure 32) have demonstrated that in GST-tagged PP-1, glutathionylation can be induced at outer-bound Cys residues (i.e. Cys¹⁴⁰, Cys²⁰² and Cys²⁴⁵) only as a consequence of oxidative stress. Also, with Cys²⁰², both complete glutathionylation and persulfide modifications were identified (Figure 33). Altogether, the findings of the mass spectrometry experiments provide strong evidence that Cys residues in PP-1 are prone to oxidation. Therefore, glutathionylation in PP-1 could be a fast response to oxidative stress that protects the protein from further damage. A major limitation of this finding is that the same experiments were not performed with different concentrations of GSH in the presence of the GST-tagged PP-1 and with different concentrations of GSH in the presence of a non-tagged protein. Therefore, it cannot be unequivocally concluded from the data that glutathionylation occurs. Also, the non-detectable Cys peptides generated with LC-MS/MS were believed to be involved with disulfide bridge formation, but they were not detectable. Therefore, these Cys residues may be altered by a hitherto unknown modification (Append 1).

Additional experiments are necessary to repeat the above findings intracellularly. This is critical for illustrating the glutathionylation state of PP-1, as GSH is present in large amounts (~10mM) in cells and reduces various oxidizing agents, including H₂O₂. Furthermore, it would be necessary to identify which modifications occur *in situ*, such as: sulfenic acid (Cys-SOH), intra-disulfide (Cys-SS) and/or mixed disulfide (Cys-SSG). Nonetheless, the above results indicate that the action of GSH to modify Cys-SOH into Cys-SSG in the intracellular context to form glutathione mixed disulfide links (PP-1-SSG), is the first reaction to oxidative stress. The results also demonstrated that the activity could be recovered with TCEP or by thioltransferase (see also Figure 21).

5.5.2 Mn²⁺ in external buffer plays a protective role for Cysteine oxidation

Nearly two decades ago, it was shown that PP-1 activity mainly relies on the di-nuclear metal center for catalysis, rather than Cys-redox modifications (Egloff et al., 1995; Goldberg et al., 1995). Later it was demonstrated by Zhang et al in a cardiomyocyte-targeted NOX2-transgenic mouse model that elevated NOX2 activity modulates cardiomyocytes SR Ca²⁺ uptake and contractile function. Which further, increased PLB phosphorylation in both heart

tissues and cardiomyocyte cells, which correlated with the inhibition of PP-1 activity. This mechanism was additionally confirmed with PKA inhibitors blocking Ang II-mediated enhancement of contractile function in transgenic myocytes. (Zhang et al., 2015). The same group later also showed that PP-1 inhibition is mainly redox-regulated by the metal center and not by the Cys oxidation. In particular, NOX4 mediate the inhibition of PP-1 resulting in enhanced eIF2 α phosphorylation and increase in ATF4 levels increase cell survival during protein misfolding stress and is strongly protective against acute cardiac or kidney injury (Santos et al., 2016).

A theoretical study on the reaction mechanisms of PP-1 has demonstrated a novel mechanism behind the different oxidation states of the Mn²⁺ at the catalytic center. Based on the high-resolution crystal structure, it was shown that the different oxidation states of Mn ion (i.e. Mn³⁺-Mn²⁺ and Mn³⁺-Mn³⁺) can shorten the bond lengths between the metal ions by 0.15 Å, which triggers the energy barriers (Zhang et al., 2013). In parallel, recently Santos et al., demonstrated that soaking of PP-1 crystals with H₂O₂ did not alter the general structural features of the active site, however a contraction of the average metal coordination sphere by 0.12 Å compared to ascorbate-treated crystals (Santos et al., 2016).

The active center is placed in proximity to Cys¹²⁷, Cys²⁷³, Cys¹⁵⁵ and Cys¹⁵⁸. Half of the Cys network, including Cys³⁹, Cys¹⁰⁵, Cys¹²⁷, Cys¹⁴⁰, Cys¹⁵⁵ and Cys¹⁵⁸, are in proximity to the metal ions and hence could be protected from oxidation. The other half is situated further from the metal ions and hence will not be protected. When the formation of disulfide bridges in our assay was observed, this separation into two halves quickly became visible (see also the two black boxes in Table 21). In addition, it was identified that extra Mn²⁺ ions in the buffer took reduced redox stress so that fewer disulfide bridges were formed as compared to the -Mn²⁺ +H₂O₂ conditions. The same was observed for other Cys-based PTM in PP-1. This result was obtained under harsh, non-physiological conditions (Table 20.C), but it could also be possible under higher H₂O₂ concentrations in the cellular context. Furthermore, the Cys sulfone levels were used as a readout of the damaging effect of H₂O₂ (Table 22). Additional Mn²⁺ in the buffer protected all Cys residues from over-oxidation, and therefore concluded that under physiological conditions, the two Mn²⁺ bound in the complex could provide protection from oxidation.

5.5.3 Network of disulfide bridges might play a protective role in maintenance of GST-tagged PP-1 activity under redox-stress

In this thesis, the role of various PTM including intra-molecular disulfide bridge formation and glutathionylation were assessed during oxidative stress. Oxidative stress has been shown

to affect the activity of the protein. This inhibition can also be reversed with the treatment of TCEP (Figure 21). S-Gluthathionylation was shown to be a fast response to a harsh oxidative treatment, but this modification may have deleterious effects if prolonged. Therefore, the formation of the disulfide bridges from the Cys residues, not in proximity to one another, may play a role in maintaining structural integrity of PP-1. Hence the structure of PP-1 could be highly dynamic, however the formation of transient intra-molecular disulfide bridges cannot be identified using typically employed approaches, such as non-reducing immunoblots. Nevertheless, these modifications may be identified using with mass spectrometry.

This approach was used in LC-MSMS experiments under four conditions: including and excluding both Mn^{2+} and H_2O_2 in the buffer solutions. A curious result that was identified under all conditions was that Cys¹⁵⁵ and Cys¹⁵⁸; Cys¹⁷¹ and Cys¹⁷² formed disulfide bridges. The direct proximity of Cys¹⁷¹ and Cys¹⁷² supports this behavior, and the disulfide bridge remains intact. This is an expected result because they are always placed on one peptide when the protein was digested with Trypsin. On the other hand, Trypsin digestion is performed at almost neutral pH, which can lead to artifact formation of disulfide bridges. The observation was because generally the detection of disulfide linked peptides is in only enabled by H_2O_2 treatment. Artifact formations did not play a major role in this experiment. Cys³⁹ and Cys¹²⁷ were not detected as free peptide spectra, which allows us to conclude that they play a major role in disulfide networking.

When a normal search was performed with all the Cys modifications, the formation of persulfides and/or dehydroalanines was observed for the following Cys residues: Cys⁶², Cys¹⁰⁵, Cys¹⁵⁵, Cys²⁰² and Cys²⁹¹, that must be formed under CID conditions from either disulfide bridges or any other type of disulfide-link. In conclusion, oxidative stress might induce disulfide bridge formations that freeze structural changes in the protein. Altogether, seven disulfide bridges were identified as true ones (Cys¹⁴⁰ XL Cys³⁹, Cys¹⁰⁵ XL Cys³⁹, Cys¹⁴⁰ XL Cys¹²⁷, Cys¹⁴⁰ XL Cys¹⁵⁴Cys¹⁵⁸ and Cys¹²⁷ XL Cys¹⁵⁴Cys¹⁵⁸). However, none of them were found to be in the appropriate proximity to form native disulfide bridges. In order to form disulfide bridges, Cys residues need more flexibility of the protein to come closer to each other. Three more disulfide bridge spectra were weaker and could be hence artifacts from the database search (Cys³⁹ XL Cys⁶², Cys³⁹ XL Cys¹²⁷ and Cys¹⁴⁰ XL Cys¹⁵⁴Cys¹⁵⁸), since the spectra do not contain enough information about the second peptide. Also from a structural point of view, these disulfide bridges are not very likely to form because the Cys residues are too far away from each other so that this could be explained by disulfide scrambling. On the other hand, not all Cys residues are involved in disulfide links when harsh oxidative stress is applied to the protein. Although experiments were performed under slightly acidic conditions,

the results from all four conditions provide sufficient information to conclude that true disulfide links were formed. Also, disulfide shuffling upon digestion with Trypsin might have also played a role.

With the aid of pymol and PDB id: 4MOV, all possible distances were measured in Ångström between all thirteen Cys. The distance between all the Cys and Mn^{2+} ions in PP-1 was measured as well. Table 21, arguments for the Cys which are closer to Mn^{2+} ions might be protected from oxidation. Figure 52.A shows close proximities of Cys²⁷³, Cys²⁰² and Cys¹²⁷. According to the distance measurements of the structure determined under non-oxidative conditions, one should also see protection for Cys²⁴⁵ and Cys⁶² (Table 21). The latter are close proximity to Cys¹⁵⁵Cys¹⁵⁸ which forms a disulfide bridges under all conditions (as detected in Figure 52.B). Cys¹⁵⁵ being in the center vicinity of all the Cys residues, it appears to be an ideal Cys to form disulfide bridges with other Cys. The same holds true for Cys²⁴⁵ (Figure 52.C) which shows a second network between Cys²⁹¹, Cys⁶², Cys²⁴⁵, Cys¹⁷¹ and Cys¹⁷². Cys¹⁷¹Cys¹⁷² could form a disulfide under all conditions. The two potential networks based on the proximities are indicated in black boxes in Table 21. To conclude, the experiments do not answer the question to which extent the Mn^{2+} ions are protective against the oxidation, since the H_2O_2 levels are quite artificially high. As stated above, Cys²⁷³ and Cys²⁹¹ are too far away from the active center and not protected by the Mn^{2+} ion, either. However, a truncated peptide was identified starting from Ser¹⁶⁸ being completely reduced without H_2O_2 , and a persulfide formation at Cys²⁹¹ when H_2O_2 was applied.

Over two decades ago, site-directed mutants of the catalytic subunit of rabbit muscle PP-1 were generated, as their activity is highly susceptible to inactivation by sulfhydryl reagents. In an experiment, they had mutated the following Cys residues: 39, 62, 171, 202, and 273 from Cys to Ser. All six mutants were active; and so did not depend on the mechanism of a cysteinyl-phosphate intermediate (Zhang et al., 1994). In the same study, interestingly, C²⁷³S mutant, this Cys is closest to the C-terminus, shows a similar activity to the wild-type recombinant enzyme, which suggests that that portion of C-terminus of PP-1 can be cleaved without loss of activity (Cohen, 1989; Bollen and Stalmans, 1992). Recent study confirming the abovementioned findings that, PP-1 Cys^{127/273}Ser double variant mutant exhibited the same catalytic activity as wild type PP-1 and responded identically to H_2O_2 treatment (Santos et al., 2016).

In the future, it would be interesting to conduct mutagenesis studies involving the replacement of redox-sensitive Cys residues in PP-1. For instance, Cys¹²⁷ would be a convincing link between disulfide bridges and PP-1 activity. It is also possible that an amino

acid switch could alter the PP-1 structure, leading to total inactivation of PP-1 and disrupting the β -adrenergic signaling pathway.

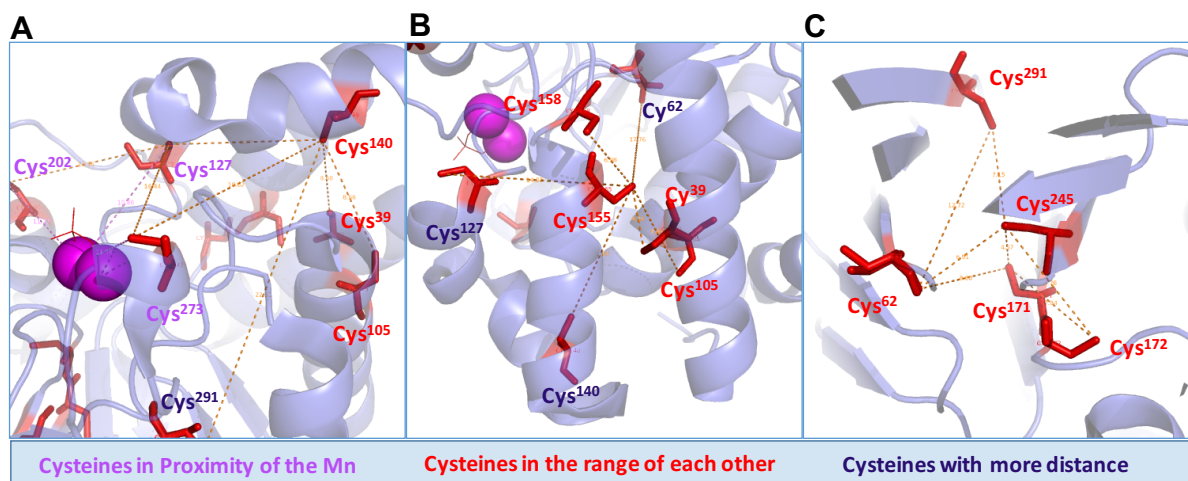


Figure 52 | Proximities of several Cys residues forming a network. Red Cys have a very high proximity, and blue Cys residues are in the range of 14 Å. (A) The cartoon representation shows close proximities towards the Mn^{2+} for Cys²⁷³, Cys²⁰² and Cys¹²⁷. The distance measurements of the structure determined under non-oxidative conditions, shows that Cys²⁴⁵ and Cys⁶² are protected (Table 21). (B) The figure shows the network of closer related Cys residues around Cys¹⁵⁵. Cys¹⁵⁵Cys¹⁵⁸ can form a disulfide under all conditions and might interact with Cys³⁹ and Cys¹⁰⁵. On the other hand, Cys¹⁴⁰ and Cys¹²⁷ are further away. With Cys¹⁵⁵ in the center vicinity of all the Cys residues, it could be ideal for forming disulfide bridges with all other Cys. (C) The same holds true for Cys²⁴⁵ which shows a second network between Cys²⁹¹, Cys⁶², Cys²⁴⁵, Cys¹⁷¹ and Cys¹⁷². Cys¹⁷¹Cys¹⁷² would also form a disulfide bridge under all conditions.

5.5.4 Redox response of His-tagged PP-1 involves sulfone formation

From the Peaks results, the first observation from the His-tagged PP-1A protein was that a large number of sulfone was formed at all Cys residues when H_2O_2 was applied, but no persulfides were formed at all. Furthermore, other amino acids were oxidized, which was not present in the GST-tagged PP-1A. This confirms the protective mechanism of GST in the buffer for all other amino acids, but also clearly shows that glutathione in GST-tagged PP-1 is protecting the protein from further oxidation and preventing the Cys from being oxidized up to the sulfone state, a mechanism missing completely in the His-tagged PP-1.

Similar to GST-tagged PP-1, the free peptides with Cys³⁹ were not visible, but some oxidized peptides comprised Cys¹²⁷. Cys³⁹ is the only disulfide bridge discovered close to Cys¹⁵⁵Cys¹⁵⁸ in the condition with non Mn^{2+} and with H_2O_2 . To conclude, the fast formation of sulfones of all the other Cys prevented more disulfide bridge formations. The distance table also shows the by far lowest distance of only 4.54 Å between Cys³⁹ and Cys¹⁵⁵, which argues for the fast formation of a disulfide bridges as a protection mechanism even more strongly.

When samples were free from Mn^{2+} and H_2O_2 , all Cys were free, and carbamidomethylation was possible. Surprisingly, when Mn^{2+} were not present in the buffer, the addition of H_2O_2 led to the formation of sulfonic acid of all Cys residues, whereas in the presence of Mn^{2+} ions this was not the case.

5.5.5 Do Histidine residues cage the dinuclear Mn^{2+} ions to shield them from Cysteine residues?

The X-ray structure of PP-1 has revealed the six residues which coordinate the Mn^{2+} ions (Asp^{64} , His^{66} , Asp^{92} , Asn^{124} , His^{173} and His^{248}). His^{66} is found next to one Mn^{2+} ion, His^{248} is next to the other Mn^{2+} ion, which excludes His^{125} from the unity sequence of the ligands amino acids. It has been well established that His^{125} is required for catalysis and that it is not a ligand to both metal ions, but that it is within the range of 5 Å (Lohse et al., 1995). However, site-directed mutagenesis of His^{125} been shown to have considerable effect on its catalytic activity as well as on the stability of the protein, which opens the question for the role of His.

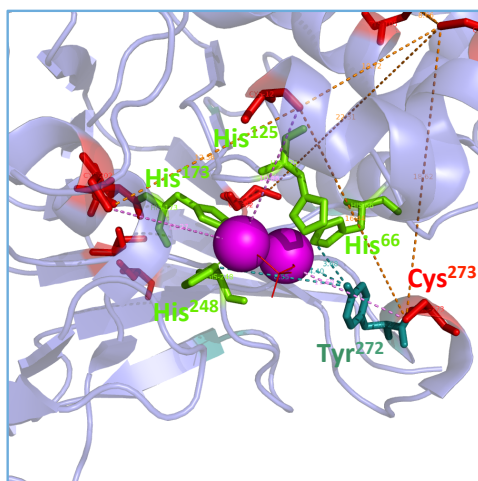


Figure 53 | His caging Mn^{2+} and Tyr²⁷² arrangement correlated to Cys network His arrangement around the dinuclear Mn^{2+} ions. In the structure of PP-1, two Mn^{2+} ions are surrounded by the four His residues (His^{66} , His^{125} , His^{173} and His^{248}). Tyr²⁷² is close by Mn^{2+} ions and gets oxidized.

Di-nuclear Mn^{2+} ions are surrounded by four His (His^{66} , His^{125} , His^{173} and His^{248}). Interestingly, in this study, His^{125} was discovered to be oxidized in the spectral data in the condition with Mn^{2+} and with H_2O_2 in His-tagged PP-1, while His^{248} was discovered to be oxidized in the GST-tagged protein (Figure 53). This lead to a conclusion that first Mn^{2+} is getting oxidized, followed by His. Cys residues might behave independently from this because they are shielded by the His residues from the protected distance of the metal ions. Mn^{2+} ions do not protect Cys from oxidation unless a certain order of oxidation (first Mn^{2+} and

later His) occurs as a protection mechanism. One possible conclusion could be that first Mn^{2+} gets oxidized and then His but that somehow Mn^{2+} ions fail to protect Cys from oxidation.

In addition, Tyr²⁷² gets oxidized in the condition with non Mn^{2+} ions and with H_2O_2 , which resides next to the Cys²⁷³ and also in close proximity of dinuclear Mn^{2+} ions. One suggestion for this oxidation could be that Tyr aids in the oxidation of both metal ions and Cys²⁷³ by transferring the electrons to them or vice versa. More experimental data are needed to prove this interesting finding.

5.5.6 Disulfide bridges determination in PP-1 using predictive computational methods and its correlation with mass spectrometry data

Cys is known as a triprotic acid in which the pK_a of the thiol group has been identified to be 8.2 (Tajc et al., 2004). Thiol groups are considered to be mild acids, where the pK_a value can be altered due to the protein microenvironment. In conclusion, the pK_a value will play a significant role, whether a thiol group will be reactive enough to oxidize, and hence to form disulfide bridges with a neighboring thiol group. In total, four different prediction software programs were used to identify the probability for disulfide bridges in PP-1 with corresponding PDB id or sequence information, namely PROPKA 3.1, COPA, DiANNA and dbGSH database.

PROPKA 3.1 software identified Cys¹⁵⁵ and Cys¹⁷¹ as the Cys with the lowest pK_a . The corresponding thiol groups containing Cys can be highly susceptible to oxidation and can later form disulfide bonds. Mass spectrometry analysis found those Cys residues to be involved in disulfide bridges in all times, but this correlates also with its simplified detection on just one Tryptic peptide. In contrast, COPA, an algorithm based disulfide bridges predictor software, identified Cys 39, 127, 155, 171, 245 and 273 to be redox sensitive. This software categorizes different Cys residues into oxidation susceptible and oxidation-non-susceptible and further classified three points for prediction of thiol oxidation susceptibility i.e. distance to the nearest Cys sulfur atom, solvent accessibility, and pK_a . Interestingly, both Cys³⁹ and Cys¹²⁷ were also not identified as free Cys peptides under all buffer conditions, and to be involved in disulfide formation. Cys²⁴⁵ is known as one target to glutathionylation. Furthermore, DiANNA software predicted mainly Cys²⁷³ to be in oxidation state with the score of 1. Also, from a structural point of view, PP-1 contains dinuclear Mn^{2+} in the pocket of the catalytic subunit, and Cys²⁷³ and Cys²⁹¹ were quite distant from it and hence could not be protected from oxidation by Mn^{2+} ions. In the mass spectrometry analysis, initially these two Cys residues were not detected at all, but a repeated search in aid with a semi-trypsin

activity that allows one non-specific cleavage, it was possible to detect a truncated peptide starting at Ser¹⁶⁸, where both Cys residues were non-oxidized in non Mn²⁺ and with H₂O₂ and hence must be protected. Under harsh oxidative conditions, Cys²⁹¹ was also identified as a persulfide, which indicated that it might form disulfide bridge or mixed disulfide bridge with glutathione. Another prediction software/database dbGSH proposed that Cys¹⁴⁰, Cys¹⁵⁸ and Cys²⁴⁵ could be S-glutathionylated, which could be correlated with the MS results that demonstrated Cys¹⁴⁰, Cys²⁰² and Cys²⁴⁵ to be S-glutathionylated (discussed in detail in Section 5.5.1).

5.6 Proposed mechanism for protection of PP-1 from irreversible loss of activity

In the native structure of PP-1, there is no disulfide bridge formation and no Cys residues are known to play any role in redox modified signaling mechanism. In this thesis, a mechanism for the redox modification of PP-1 is proposed (Figure 54). At this point, it is uncertain which part of the mechanism described below may be responsible for the redox-based activity of PP-1, but it seems clear that the GST activity and GSH at high concentrations actively protects the Cys residues from the formation of an irreversible state of sulfonic acid, which further leads to a protective mechanism that involves formation of various disulfide bridges. However, external addition of Mn²⁺ in the buffer also leads to the novel protection of Cys and His from oxidation.

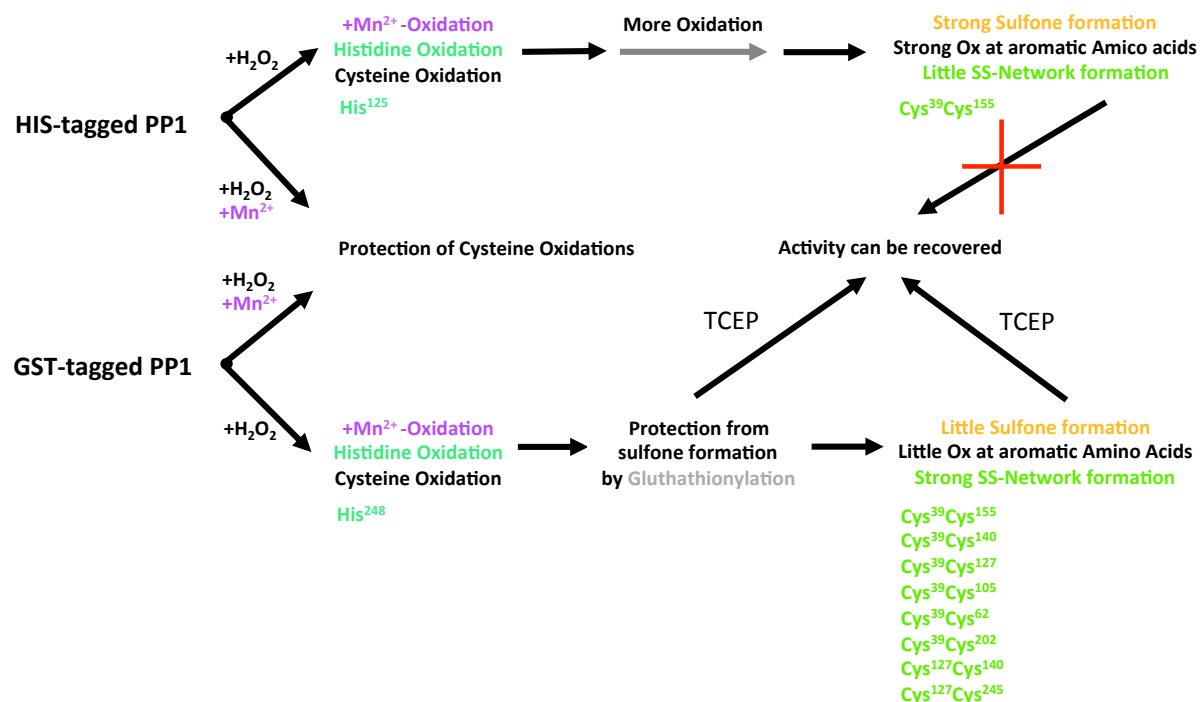


Figure 54 | A proposed mechanism showing the vital role of glutathione, His, Cys and Mn²⁺ ions in the activity of PP-1. With the aid of two His-tagged and GST-tagged rPP-1, glutathione

oxidation specifically in context of cardiovascular research (Zhang et al., 2015; Santos et al., 2016).

PP-1 is found as a target to oxidative stress in the brain, forming transient disulfide bridges (Foley et al., 2016), but the exact mechanism and the extent of the disulfide formation have not been determined. Repeated psychological stress might increase disulfide formation and the inhibition of the four non-Peridoxin-like proteins in the brain which directly increases the vulnerability for disturbed glutamate neurotransmission. In this context, thioredoxin was also mentioned as a marker protein in the early development of the disease. In particular in schizophrenia, a disturbed antioxidant defense system in combination with increased formation of reactive oxygen species plays a crucial role (Wu et al., 2013).

In conclusion, these results describe in detail a potential role of disulfide bridges and PTMs of the PP-1 alpha as a protection mechanism to maintain the activity of the protein under oxidative stress conditions in the context of heart disease, which may hold clinical and therapeutic implications.

5.8 Regulation of CTGF in response to ER stress

The number of cardiomyocytes usually decreases during HF (Nakano et al., 2012). Although the cause of this loss has not been fully clarified, it is known that cardiomyocytes are exposed to many different stressors in HF (Richardson et al., 1996; Chien, 1999). Among the stressors, mechanical stress is considered to induce growth response in the overloaded myocardium by the release of the growth promoting factors, such as Ang II, endothelin-1 and TGF- β (Ruwhof and van der Laarse, 2000). Besides mechanical stress, cardiomyocytes are also constantly exposed to oxidative stress (Santos et al., 2011).

In the first part of this thesis, a mechanism was suggested depicting the S-glutathionylation of PP-1 that could further lead to intra- and inter- disulfide bond formation and protect the protein from irreversible state of sulfonic acid. After establishing PP-1 a well-defined role in folding mechanisms, it will be really interesting to identify, which component of the cell plays role in the folding of the protein and maintains the hemostasis of the cell. To answer that question, one of the classic and little known secretory proteins called as CTGF was targeted. Various cellular functions, including processing of secreted proteins, calcium storage and folding of proteins, are controlled by ER and disruption to the ER function leads to ER stress. In the following sections of the discussion, the main focus is to identify whether the ER and CTGF have any co-relationship in maintaining the physiological balance of the cell.

The in this thesis presented data demonstrates that an increase in oxidative stress as elicited by the application of H₂O₂ led to a slight increase of intracellular CTGF levels, which were however not significant. Trends toward an up-regulation of CTGF were observed 6 min and 4 h after H₂O₂ addition (Figure 41.A). The long-term up-regulation of CTGF under stress conditions was further confirmed by the conduction of heat-shock experiments. These results are in accordance with previous findings of up-regulation of CTGF under stress conditions, in particular mechanical stress (Chudgar et al., 2006). These findings therefore indicate that CTGF up-regulation may be an initial response to different kinds of stressors in cardiomyocytes.

It has previously been shown that ER stress can be initiated by chemicals such as dithiothreitol (DTT), thapsigargin (TGN) and tunicamycin (Tm) which change the redox balance, Ca²⁺ homeostasis and protein glycosylation state in the ER, respectively, as well as brefeldin A, which inhibits transportation of proteins from the ER to the Golgi complex (Kozutsumi et al., 1988; Kaufman, 1999; Breckenridge et al., 2003; Merksamer et al., 2008). When these chemicals were applied to the cells, the ER protein folding machinery deteriorates. The aggregation of malfunctioned, misfolded proteins is a hallmark signal of ER stress (Chang et al., 1987). In this thesis, results obtained from cells exposed to DTT demonstrated that CTGF may form an intramolecular disulfide bridge as demonstrated with immunoblots showing molecular weight shifts from between 36 and 38 kDa under non-reducing and reducing SDS-PAGE conditions (Figure 42).

Furthermore, results also demonstrated that when NRCM were treated with TGN, it induced ER stress by emptying intracellular Ca²⁺ stores, which led to an up regulation of CTGF after 6 h (Figure 43). To determine if glycosylation was essential for rat CTGF localization and secretion, NRCM was also incubated with Tm. In contrast to TGN, incubation of NRCM with Tm did not affect CTGF expression. These results are perhaps not surprising as in rat CTGF, no N-linked glycosylation site has been identified. Thus, N-linked glycosylation could be excluded from a process influencing CTGF expression and secretion.

A liver study showed that hsp47, TGF-β1 and CTGF are involved in the pathogenesis of hepatic fibrosis infected by *Schistosoma japonicum*, and that downregulation of hsp47 in a hepatic mouse model of schistosomiasis led to downregulation of CTGF (Huang et al., 2014). The expression of CTGF in hsp47 knockout mouse embryonic fibroblasts was analyzed and results demonstrated that in these cells CTGF expression was markedly downregulated supporting a link between the collagen processing hsp47 and CTGF (Figure 45).

5.8.1 No evidence for the impact of pH, MG132 and BFA on CTGF expression in NRCM

In human airway smooth muscle cells, it has been demonstrated that extracellular acidification of pH 6.3 can trigger the CTGF expression and that this plays a major role in the formation of ECM proteins and necessary for airway remodeling via the GPR68-G_{q/11}-IP₃-Ca²⁺ signaling (Ichimonji et al., 2010). Within the cardiovascular field the impact of pH has not been studied in relation to CTGF expression. To assess the effects of pH on CTGF expression, NRCM were exposed to a wide range of pH conditions. Results demonstrated that in NRCM, different pH conditions had no major influence on CTGF expression (Figure 46.A). Next, MG132 (a potent, membrane-permeable proteasome inhibitor) was used to assess the correlation between proteasome degradation and CTGF expression in NRCM. CTGF showed no concentration dependent change in expression with MG132 treatment; indicating that CTGF, under these conditions, does not appear to have a role in proteasome degradation (Figure 46.B). In 2002, it was demonstrated that BFA-induced Golgi disruption blocks CTGF secretion (Chen et al., 2001). However, in this study no change was observed in the expression of CTGF with increasing concentrations of BFA in NRCM (Figure 46.C).

5.8.2 Knockdown of CTGF affects ER stress markers in NRCM

During I/R, all sources of oxygen and energy substrates are diminished in the myocardium, leading to an increased production of ROS. This eventually triggers the UPR signaling pathway. In this context, it has been reported that an increased expression of UPR-related genes in cardiomyocytes occurs such as BiP, XBP-1, and PDI, which have been identified following myocardial infarction in mouse and human hearts (Thuerlauf et al., 2006; Severino et al., 2007). As a consequence, it could result in perturbation of ER oxidative balance and Ca²⁺ homeostasis, and hence the loss of cardiac function and ultimately apoptosis (Scarabelli and Gottlieb, 2004). More than two decades ago the concept of ER stress was identified and recently its role in cardiovascular functioning has been increasingly recognized (Kozutsumi et al., 1988). Various external and physiological changes such as ischemia, heat, hypoxia, glucose and metabolic starvations are strong inducers of the ER stress signaling pathway (Toth et al., 2007).

In this thesis, different stressors were used to analyze their effect on CTGF and its role in ER stress signaling pathway in cardiomyocytes. The obtained results demonstrate that certain factors inducing ER stress can increase CTGF expression. However, whether CTGF can

affect ER stress was not clear. Therefore, the regulation of various ER stress related proteins and their dependence on CTGF were examined.

When the unfolded protein response (UPR) is initiated various UPR signaling pathways are activated. One such pathway involves the transmembrane activating transcription factor 6 (ATF6) which is sequentially cleaved by site-1 protease (S1P) and S2P inside the Golgi (Ye et al., 2000). This allows the cytosolic fragment of ATF6 to enter the nucleus. In this study, the putative roles of CTGF and ATF6 in NRCM were investigated by siRNA-mediated silencing of CTGF *in vitro*. Immunofluorescence analysis demonstrated that siCTGF-transfected cells had a lower CTGF and ATF6 expression (mainly in the nucleus) than siControl-transfected cells (Figure 47). In a previous study, it was shown that when ATF6 is conditionally active in cardiomyocytes, as achieved by a transgenic mouse line, and upon *in vivo* ischemic injury, ATF6 triggers cytoprotective ER stress proteins involving BiP and GRP94, which can function to reduce ischemic injury (Martindale et al., 2006). Moreover, in a mouse model of pressure overload hypertrophy, ATF6 has been suggested to play an adaptive role (Lynch et al., 2012).

Next, the relationship between CTGF and the third UPR activation pathway was analyzed, which is governed by the dimerization and autophosphorylation of IRE1- α . Under basal non-stress conditions, IRE1- α is inactive, but upon stress, there is a conformational alteration of IRE1- α induced by its phosphorylation, which exposes a ribonuclease capacity that removes an intron from XBP1 mRNA (XBP1US). A recent study from Lyons group has demonstrated that deletion of CTGF can induce cellular stress and plays a protective role in the survival of chondrocytes (Hall-Glenn et al., 2013). Another recent study demonstrated that, an adenovirus (Ad5-CMV-CCN2) mediated gene transfer induced ER stress and UPR in primary hepatic stellate cells and hepatocytes (Borkham-Kamphorst et al., 2016). Results have demonstrated the partial knockdown of CTGF in NRCM, leads to significant downregulation of the ER stress markers IRE-1 α , PDI, and BiP (Figure 48), which is in line with research as discussed above. However, the same results were not established at the transcription level, as ER stress markers expressions were almost the same (Figure 50). The length of XBP1S was observed to be 263 base pairs, and the US variant had 289 base pairs for the siCTGF partial knockdown and conclusive of proteins expression data from the partial knockdown of CTGF in NRCM (Figure 49). In conclusion, the data suggest that either CTGF is governing the expression of ER stress markers or vice versa.

5.9 Role of secretory cells with respect to ER stress

Different cells respond in various ways to ER stress which leads to the activation of UPR by the secretory apparatus. The purpose of UPR is to increase the competence of a cell to carry out protein secretion and protect the cell from ER stress (Ron and Walter, 2007). Few publications exist on the relationship between UPR, ER stress and the secretory pathway, and how secretory proteins relate to the survival of the cell during ER stress. The targeting of CTGF proteins in cardiomyocytes and their role in UPR represents a unique aspect of this study. Previously this has only been examined in chondrocytes and hepatocytes (Hall-Glenn et al., 2013; Wu et al., 2015).

Mammalian cells, including antibody-secreting plasma cells and insulin secreting pancreatic β -cells, are involved in maintaining the balance between ER competence to the protein folding demand and have large fluxes in their secretory loads (Moore and Hollien, 2012). The first work done to understand the relationship between secretory cells and the UPR was done in plasma cell differentiation. Here it was shown that XBP-1 plays an important factor in this process, as without it cells undergo apoptosis (Iwakoshi et al., 2003). Furthermore, it was previously discovered that during early B-cell development there is an IRE1- α deficiency (Zhang et al., 2005). In contrast to plasma cells, deletion or mutation of Perk or perturbation of the eIF2 α phosphorylation site induces β -cell deficiency, deregulation of glucose metabolism and early-onset diabetes (Harding et al., 2001; Zhang et al., 2002). Also, deletion of XBP-1 in β -cells damages secretion, insulin processing and *in vivo* proliferation (Lee et al., 2011). Similarly, lack in any of the three primary signaling pathways in the liver negotiates the response to acute ER stress, inducing suppression of metabolic gene expression, which is regulated by up-regulation of CHOP (Rutkowski et al., 2008). Furthermore, osteoblasts also highly express PERK, ATF4 and XBP1 (Clauss et al., 1993; Zhang et al., 2002; Saito et al., 2011) and both PERK and IRE1- α (Murakami et al., 2009; Saito et al., 2011) are activated during differentiation. The triggering of UPR in osteoblasts is likely to be involved in bone morphogenetic protein 2 (Bmp2) signaling, which is required for osteoblast differentiation and bone formation. Thorough research has been done in various secretory cell types, but there is much to be learned about the UPR in specific tissues and organs.

5.10 Higher expression of CTGF in the end stage heart failure

In the left ventricular tissue CTGF expression was significantly up-regulated in DCM and showed a trend toward elevation in ICM heart samples (Figure 40). These results are in accordance with previous studies demonstrating that CTGF is up-regulated in both animal and human models of HF (Daniels et al., 2009). In the context of HF and cardiac

hypertrophy, downstream effectors of $G_{\alpha q}$ -coupled receptors for endothelin-1, norepinephrine and Ang II regulate CTGF expression (Kemp et al., 2004). However, the role of CTGF as a marker for fibrosis or triggering protein for interstitial fibrosis of the heart remains to be fully elucidated. Interestingly, in the heart and other organs, CTGF's modular domain structure influences the binding and consequent signaling of TGF- β which is known to be a regulator of fibrillar collagen gene transcription (Abreu et al., 2002).

Figure 56 represents a summary of all the results related to the effect of various stressors on CTGF expression. Red boxes, including changes in BFA, MG132 and pH demonstrated no effect on CTGF expression. However, green boxes including oxidizing agents, ER stress reducing agents, ER stress markers, heat shock, HSP47 and end stage heart failure, showed changes on the CTGF expression. The CTGF data argue for an interconnection of CTGF and ER stress, as ER stress modulates CTGF and *vice versa*, CTGF expression modulates proteins of the ER stress cascade.

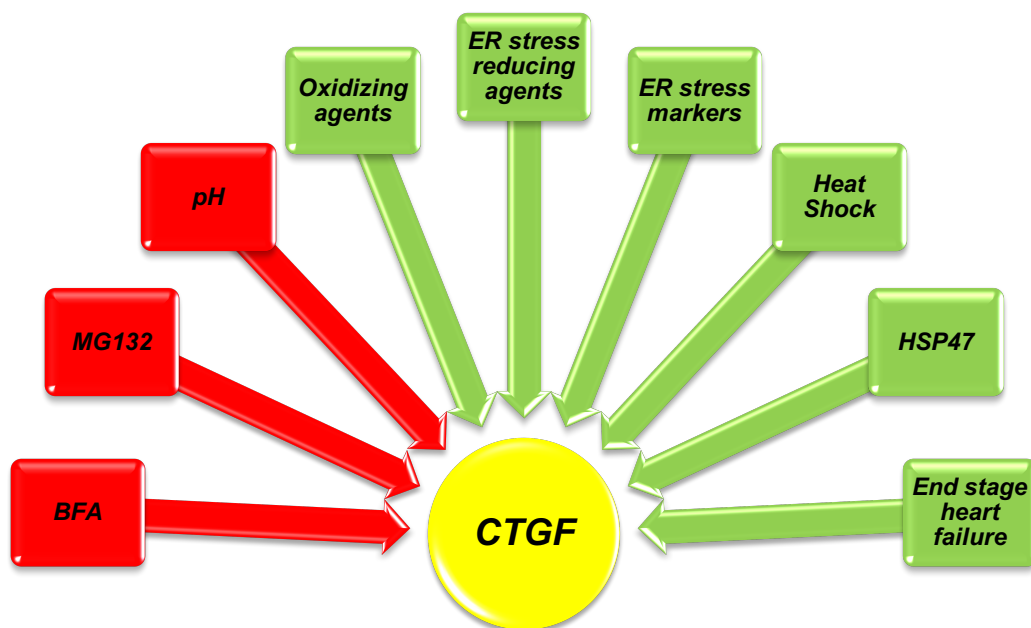
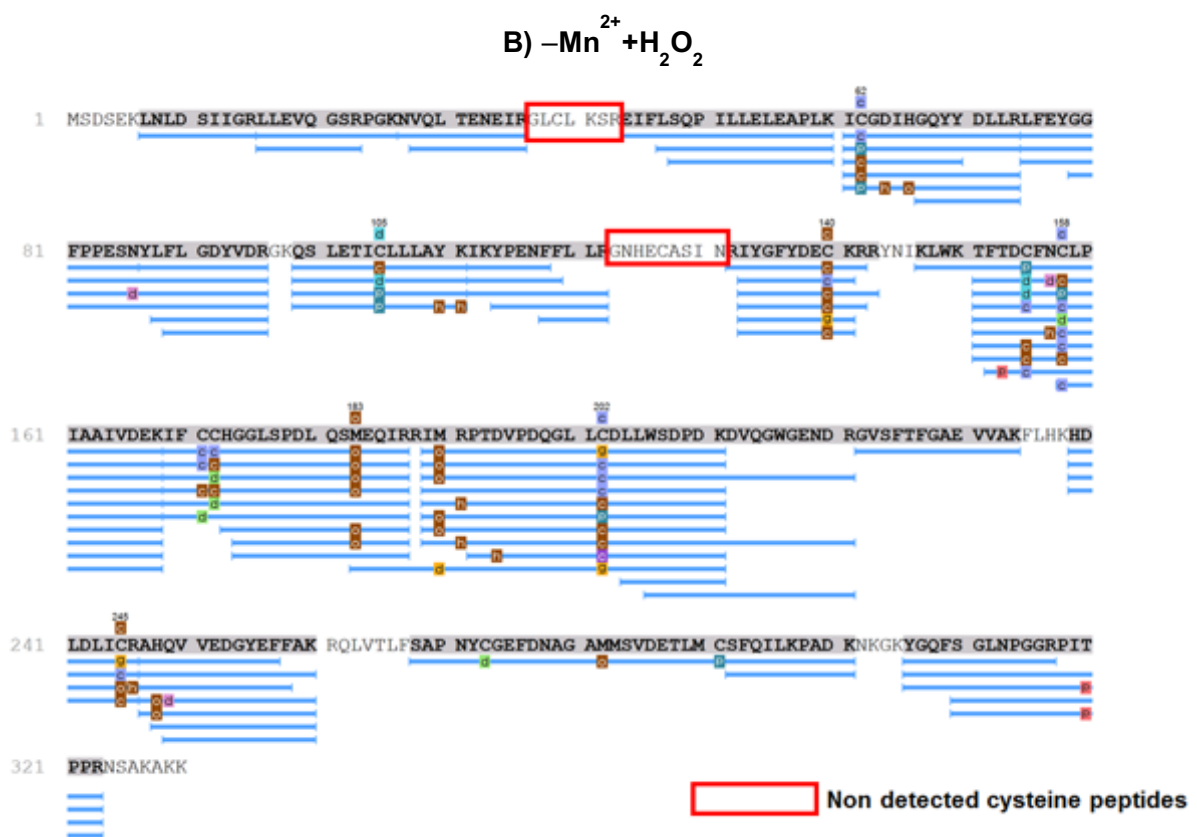


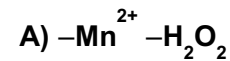
Figure 56 | Summary of all effectors on CTGF. Cartoon picture representing all the stressors used during the experiments. Boxes in red show no effect on CTGF expression, whereas green boxes represent with effect on CTGF expression.

6 Appendix

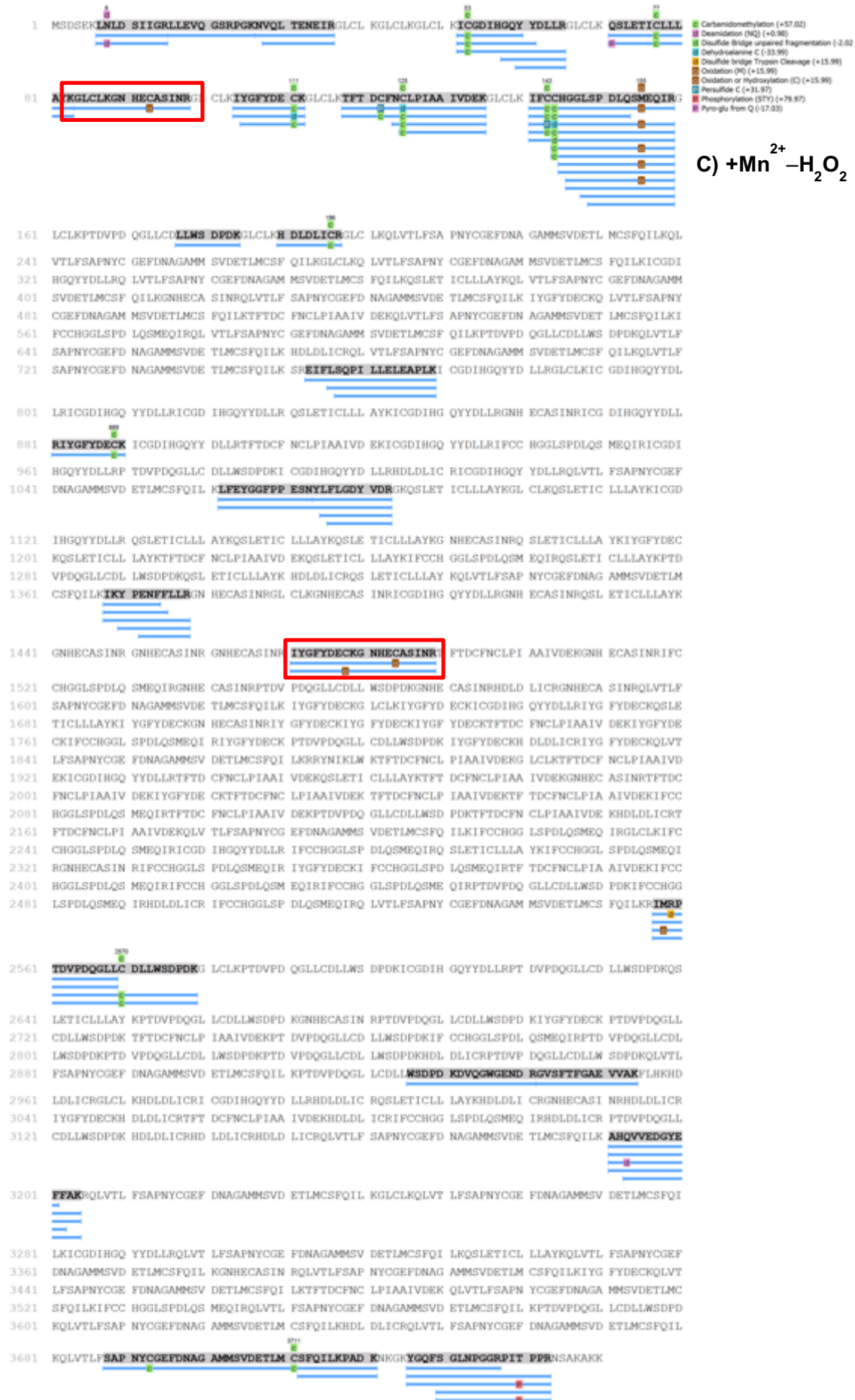
6.1 Spectrum covered by MS



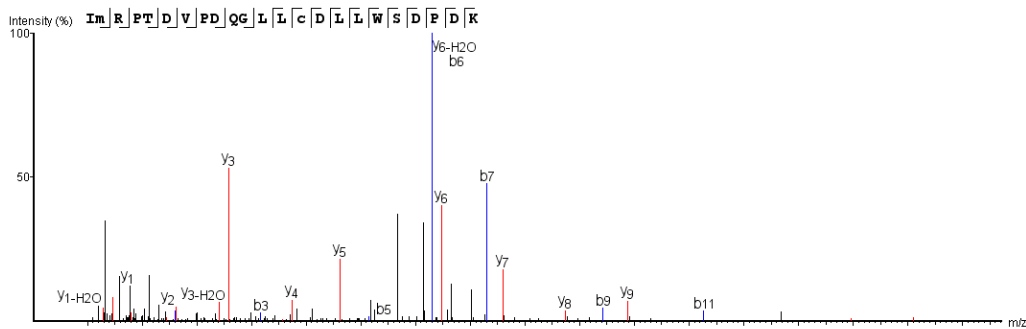
Append 1 | Peak results indicating the Cys peptides that were not detected with red boxes. No detection might point at an unknown modification or involvement in disulfide bridges.





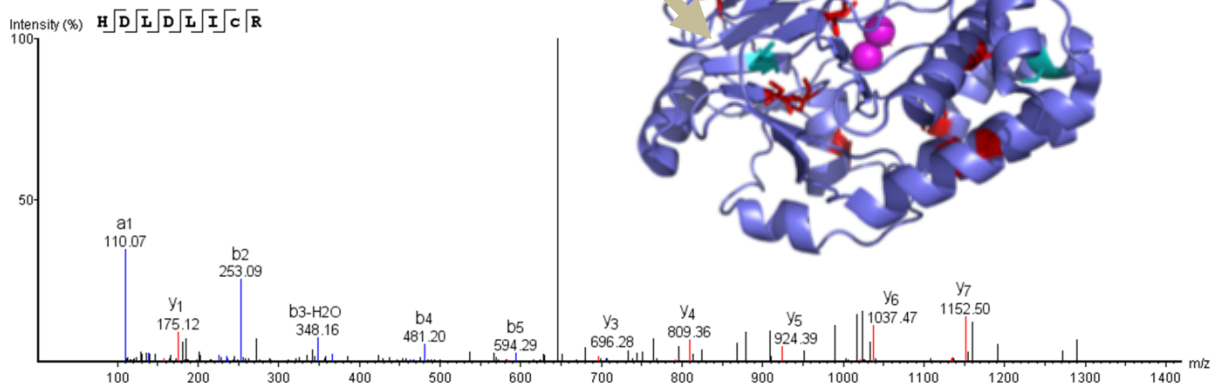


Cys²⁰²



#	b	b-H2O	b (2+)	Seq	y	y-H2O	y (2+)	#
1	114.09	96.08	57.55	I				23
2	261.13	243.12	131.06	M(+15.99)	2835.26	2817.25	1418.13	22
3	417.23	399.22	209.11	R	2688.23	2670.22	1344.61	21
4	514.28	496.27	257.64	P	2532.13	2514.12	1266.56	20
5	615.32	597.32	308.16	T	2435.07	2417.06	1218.04	19
6	730.35	712.35	365.68	D	2334.03	2316.02	1167.51	18
7	829.42	811.41	415.21	V	2219.00	2200.99	1110.00	17
8	926.48	908.47	463.74	P	2119.93	2101.92	1060.47	16
9	1041.49	1023.49	521.25	D	2022.88	2004.87	1011.94	15
10	1169.56	1151.55	585.28	Q	1907.85	1889.84	954.43	14
11	1226.57	1208.57	613.79	G	1779.79	1761.78	890.40	13
12	1339.67	1321.66	670.33	L	1722.77	1704.76	861.89	12
13	1452.75	1434.74	726.88	L	1609.67	1591.68	805.34	11
14	1860.83	1842.82	930.91	C(+305.07)	1496.58	1478.59	748.80	10
15	1975.86	1957.85	988.43	D	1088.52	1070.52	544.76	9
16	2088.94	2070.93	1044.97	L	973.50	955.49	487.25	8
17	2202.02	2184.01	1101.51	L	860.41	842.40	430.71	7
18	2388.10	2370.09	1194.55	W	747.32	729.32	374.17	6
19	2475.14	2457.13	1238.07	S	561.25	543.24	281.13	5
20	2590.16	2572.15	1295.58	D	474.22	456.21	237.61	4
21	2687.22	2669.21	1344.11	P	359.19	341.14	180.10	3
22	2802.24	2784.23	1401.62	D	262.14	244.09	131.57	2
23				K	147.11	129.10	74.06	1

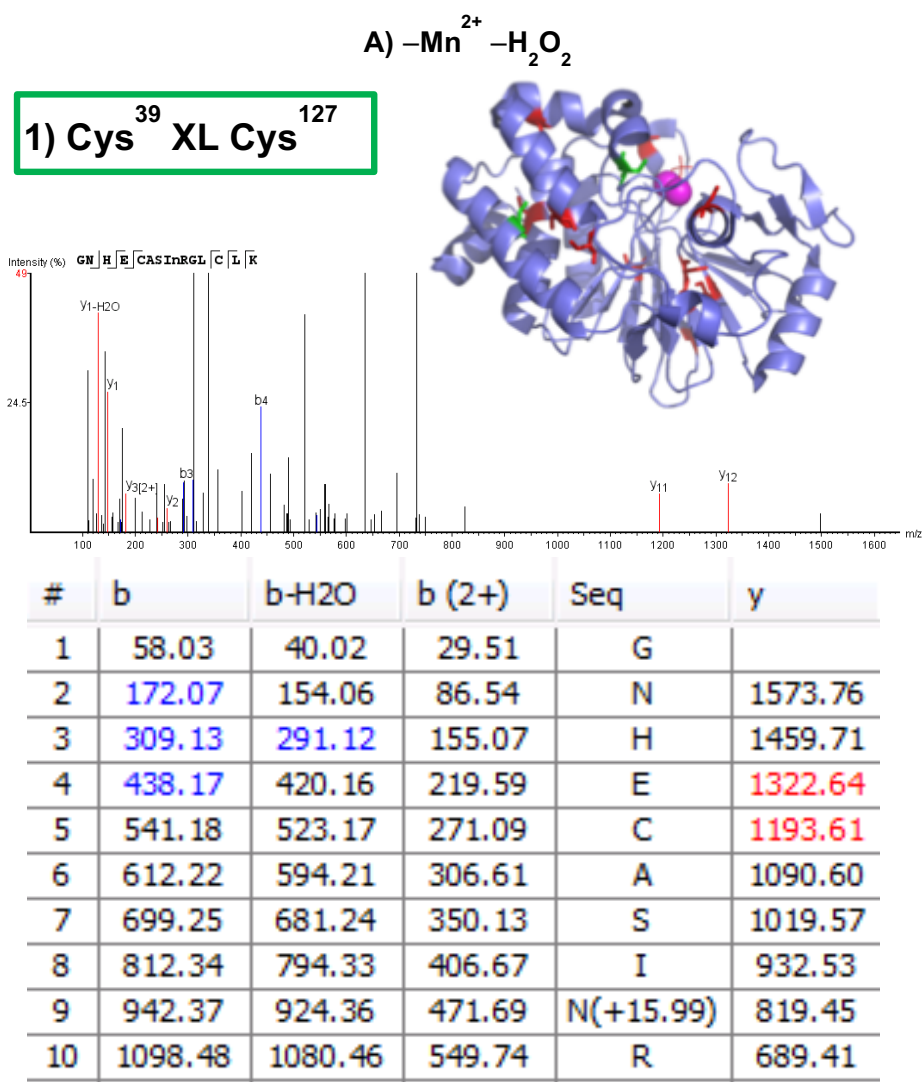
Cys²⁴⁵



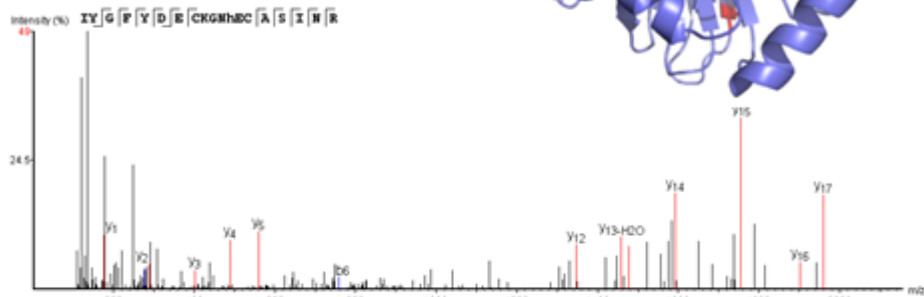
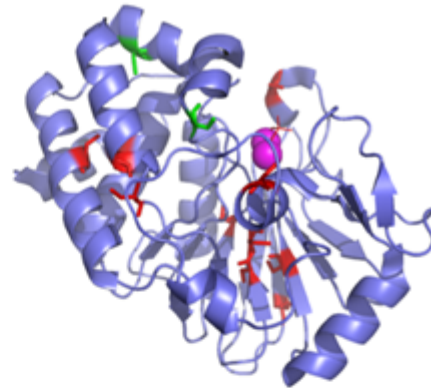
#	Immonium	b	b-H2O	b-NH3	a	b (2+)	Seq	y	y-H2O	y-NH3	y (2+)	#
1	110.07	138.07	120.06	121.04	110.07	69.53	H					8
2	88.04	253.09	235.08	236.07	225.10	127.05	D	1152.50	1134.48	1135.46	576.75	7
3	86.10	366.17	348.16	349.15	338.18	183.59	L	1037.47	1019.46	1020.46	519.24	6
4	88.04	481.20	463.19	464.18	453.21	241.10	D	924.39	906.38	907.36	462.70	5
5	86.10	594.29	576.28	577.26	566.29	297.64	L	809.36	791.35	792.36	405.18	4
6	86.10	707.37	689.36	690.35	679.38	354.19	I	696.28	678.27	679.25	348.64	3
7	381.09	1115.45	1097.44	1098.42	1087.46	558.23	C(+305.07)	583.19	565.19	566.17	292.10	2
8	129.11						R	175.12	157.11	158.09	88.06	1

Append 3 | Spectra and positions of the glutathione modified Cys²⁰² and Cys²⁴⁵.

6.2 Summary of all disulfide bridges

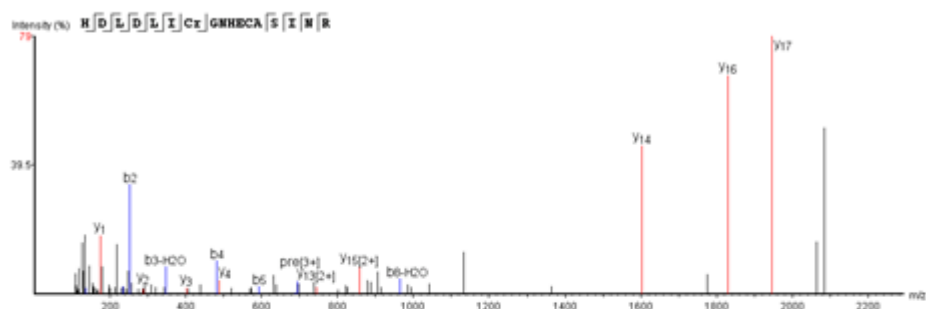


2) Cys¹²⁷ XL Cys¹⁴⁰

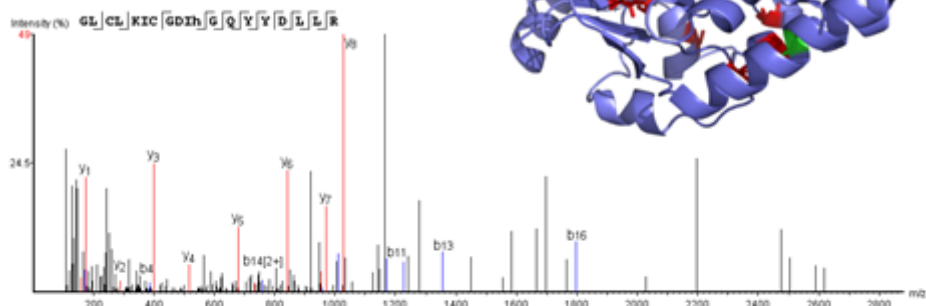


#	b	b-H ₂ O	b (2+)	Seq	y	y-H ₂ O	y (2+)	#
1	114.09	96.08	57.55	I				19
2	277.15	259.14	139.08	Y	2121.88	2103.86	1061.44	18
3	334.18	316.17	167.59	G	1958.81	1940.80	979.91	17
4	481.25	463.23	241.12	F	1901.79	1883.78	951.40	16
5	644.31	626.30	322.65	Y	1754.72	1736.71	877.86	15
6	759.35	741.32	380.17	D	1591.65	1573.65	796.33	14
7	888.38	870.37	444.69	E	1476.63	1458.60	738.82	13
8	991.39	973.38	496.19	C	1347.59	1329.58	674.29	12
9	1119.48	1101.47	560.24	K	1244.58	1226.57	622.79	11
10	1176.50	1158.49	588.75	G	1116.49	1098.47	558.74	10
11	1290.55	1272.54	645.77	N	1059.46	1041.45	530.23	9
12	1443.60	1425.59	722.30	H(+15.99)	945.42	927.41	473.21	8
13	1572.64	1554.63	786.82	E	792.37	774.36	396.68	7
14	1675.65	1657.64	838.33	C	663.32	645.31	332.16	6
15	1746.69	1728.68	873.84	A	560.31	542.30	280.66	5
16	1833.72	1815.71	917.36	S	489.28	471.27	245.14	4
17	1946.81	1928.79	973.90	I	402.24	384.24	201.62	3
18	2060.85	2042.84	1030.92	N	289.16	271.15	145.08	2
19				R	175.12	157.11	88.06	1

3) Cys¹²⁷ XL Cys²⁴⁵

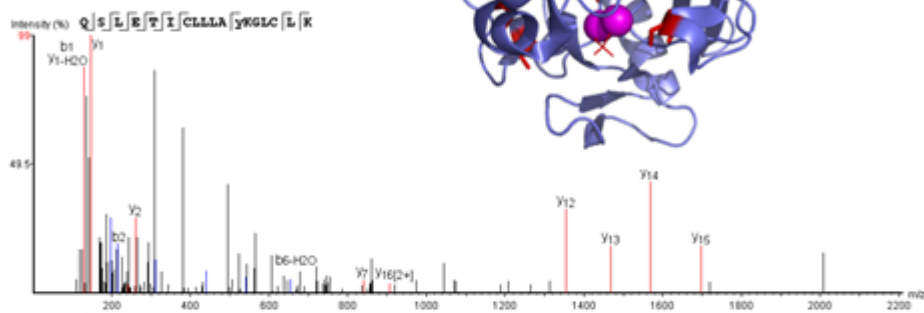
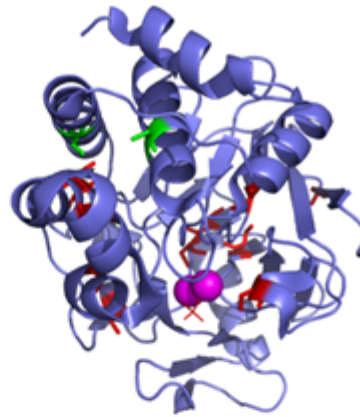


#	b	b-H ₂ O	b (2+)	Seq	y	y-H ₂ O	y (2+)	#
1	138.06	120.06	69.53	H				18
2	253.09	235.08	127.05	D	1944.89	1926.89	972.95	17
3	366.18	348.16	183.59	L	1829.87	1811.86	915.44	16
4	481.20	463.19	241.10	D	1716.79	1698.78	858.90	15
5	594.28	576.28	297.64	L	1601.74	1583.75	801.38	14
6	707.37	689.31	354.19	I	1488.68	1470.67	744.84	13
7	810.38	792.37	405.69	C	1375.60	1357.58	688.30	12
8	982.48	964.44	491.74	R(+15.99)	1272.59	1254.58	636.79	11
9	1039.50	1021.49	520.25	G	1100.49	1082.48	550.75	10
10	1153.54	1135.53	577.27	N	1043.47	1025.46	522.23	9
11	1290.60	1272.59	645.80	H	929.43	911.42	465.21	8
12	1419.64	1401.63	710.32	E	792.37	774.36	396.68	7
13	1522.65	1504.64	761.83	C	663.32	645.31	332.16	6
14	1593.69	1575.68	797.35	A	560.32	542.30	280.66	5
15	1680.72	1662.71	840.86	S	489.27	471.27	245.14	4
16	1793.81	1775.80	897.40	I	402.24	384.24	201.62	3
17	1907.85	1889.84	954.42	N	289.16	271.15	145.08	2
18				R	175.12	157.11	88.06	1

B) $-Mn^{2+} + H_2O_2$ 1) Cys³⁹ XL Cys⁶²

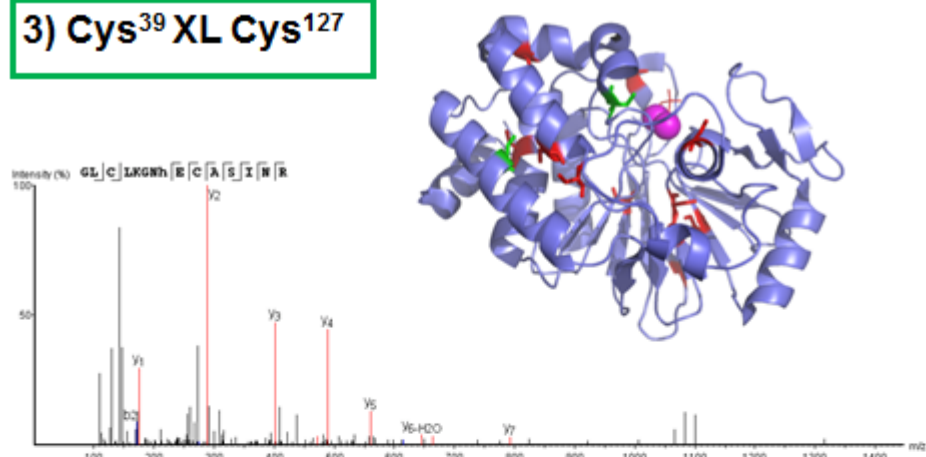
#	b	b-H ₂ O	b (2+)	Seq	y	y-H ₂ O	y (2+)	#
1	58.03	40.02	29.51	G				19
2	171.11	153.10	86.06	L	2139.07	2121.06	1070.04	18
3	274.12	256.11	137.56	C	2025.99	2007.98	1013.49	17
4	387.20	369.20	194.10	L	1922.98	1904.97	961.99	16
5	515.30	497.29	258.15	K	1809.90	1791.88	905.45	15
6	628.39	610.38	314.69	I	1681.80	1663.79	841.40	14
7	731.39	713.38	366.20	C	1568.72	1550.71	784.86	13
8	788.42	770.41	394.71	G	1465.71	1447.70	733.37	12
9	903.44	885.43	452.22	D	1408.69	1390.68	704.84	11
10	1016.53	998.52	508.76	I	1293.66	1275.65	647.33	10
11	1169.58	1151.57	585.29	H(+15.99)	1180.57	1162.56	590.79	9
12	1226.60	1208.59	613.80	G	1027.52	1009.51	514.26	8
13	1354.65	1336.65	677.83	Q	970.49	952.48	485.75	7
14	1517.72	1499.71	759.37	Y	842.44	824.43	421.72	6
15	1680.79	1662.78	840.89	Y	679.38	661.37	340.19	5
16	1795.81	1777.80	898.41	D	516.31	498.30	258.66	4
17	1908.90	1890.89	954.95	L	401.29	383.28	201.14	3
18	2021.98	2003.97	1011.47	L	288.20	270.19	144.60	2
19				R	175.12	157.11	88.06	1

2) Cys³⁹ XL Cys¹⁰⁵



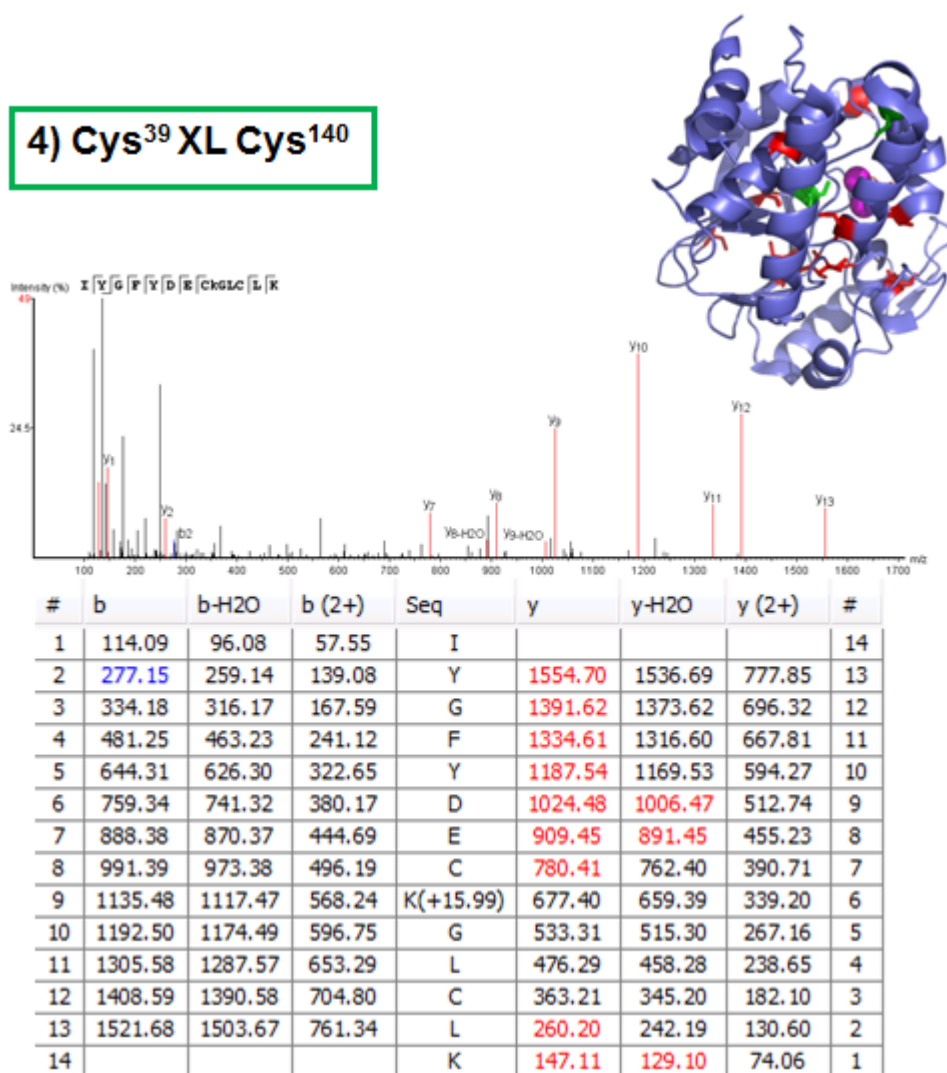
#	b	b-H ₂ O	b (2+)	Seq	y	y-H ₂ O	y (2+)	#
1	129.07	111.06	65.03	Q				18
2	216.10	198.09	108.55	S	1897.05	1879.04	949.03	17
3	329.18	311.17	165.09	L	1810.02	1792.01	905.50	16
4	458.23	440.21	229.61	E	1696.93	1678.93	848.97	15
5	559.27	541.26	280.14	T	1567.89	1549.88	784.45	14
6	672.36	654.34	336.68	I	1466.85	1448.84	733.92	13
7	775.37	757.36	388.18	C	1353.75	1335.75	677.38	12
8	888.45	870.44	444.73	L	1250.75	1232.74	625.88	11
9	1001.53	983.52	501.27	L	1137.67	1119.66	569.33	10
10	1114.62	1096.61	557.81	L	1024.59	1006.58	512.79	9
11	1185.66	1167.64	593.33	A	911.50	893.49	456.25	8
12	1364.71	1346.70	682.86	Y(+15.99)	840.47	822.45	420.73	7
13	1492.81	1474.80	746.90	K	661.41	643.40	331.20	6
14	1549.83	1531.82	775.41	G	533.31	515.30	267.16	5
15	1662.91	1644.90	831.96	L	476.29	458.28	238.65	4
16	1765.92	1747.91	883.46	C	363.21	345.20	182.10	3
17	1879.01	1861.00	940.00	L	260.20	242.18	130.60	2
18				K	147.11	129.10	74.06	1

3) Cys³⁹ XL Cys¹²⁷

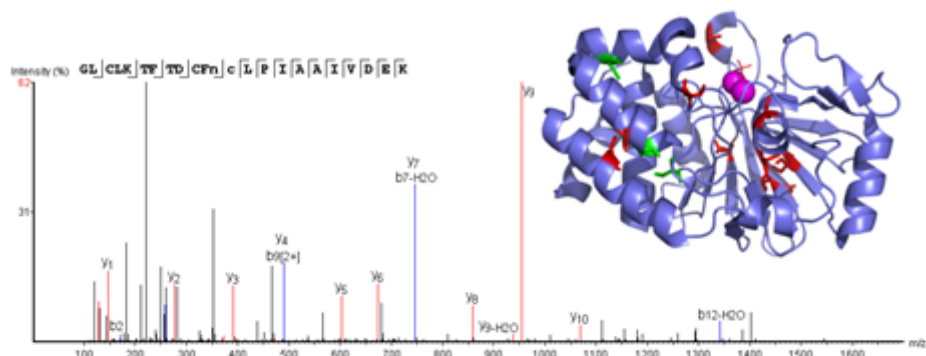


#	b	b-H ₂ O	b (2+)	Seq	y	y-H ₂ O	y (2+)	#
1	58.03	40.02	29.51	G				15
2	171.11	153.10	86.06	L	1573.76	1555.75	787.38	14
3	274.12	256.11	137.56	C	1460.67	1442.66	730.84	13
4	387.21	369.20	194.10	L	1357.66	1339.65	679.33	12
5	515.30	497.29	258.15	K	1244.58	1226.57	622.79	11
6	572.32	554.31	286.66	G	1116.49	1098.47	558.74	10
7	686.37	668.36	343.68	N	1059.46	1041.45	530.23	9
8	839.42	821.41	420.21	H(+15.99)	945.42	927.41	473.21	8
9	968.46	950.45	484.73	E	792.37	774.36	396.68	7
10	1071.47	1053.46	536.24	C	663.32	645.31	332.16	6
11	1142.51	1124.50	571.75	A	560.31	542.30	280.66	5
12	1229.54	1211.53	615.27	S	489.28	471.27	245.14	4
13	1342.62	1324.61	671.81	I	402.24	384.24	201.62	3
14	1456.67	1438.66	728.83	N	289.16	271.15	145.08	2
15				R	175.12	157.11	88.06	1

4) Cys³⁹ XL Cys¹⁴⁰

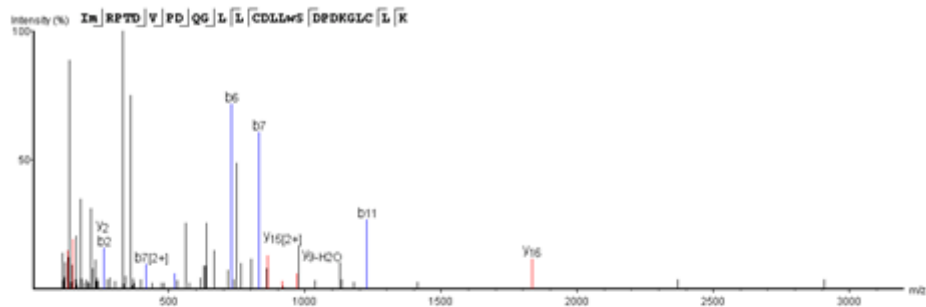


5) Cys³⁹XL Cys¹⁵⁵Cys¹⁵⁸

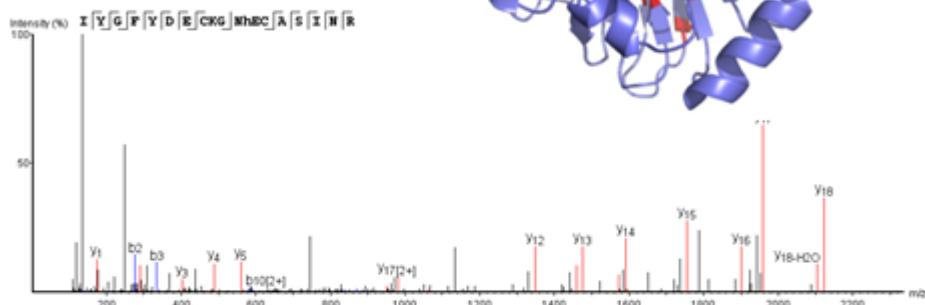
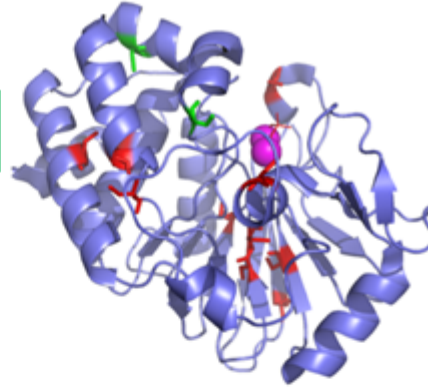


#	b	b-H2O	b (2+)	Seq	y	y-H2O	y (2+)	#
1	58.03	40.02	29.51	G				23
2	171.11	153.10	86.06	L	2521.20	2503.19	1261.10	22
3	274.12	256.11	137.56	C	2408.12	2390.11	1204.56	21
4	387.21	369.20	194.10	L	2305.11	2287.10	1153.05	20
5	515.30	497.29	258.14	K	2192.02	2174.01	1096.51	19
6	616.35	598.34	308.67	T	2063.93	2045.92	1032.46	18
7	763.42	745.40	382.21	F	1962.88	1944.87	981.94	17
8	864.47	846.45	432.73	T	1815.81	1797.80	908.41	16
9	979.49	961.48	490.25	D	1714.77	1696.76	857.88	15
10	1082.50	1064.49	541.75	C	1599.74	1581.73	800.37	14
11	1229.57	1211.56	615.28	F	1496.73	1478.72	748.87	13
12	1359.60	1341.59	680.30	N(+15.99)	1349.66	1331.65	675.33	12
13	1510.60	1492.59	755.80	C(+47.98)	1219.62	1201.61	610.31	11
14	1623.69	1605.68	812.34	L	1068.63	1050.62	534.81	10
15	1720.74	1702.73	860.87	P	955.54	937.54	478.27	9
16	1833.82	1815.81	917.41	I	858.49	840.48	429.75	8
17	1904.86	1886.85	952.93	A	745.40	727.40	373.20	7
18	1975.90	1957.89	988.45	A	674.37	656.36	337.69	6
19	2088.98	2070.97	1044.99	I	603.33	585.33	302.17	5
20	2188.05	2170.04	1094.52	V	490.25	472.24	245.63	4
21	2303.08	2285.07	1152.04	D	391.18	373.17	196.09	3
22	2432.12	2414.11	1216.56	E	276.15	258.14	138.58	2
23				K	147.11	129.10	74.06	1

6) Cys³⁹ XL Cys²⁰²

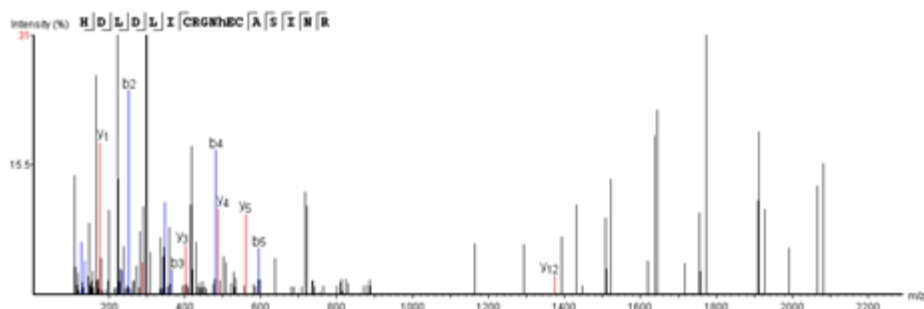


#	b	b-H ₂ O	b (2+)	Seq	y	y-H ₂ O	y (2+)	#
1	114.09	96.08	57.55	I				28
2	261.13	243.12	131.06	M(+15.99)	3060.48	3042.47	1530.74	27
3	417.23	399.22	209.11	R	2913.45	2895.44	1457.22	26
4	514.28	496.27	257.64	P	2757.35	2739.34	1379.17	25
5	615.33	597.32	308.16	T	2660.29	2642.28	1330.65	24
6	730.35	712.35	365.68	D	2559.25	2541.24	1280.12	23
7	829.42	811.41	415.21	V	2444.22	2426.21	1222.61	22
8	926.48	908.47	463.74	P	2345.15	2327.14	1173.08	21
9	1041.50	1023.49	521.25	D	2248.10	2230.09	1124.55	20
10	1169.56	1151.55	585.28	Q	2133.07	2115.06	1067.04	19
11	1226.57	1208.57	613.79	G	2005.01	1987.00	1003.01	18
12	1339.67	1321.66	670.33	L	1947.99	1929.98	974.50	17
13	1452.75	1434.74	726.88	L	1834.89	1816.90	917.95	16
14	1555.76	1537.75	778.38	C	1721.82	1703.81	861.41	15
15	1670.79	1652.78	835.89	D	1618.81	1600.80	809.91	14
16	1783.87	1765.86	892.44	L	1503.79	1485.78	752.39	13
17	1896.96	1878.95	948.98	L	1390.70	1372.69	695.85	12
18	2099.03	2081.02	1050.02	W(+15.99)	1277.62	1259.61	639.31	11
19	2186.06	2168.05	1093.53	S	1075.55	1057.53	538.27	10
20	2301.09	2283.08	1151.04	D	988.51	970.52	494.76	9
21	2398.14	2380.13	1199.57	P	873.49	855.48	437.24	8
22	2513.17	2495.16	1257.08	D	776.43	758.42	388.72	7
23	2641.26	2623.25	1321.13	K	661.41	643.40	331.20	6
24	2698.29	2680.28	1349.64	G	533.31	515.30	267.16	5
25	2811.37	2793.36	1406.18	L	476.29	458.28	238.65	4
26	2914.38	2896.37	1457.69	C	363.21	345.20	182.10	3
27	3027.46	3009.45	1514.23	L	260.20	242.19	130.60	2
28				K	147.11	129.10	74.06	1

7) Cys¹²⁷ XL Cys¹⁴⁰

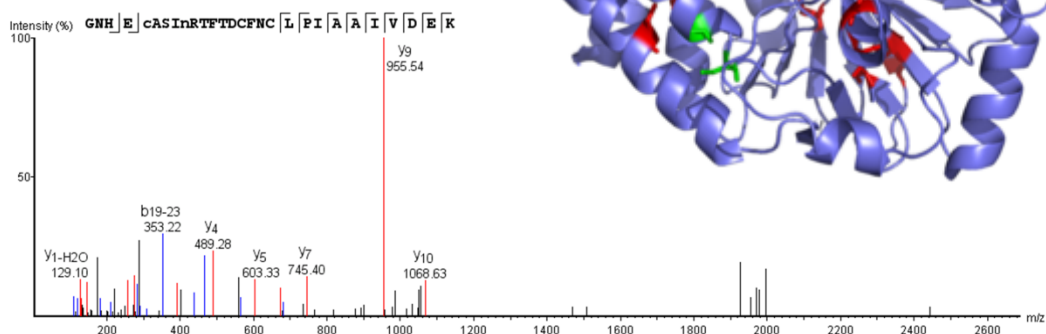
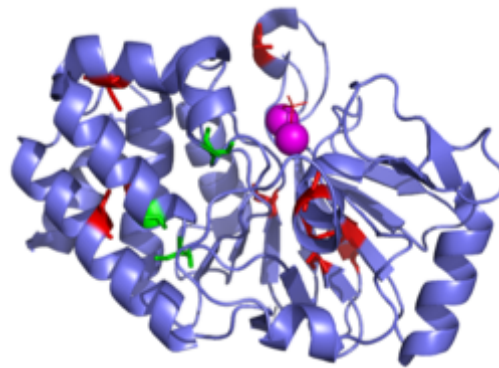
#	b	b-H ₂ O	b (2+)	Seq	y	y-H ₂ O	y (2+)	#
1	114.09	96.08	57.55	I				19
2	277.15	259.14	139.09	Y	2121.86	2103.86	1061.43	18
3	334.18	316.17	167.59	G	1958.80	1940.80	979.91	17
4	481.25	463.23	241.12	F	1901.79	1883.78	951.40	16
5	644.31	626.30	322.65	Y	1754.71	1736.71	877.86	15
6	759.34	741.32	380.17	D	1591.66	1573.63	796.33	14
7	888.38	870.35	444.69	E	1476.63	1458.61	738.82	13
8	991.39	973.38	496.19	C	1347.60	1329.58	674.29	12
9	1119.48	1101.47	560.24	K	1244.58	1226.57	622.79	11
10	1176.50	1158.49	588.77	G	1116.49	1098.47	558.74	10
11	1290.55	1272.54	645.77	N	1059.46	1041.45	530.23	9
12	1443.60	1425.59	722.30	H(+15.99)	945.42	927.41	473.21	8
13	1572.64	1554.63	786.82	E	792.37	774.36	396.68	7
14	1675.65	1657.64	838.35	C	663.32	645.31	332.16	6
15	1746.69	1728.68	873.84	A	560.31	542.30	280.66	5
16	1833.72	1815.71	917.36	S	489.28	471.27	245.14	4
17	1946.81	1928.79	973.90	I	402.24	384.24	201.62	3
18	2060.85	2042.84	1030.92	N	289.16	271.15	145.08	2
19				R	175.12	157.11	88.06	1

8) Cys¹²⁷ XL Cys²⁴⁵



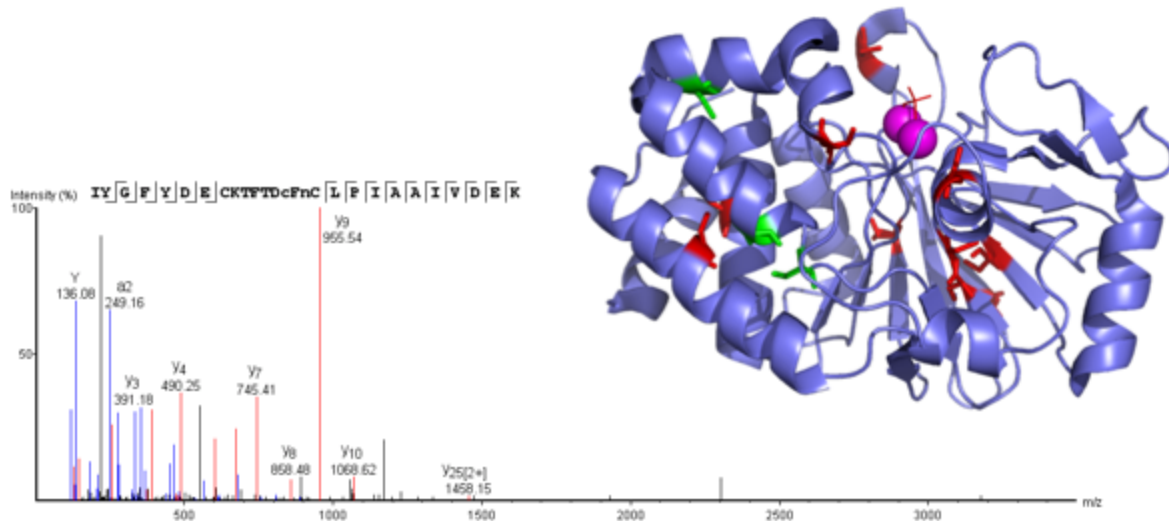
#	b	b-H ₂ O	b (2+)	Seq	y	y-H ₂ O	y (2+)	#
1	138.07	120.06	69.53	H				18
2	253.09	235.08	127.05	D	1944.90	1926.89	972.95	17
3	366.18	348.16	183.59	L	1829.87	1811.86	915.44	16
4	481.20	463.19	241.10	D	1716.79	1698.78	858.90	15
5	594.29	576.28	297.64	L	1601.76	1583.75	801.38	14
6	707.37	689.36	354.19	I	1488.68	1470.67	744.84	13
7	810.38	792.37	405.69	C	1375.60	1357.58	688.30	12
8	966.48	948.47	483.74	R	1272.59	1254.58	636.79	11
9	1023.50	1005.49	512.25	G	1116.49	1098.47	558.74	10
10	1137.55	1119.54	569.27	N	1059.46	1041.45	530.23	9
11	1290.60	1272.59	645.80	H(+15.99)	945.42	927.41	473.21	8
12	1419.64	1401.63	710.32	E	792.37	774.36	396.68	7
13	1522.65	1504.64	761.83	C	663.32	645.31	332.16	6
14	1593.69	1575.68	797.35	A	560.31	542.30	280.66	5
15	1680.72	1662.71	840.86	S	489.28	471.27	245.14	4
16	1793.81	1775.80	897.40	I	402.24	384.24	201.62	3
17	1907.85	1889.84	954.42	N	289.16	271.15	145.08	2
18				R	175.12	157.11	88.06	1

9) Cys¹²⁷ XL Cys¹⁵⁵Cys¹⁵⁸



#	Immonium	b	b-H2O	b-NH3	a	b (2+)	Seq	y	y-H2O	y-NH3	y (2+)	#
1	30.03	58.03	40.02	41.00	30.03	29.51	G					28
2	87.06	172.07	154.06	155.05	144.08	86.54	N	3088.38	3070.37	3071.35	1544.69	27
3	110.07	309.13	291.12	292.10	281.14	155.07	H	2974.34	2956.33	2957.31	1487.67	26
4	102.06	438.17	420.16	421.15	410.18	219.59	E	2837.28	2819.27	2820.25	1419.14	25
5	124.01	589.17	571.16	572.14	561.17	295.08	C(+47.98)	2708.24	2690.23	2691.21	1354.62	24
6	44.05	660.20	642.19	643.18	632.21	330.60	A	2557.24	2539.23	2540.22	1279.12	23
7	60.04	747.24	729.23	730.21	719.24	374.12	S	2486.21	2468.19	2469.18	1243.60	22
8	86.10	860.32	842.31	843.29	832.33	430.66	I	2399.17	2381.16	2382.15	1200.09	21
9	103.05	990.36	972.35	973.33	962.36	495.68	N(+15.99)	2286.09	2268.08	2269.06	1143.54	20
10	129.10	1146.46	1128.45	1129.43	1118.46	573.73	R	2156.05	2138.04	2139.02	1078.53	19
11	74.06	1247.51	1229.50	1230.48	1219.51	624.25	T	1999.95	1981.94	1982.92	1000.48	18
12	120.08	1394.58	1376.57	1377.55	1366.58	697.79	F	1898.90	1880.89	1881.88	949.95	17
13	74.06	1495.62	1477.61	1478.60	1467.63	748.31	T	1751.83	1733.82	1734.81	876.42	16
14	88.04	1610.65	1592.64	1593.62	1582.66	805.83	D	1650.79	1632.78	1633.76	825.89	15
15	76.02	1713.66	1695.65	1696.63	1685.66	857.33	C	1535.76	1517.75	1518.73	768.38	14
16	120.08	1860.73	1842.72	1843.70	1832.73	930.86	F	1432.75	1414.74	1415.72	716.88	13
17	87.06	1974.77	1956.76	1957.74	1946.78	987.89	N	1285.68	1267.67	1268.66	643.34	12
18	76.02	2077.78	2059.77	2060.75	2049.79	1039.39	C	1171.64	1153.63	1154.61	586.32	11
19	86.10	2190.86	2172.85	2173.84	2162.87	1095.93	L	1068.63	1050.62	1051.60	534.81	10
20	70.07	2287.92	2269.91	2270.89	2259.92	1144.46	P	955.54	937.54	938.52	478.27	9
21	86.10	2401.00	2382.99	2383.97	2373.01	1201.00	I	858.49	840.48	841.47	429.75	8
22	44.05	2472.04	2454.03	2455.01	2444.04	1236.52	A	745.40	727.40	728.38	373.20	7
23	44.05	2543.08	2525.06	2526.05	2515.08	1272.04	A	674.37	656.36	657.34	337.69	6
24	86.10	2656.16	2638.15	2639.13	2628.16	1328.58	I	603.33	585.32	586.31	302.17	5
25	72.08	2755.23	2737.22	2738.20	2727.23	1378.11	V	490.25	472.24	473.22	245.63	4
26	88.04	2870.25	2852.24	2853.23	2842.26	1435.63	D	391.18	373.17	374.16	196.09	3
27	102.06	2999.30	2981.29	2982.27	2971.30	1500.15	E	276.15	258.14	259.13	138.58	2
28	101.11						K	147.11	129.10	130.09	74.06	1

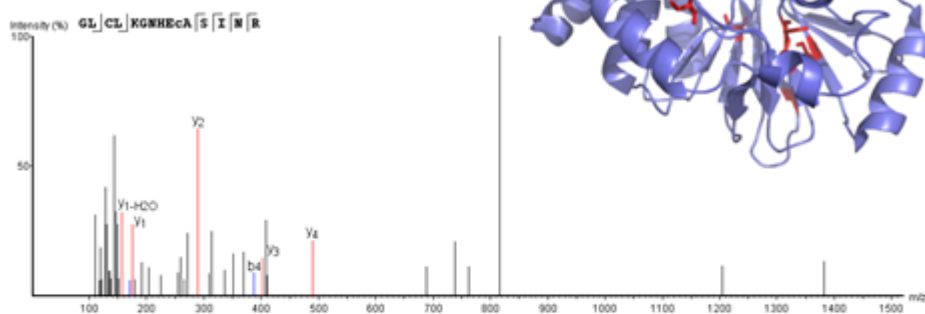
10) Cys¹⁴⁰ XL Cys¹⁵⁵Cys¹⁵⁸



#	Immonium	b	b-H ₂ O	b-NH ₃	a	b (2+)	Seq	y	y-H ₂ O	y-NH ₃	y (2+)	#
1	86.10	114.09	96.08	97.06	86.10	57.55	I					27
2	136.08	277.15	259.14	260.13	249.16	139.08	Y	3078.36	3060.35	3061.33	1539.68	26
3	30.03	334.17	316.17	317.15	306.18	167.59	G	2915.29	2897.28	2898.27	1458.15	25
4	120.08	481.24	463.23	464.21	453.25	241.12	F	2858.27	2840.26	2841.24	1429.64	24
5	136.08	644.31	626.30	627.28	616.31	322.65	Y	2711.20	2693.19	2694.18	1356.10	23
6	88.04	759.33	741.32	742.31	731.34	380.17	D	2548.14	2530.13	2531.11	1274.57	22
7	102.06	888.38	870.37	871.35	860.38	444.69	E	2433.11	2415.10	2416.09	1217.06	21
8	76.02	991.39	973.38	974.36	963.39	496.19	C	2304.07	2286.06	2287.04	1152.54	20
9	101.11	1119.48	1101.47	1102.46	1091.49	560.24	K	2201.06	2183.05	2184.03	1101.03	19
10	74.06	1220.53	1202.52	1203.50	1192.53	610.76	T	2072.97	2054.96	2055.94	1036.98	18
11	120.08	1367.60	1349.59	1350.57	1339.60	684.30	F	1971.92	1953.91	1954.89	986.46	17
12	74.06	1468.65	1450.64	1451.62	1440.65	734.82	T	1824.85	1806.84	1807.82	912.93	16
13	88.04	1583.67	1565.66	1566.65	1555.68	792.34	D	1723.80	1705.79	1706.78	862.40	15
14	133.04	1743.70	1725.69	1726.68	1715.71	872.35	C(+57.02)	1608.78	1590.77	1591.75	804.89	14
15	120.08	1890.77	1872.76	1873.74	1862.78	945.89	F	1448.75	1430.73	1431.72	724.87	13
16	103.05	2020.81	2002.80	2003.78	1992.81	1010.90	N(+15.99)	1301.68	1283.67	1284.65	651.34	12
17	76.02	2123.82	2105.81	2106.79	2095.82	1062.41	C	1171.64	1153.63	1154.61	586.32	11
18	86.10	2236.90	2218.89	2219.88	2208.91	1118.95	L	1068.62	1050.62	1051.60	534.81	10
19	70.07	2333.96	2315.95	2316.93	2305.96	1167.48	P	955.54	937.54	938.52	478.28	9
20	86.10	2447.04	2429.03	2430.01	2419.04	1224.02	I	858.48	840.48	841.47	429.75	8
21	44.05	2518.08	2500.07	2501.05	2490.08	1259.54	A	745.41	727.40	728.38	373.20	7
22	44.05	2589.11	2571.10	2572.09	2561.12	1295.06	A	674.37	656.36	657.34	337.69	6
23	86.10	2702.20	2684.19	2685.17	2674.20	1351.60	I	603.33	585.32	586.31	302.17	5
24	72.08	2801.27	2783.26	2784.24	2773.27	1401.13	V	490.25	472.24	473.22	245.63	4
25	88.04	2916.29	2898.28	2899.27	2888.30	1458.65	D	391.18	373.17	374.16	196.09	3
26	102.06	3045.34	3027.33	3028.31	3017.34	1523.17	E	276.16	258.14	259.13	138.58	2
27	101.11						K	147.11	129.10	130.09	74.06	1

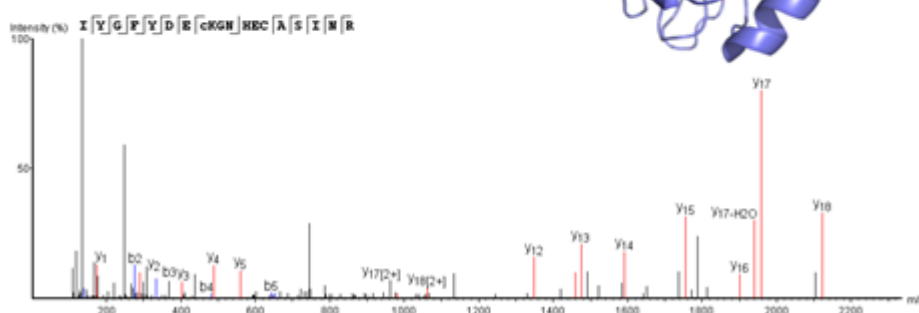
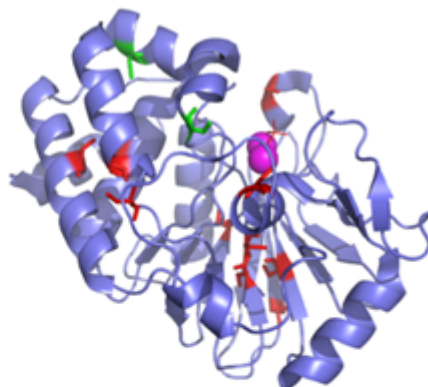
C) $+Mn^{2+} -H_2O_2$

1) Cys³⁹ XL Cys¹²⁷



#	b	b-H2O	b (2+)	Seq	y	y-H2O	y (2+)	#
1	58.03	40.02	29.51	G				15
2	171.11	153.10	86.06	L	1573.76	1555.75	787.38	14
3	274.12	256.11	137.56	C	1460.67	1442.66	730.84	13
4	387.20	369.20	194.10	L	1357.66	1339.65	679.33	12
5	515.30	497.29	258.15	K	1244.58	1226.57	622.79	11
6	572.32	554.31	286.66	G	1116.49	1098.47	558.74	10
7	686.37	668.36	343.68	N	1059.46	1041.45	530.23	9
8	823.42	805.41	412.21	H	945.42	927.41	473.21	8
9	952.47	934.46	476.73	E	808.36	790.35	404.68	7
10	1071.47	1053.46	536.24	C(+15.99)	679.32	661.31	340.16	6
11	1142.51	1124.50	571.75	A	560.32	542.30	280.66	5
12	1229.54	1211.53	615.27	S	489.28	471.27	245.14	4
13	1342.62	1324.61	671.81	I	402.25	384.24	201.62	3
14	1456.67	1438.66	728.83	N	289.16	271.15	145.08	2
15				R	175.12	157.08	88.06	1

2) Cys¹²⁷ XL Cys¹⁴⁰



#	b	b-H ₂ O	b (2+)	Seq	y	y-H ₂ O	y (2+)	#
1	114.09	96.08	57.55	I				19
2	277.15	259.14	139.09	Y	2121.87	2103.86	1061.44	18
3	334.17	316.17	167.59	G	1958.81	1940.78	979.91	17
4	481.20	463.23	241.12	F	1901.78	1883.78	951.40	16
5	644.29	626.30	322.65	Y	1754.70	1736.71	877.86	15
6	759.34	741.32	380.17	D	1591.64	1573.65	796.33	14
7	888.38	870.37	444.69	E	1476.63	1458.61	738.82	13
8	1007.38	989.37	504.19	C(+15.99)	1347.58	1329.58	674.29	12
9	1135.48	1117.47	568.24	K	1228.59	1210.57	614.79	11
10	1192.50	1174.49	596.75	G	1100.49	1082.48	550.75	10
11	1306.54	1288.53	653.79	N	1043.47	1025.46	522.23	9
12	1443.60	1425.59	722.30	H	929.43	911.42	465.21	8
13	1572.64	1554.63	786.82	E	792.37	774.36	396.68	7
14	1675.65	1657.64	838.33	C	663.32	645.31	332.16	6
15	1746.69	1728.68	873.84	A	560.31	542.30	280.66	5
16	1833.72	1815.71	917.36	S	489.28	471.27	245.14	4
17	1946.81	1928.79	973.90	I	402.24	384.24	201.62	3
18	2060.85	2042.84	1030.92	N	289.16	271.15	145.08	2
19				R	175.12	157.11	88.06	1

Append 4 | All disulfide-peptide conjugates are shown in their spectrum and fragment table. In the structure plot, the two Cys involved are indicated in green.

7 References

- Abreu, J.G., Ketpura, N.I., Reversade, B., and Robertis, E.M. de (2002). Connective-tissue growth factor (CTGF) modulates cell signalling by BMP and TGF-beta. *Nature cell biology* 4, 599-604.
- Ahmed, M.S., Gravning, J., Martinov, V.N., Lueder, T.G. von, Edvardsen, T., Czibik, G., Moe, I.T., Vinge, L.E., Oie, E., and Valen, G., et al. (2011). Mechanisms of novel cardioprotective functions of CCN2/CTGF in myocardial ischemia-reperfusion injury. *American journal of physiology. Heart and circulatory physiology* 300, H1291-302.
- Alfaro, M.P., Deskins, D.L., Wallus, M., DasGupta, J., Davidson, J.M., Nanney, L.B., A Guney, M., Gannon, M., and Young, P.P. (2013). A physiological role for connective tissue growth factor in early wound healing. *Laboratory investigation; a journal of technical methods and pathology* 93, 81-95.
- Arnott, J.A., Lambi, A.G., Mundy, C., Hendsi, H., Pixley, R.A., Owen, T.A., Safadi, F.F., and Popoff, S.N. (2011). The role of connective tissue growth factor (CTGF/CCN2) in skeletogenesis. *Critical reviews in eukaryotic gene expression* 21, 43-69.
- Au, C.G., Butler, T.L., Sherwood, M.C., Egan, J.R., North, K.N., and Winlaw, D.S. (2010). Increased connective tissue growth factor associated with cardiac fibrosis in the mdx mouse model of dystrophic cardiomyopathy. *International Journal of Experimental Pathology* 92, 57-65.
- Barrett, W.C., DeGnore, J.P., Konig, S., Fales, H.M., Keng, Y.F., Zhang, Z.Y., Yim, M.B., and Chock, P.B. (1999). Regulation of PTP1B via glutathionylation of the active site cysteine 215. *Biochemistry* 38, 6699-6705.
- Berlett, B.S., and Stadtman, E.R. (1997). Protein Oxidation in Aging, Disease, and Oxidative Stress. *Journal of Biological Chemistry* 272, 20313-20316.
- Berry, C.E., and Hare, J.M. (2004). Xanthine oxidoreductase and cardiovascular disease: molecular mechanisms and pathophysiological implications. *The Journal of physiology* 555, 589-606.
- Bers, D.M. (2002). Cardiac excitation-contraction coupling. *Nature* 415, 198-205.
- Bertolotti, A., Zhang, Y., Hendershot, L.M., Harding, H.P., and Ron, D. (2000). Dynamic interaction of BiP and ER stress transducers in the unfolded-protein response. *Nature cell biology* 2, 326-332.
- Biemann, K. (1988). Contributions of mass spectrometry to peptide and protein structure. *Biol. Mass Spectrom.* 16, 99-111.
- Bollen, M., Peti, W., Ragusa, M.J., and Beullens, M. (2010). The extended PP1 toolkit: designed to create specificity. *Trends in Biochemical Sciences* 35, 450-458.
- Bollen, M., and Stalmans, W. (1992). The structure, role, and regulation of type 1 protein phosphatases. *Critical reviews in biochemistry and molecular biology* 27, 227-281.
- Bork, P. (1993). The modular architecture of a new family of growth regulators related to connective tissue growth factor. *FEBS letters* 327, 125-130.
- Borkham-Kamphorst, E., Steffen, B.T., van de Leur, E., Tihaa, L., Haas, U., Woitok, M.M., Meurer, S.K., and Weiskirchen, R. (2016). Adenoviral CCN gene transfers induce in vitro and in vivo endoplasmic reticulum stress and unfolded protein response. *Biochimica et biophysica acta* 1863, 2604-2612.
- Bradham DM, Igarashi A, and Potter RL and Grotendorst GR. (1991). Connective-tissue growth-factor – a cysteine-rich mitogen secreted by human vascular endothelial-cells is related to the src-induced immediate early gene-product Cef-10. *The Journal of cell biology* 114, 1285-1294.

- Brautigan, D.L., and Shriener, C.L. (1989). Protein phosphatase type 1 catalytic subunit forms nondissociable dimers. *Archives of biochemistry and biophysics* 275, 44-52.
- Breckenridge, D.G., Germain, M., Mathai, J.P., Nguyen, M., and Shore, G.C. (2003). Regulation of apoptosis by endoplasmic reticulum pathways. *Oncogene* 22, 8608-8618.
- Brennan, J.P., Bardswell, S.C., Burgoyne, J.R., Fuller, W., Schroder, E., Wait, R., Begum, S., Kentish, J.C., and Eaton, P. (2006). Oxidant-induced activation of type I protein kinase A is mediated by RI subunit interprotein disulfide bond formation. *The Journal of biological chemistry* 281, 21827-21836.
- Brigstock, D.R. (1999). The connective tissue growth factor/cysteine-rich 61/nephroblastoma overexpressed (CCN) family. *Endocrine reviews* 20, 189-206.
- Burgoyne, J.R., Madhani, M., Cuello, F., Charles, R.L., Brennan, J.P., Schroder, E., Browning, D.D., and Eaton, P. (2007). Cysteine redox sensor in PKG α enables oxidant-induced activation. *Science (New York, N.Y.)* 317, 1393-1397.
- Burgoyne, JR, Madhani, M., Cuello, F., Charles, R.L., Brennan, J.P., Schroder, E., Browning, D.D., and Eaton, P. (2007). Cysteine redox sensor in PKG α enables oxidant-induced activation. *Science (New York, N.Y.)* 317, 1393-1397.
- Calfon, M., Zeng, H., Urano, F., Till, J.H., Hubbard, S.R., Harding, H.P., Clark, S.G., and Ron, D. (2002). IRE1 couples endoplasmic reticulum load to secretory capacity by processing the XBP-1 mRNA. *Nature* 415, 92-96.
- Chai, Y.C., Ashraf, S.S., Rokutan, K., Johnston, R.B., JR, and Thomas, J.A. (1994). S-thiolation of individual human neutrophil proteins including actin by stimulation of the respiratory burst: evidence against a role for glutathione disulfide. *Archives of biochemistry and biophysics* 310, 273-281.
- Chang, S.C., Wooden, S.K., Nakaki, T., Kim, Y.K., Lin, A.Y., Kung, L., Attenello, J.W., and Lee, A.S. (1987). Rat gene encoding the 78-kDa glucose-regulated protein GRP78: its regulatory sequences and the effect of protein glycosylation on its expression. *Proceedings of the National Academy of Sciences of the United States of America* 84, 680-684.
- Chaqour, B., and Goppelt-Struebe, M. (2006). Mechanical regulation of the Cyr61/CCN1 and CTGF/CCN2 proteins. *The FEBS journal* 273, 3639-3649.
- Charles, R.L., and Eaton, P. (2008). Redox signalling in cardiovascular disease. *Proteomics. Clinical applications* 2, 823-836.
- Chen, C.-Y., Willard, D., and Rudolph, J. (2009). Redox regulation of SH2-domain-containing protein tyrosine phosphatases by two backdoor cysteines. *Biochemistry* 48, 1399-1409.
- Chen, Y., Segarini, P., Raoufi, F., Bradham, D., and Leask, A. (2001). Connective tissue growth factor is secreted through the Golgi and is degraded in the endosome. *Experimental cell research* 271, 109-117.
- Chen, Y.-R., and Zweier, J.L. (2014). Cardiac mitochondria and reactive oxygen species generation. *Circulation research* 114, 524-537.
- Chiang, B.-Y., Chou, C.-C., Hsieh, F.-T., Gao, S., Lin, J.C.-Y., Lin, S.-H., Chen, T.-C., Khoo, K.-H., and Lin, C.-H. (2012). In vivo tagging and characterization of S-glutathionylated proteins by a chemoenzymatic method. *Angewandte Chemie (International ed. in English)* 51, 5871-5875.
- Chiarugi, P. (2005). PTPs versus PTKs: the redox side of the coin. *Free radical research* 39, 353-364.
- Chien, K.R. (1999). Stress pathways and heart failure. *Cell* 98, 555-558.

- Chudgar, S.M., Deng, P., Maddala, R., Epstein, D.L., and Rao, P.V. (2006). Regulation of connective tissue growth factor expression in the aqueous humor outflow pathway. *Molecular vision* 12, 1117-1126.
- Clauss, I.M., Gravallesse, E.M., Darling, J.M., Shapiro, F., Glimcher, M.J., and Glimcher, L.H. (1993). In situ hybridization studies suggest a role for the basic region-leucine zipper protein hXBP-1 in exocrine gland and skeletal development during mouse embryogenesis. *Developmental dynamics : an official publication of the American Association of Anatomists* 197, 146-156.
- Cohen, P. (1989). The structure and regulation of protein phosphatases. *Annual review of biochemistry* 58, 453-508.
- Copley, S.D., Novak, W.R.P., and Babbitt, P.C. (2004). Divergence of function in the thioredoxin fold suprafamily: evidence for evolution of peroxiredoxins from a thioredoxin-like ancestor. *Biochemistry* 43, 13981-13995.
- Cox, J.S., Shamu, C.E., and Walter, P. (1993). Transcriptional induction of genes encoding endoplasmic reticulum resident proteins requires a transmembrane protein kinase. *Cell* 73, 1197-1206.
- Cyert, M.S., and Thorner, J. (1989). Putting it on and taking it off: phosphoprotein phosphatase involvement in cell cycle regulation. *Cell* 57, 891-893.
- Daniels, A., van Bilsen, M., Goldschmeding, R., van der Vusse, G J, and van Nieuwenhoven, F.A. (2009). Connective tissue growth factor and cardiac fibrosis. *Acta physiologica (Oxford, England)* 195, 321-338.
- den Hertog, J., Groen, A., and van der Wijk, T. (2005). Redox regulation of protein-tyrosine phosphatases. *Archives of biochemistry and biophysics* 434, 11-15.
- Denu, J.M., and Tanner, K.G. (1998). Specific and Reversible Inactivation of Protein Tyrosine Phosphatases by Hydrogen Peroxide: Evidence for a Sulfenic Acid Intermediate and Implications for Redox Regulation. *Biochemistry* 37, 5633-5642.
- Diez, J. (2014). Arterial hypertension in patients with heart failure. *Heart failure clinics* 10, 233-242.
- Drazner, M.H. (2011). The progression of hypertensive heart disease. *Circulation* 123, 327-334.
- Egloff, M.P., Cohen, P.T., Reinemer, P., and Barford, D. (1995). Crystal structure of the catalytic subunit of human protein phosphatase 1 and its complex with tungstate. *Journal of molecular biology* 254, 942-959.
- El-Armouche, A., and Eschenhagen, T. (2009). Beta-adrenergic stimulation and myocardial function in the failing heart. *Heart failure reviews* 14, 225-241.
- El-Armouche, A., Rau, T., Zolk, O., Ditz, D., Pamminger, T., Zimmermann, W.H., Jackel, E., Harding, S.E., Boknik, P., and Neumann, J., et al. (2003). Evidence for protein phosphatase inhibitor-1 playing an amplifier role in beta-adrenergic signaling in cardiac myocytes. *FASEB journal: official publication of the Federation of American Societies for Experimental Biology* 17, 437-439.
- Erickson, J.R., He, B.J., Grumbach, I.M., and Anderson, M.E. (2011). CaMKII in the cardiovascular system: sensing redox states. *Physiological reviews* 91, 889-915.
- Ferre, F., and Clote, P. (2005). DiANNA: a web server for disulfide connectivity prediction. *Nucleic acids research* 33, W230-2.
- Fetrow., Naomi S., and Jeffrey S. (1999). Structure-based functional motif identifies a potential disulfide oxidoreductase active site in the serine/ threonine protein phosphatase-1 subfamily. *FASEB journal: official publication of the Federation of American Societies for Experimental Biology* 13, 1866-1874.

- Foley, T.D., Katchur, K.M., and Gillespie, P.F. (2016). Disulfide Stress Targets Modulators of Excitotoxicity in Otherwise Healthy Brains. *Neurochemical research* 41, 2763-2770.
- Foley, T.D., Petro, L.A., Stredny, C.M., and Coppa, T.M. (2007). Oxidative inhibition of protein phosphatase 2A activity: role of catalytic subunit disulfides. *Neurochemical research* 32, 1957-1964.
- Forrester, M.T., Foster, M.W., Benhar, M., and Stamler, J.S. (2009). Detection of protein S-nitrosylation with the biotin-switch technique. *Free radical biology & medicine* 46, 119-126.
- Fribley, A., Zhang, K., and Kaufman, R.J. (2009). Regulation of apoptosis by the unfolded protein response. *Methods in molecular biology (Clifton, N.J.)* 559, 191-204.
- Glembotski, C.C. (2007). Endoplasmic reticulum stress in the heart. *Circulation research* 101, 975-984.
- Glembotski, C.C. (2008). The role of the unfolded protein response in the heart. *Journal of molecular and cellular cardiology* 44, 453-459.
- Glembotski, C.C. (2014). Roles for ATF6 and the sarco/endoplasmic reticulum protein quality control system in the heart. *Journal of molecular and cellular cardiology* 71, 11-15.
- Go, Y.-M., Chandler, J.D., and Jones, D.P. (2015). The cysteine proteome. *Free radical biology & medicine* 84, 227-245.
- Gojniczek, K., Jurzak, M., and Garnarczyk, A. (2008). The Role of Connective Tissue Growth Factor (CTGF) in Fibroproliferative Processes and Tissues Fibrosis. *Advances in Cell Biology -1*, 1-17.
- Goldberg, J., Huang, H.B., Kwon, Y.G., Greengard, P., Nairn, A.C., and Kuriyan, J. (1995). Three-dimensional structure of the catalytic subunit of protein serine/threonine phosphatase-1. *Nature* 376, 745-753.
- Görlach, A., Bertram, K., Hudecova, S., and Krizanova, O. (2015). Calcium and ROS: A mutual interplay. *Redox Biology* 6, 260-271.
- Gotze, M., Pettelkau, J., Schaks, S., Bosse, K., Ihling, C.H., Krauth, F., Fritzsche, R., Kuhn, U., and Sinz, A. (2012). StavroX--a software for analyzing crosslinked products in protein interaction studies. *Journal of the American Society for Mass Spectrometry* 23, 76-87.
- Gough, and Cotter, T.G. (2011). Hydrogen peroxide: a Jekyll and Hyde signalling molecule. *Cell death & disease* 2, e213.
- Gravning, J., Ahmed, M.S., Lueder, T.G. von, Edvardsen, T., and Attramadal, H. (2013a). CCN2/CTGF attenuates myocardial hypertrophy and cardiac dysfunction upon chronic pressure-overload. *International journal of cardiology* 168, 2049-2056.
- Gravning, J., Ahmed, M.S., Qvigstad, E., Krobert, K., Edvardsen, T., Moe, I.T., Hagelin, E.M.V., Sagave, J., Valen, G., and Levy, F.O., et al. (2013b). Connective tissue growth factor/CCN2 attenuates beta-adrenergic receptor responsiveness and cardiotoxicity by induction of G protein-coupled receptor kinase-5 in cardiomyocytes. *Molecular pharmacology* 84, 372-383.
- Grek, C.L., Zhang, J., Manevich, Y., Townsend, D.M., and Tew, K.D. (2013). Causes and consequences of cysteine S-glutathionylation. *The Journal of biological chemistry* 288, 26497-26504.
- Griendling, K.K., and FitzGerald, G.A. (2003). Oxidative stress and cardiovascular injury: Part I: basic mechanisms and in vivo monitoring of ROS. *Circulation* 108, 1912-1916.
- Groenendyk, J., Agellon, L.B., and Michalak, M. (2013). Coping with endoplasmic reticulum stress in the cardiovascular system. *Annual review of physiology* 75, 49-67.

- Grotendorst, G.R., and Duncan, M.R. (2005). Individual domains of connective tissue growth factor regulate fibroblast proliferation and myofibroblast differentiation. *FASEB journal : official publication of the Federation of American Societies for Experimental Biology* 19, 729-738.
- Guo, Z., Kozlov, S., Lavin, M.F., Person, M.D., and Paull, T.T. (2010). ATM activation by oxidative stress. *Science (New York, N.Y.)* 330, 517-521.
- Hall-Glenn, F., Aivazi, A., Akopyan, L., Ong, J.R., Baxter, R.R., Benya, P.D., Goldschmeding, R., van Nieuwenhoven, F.A., Hunziker, E.B., and Lyons, K.M. (2013). CCN2/CTGF is required for matrix organization and to protect growth plate chondrocytes from cellular stress. *Journal of cell communication and signaling* 7, 219-230.
- Halliwell, B., Clement, M.V., and Long, L.H. (2000). Hydrogen peroxide in the human body. *FEBS letters* 486, 10-13.
- Harding, H.P., Zeng, H., Zhang, Y., Jungries, R., Chung, P., Plesken, H., Sabatini, D.D., and Ron, D. (2001). Diabetes mellitus and exocrine pancreatic dysfunction in *perk*^{-/-} mice reveals a role for translational control in secretory cell survival. *Molecular cell* 7, 1153-1163.
- Harding, H.P., Zhang, Y., and Ron, D. (1999). Protein translation and folding are coupled by an endoplasmic-reticulum-resident kinase. *Nature* 397, 271-274.
- Hartzell, H.C. (2007). Cell biology. The stress of relaxation. *Science (New York, N.Y.)* 317, 1331-1332.
- Heijman, J., Dewenter, M., El-Armouche, A., and Dobrev, D. (2013). Function and regulation of serine/threonine phosphatases in the healthy and diseased heart. *Journal of molecular and cellular cardiology* 64, 90-98.
- Herren, A.W., Bers, D.M., and Grandi, E. (2013). Post-translational modifications of the cardiac Na channel: contribution of CaMKII-dependent phosphorylation to acquired arrhythmias. *American Journal of Physiology - Heart and Circulatory Physiology* 305, H431-H445.
- Herzig, S., and Neumann, J. (2000). Effects of serine/threonine protein phosphatases on ion channels in excitable membranes. *Physiological reviews* 80, 173-210.
- Holbourn, K.P., Acharya, K.R., and Perbal, B. (2008). The CCN family of proteins: structure–function relationships. *Trends in Biochemical Sciences* 33, 461-473.
- Hoshino, A., Okawa, Y., Ariyoshi, M., Kaimoto, S., Uchihashi, M., Fukai, K., Iwai-Kanai, E., and Matoba, S. (2014). Oxidative post-translational modifications develop LONP1 dysfunction in pressure overload heart failure. *Circulation. Heart failure* 7, 500-509.
- Hsiao, H.-H., Meulmeester, E., Frank, B.T.C., Melchior, F., and Urlaub, H. (2009a). "ChopNSpice," a mass spectrometric approach that allows identification of endogenous small ubiquitin-like modifier-conjugated peptides. *Molecular & cellular proteomics: MCP* 8, 2664-2675.
- Hsiao, H.-H., Meulmeester, E., Frank, B.T.C., Melchior, F., and Urlaub, H. (2009b). "ChopNSpice," a mass spectrometric approach that allows identification of endogenous small ubiquitin-like modifier-conjugated peptides. *Molecular & cellular proteomics : MCP* 8, 2664-2675.
- Huang, J.-Q., Tao, R., Li, L., Ma, K., Xu, L., Ai, G., Fan, X.-X., Jiao, Y.-T., and Ning, Q. (2014). Involvement of heat shock protein 47 in *Schistosoma japonicum*-induced hepatic fibrosis in mice. *International journal for parasitology* 44, 23-35.
- Huebsch, N., Loskill, P., Mandegar, M.A., Marks, N.C., Sheehan, A.S., Ma, Z., Mathur, A., Nguyen, T.N., Yoo, J.C., and Judge, L.M., et al. (2015). Automated Video-Based Analysis of Contractility and Calcium Flux in Human-Induced Pluripotent Stem Cell-Derived Cardiomyocytes Cultured over Different Spatial Scales. *Tissue engineering. Part C, Methods* 21, 467-479.

- Hwa, V., Oh, Y., and Rosenfeld, R.G. (1999). The insulin-like growth factor-binding protein (IGFBP) superfamily. *Endocrine reviews* 20, 761-787.
- Ichimonji, I., Tomura, H., Mogi, C., Sato, K., Aoki, H., Hisada, T., Dobashi, K., Ishizuka, T., Mori, M., and Okajima, F. (2010). Extracellular acidification stimulates IL-6 production and Ca(2+) mobilization through proton-sensing OGR1 receptors in human airway smooth muscle cells. *American journal of physiology. Lung cellular and molecular physiology* 299, L567-77.
- Ingebritsen, T.S., and Cohen, P. (1983). Protein phosphatases: properties and role in cellular regulation. *Science (New York, N.Y.)* 221, 331-338.
- Ivkovic, S., Yoon, B.S., Popoff, S.N., Safadi, F.F., Libuda, D.E., Stephenson, R.C., Daluiski, A., and Lyons, K.M. (2003). Connective tissue growth factor coordinates chondrogenesis and angiogenesis during skeletal development. *Development (Cambridge, England)* 130, 2779-2791.
- Iwakoshi, N.N., Lee, A.-H., Vallabhajosyula, P., Otipoby, K.L., Rajewsky, K., and Glimcher, L.H. (2003). Plasma cell differentiation and the unfolded protein response intersect at the transcription factor XBP-1. *Nature immunology* 4, 321-329.
- Jacobson, A., and Cunningham, J.L. (2012). Connective tissue growth factor in tumor pathogenesis. *Fibrogenesis & Tissue Repair* 5, 1-7.
- Jatho, A., Hartmann, S., Kittana, N., Mugge, F., Wuertz, C.M., Tiburcy, M., Zimmermann, W.-H., Katschinski, D.M., and Lutz, S. (2015). RhoA Ambivalently Controls Prominent Myofibroblast Characteristics by Involving Distinct Signaling Routes. *PLoS ONE* 10, e0137519.
- Jeong, D., Lee, M.-A., Li, Y., Yang, D.K., Kho, C., Oh, J.G., Hong, G., Lee, A., Song, M.H., and LaRocca, T.J., et al. (2016). Matricellular Protein CCN5 Reverses Established Cardiac Fibrosis. *Journal of the American College of Cardiology* 67, 1556-1568.
- Johnston, A.S., Lehnart, S.E., and Burgoyne, JR (2015). Ca(2+) signaling in the myocardium by (redox) regulation of PKA/CaMKII. *Frontiers in pharmacology* 6, 166.
- Kaufman, R.J. (1999). Stress signaling from the lumen of the endoplasmic reticulum: coordination of gene transcriptional and translational controls. *Genes & Development* 13, 1211-1233.
- Kemp, T.J., Aggeli, I.-K., Sugden, P.H., and Clerk, A. (2004). Phenylephrine and endothelin-1 upregulate connective tissue growth factor in neonatal rat cardiac myocytes. *Journal of molecular and cellular cardiology* 37, 603-606.
- Kim, J.H., Johannes, L., Goud, B., Antony, C., Lingwood, C.A., Daneman, R., and Grinstein, S. (1998). Noninvasive measurement of the pH of the endoplasmic reticulum at rest and during calcium release. *Proceedings of the National Academy of Sciences* 95, 2997-3002.
- Kimata, Y., and Kohno, K. (2011). Endoplasmic reticulum stress-sensing mechanisms in yeast and mammalian cells. *Current opinion in cell biology* 23, 135-142.
- Kozutsumi, Y., Segal, M., Normington, K., Gething, M.J., and Sambrook, J. (1988). The presence of malfolded proteins in the endoplasmic reticulum signals the induction of glucose-regulated proteins. *Nature* 332, 462-464.
- Kwon, S.H., Pimentel, D.R., Remondino, A., Sawyer, D.B., and Colucci, W.S. (2003). H(2)O(2) regulates cardiac myocyte phenotype via concentration-dependent activation of distinct kinase pathways. *Journal of molecular and cellular cardiology* 35, 615-621.
- Lacle, M.M., van Diest, P.J., Goldschmeding, R., van der Wall, E., and Nguyen, T.Q. (2015). Expression of connective tissue growth factor in male breast cancer: clinicopathologic correlations and prognostic value. *PLoS ONE* 10, e0118957.

- Lau, L.F., and Lam, S.C. (1999). The CCN family of angiogenic regulators: the integrin connection. *Experimental cell research* 248, 44-57.
- Leask, A., and Abraham, D.J. (2006). All in the CCN family: essential extracellular signaling modulators emerge from the bunker. *Journal of cell science* 119, 4803-4810.
- Lee, A.-H., Heidtman, K., Hotamisligil, G.S., and Glimcher, L.H. (2011). Dual and opposing roles of the unfolded protein response regulated by IRE1 α and XBP1 in proinsulin processing and insulin secretion. *Proceedings of the National Academy of Sciences of the United States of America* 108, 8885-8890.
- Leeuwis, J.W., Nguyen, T.Q., Theunissen, M.G.J., Peeters, W., Goldschmeding, R., Pasterkamp, G., and Vink, A. (2010). Connective tissue growth factor is associated with a stable atherosclerotic plaque phenotype and is involved in plaque stabilization after stroke. *Stroke; a journal of cerebral circulation* 41, 2979-2981.
- Li, S., Wang, X., Klee, C.B., and Krieger, C. (2004). Overexpressed mutant G93A superoxide dismutase protects calcineurin from inactivation. *Brain research. Molecular brain research* 125, 156-161.
- Lim, A., Wally, J., Walsh, M.T., Skinner, M., and Costello, C.E. (2001). Identification and location of a cysteinyl posttranslational modification in an amyloidogenic kappa1 light chain protein by electrospray ionization and matrix-assisted laser desorption/ionization mass spectrometry. *Analytical biochemistry* 295, 45-56.
- Lip, G.Y.H., Heinzel, F.R., Gaita, F., Juanatey, J.R.G., Le Heuzey, J.Y., Potpara, T., Svendsen, J.H., Vos, M.A., Anker, S.D., and Coats, A.J., et al. (2016). European Heart Rhythm Association/Heart Failure Association joint consensus document on arrhythmias in heart failure, endorsed by the Heart Rhythm Society and the Asia Pacific Heart Rhythm Society. *Europace: European pacing, arrhythmias, and cardiac electrophysiology: journal of the working groups on cardiac pacing, arrhythmias, and cardiac cellular electrophysiology of the European Society of Cardiology* 18, 12-36.
- Liu, F., Rijkers, D.T.S., Post, H., and Heck, A.J.R. (2015). Proteome-wide profiling of protein assemblies by cross-linking mass spectrometry. *Nature methods* 12, 1179-1184.
- Liu, F., van Breukelen, B., and Heck, A.J.R. (2014a). Facilitating protein disulfide mapping by a combination of pepsin digestion, electron transfer higher energy dissociation (ETHcD), and a dedicated search algorithm SlinkS. *Molecular & cellular proteomics : MCP* 13, 2776-2786.
- Liu, S.-C., Chuang, S.-M., Hsu, C.-J., Tsai, C.-H., Wang, S.-W., and Tang, C.-H. (2014b). CTGF increases vascular endothelial growth factor-dependent angiogenesis in human synovial fibroblasts by increasing miR-210 expression. *Cell death & disease* 5, e1485.
- Lo Conte, M., and Carroll, K.S. (2013). The redox biochemistry of protein sulfenylation and sulfinylation. *The Journal of biological chemistry* 288, 26480-26488.
- Lohse, D.L., Denu, J.M., and Dixon, J.E. (1995). Insights derived from the structures of the Ser/Thr phosphatases calcineurin and protein phosphatase 1. *Structure* 3, 987-990.
- Lok, S.I., Nous, F.M.A., van Kuik, J., van der Weide, P., Winkens, B., Kemperman, H., Huisman, A., Lahpor, J.R., Weger, R.A. de, and Jonge, N. de (2015). Myocardial fibrosis and pro-fibrotic markers in end-stage heart failure patients during continuous-flow left ventricular assist device support. *European journal of cardio-thoracic surgery : official journal of the European Association for Cardio-thoracic Surgery* 48, 407-415.
- Luo, M., and Anderson, M.E. (2013). Mechanisms of altered Ca²⁺ handling in heart failure. *Circulation research* 113, 690-708.

- Lynch, J.M., Maillet, M., Vanhoutte, D., Schloemer, A., Sargent, M.A., Blair, N.S., Lynch, K.A., Okada, T., Aronow, B.J., and Osinska, H., et al. (2012). A thrombospondin-dependent pathway for a protective ER stress response. *Cell* 149, 1257-1268.
- Ma, K., Vattam, K.M., and Wek, R.C. (2002). Dimerization and release of molecular chaperone inhibition facilitate activation of eukaryotic initiation factor-2 kinase in response to endoplasmic reticulum stress. *The Journal of biological chemistry* 277, 18728-18735.
- MacMillan, L.B., Bass, M.A., Cheng, N., Howard, E.F., Tamura, M., Strack, S., Wadzinski, B.E., and Colbran, R.J. (1999). Brain actin-associated protein phosphatase 1 holoenzymes containing spinophilin, neurabin, and selected catalytic subunit isoforms. *The Journal of biological chemistry* 274, 35845-35854.
- Marti-Carvajal, A.J., and Kwong, J.S. (2016). Pharmacological interventions for treating heart failure in patients with Chagas cardiomyopathy. *The Cochrane database of systematic reviews* 7, CD009077.
- Martindale, J.J., Fernandez, R., Thuerauf, D., Whittaker, R., Gude, N., Sussman, M.A., and Glembotski, C.C. (2006). Endoplasmic reticulum stress gene induction and protection from ischemia/reperfusion injury in the hearts of transgenic mice with a tamoxifen-regulated form of ATF6. *Circulation research* 98, 1186-1193.
- Martinez-Finley, E.J., Chakraborty, S., and Aschner, M. (2013). Manganese in Biological Systems. In *Encyclopedia of Metalloproteins*, R.H. Kretsinger, V.N. Uversky and E.A. Permyakov, eds. (New York, NY: Springer New York), pp. 1297–1303.
- Matsushima, S., Ide, T., Yamato, M., Matsusaka, H., Hattori, F., Ikeuchi, M., Kubota, T., Sunagawa, K., Hasegawa, Y., and Kurihara, T., et al. (2006). Overexpression of mitochondrial peroxiredoxin-3 prevents left ventricular remodeling and failure after myocardial infarction in mice. *Circulation* 113, 1779-1786.
- Maytin, M., Siwik, D.A., Ito, M., Xiao, L., Sawyer, D.B., Liao, R., and Colucci, W.S. (2004). Pressure overload-induced myocardial hypertrophy in mice does not require gp91phox. *Circulation* 109, 1168-1171.
- McCluskey, A., Keane, M.A., Walkom, C.C., Bowyer, M.C., Sim, A.T.R., Young, D.J., and Sakoff, J.A. (2002). The first two cantharidin analogues displaying PP1 selectivity. *Bioorganic & medicinal chemistry letters* 12, 391-393.
- Meng C.T., Lou W. Y., Chen Y. Y., Hsu F. S., and Huang F.F. (2006). Cys-Oxidation of Protein Tyrosine Phosphatases: Its Role in Regulation of Signal Transduction and Its Involvement in Human Cancers. *Journal of Cancer Molecules* 14, 9-16.
- Merksamer, P.I., Trusina, A., and Papa, F.R. (2008). Real-time redox measurements during endoplasmic reticulum stress reveal interlinked protein folding functions. *Cell* 135, 933-947.
- Minamino, T., and Kitakaze, M. (2010). ER stress in cardiovascular disease. *Journal of molecular and cellular cardiology* 48, 1105-1110.
- Minicucci, M.F., Azevedo, P.S., Polegato, B.F., Paiva, S.A.R., and Zornoff, L.A.M. (2011). Heart failure after myocardial infarction: clinical implications and treatment. *Clinical cardiology* 34, 410-414.
- Moe, I.T., Pham, T.A., Hagelin, E.M.V., Ahmed, M.S., and Attramadal, H. (2013). CCN2 exerts direct cytoprotective actions in adult cardiac myocytes by activation of the PI3-kinase/Akt/GSK-3beta signaling pathway. *Journal of cell communication and signaling* 7, 31-47.
- Moore, K.A., and Hollien, J. (2012). The unfolded protein response in secretory cell function. *Annual review of genetics* 46, 165-183.

- Mori, K., Ma, W., Gething, M.J., and Sambrook, J. (1993). A transmembrane protein with a cdc2+/CDC28-related kinase activity is required for signaling from the ER to the nucleus. *Cell* 74, 743-756.
- Mozaffarian, D., Benjamin, E.J., Go, A.S., Arnett, D.K., Blaha, M.J., Cushman, M., Ferranti, S. de, Després, J.-P., Fullerton, H.J., and Howard, V.J., et al. (2015). Heart Disease and Stroke Statistics—2015 Update: A Report From the American Heart Association. *Circulation* 131, e29-e322.
- Murakami, T., Saito, A., Hino, S.-i., Kondo, S., Kanemoto, S., Chihara, K., Sekiya, H., Tsumagari, K., Ochiai, K., and Yoshinaga, K., et al. (2009). Signalling mediated by the endoplasmic reticulum stress transducer OASIS is involved in bone formation. *Nature cell biology* 11, 1205-1211.
- Murray, C.I., and van Eyk, J.E. (2012). Chasing cysteine oxidative modifications: proteomic tools for characterizing cysteine redox status. *Circulation. Cardiovascular genetics* 5, 591.
- Nakano, S., Muramatsu, T., Nishimura, S., and Senbonmatsu, T. (2012). Cardiomyocyte and Heart Failure. In *Role of Prokineticin in Epicardial Progenitor Cell Differentiation to Regenerate Heart*, Canan G. Nebigil, ed. (INTECH Open Access Publisher).
- Neumann, J., Eschenhagen, T., Jones, L.R., Linck, B., Schmitz, W., Scholz, H., and Zimmermann, N. (1997). Increased expression of cardiac phosphatases in patients with end-stage heart failure. *Journal of molecular and cellular cardiology* 29, 265-272.
- O’Loughlen, A., Pérez-Morgado, M., Salinas, M., and Martín, M. (2003). Reversible inhibition of the protein phosphatase 1 by hydrogen peroxide. Potential regulation of eIF2 α phosphorylation in differentiated PC12 cells. *Archives of biochemistry and biophysics* 417, 194-202.
- Ongherth, A., Pasch, S., Wuertz, C.M., Nowak, K., Kittana, N., Weis, C.A., Jatho, A., Vettel, C., Tiburcy, M., and Toischer, K., et al. (2015). p63RhoGEF regulates auto- and paracrine signaling in cardiac fibroblasts. *Journal of molecular and cellular cardiology* 88, 39-54.
- Paulech, J., Liddy, K.A., Engholm-Keller, K., White, M.Y., and Cordwell, S.J. (2015). Global analysis of myocardial peptides containing cysteines with irreversible sulfinic and sulfonic acid post-translational modifications. *Molecular & cellular proteomics: MCP* 14, 609-620.
- Perbal, B., Martinerie, C., Sainson, R., Werner, M., He, B., and Roizman, B. (1998). The C-terminal domain of the regulatory protein NOVH is sufficient to promote interaction with fibulin 1C: A clue for a role of NOVH in cell-adhesion signaling. *Proceedings of the National Academy of Sciences of the United States of America* 96, 869-874.
- Peti, W., Nairn, A.C., and Page, R. (2013). Structural basis for protein phosphatase 1 regulation and specificity. *The FEBS journal* 280, 596-611.
- Prysyazhna, O., and Eaton, P. (2015). Redox regulation of cGMP-dependent protein kinase I α in the cardiovascular system. *Frontiers in pharmacology* 6, 139.
- Purdom, S., and Chen, Q.M. (2005). Epidermal growth factor receptor-dependent and -independent pathways in hydrogen peroxide-induced mitogen-activated protein kinase activation in cardiomyocytes and heart fibroblasts. *The Journal of pharmacology and experimental therapeutics* 312, 1179-1186.
- Rachfal, A.W., and Brigstock, D.R. (2005). Structural and Functional Properties of CCN Proteins. In *Vitamins and hormones. Advances in research and applications*, G. Litwak, ed. (Amsterdam: Elsevier Academic Press), pp. 69–103.
- Rahal, A., Kumar, A., Singh, V., Yadav, B., Tiwari, R., Chakraborty, S., and Dhama, K. (2014). Oxidative stress, prooxidants, and antioxidants: the interplay. *BioMed research international* 2014, 761264.

- Rappsilber, J., Mann, M., and Ishihama, Y. (2007). Protocol for micro-purification, enrichment, pre-fractionation and storage of peptides for proteomics using StageTips. *Nature protocols* 2, 1896-1906.
- Reuter H. (1983). Calcium channel modulation by neurotransmitters, enzymes and drugs. *Nature* 301, 569-574.
- Richardson, P., McKenna, W., Bristow, M., Maisch, B., Mautner, B., O'Connell, J., Olsen, E., Thiene, G., Goodwin, J., and Gyarfás, I., et al. (1996). Report of the 1995 World Health Organization/International Society and Federation of Cardiology Task Force on the Definition and Classification of cardiomyopathies. *Circulation* 93, 841-842.
- Ron, D., and Walter, P. (2007). Signal integration in the endoplasmic reticulum unfolded protein response. *Nature reviews. Molecular cell biology* 8, 519-529.
- Rutkowski, D.T., Wu, J., Back, S.-H., Callaghan, M.U., Ferris, S.P., Iqbal, J., Clark, R., Miao, H., Hassler, J.R., and Fornek, J., et al. (2008). UPR pathways combine to prevent hepatic steatosis caused by ER stress-mediated suppression of transcriptional master regulators. *Developmental cell* 15, 829-840.
- Ruwhof, C., and van der Laarse, A. (2000). Mechanical stress-induced cardiac hypertrophy: mechanisms and signal transduction pathways. *Cardiovascular research* 47, 23-37.
- Rybka, J., Kupczyk, D., Kedziora-Kornatowska, K., Motyl, J., Czuczejko, J., Szewczyk-Golec, K., Kozakiewicz, M., Pawluk, H., Carvalho, L.A., and Kedziora, J. (2011). Glutathione-related antioxidant defense system in elderly patients treated for hypertension. *Cardiovascular toxicology* 11, 1-9.
- Sabri, A., Byron, K.L., Samarel, A.M., Bell, J., and Lucchesi, P.A. (1998). Hydrogen peroxide activates mitogen-activated protein kinases and Na⁺-H⁺ exchange in neonatal rat cardiac myocytes. *Circulation research* 82, 1053-1062.
- Sag, C.M., Santos, C.X., and Am Shah (2014). Redox regulation of cardiac hypertrophy. *Journal of molecular and cellular cardiology* 73, 103-111.
- Saito, A., Ochiai, K., Kondo, S., Tsumagari, K., Murakami, T., Cavener, D.R., and Imaizumi, K. (2011). Endoplasmic reticulum stress response mediated by the PERK-eIF2(α)-ATF4 pathway is involved in osteoblast differentiation induced by BMP2. *The Journal of biological chemistry* 286, 4809-4818.
- Sandra, K., Vandenheede, I., and Sandra, P. (2014). Modern chromatographic and mass spectrometric techniques for protein biopharmaceutical characterization. *Journal of chromatography. A* 1335, 81-103.
- Santos, C.X., Anilkumar, N., Zhang, M., Brewer, A.C., and Am Shah (2011). Redox signaling in cardiac myocytes. *Free radical biology & medicine* 50, 777-793.
- Santos, C.X.C., Hafstad, A.D., Beretta, M., Zhang, M., Molenaar, C., Kopec, J., Fotinou, D., Murray, T.V., Cobb, A.M., and Martin, D., et al. (2016). Targeted redox inhibition of protein phosphatase 1 by Nox4 regulates eIF2α-mediated stress signaling. *The EMBO journal* 35, 319-334.
- Santos CX, Tanaka LY, Wosniak J and Laurindo FR (2009). Mechanisms and implications of reactive oxygen species generation during the unfolded protein response: roles of endoplasmic reticulum oxidoreductases, mitochondrial electron transport, and NADPH oxidase. *Antioxidants & Redox signaling*, 11 (10): 2409-2427.
- Scarabelli, T.M., and Gottlieb, R.A. (2004). Functional and clinical repercussions of myocyte apoptosis in the multifaceted damage by ischemia/reperfusion injury: old and new concepts after 10 years of contributions. *Cell death and differentiation* 11 Suppl 2, S144-52.

- Schroder, E., and Eaton, P. (2008). Hydrogen peroxide as an endogenous mediator and exogenous tool in cardiovascular research: issues and considerations. *Current opinion in pharmacology* 8, 153-159.
- Schulz, E.M., and Wieczorek, D.F. (2013). Tropomyosin de-phosphorylation in the heart: what are the consequences? *Journal of muscle research and cell motility* 34, 239-246.
- Seoyoung C. Kim, Sebastian Schneeweiss, Niteesh Choudhry, Jun Liu, Robert J. Glynn, and Daniel H. Solomon (2015). Effects of Xanthine Oxidase Inhibitors on Cardiovascular Disease in Patients with Gout: A Cohort Study. *The American journal of medicine* 128, 653.e7 - 653.e16.
- Severino, A., Campioni, M., Straino, S., Salloum, F.N., Schmidt, N., Herbrand, U., Frede, S., Toietta, G., Di Rocco, G., and Bussani, R., et al. (2007). Identification of protein disulfide isomerase as a cardiomyocyte survival factor in ischemic cardiomyopathy. *Journal of the American College of Cardiology* 50, 1029-1037.
- Shaked, Z., Szajewski, R.P., and Whitesides, G.M. (1980). Rates of thiol-disulfide interchange reactions involving proteins and kinetic measurements of thiol pKa values. *Biochemistry* 19, 4156-4166.
- Sharov, V.S., Dremina, E.S., Galeva, N.A., Williams, T.D., and Schoneich, C. (2006). Quantitative mapping of oxidation-sensitive cysteine residues in SERCA in vivo and in vitro by HPLC-electrospray-tandem MS: selective protein oxidation during biological aging. *The Biochemical journal* 394, 605-615.
- Shi, Y. (2009). Serine/threonine phosphatases: mechanism through structure. *Cell* 139, 468-484.
- Shi, Y., Vattem, K.M., Sood, R., An, J., Liang, J., Stramm, L., and Wek, R.C. (1998). Identification and characterization of pancreatic eukaryotic initiation factor 2 alpha-subunit kinase, PEK, involved in translational control. *Molecular and Cellular Biology* 18, 7499-7509.
- Sies, H. (1997). Oxidative stress: oxidants and antioxidants. *Experimental physiology* 82, 291-295.
- Solaro, R.J., and Kobayashi, T. (2011). Protein phosphorylation and signal transduction in cardiac thin filaments. *The Journal of biological chemistry* 286, 9935-9940.
- Søndergaard, C.R., Olsson, M.H.M., Rostkowski, M., and Jensen, J.H. (2011). Improved Treatment of Ligands and Coupling Effects in Empirical Calculation and Rationalization of pKa Values. *J. Chem. Theory Comput.* 7, 2284-2295.
- Sonnyal, S., Xu, S., Jones, H., Tam, A., Sreeram, V.R., Ponticos, M., Norman, J., Agrawal, P., Abraham, D., and Crombrughe, B. de (2013). Connective tissue growth factor causes EMT-like cell fate changes in vivo and in vitro. *Journal of cell science* 126, 2164-2175.
- Steinhubl, S.R. (2008). Why have antioxidants failed in clinical trials? *The American journal of cardiology* 101, 14D-19D.
- Stull, L.B., Leppo, M.K., Szweda, L., Gao, W.D., and Marban, E. (2004). Chronic treatment with allopurinol boosts survival and cardiac contractility in murine postischemic cardiomyopathy. *Circulation research* 95, 1005-1011.
- Sullivan, L.B., and Chandel, N.S. (2014). Mitochondrial reactive oxygen species and cancer. *Cancer & metabolism* 2, 17.
- Szabo, Z., Magga, J., Alakoski, T., Ulvila, J., Piuholta, J., Vainio, L., Kivirikko, K.I., Vuolteenaho, O., Ruskoaho, H., and Lipson, K.E., et al. (2014). Connective tissue growth factor inhibition attenuates left ventricular remodeling and dysfunction in pressure overload-induced heart failure. *Hypertension* 63, 1235-1240.
- Tajc, S.G., Tolbert, B.S., Basavappa, R., and Miller, B.L. (2004). Direct Determination of Thiol pKa by Isothermal Titration Microcalorimetry. *J. Am. Chem. Soc.* 126, 10508-10509.

- Tan, K., Duquette, M., Liu, J.-h., Dong, Y., Zhang, R., Joachimiak, A., Lawler, J., and Wang, J.-h. (2002). Crystal structure of the TSP-1 type 1 repeats: a novel layered fold and its biological implication. *The Journal of cell biology* 159, 373-382.
- Thuerauf, D.J., Marcinko, M., Gude, N., Rubio, M., Sussman, M.A., and Glembotski, C.C. (2006). Activation of the unfolded protein response in infarcted mouse heart and hypoxic cultured cardiac myocytes. *Circulation research* 99, 275-282.
- Tonks, N.K. (2005). Redox redux: revisiting PTPs and the control of cell signaling. *Cell* 121, 667-670.
- Toth, A., Nickson, P., Mandl, A., Bannister, M., Toth, K., and Erhardt, P. (2007). Endoplasmic Reticulum Stress as a Novel Therapeutic Target in Heart Diseases. *CHDDT* 7, 205-218.
- van Empel, Vanessa P M, Bertrand, A.T., van der Nagel, R., Kostin, S., Doevendans, P.A., Crijns, H.J., Wit, E. de, Sluiter, W., Ackerman, S.L., and Windt, L.J. de (2005). Downregulation of apoptosis-inducing factor in harlequin mutant mice sensitizes the myocardium to oxidative stress-related cell death and pressure overload-induced decompensation. *Circulation research* 96, e92-e101.
- Virshup, D.M., and Shenolikar, S. (2009). From promiscuity to precision: protein phosphatases get a makeover. *Molecular cell* 33, 537-545.
- Wang, Z.V., Deng, Y., Gao, N., Pedrozo, Z., Li, D.L., Morales, C.R., Criollo, A., Luo, X., Tan, W., and Jiang, N., et al. (2014). Spliced X-box binding protein 1 couples the unfolded protein response to hexosamine biosynthetic pathway. *Cell* 156, 1179-1192.
- Wefing, S., Schnaible, V., and Hoffmann, D. (2006). SearchXLinks. A program for the identification of disulfide bonds in proteins from mass spectra. *Analytical chemistry* 78, 1235-1241.
- Winter, P. de, Leoni, P., and Abraham, D. (2008). Connective tissue growth factor: structure-function relationships of a mosaic, multifunctional protein. *Growth factors (Chur, Switzerland)* 26, 80-91.
- Wisniewski, J.R., Zougman, A., Nagaraj, N., and Mann, M. (2009). Universal sample preparation method for proteome analysis. *Nature methods* 6, 359-362.
- Wu, H., Wei, L., Fan, F., Ji, S., Zhang, S., Geng, J., Hong, L., Fan, X., Chen, Q., and Tian, J., et al. (2015). Integration of Hippo signalling and the unfolded protein response to restrain liver overgrowth and tumorigenesis. *Nature communications* 6, 6239.
- Wu, J.Q., Kosten, T.R., and Zhang, X.Y. (2013). Free radicals, antioxidant defense systems, and schizophrenia. *Progress in neuro-psychopharmacology & biological psychiatry* 46, 200-206.
- Yancy, C.W., Jessup, M., Bozkurt, B., Butler, J., Casey, D.E., Drazner, M.H., Fonarow, G.C., Geraci, S.A., Horwich, T., and Januzzi, J.L., et al. (2013). 2013 ACCF/AHA Guideline for the Management of Heart Failure. Executive Summary. *Journal of the American College of Cardiology* 62, 1495-1539.
- Yates, J.R., Ruse, C.I., and Nakorchevsky, A. (2009). Proteomics by mass spectrometry: approaches, advances, and applications. *Annual review of biomedical engineering* 11, 49-79.
- Ye, J., Rawson, R.B., Komuro, R., Chen, X., Dave, U.P., Prywes, R., Brown, M.S., and Goldstein, J.L. (2000). ER stress induces cleavage of membrane-bound ATF6 by the same proteases that process SREBPs. *Molecular cell* 6, 1355-1364.
- Yoon, P.O., Lee, M.-A., Cha, H., Jeong, M.H., Kim, J., Jang, S.P., Choi, B.Y., Jeong, D., Yang, D.K., and Hajjar, R.J., et al. (2010). The opposing effects of CCN2 and CCN5 on the development of cardiac hypertrophy and fibrosis. *Journal of molecular and cellular cardiology* 49, 294-303.
- Zambrano, C.A., Egana, J.T., Nunez, M.T., Maccioni, R.B., and Gonzalez-Billault, C. (2004). Oxidative stress promotes tau dephosphorylation in neuronal cells: the roles of cdk5 and PP1. *Free radical biology & medicine* 36, 1393-1402.

- Zhang, H., Ma, Y., Liu, K., and Yu, J.G. (2013). Theoretical studies on the reaction mechanism of PP1 and the effects of different oxidation states of the Mn-Mn center on the mechanism. *Journal of biological inorganic chemistry : JBIC : a publication of the Society of Biological Inorganic Chemistry* 18, 451-459.
- Zhang, K., Wong, H.N., Song, B., Miller, C.N., Scheuner, D., and Kaufman, R.J. (2005). The unfolded protein response sensor IRE1alpha is required at 2 distinct steps in B cell lymphopoiesis. *The Journal of clinical investigation* 115, 268-281.
- Zhang, M., Prosser, B.L., Bamboye, M.A., Gondim, A.N.S., Santos, C.X., Martin, D., Ghigo, A., Perino, A., Brewer, A.C., and Ward, C.W., et al. (2015). Contractile Function During Angiotensin-II Activation: Increased Nox2 Activity Modulates Cardiac Calcium Handling via Phospholamban Phosphorylation. *Journal of the American College of Cardiology* 66, 261-272.
- Zhang, P., McGrath, B., Li, S., Frank, A., Zambito, F., Reinert, J., Gannon, M., Ma, K., McNaughton, K., and Cavener, D.R. (2002). The PERK eukaryotic initiation factor 2 alpha kinase is required for the development of the skeletal system, postnatal growth, and the function and viability of the pancreas. *Molecular and Cellular Biology* 22, 3864-3874.
- Zhang, Z., Zhao, S., Deans-Zirattu, S., Bai, G., and Lee, E.Y.C. (1994). Mutagenesis of the catalytic subunit of rabbit muscle protein phosphatase-1. In *Reversible Protein Phosphorylation in Cell Regulation*, R.L. Khandelwal and J.H. Wang, eds. (Boston, MA: Springer US), pp. 113-119.
- Zhang, Z.-Y., Liu, X.-H., Hu, W.-C., Rong, F., and Wu, X.-D. (2010). The calcineurin-myocyte enhancer factor 2c pathway mediates cardiac hypertrophy induced by endoplasmic reticulum stress in neonatal rat cardiomyocytes. *American journal of physiology. Heart and circulatory physiology* 298, H1499-509.
- Zhu, C., Johansen, F.E., and Prywes, R. (1997). Interaction of ATF6 and serum response factor. *Molecular and Cellular Biology* 17, 4957-4966.

8 Curriculum vitae

Simranjit Singh

Date of birth: 19 July, 1987, **Nationality:** Indian

Adresse: Am Vogelsang 3, # 001, 37075 Göttingen

Phone: 0049-176-85122862, **E-Mail:** singhsimranjit1987@gmail.com



Experience

Ph.D. graduate student

April.2013-June.2017

Ph.D. thesis title - 'Redox regulation of protein phosphatase-1 and connective tissue growth factor in the heart'

Institute of Pharmacology and Toxicology,
University of Medical Center,
Goettingen, Germany

Master thesis

Novemeber.2011-Novemeber.2012

Master thesis title – 'Identification of novel endothelial-specific molecules involved in the regulation of tumor cell extravasation'

Pharmacology department
Max Planck Institute for Heart and Lung Research,
Bad Nauheim, Germany

Hiwi job

August.2011-January.2012

Histology Department
Pharmacology department,
Max Planck Institute for Heart and Lung Research,
Bad Nauheim, Germany

Lecturer

January.2010-May.2010

Biotechnology Department
Beant Singh College of Engineering and Technology (BCET),
Gurdaspur, India

Education

Ph.D. In Cardiovascular medicine

April.2013-June.2017

George August University, Goettingen, Germany

Master of Science in Agrobiotechnology

October.2010-December.2013

Justus-Liebig-Universität, Giessen, Germany

Bachelor of Technology in Biotechnology

August.2005-July.2009

Saheed Udham Singh College of Engineering and Technology (SUSCET),
Punjab Technical University, Chandigarh, India

Skills**Language skills**

English: Fluent in speech, writing and reading (IELTS band score =7.0)
Hindi: Fluent in speech, writing and reading
German: Intermediate Knowledge (B1)
Punjabi: Native Speaker

Extra qualification

Vice president (external relations), AIESEC Giessen, Germany
March-September, 2011
Exchange Coordinator (AIDS/HIV awareness related), AIESEC
Chandigarh, India, February-December, 2008

Posters presentation

Singh S., Saadatmand A.R., Vettel C., El-Armouche A. (2014). Redox regulation of protein phosphates -1 in cardiomyocytes. Poster presentation at the 80th Annual Meeting of the German Society for Experimental and Clinical Pharmacology and Toxicology (DGPT), Hannover, Germany.

Simranjit Singh, Susanne Lutz (2015). Endoplasmic reticulum stress and oxidative stress – A mixed blessing for connective tissue growth factor in cardiomyocytes. Poster presentation at the Stress Proteins in Growth, Development & Disease, Gordon Research Conference, Tuscany, Italy.